Universidad Autónoma de Querétaro
Facultad de Ingeniería

Sensores colaborativos para detección de fallas en máquinas eléctricas

Tesis
Que como parte de los requisitos para obtener el grado de
Doctor en Ingeniería

Presenta
M. en I. Armando Guadalupe García Ramírez

Dirigido por:

Dr. René de Jesús Romero Troncoso

San Juan del Río, Qro. Octubre 2014

Universidad Autónoma de Querétaro
Facultad de Ingeniería
Doctorado en Ingeniería

Sensores colaborativos para detección de fallas en máquinas eléctricas

Tesis
Que como parte de los requisitos para obtener el grado de
Doctor en Ingeniería

Presenta
M. en I. Armando Guadalupe García Ramírez

Dirigido por:

Dr. René de Jesús Romero Troncoso

SINODALES

Dr. René de Jesús Romero Troncoso
Presidente — Firma

Dr. Roque Alfredo Osornio Rios
Secretario — Firma

Dr. Luis Alberto Morales Hernández
Vocal — Firma

Dr. Arturo García Pérez
Suplente — Firma

Dr. Juan Primo Benítez Rangel
Suplente — Firma

Dr. Aurelio Domínguez González
Director de la Facultad

Dr. Iñigo Torres Pacheco
Director de Investigación y Posgrado

Centro Universitario
Querétaro, Qro.
México
Octubre 2014

RESUMEN

Actualmente, el monitoreo de máquinas eléctricas ha llamado la atención de un gran número de investigadores debido a la importancia que tienen éstas en la industria y vida diaria y como éstas afectan la calidad de la energía por la serie de problemas originados en la electricidad, el suministro de energía no regulado, ya que son fuente de perturbaciones en voltaje y corriente. Por otro lado, el uso de sensores colaborativos mejoran las demandas de los sistemas de monitoreo debido a sus características de comunicación, procesamiento de datos, versatilidad y habilidad de trabajar en ambientes donde el acceso a trabajadores es limitado. En este trabajo se proponen diferentes metodologías para sensores inteligentes los cuales colaboran entre sí para monitorear y evaluar las máquinas eléctricas; éstos, se enfocan principalmente a la detección de fallas bajo diferentes criterios de operación y de número de fallas respaldados por la literatura así como también estándares internacionales los cuales pocos han sido reportados en la literatura.

Entre otros resultados obtenidos de esta investigación, figuran dos publicaciones en revistas indizadas y dos artículos en congreso internacional.

Palabras claves: Máquinas eléctricas, sensores inteligentes, redes neuronales, sensores colaborativos, FPGA

SUMMARY

Nowadays , monitoring of electrical machines has caught the attention of many researchers due to the importance of these in industry and daily life and how they affect power quality for the range of problems arising in the electricity, unregulated power supply , since they are a source of disturbances in voltage and current. On the other hand, the use of collaborative sensors enhance the demands of monitoring systems due to its characteristics of communication, data processing, versatility and ability to work in environments where access to workers is limited. In this work different methodologies for smart sensors which collaborate with each other to monitor and evaluate the electrical machines are proposed; they are mainly focus on fault detection under different operating criteria and number of failures supported in the literature as well as international standards which few have been reported in the literature

Other obtained results of this investigation are the publication of two papers in indexed journals and two international congress papers.

Keywords: Electric machines, smart sensors, neural networks, collaborative sensors, FPGA

DEDICATORIA

Con todo mi amor y agradecimiento dedico este trabajo a las personas que hicieron realidad este logro, mis padres Rosa María y Jesús Armando, a mi esposa Carmen Nereyda, a mi sobrina Nayeli Yarazeth y en memoria a mi mamá Tachita, quien ha marcado mi camino.

AGRADECIMIENTOS

A mis padres y hermanos por el apoyo incondicional brindado en todo momento, siendo mi principal motivación para seguir avanzando y salir adelante.

A mis asesores, el Dr. René de Jesús Romero Troncoso y el Dr. Roque Alfredo Osornio Ríos, por confiar en mí y apoyarme en mis estudios doctorales, por sus invaluables consejos y enseñanzas durante mi formación profesional.

A mis compañeros de trabajo, tanto a las generaciones que ya culminaron sus estudios como a las generaciones que siguen en este camino, en especial a: Arturo, Arturin, Carlos, Claudia, Martín, Iván, David, Juan José, Benigno, Lieberman, Rooney, Uriel.

A todos los integrantes del grupo HSPdigital por el apoyo y amistad que me han brindado haciendo que lo difícil sea fácil.

A todos mis alumnos de la Universidad Autónoma de Querétaro por todas las experiencias vividas dentro y fuera del aula de clases.

A todos los colegas y personal de trabajo de la Universidad Autónoma de Querétaro que ayudaron, facilitaron y brindaron su ayuda laboral y personal.

Al Consejo Nacional de Ciencia y Tecnología (CONACyT) por el apoyo No. 328330 otorgado a través del Programa de Becas para Estudios de Posgrado y realizar mis estudios doctorales en la Universidad Autónoma de Querétaro.

ÍNDICE

ÍNDICE DE TABLAS

ÍNDICE DE FIGURAS

1. INTRODUCCIÓN

Actualmente, más de la mitad de la energía producida en países desarrollados es transformada a energía mecánica a través de motores eléctricos, liberando a la sociedad de trabajos tediosos y algunas labores físicas. Entre una amplia variedad de motores, las máquinas de inducción trifásicas aún conservan la popularidad que han tenido desde hace un siglo. Al menos el 90% de la industria maneja sistemas que emplean motores de inducción. Aunque los motores de inducción son seguros y robustos, la posibilidad de fallas es inevitable, donde los porcentajes de fallas en motores más comunes son: 41% debido a daños en rodamientos, el 37% a fallas en el estator, el 10% a fallas en el rotor y el 12% debido a otro tipo de fallas, Garcia-Perez (2013). La detección temprana de fallas permite programar un mantenimiento preventivo para motores de inducción. Esto también puede prevenir periodos extendidos de inactividad o incluso consecuencias catastróficas causadas por la falla de un motor. Por eso recientemente las condiciones de monitoreo y diagnóstico de fallas han recibido una atención considerable que han generado la propuesta de nuevas técnicas aplicadas a la detección de fallas en motores de inducción trifásicos.

1.1 ANTECEDENTES

En los antecedentes de este trabajo se presenta una descripción de las máquinas eléctricas y sus problemas, un análisis sobre el monitoreo en máquinas eléctricas y las principales técnicas, una descripción conceptual de sensores inteligentes y finalmente los trabajos sobre detección de fallas en máquinas eléctricas, sensores inteligentes y colaborativos que han sido desarrollados dentro del grupo de investigación HSPdigital y la Universidad Autónoma de Querétaro.

1.1.1 Máquinas eléctricas y sus problemas

Una máquina eléctrica es un dispositivo que puede convertir energía mecánica en energía eléctrica o viceversa. Cuando dicho dispositivo se usa para convertir energía mecánica en eléctrica se le llama generador. Asimismo, cuando

convierte energía eléctrica en mecánica se le llama motor, Chapman (2005). Las máquinas eléctricas son un componente crítico en muchos de los procesos industriales. Una de las máquinas eléctricas más utilizadas en la industria es sin duda el motor de inducción ya que su robustez, bajo costo, fácil mantenimiento y versatilidad los han hecho populares. Botha (1997), describe que la mayoría de las fallas en máquinas eléctricas pueden ser clasificadas en dos grupos: fallas eléctricas y mecánicas; así como también presenta las causas que pueden llevar a la ocurrencia de fallas en motores eléctricos de inducción. Las fallas eléctricas son caracterizadas por dañar las espiras del estator, conocidas como cortocircuito en el enrollamiento del estator. Las fallas mecánicas están asociadas con el rotor, dentro de las principales fallas mecánicas se pueden destacar en la literatura las siguientes: Daños en baleros, quiebre de barras, desbalance. Tandon (1999), menciona que más del 40% de fallas en máquinas eléctricas están relacionadas con baleros así como Ordaz (2008), comenta que las barras rotas es la falla en el rotor más común la cual afecta la máquina eléctrica y es difícil de percibir ya que aparentemente la máquina trabaja en condiciones normales representando un 10% de las fallas. Betta (2002), explica que cada máquina produce vibraciones con características distintivas en cada falla dentro de ellas se mencionan desbalance y desalineamiento, siendo estos <10% de las fallas. Por otra parte los transformadores eléctricos de potencia se utilizan para subir o bajar voltaje y son un componente importante en cualquier red de distribución de energía. Morgan (1998), dice que la vida y el envejecimiento de los transformadores están relacionados con la degradación del aislamiento, causado principalmente por el estrés térmico del aislamiento del papel junto con la descomposición química del papel.

Las fallas que se centran máquinas eléctricas ha tomado gran interés en la investigación debido a cómo afectan la calidad de la energía por la serie de problemas originados en la electricidad, el suministro de energía no regulado, ya que son fuente de perturbaciones en voltaje y corriente, Stones (2001). Debido a que estos problemas afectan directamente a las industrias, en tiempos y costos, se demandan sistemas de monitoreo para máquinas eléctricas bajo las normas

IEC 61000-4-3 (2003), IEEE-519(1999). La calidad de la energía eléctrica es el término que relaciona las características óptimas de la señal del suministro de voltaje y corriente consumidos por la carga de forma lineal o no lineal. Esta calidad está referida a una onda senoidal ideal compuesta por una sola componente fundamental, de amplitud constante y sin desviaciones en frecuencia, Bollen (2003). Hay estándares como el IEEE-519 (1999) que establece los límites de contenido armónico en la línea así como la distorsión armónica del voltaje de alimentación, mientras que el IEEE-1159 (1995) clasifica fenómenos electromagnéticos como: impulsos, oscilaciones, sobretensiones, subtensiones, interrupciones, offset DC, fluctuaciones de tensión y frecuencia, entre otros que establecen índices sobre parámetros eléctricos acorde a las formas de onda de las señales de corriente y voltaje con los cuales se puede estimar perfectamente la calidad de la energía. Estos índices sirven para cuantificar y diagnosticar disturbios eléctricos sobre el contenido armónico, desequilibrio de tensión entre fases, cambios rápidos de tensión, fluctuaciones (*Flickers*), huecos de tensión (*Dips*), interrupciones, transitorios, etc. Granados (2010). Existen cargas que al ser alimentadas consumen corriente no lineal, por ejemplo, hornos de arco eléctrico, variadores de velocidad, máquinas soldadoras, balastras electrónicas, sistemas alimentados con fuentes conmutadas, entre otras, Caupa (2001). Estas cargas inducen armónicos en el suministro de voltaje que generan problemas como: disminución de la vida útil de máquinas de inducción, vibraciones mecánicas, mala operación de bancos de capacitores, error en instrumentos de medición, interferencia telefónica, falso accionamiento de sistemas de protección, Podesta (2002), corrientes excesivas en el neutro, sobrecalentamiento de transformadores, motores y cableado en general. Existen trabajos sobre la medición de ciertos parámetros relacionados con la calidad de la energía los cuales han estudiado de manera específica a máquinas eléctricas como motores, trasformadores, generadores, etc. y no como a un sistema que incorpore el uso en conjunto de varios elementos. Tal es el caso de la medición del factor de potencia en máquinas rotatorias en condiciones de desbalance de voltajes, Eren (1999), efectos de perturbaciones en la línea de alimentación de motores como variación

en la frecuencia y la distorsión de la forma de onda de la tensión, Wakileh (2003). También se han realizados estudios con cargas variables en motores, Yen-Nien (2001), presentando resultados del comportamiento del par motor ante la presencia de armónicos en la línea.

Las investigaciones relacionadas con la calidad de la energía han tomado gran importancia en años recientes, debido a que el consumo eficiente de energía eléctrica implica ahorro de recursos naturales y económicos. El accionamiento de máquinas y equipamientos mecánicos por motores eléctricos es de gran importancia económica en la industria. Según la secretaria de energía alrededor del 70% del consumo de la energía eléctrica generada se debe al funcionamiento de las máquinas eléctricas, Garcia-Ramirez (2013).

1.1.2 Monitoreo en máquinas eléctricas

El monitoreo de máquinas es uno de los intereses principales en la industria moderna con el fin de garantizar la eficiencia durante el proceso de producción, Contreras (2008). El mantenimiento preventivo en el ámbito industrial permite detectar fallas en equipo eléctrico de potencia como transformadores, generadores y motores (máquinas eléctricas). Permitiendo con esto incrementar la vida útil de la máquina y evitar daños catastróficos, además de reducir el tiempo de paro en la línea de producción y gastos a causa del mantenimiento correctivo.

Benbouzid (1999), argumenta que el mantenimiento correctivo ha impulsado el desarrollo de diversas técnicas para el monitoreo y detección de fallas. Nelson clasifica las principales técnicas de monitoreo como: análisis de variables eléctricas, análisis de vibraciones, termografía, tintas penetrantes, radiografía y ultrasonido; sin embargo, la mayoría de estas técnicas tienen la desventaja de ser invasivas o fuera de línea, lo que origina pérdida de tiempo en el desmontaje del motor, paro de la producción, costos por el análisis en laboratorio, etc.

El análisis de las señales de vibración, corriente, voltaje, termografía y ultrasonido es principalmente realizado en el dominio de la frecuencia. Técnicas de procesamiento como la Transformada Rápida de Fourier (FFT, Fast Fourier Transform), Transformada Wavelet, Entropía, entre otros, son utilizadas ampliamente para el monitoreo de máquinas eléctricas. El análisis tradicional es realizado generalmente con un análisis espectral basado en la transformada rápida de Fourier o la transformada corta de Fourier, Yen (2000). Peng (2004), argumentó que la transformada Wavelet para monitoreo de máquinas eléctricas ha sido usada por más de 10 años con un rápido desarrollo correspondiente al monitoreo de la corriente. Romero (2004), presentó un algoritmo para el procesamiento de las señales de corriente en máquinas CNC proponiendo un sistema de monitoreo de la condición de las herramientas que permite la detección de su ruptura. Franco (2006), desarrolló un sistema para el monitoreo de la señal de corriente en los servomotores para determinar los daños o desgaste en la maquinaria CNC este trabajo fue desarrollado a partir de la trasformada Wavelet para encontrar las frecuencias originadas por la fuerza de corte de la máquina, los algoritmos diseñados fueron implementados en un FPGA para poder realizar el monitoreo en línea y fueron probados en una máquina CNC Baker-422 bajo distintas condiciones de corte. Posteriormente Franco (2008), realizó un sistema de acondicionamiento sobre señales de este sistema. Zhang (2006), desarrolló el monitoreo de máquinas eléctricas rotatorias, por medio de análisis en señales de vibración hace una comparación entre procesamientos tiempo-frecuencia como la transformada corta de Fourier y la transformada Wavelet. Didier (2007), realizó el monitoreo de la corriente en motores de inducción utilizando el procesamiento de la transformada de Fourier para detectar barras rotas así como también la transformada de Hilbert. Zhu (2009), afirmó que la transformada Wavelet es la herramienta más importante y popular para el procesamiento de señales no estacionarias, así como para monitorear máquinas eléctricas.

1.1.3. Sensores inteligentes

Los sensores inteligentes, recopilan, analizan y transmiten los datos haciéndolos más sofisticados que los sensores tradicionales. De acuerdo a las especificaciones del IEEE 1451.2 (1997), un sensor inteligente proporciona funciones para generar una representación correcta de la cantidad sensada o controlada. La independencia de las variables que componen cualquier sistema hace necesario establecer algún tipo de sensado inteligente para conocer el estado del mismo. La necesidad principal de desarrollar sensores inteligentes es sin duda para tener un diagnóstico rápido del sistema a monitorear ya que dentro del mismo contiene técnicas de procesamiento.

Korkua (2009), propuso una red inalámbrica (ZigBee™/ Estándar IEEE802.15.4) de sensores inteligentes para un sistema de monitoreo y recolección de datos de máquinas eléctricas. Jong-Duk (2009), realizó un sistema de sensores inteligentes que adquiere tres tipos de señales vibraciones, corriente y flujo en motores de inducción y después en una máquina de vectores, hace un análisis lineal, k-enésimo vecino más cercano y el algoritmo de forest empleados para clasificar el diagnóstico de la falla, los parámetros son clasificados y optimizados usando el método de validación de cruce.

1.1.4. Antecedentes del grupo de investigación y la Universidad Autónoma de Querétaro

Parte del grupo de investigación HSP-digital ubicado en la Universidad de Guanajuato (UG), ha realizado trabajos que involucran detección de fallas en máquinas eléctricas. Rangel (2009), presentó un sistema en un chip (SoC, System-on-a-Chip) para la detección de media barra rota en un motor de inducción con un análisis frecuencial por medio de la FFT y la correlación de los espectros de la señal para mejorar la detectabilidad, para la operación en línea, con el desarrollo de una unidad que toma decisiones. Valtierra (2010), realizó el monitoreo de las vibraciones de un motor de inducción para la detección de fallas múltiples combinadas, realizando el cálculo de la Entropía para señales de

vibraciones, para que después sean clasificadas por una red neuronal multicapa y así diagnosticar la condición física del motor, todo esto en software y hardware FPGA. Saucedo (2010), presenta un sistema difuso para la detección de fallas en motores de inducción mediante las señales de corriente y vibraciones, también en software y hardware FPGA. Por parte de la Universidad Autónoma de Querétaro (UAQ), Trejo (2010), desarrolló un sensor inteligente, basado en FPGA para mejorar la estimación cuantitativa en línea del flanco de desgaste en máquinas de control numérico por computadora (CNC, Computer Numerical Control) a partir de la información proporcionada por dos sensores principales: corriente y acelerómetro. Moreno et al. (2010), crearon una red de sensores inteligentes para el monitoreo de máquinas CNC. Por otro lado Osornio et al. (2008) presentaron una plataforma FPGA con IP Cores (Intellectual Property Cores) para dar soporte a la investigación y desarrollo de productos para aplicaciones de tiempo real en mecatrónica. Morales et al. (2010) presentaron un diseño software-hardware con funciones reconfigurables de control y monitoreo para máquinas CNC.

Como se podrá observar en los trabajos citados aún no se han desarrollado investigaciones relacionadas con sensores colaborativos. Principalmente en la arquitectura de las redes de sensores inteligentes para la detección de fallas en máquinas eléctricas.

1.2 DESCRIPCIÓN DEL PROBLEMA

Las fallas en máquinas eléctricas son imprescindibles y las consecuencias de estas fallas en el mejor de los casos se pueden ver reflejadas en pérdidas económicas debido al tiempo de mantenimiento correctivo no previsto o en el peor de los casos daños mayores a la máquina operada por el motor o posibles accidentes que causen algún daño al operador de la máquina. Por consiguiente; las máquinas eléctricas requieren de monitoreo y diagnóstico donde muchas veces es complicado debido a que el acceso es limitado para técnicos y trabajadores.

En términos generales el monitoreo clásico de máquinas eléctricas bajo las normas IEC 61000-4-3 (2003), IEEE-519 (1999) como se muestra en la Figura 1.1a, consiste en el sensado y adquisición de datos para ser transmitidos hacia una computadora personal (PC, Personal Computer), una vez almacenados se realiza un análisis fuera de línea mediante algún software especializado (MATLAB, etc.), ahí se realiza el procesamiento (FFT, Wavelets, etc.) y posteriormente se hace un análisis para conocer la falla. El problema a resolver es crear un sistema el cual cuente con sensores colaboradores y así monitorear en tiempo real, de forma continua y sin necesidad del procesamiento en PC (Figura 1.1b).

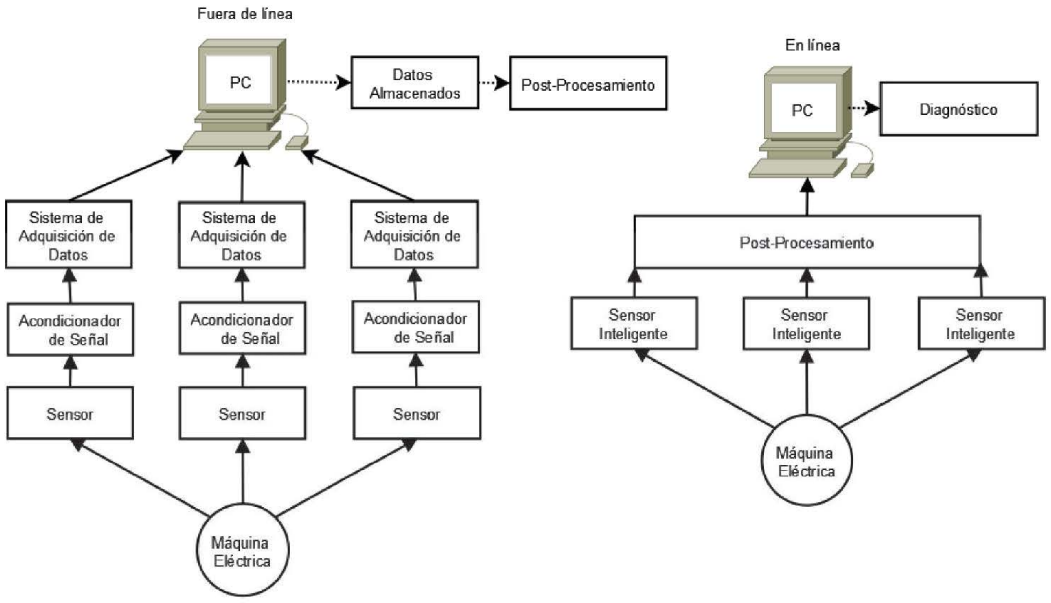

Figura 1.1: a) Sistema de monitoreo clásico, b) Sistema de monitoreo propuesto.

1.3 HIPÓTESIS Y OBJETIVOS

1.3.1 Hipótesis

El diseño de sensores colaborativos que incorporen técnicas de procesamiento o su combinación incrementa la precisión del monitoreo automático de máquinas eléctricas en procesos industriales en línea.

1.3.2 Objetivos

General:

Desarrollar arquitectura en hardware para los sensores colaborativos así como sensores colaborativos para el monitoreo en máquinas eléctricas.

Específicos:

1. Desarrollar e integrar la tecnología en la elaboración de instrumentos para monitoreo en máquinas eléctricas.

2. Probar la red de sensores diseñada en dos o más metodologías hasta ahora reportadas en software para mostrar las mejoras en los instrumentos diseñados.

3. Publicar dos artículos en revistas indexadas, mediante el estudio y desarrollo de la arquitectura e instrumentos generados de este proyecto para la difusión de la presente investigación.

4. Generar tesis de grado mediante la presente investigación para la formación de recursos humanos en esta línea de investigación.

1.4 JUSTIFICACIÓN

La principal motivación para realizar esta investigación consiste en que hasta la fecha en la literatura revisada no se ha reportado la existencia de una arquitectura flexible y genérica en hardware de sensores colaborativos con características para detectar fallas en diversas máquinas, donde además sus parámetros de diseño sean versátiles tales como: estructura, paralelismo, velocidad y consumo de recursos. El desarrollo de instrumentos para el monitoreo de máquinas eléctricas, beneficia a la industria en diferentes factores como disminución de costos en producción, incremento del tiempo de vida de las máquinas, disminuirá los costos en el mantenimiento correctivo, ahorro en compra de equipos costosos, consumo de energía ya que se reporta en trabajos de todo el mundo, que las máquinas eléctricas consumen el 85% de la energía. Mediante

este desarrollo se superarán aspectos de flexibilidad, velocidad de diagnóstico y costo a las metodologías propuestas a la fecha.

El campo de investigación sobre monitoreo y diagnóstico de las máquinas eléctricas es una de las tantas áreas de aplicación de sensores colaborativos. La importancia del monitoreo de las máquinas eléctricas es debido a la gran importancia que tienen éstas en la industria y vida diaria, por la presencia de diferentes fallas en las máquinas eléctricas. Esta situación demanda sistemas en línea para el monitoreo de las máquinas eléctricas. Las soluciones identificadas hasta ahora acerca del monitoreo de máquinas eléctricas son artículos reportados en congresos internacionales y revistas indexadas las cuales presentan metodologías basadas en redes de sensores procesadas en software con limitantes en máquinas eléctricas en específico, lo anterior demanda una red de sensores inteligentes que colaboren entre sí para tener un diagnóstico de diferentes máquinas eléctricas; también existen instrumentos ya disponibles en el mercado (Fluke Corporation, Extech Instruments Corporation, Hioki Corporation) pero con la principal desventaja de un alto costo.

Otro factor que motiva el diseño y desarrollo de sensores colaborativos es el campo de aplicación de los microprocesadores y sistemas en un mismo chip (Microprocessors and systems-on-a-chip) en áreas como: electrónica, electricidad, mecánica, control y muchas otras más. En todas éstas se desarrollan instrumentos que poseen sensores inteligentes para control, clasificación, predicción, etc. Esta investigación permitirá desarrollar un sistema que pueda ayudar y ser utilizado en estas áreas de investigación para el desarrollo de estos sensores colaborativos.

El diseño de sensores colaborativos permitirá la implementación de diversos sensores de forma eficiente y versátil para atender las características que las metodologías de monitoreo sugieren en su algoritmo de diagnóstico, con esto, el aporte para el campo de innovación en el desarrollo de instrumentos será muy grande ya que esto no se ha realizado en hardware.

1.5 PLANTEAMIENTO GENERAL

El planteamiento general de la metodología de este trabajo consiste principalmente de cuatro módulos: (1) Análisis y comparativa de técnicas aplicadas en fallas de máquinas eléctricas, (2) diseño, desarrollo e implementación de los sensores inteligentes, (3) fusión de los sensores inteligentes (sensores colaborativos), (4) pruebas y resultados para validar y probar las metodologías y el sensor colaborativo desarrollado.

Una descripción más detallada del planteamiento general de la metodología es la siguiente:

Análisis y comparativa de técnicas aplicadas en fallas de máquinas eléctricas: Primeramente en esta parte se realizó una revisión bibliográfica exhaustiva sobre el tema. Se realizó también la comparativa de la teoría y las técnicas utilizadas en el área de procesamiento digital de señales aplicada al monitoreo de máquinas eléctricas como la FFT, STFT, Wavelet, entropía, transformada Park o la combinación entre ellas y se determinó en base al estudio las mejores técnicas a utilizar en cuanto resolución, precisión y tiempo de cómputo.

Diseño, desarrollo e implementación de los sensores inteligentes: Esta etapa consiste en el desarrollo de los algoritmos revisados para realizar el monitoreo de máquinas eléctricas en sensores inteligentes, esta metodología será implementada en FPGA, la cual será programada mediante lenguaje de descripción de hardware (Very high speed integrated circuit Hardware Description Language, VHDL).

Fusión de los sensores inteligentes (sensor colaborativo): En esta etapa se usará una red de sensores inteligentes para colaborar entre sí (Figura1.2). A continuación se describe cada uno de los elementos que se desarrollarán en la metodología propuesta.

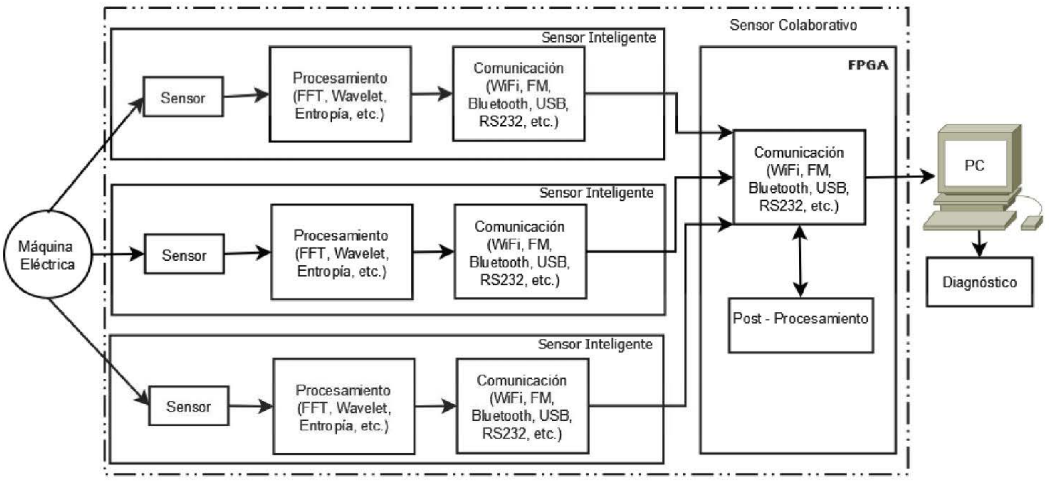

Figura 1.2: Diagrama ejemplo de un sensor colaborativo.

- Sensor inteligente: Está conformado principalmente por un sensor primario, un módulo de procesamiento y un módulo de comunicación.

- Procesamiento: Este módulo realizará la técnica matemática de los datos adquiridos mediante el sensor con el fin de analizar la señal. Este módulo podrá realizar uno o más procesamientos para cada señal de voltaje, corriente, vibraciones, etc.

- Comunicación: Dentro de estos bloques se pretende realizar un módulo de comunicación entre sensores inteligentes mediante una interfaz inalámbrica o alámbrica según sea la necesidad, con la finalidad de analizar, almacenar, comparar, procesar y desplegar información en la PC.

- Sensor colaborativo: Conformado por una red de sensores inteligentes, la cual es importante para que colaboren entre sí y exista una fusión de datos, así como un post-procesamiento que entrega el diagnóstico.

- Post-procesamiento: Es el módulo que incluirá un desarrollo inteligente o matemático para conocer el estado de la máquina eléctrica.

Pruebas y resultados: Finalmente en esta etapa se desarrollarán pruebas en máquinas eléctricas de los algoritmos implementados para diferentes tipos de procesos durante su ciclo de trabajo. Además se comparará con los resultados obtenidos por otros trabajos y/o instrumentos. Así como probar diferentes combinaciones de procesamientos y metodologías de post-procesamiento para tener un diagnóstico en línea de la máquina a monitorear.

2. REVISIÓN DE LA LITERATURA

Como se mostró en el capítulo anterior, en éste trabajo se desarrollan sensores colaborativos utilizando a partir de sensores inteligentes con diferentes sensores primarios y metodologías para lograr un procesamiento y diagnóstico inteligente. Éste se puede lograr con procesamientos basados en técnicas de procesamiento de señales y post-procesamiento en este trabajo en particular: redes neuronales, las cuales permiten detectar y clasificar fallas simples, múltiples y combinadas así como algunos de ellos evaluarlos con la ayuda de los estándares y normativas internacionales. En este capítulo se presenta las herramientas teóricas que respaldan esta investigación. Como primer punto se presenta la una introducción a los sensores inteligentes y colaborativos. Cómo siguiente punto, las técnicas de procesamiento más utilizadas en el análisis de fallas en máquinas eléctricas. Posteriormente, se muestran las técnicas de clasificación que los conforman sistemas inteligentes basados en redes neuronales, describiendo básicamente su desarrollo e implementación. Finalmente se muestra una sección que introduce a la lógica programable como fundamento de la tecnología de implementación de estas metodologías.

2.1 SENSORES INTELIGENTES Y COLABORATIVOS

2.1.1 Sensores inteligentes

En 1997 según el estándar IEEE 1451.2 un transductor inteligente es aquél que proporciona más funciones de las necesarias para generar una correcta representación de la variable monitorizada, dichas funcionalidades típicamente están orientadas a facilitar la integración del transductor con las aplicaciones del entorno de red. La definición que se aporta para el término sensor inteligente es: "La versión en sensor de un transductor inteligente". Se desprende pues que un sensor inteligente añade valor a los datos para dar soporte a la toma de decisiones y al procesamiento distribuido. Los ambientes inteligentes representan el nuevo paso en la evolución en la automatización de los sistemas industriales,

domésticos, de transporte y de la construcción. Al igual que un organismo sensitivo, un entorno inteligente confía en los datos sensoriales obtenidos del mundo real. Los datos sensoriales provienen de múltiples sensores, de múltiples propósitos distribuidos por múltiples localizaciones. Los ambientes inteligentes necesitan tanto la información del entorno que les rodea como la información de su propio funcionamiento. En la Figura 2.1 se puede observar la estructura básica de un sensor inteligente.

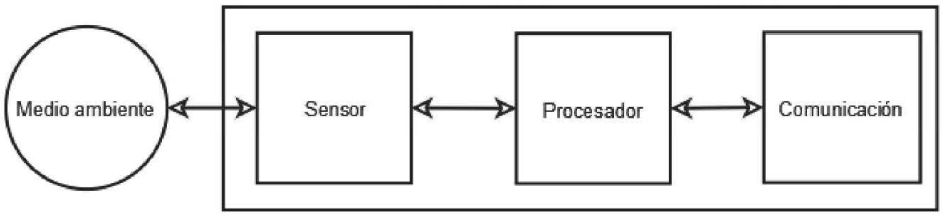

Figura 2.1: Estructura básica de un sensor inteligente.

Un sensor inteligente combina la función de detección y funciones de procesamiento de la señal y comunicación. Dado que estas funciones adicionales suele realizarlas un microprocesador, cualquier combinación de sensor y microprocesador es denominada a veces sensor inteligente. Un sensor inteligente es inevitablemente más caro que un sensor convencional. Pero si además del costo de compra se consideran el mantenimiento, fiabilidad, etc., el costo total de un sensor convencional puede ser mucho mayor. El nivel de complejidad de un sensor inteligente puede ser muy variado. Mekid (2006) menciona que además de la detección o traducción puede incluir: acondicionamiento de señal, correcciones de cero, ganancia y linealidad, compensación ambiental, escala de conversión de unidades, comunicación digital, autodiagnóstico, decisión e incluso activación sobre el sistema donde se conecta. De esta manera los sensores inteligentes incluyen, además del sensor primario, cuando menos algún algoritmo de control, memoria y capacidad de comunicación digital.

Una de las funciones que debe realizar la interfaz como un sensor es compensar interferencias y perturbaciones que afectan a su salida. Una forma de

hacerlo es mediante un procesador que almacene en memoria el valor de una serie de parámetros de referencia que permitan corregir el valor de salida del sensor. Rivera (2008), argumenta que este procesador puede ser un microcontrolador, microprocesador, FPGA, Procesador Digital de Señales (DSP, Digital Signal Processor), etc. en los cuales se pueden implementar algoritmos para así obtener otro tipo de información de la señal sensada.

2.1.2 Sensores colaborativos

Los sensores colaborativos son una red de dispositivos distribuidos espacialmente, que utilizan sensores inteligentes para controlar diversas condiciones en distintos puntos, entre ellas temperatura, sonido, vibración, presión, etc. Los dispositivos son unidades autónomas que constan de un procesador, una fuente de energía y un sensor. En su forma más simple, los sensores colaborativos pueden basarse en una estación base en la que se realiza la recogida de los datos que se han sensado en los otros dispositivos de una manera sincronizada y estructurada. La funcionalidad de la red, es decir, las rutas y protocolos de comunicación se implementan en software y se ejecuta generalmente en microcontroladores de una gama baja.

El objetivo es hacer posible que se puedan fabricar sensores inteligentes y conectarlos a las redes de forma sencilla. Entre los objetivos de los sensores colaborativos se encuentra acercar el conocimiento al punto de medida, hacer viable en términos de costos la integración y mantenimiento de los sistemas distribuidos de sensores, crear un punto de encuentro entre los sensores, monitorización, computación y la comunicación con el fin de alcanzar un objetivo común, e interconectar numerosos sensores de diferente naturaleza, así como también llevar a cabo una arquitectura para conjuntar los diferentes tipos de procesamientos que están implementados en los sensores inteligentes. Algunos trabajos que integran sensores inteligentes en sus metodologías obtienen información la cual es procesada y es enviada a la PC para dar un diagnóstico de la máquina eléctrica fuera de línea, la propuesta de este trabajo, es algo novedoso

ya que es una gran necesidad, el de tomar los datos de los sensores inteligentes y fusionarlos para dar un diagnóstico de la máquina eléctrica en línea con un bloque de post-procesamiento. A continuación en la Tabla 2.1 se muestran las diferencias entre la funcionalidad de sensores colaborativos contra los sensores inteligentes.

Tabla 2.1. Clasificación de sensores inteligentes con base a su funcionalidad.

Sensores Colaborativos	Sensores Inteligentes
Procesamiento Comunicación Validación Fusión de datos	Procesamiento Comunicación

2.2 TÉCNICAS DE ANÁLISIS PARA FALLAS EN MÁQUINAS ELÉCTRICAS

Para el análisis de las señales de voltaje y corriente en máquinas eléctricas es necesario conocer primeramente las componentes que integran las señales. Para ello existen diversas herramientas que permiten transformar del dominio del tiempo al dominio de la frecuencia. Así mismo, esta transformación de espacios puede ser llevada a cabo dominios simultáneos entre el tiempo y frecuencia, con lo que se obtiene información de las componentes frecuenciales de la señal en el momento en que éstas se presentan. Otro tipo de herramientas son las estadísticas así como también la transformación de espacios de tres dimensiones a otros de dos dimensiones en cuadratura. A continuación se muestran las principales técnicas de análisis en fallas de máquinas eléctricas.

2.2.1 Análisis espectral

2.2.1.1 Transformada rápida de Fourier

La forma más común para conocer las componentes armónicas en una señal es mediante el uso de la transformada de Fourier. La transformada discreta de Fourier (DFT, *Discrete Fourier Transform*) descrita en la ecuación (2.1) es optimizada aprovechando su periodicidad, lo que se conoce como la Transformada Rápida de Fourier (FFT, *Fast Fourier Transform*). La FFT debe su éxito al hecho que el algoritmo reduce el número de multiplicaciones y adiciones requeridas en el cálculo respecto a la DFT.

$$X[k] = \sum_{n=0}^{N-1} x[n] \cdot e^{-j\frac{2\pi}{N}nk}, k = 0,1,..., N-1 \qquad (2.1)$$

Dicha transformada proporciona el espectro de una señal en frecuencia, desde 0 Hz hasta la frecuencia de muestreo, la cual es dividida entre el número de muestras adquiridas con lo que se obtiene la resolución Δf del algoritmo, esto es

$$\Delta f = \frac{fs}{N} \qquad (2.2)$$

Donde

fs = frecuencia de muestreo

N = Número de muestras adquiridas

El espectro resultante es solo válido en la mitad de la frecuencia de muestreo de forma que se cumple con el teorema de Nyquist.

2.2.1.2 Short-Time Fourier Transform (STFT)

Existe una posibilidad de analizar una señal en tiempo-frecuencia con transformadas de Fourier consecutivas y de corta duración, a esto se le llama Transformada Corta de Fourier (STFT, Short-Time Fourier Transform). El análisis

de la STFT consiste en tomar pequeñas secciones en intervalos de tiempo de una señal realizando un enventanado al cual se calcula la FFT en esa sección y así poder conocer los componentes frecuenciales de esa sección. Así analizando cada transformada de Fourier se observa el cambio de dichas componentes frecuenciales en el tiempo (Figura 2.2).

La elección del tamaño de la ventana es crítica a la hora de obtener buena resolución. Si lo que se desea es obtener una resolución grande en el dominio temporal, se elige una ventana de poca longitud, en cambio, la distribución espectral estará muy dispersa y no se podrá conocer con exactitud sus componentes. Por el contrario, la elección de una ventana grande mostrará con más precisión las componentes de frecuencia, pero se pierde la idea del momento en que se produjeron cada una de ellas.

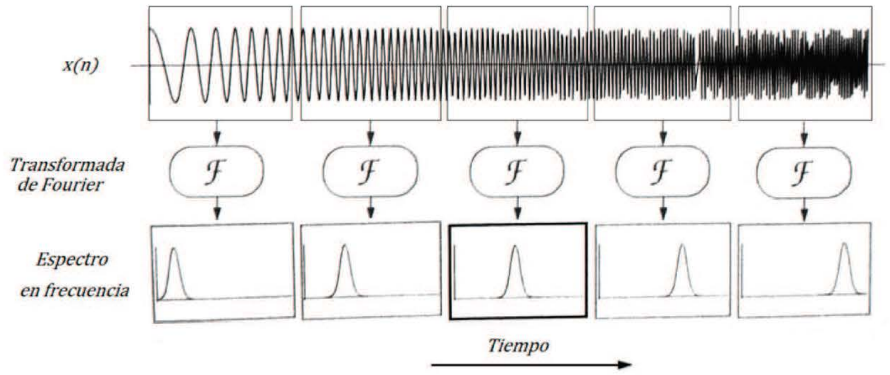

Figura 2.2.- Interpretación de la STFT.

2.2.1.3 Wavelets

Entre las herramientas tradicionales de análisis de sistemas eléctricos de potencia se encuentran algoritmos basados en la transformada de Fourier, filtros de Kalman, etc. Estas herramientas son apropiadas para el monitoreo en estado estacionario, pero para perturbaciones no estacionarias como los sags, swells, transitorios oscilatorios o impulsivos, o fluctuaciones de tensión se tienen limitaciones. Si ocurre un transitorio, las formas de onda asociadas no son

periódicas conteniendo oscilaciones de alta y baja frecuencia superpuestas a la frecuencia del sistema eléctrico. En tal situación, debido a que la transformada de Fourier realiza un promedio de la contribución de las frecuencias se pierde la localización de la perturbación en el tiempo.

El análisis mediante Wavelets supera esta limitación, realizando un procesado de la señal que proporciona información en tiempo y en frecuencia. Por ello, la transformada Wavelet es una potente ayuda para el análisis, estudio e interpretación de los distintos fenómenos transitorios que se pueden presentar en un sistema eléctrico de potencia. De una forma sencilla puede decirse que las condiciones que una onda debe cumplir para ser una Wavelet son:

- Debe ser oscilatoria.
- Debe decaer rápidamente a cero (es distinta de cero en un corto período de la función).
- Debe tener un valor medio nulo.

Un ejemplo de Wavelet se muestra en la Figura 2.3.

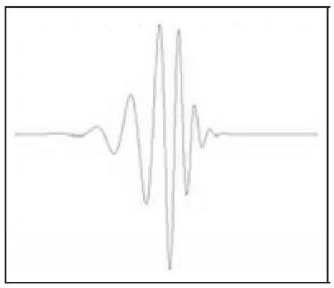

Figura 2.3: Wavelet Daubechies.

A través de la transformada Wavelet, la señal original es representada como la suma de Wavelets en diferentes localizaciones (posiciones) y escalas (duración). Los coeficientes de la transformada son los pesos de cada Wavelet para representar la señal en esas localizaciones y escalas. La transformada Wavelet discreta (DWT) es suficiente para descomponer y reconstruir la mayoría de los problemas de calidad de la energía. Brinda suficiente información y su uso

significa una importante reducción en tiempos de operación computacional. El modo de empleo de la transformada DWT es realizado a través de un árbol de descomposiciones por nivel frecuencial, el cual consiste en la separación sucesiva de componentes de baja y alta frecuencia conocidos como aproximación y detalle respectivamente. En donde cada nivel de descomposición parte de un nodo '0', '1', '2' y '3' que representa la banda en frecuencia. Este árbol se ilustra en la figura 2.4.

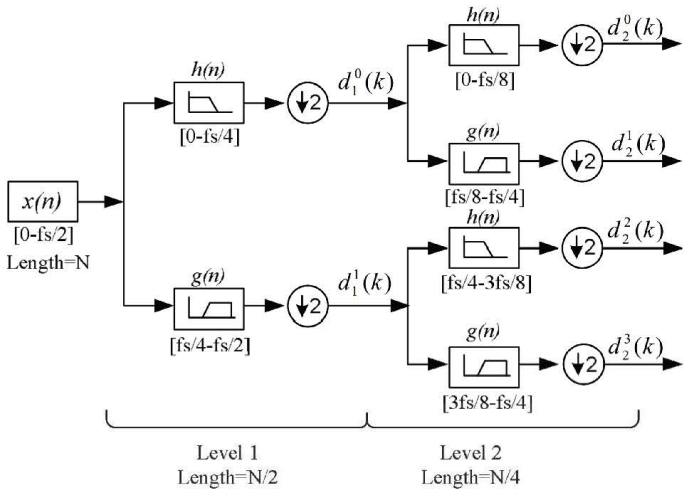

Figura 2.4: Árbol de descomposición Wavelet

Los coeficientes para cada nivel de descomposición *j* y nodo *k* en el árbol de descomposición puede ser computado mediante las siguientes ecuaciones recursivas 2.4 y 2.5:

$$d_j^{2i}(k) = \sum_n h(n) d_{j-1}^i(2k-n) \tag{2.4}$$

$$d_j^{2i+1}(k) = \sum_n g(n) d_{j-1}^i(2k-n) \tag{2.5}$$

donde *i* es el número del nodo o índice en la banda de frecuencia.

2.2.1.4 Métodos paramétricos y no paramétricos

Un problema muy común y con grandes aplicaciones prácticas en procesamiento de señales es estimar la densidad espectral de potencia de una señal aleatoria estacionaria. Se dice "estimar" puesto que, como la señal es un proceso estocástico (estacionario) dada la naturaleza estocástica del mismo no es posible determinar con absoluta precisión su densidad espectral de potencia a no ser que se disponga de un registro infinito de la señal.

Las técnicas de estimación se dividen en dos grupos:

No Paramétricas. Están basadas siempre de una u otra forma en el cálculo del periodograma. Algunos ejemplos de técnicas no paramétrica son calcular la transformada de Fourier de una señal para estimar su espectro, suavizado utilizando una ventana espectral, método de Welch, etc.

Paramétricas. Consisten en suponer un determinado modelo para el proceso estocástico (método de Burg, método de la covarianza modificado, MUSIC, Yule-walker, modelos AR, MA, ARMA, la transformada Chirp Z, etc.) y en la estimación de los parámetros de estos modelos mediante técnicas de predicción lineal (filtrado lineal óptimo) u otros métodos.

2.2.2 Análisis estadístico

2.2.2.1 Entropía

Shannon en 1948 define la entropía como medida de cuanta información es producida por una fuente de información discreta. Dado que la entropía es sensible y objetiva puede ser considerada como una herramienta para detectar algunas características específicas en los datos, que proporcionan información relevante. Esto con el fin de minimizar tiempo de procesamiento, optimizar

recursos y mejorar el desempeño al momento de analizar las fuentes de información.

Si se considera un evento aleatorio x con n posibles resultados x_1, x_2, x_3,..., x_n y cada x_i con una probabilidad de aparición $p(x_i)$, entonces la Entropía $H(X)$ de un evento aleatorio x está definida por la Ecuación 2.6.

$$H(X) = -\sum_{i=1}^{n} p(x_i)\log_2[p(x_i)] \quad para \ 1 < i \leq n \tag{2.6}$$

Si el número total de datos en un evento aleatorio x es N, entonces la probabilidad $p(x_i)$ está dada por la Ecuación 2.7.

$$p(x_i) = \frac{r_i}{N} \tag{2.7}$$

Donde r_i representa la razón de incidencia de cada posible dato xi. El número total de datos en el evento está dado por la Ecuación 2.8. Entonces la Ecuación 3 puede ser reescrita como en la Ecuación 2.9 lo que da una expresión matemática para el cálculo de la entropía mucho más fácil de implementar en hardware, Cabal (2010).

$$N = \sum_{i=1}^{n} r_i \quad para \ 1 < i \leq n \tag{2.8}$$

$$H(X) = \log_2(N) - (\frac{1}{N})\sum_{i=1}^{n} r_i \log_2(r_i) \quad para \ 1 < i \leq n \tag{2.9}$$

2.2.3 Transformación de espacios de tres dimensiones a dos dimensiones en cuadratura

2.2.3.1 Transformada Park

La transformada de Park permite obtener valores trifásicos de un sistema con eje de referencia fijo (A,B,C) de una magnitud x expresada en un sistema

con eje de referencia ortonormal giratorio (d,q) y conociendo el ángulo de desfase entre los sistemas (ecuaciones 2.10 y 2.11). La transformada inversa permite hacer lo contrario, si se tiene un sistema ortonormal con eje de referencia fijo y el desfase se puede obtener el sistema con eje de referencia giratorio.

$$i_D = \sqrt{\frac{2}{3}} i_A - \sqrt{\frac{1}{6}} i_B - \sqrt{\frac{1}{6}} i_C \tag{2.10}$$

$$i_Q = \sqrt{\frac{1}{6}} i_B - \sqrt{\frac{1}{6}} i_C \tag{2.11}$$

2.3 SISTEMAS INTELIGENTES

Son definidos como aquellos sistemas (elementos, objetos, instrumentos, etc.) que emulen un comportamiento similar a la inteligencia humana. Entre estos comportamientos se puede citar: reconocimiento de patrones, toma de decisiones, aprendizaje, razonamiento, etc. Dentro de los algoritmos inteligentes se puede mencionar que las redes neuronales y los sistemas difusos son los más utilizados para la clasificación y reconocimiento de patrones.

2.3.1 Redes neuronales

Uno de los principales objetivos de los científicos de hoy en día es imaginar, diseñar y realizar máquinas capaces de realizar procesos con inteligencia, los cuales son llamados autómatas que básicamente son máquinas que realizan alguna función típica de los seres humanos.

A pesar de disponer de herramientas y de lenguajes de programación diseñados para el desarrollo de máquinas inteligentes, existe un problema que limita los resultados que se pueden obtener: estas máquinas se implementan sobre ordenadores basados en la filosofía de funcionamiento expuesta por Von Neumann, y se apoyan en una descripción secuencial del proceso de tratamiento

de la información de elevado nivel y desarrollo, por espectacular y complejo que haya llegado a ser, no deja de seguir la línea antes descrita: una máquina puramente mecánica que es capaz de realizar tareas mecánicas de forma rápida como, cálculo, ordenación o control, pero incapaz de obtener resultados aceptables cuando se trata de tareas sencillas como reconocimiento de patrones, formas, habla, etc., Martín *et al.* (2010). Alan Turing (1936), fue el primero en estudiar el cerebro como una forma de ver el mundo de la computación, pero los primeros teóricos que concibieron los fundamentos de la computación neuronal fueron Warren McCulloch un neurofisiólogo y Walter Pitts un matemático, quienes en 1943, lanzaron una teoría acerca de la forma de trabajar de las neuronas. Modelaron una red neuronal simple mediante circuitos eléctricos. En 1957, Frank Rosenblatt comenzó el desarrollo del Perceptrón, la más antigua red neuronal, se usa hoy en día en varias formas, una de ellas es el reconocimiento de patrones. Este modelo era capaz de generalizar: después de haber aprendido una serie de patrones tenía la capacidad de reconocer otros similares, aunque no se le hubieran presentado anteriormente. Sin embargo, tenía una serie de limitaciones, quizás la más conocida era la incapacidad de resolver el problema de la OR-exclusiva y en general, no era capaz de clasificar las clases no separables linealmente. En 1969 surgieron críticas de parte de Marvin Minsky y Seymour Paper, con su libro publicado Perceptrons, en el cual hacían un análisis matemático describiendo las limitaciones del perceptrón para resolver problemas interesantes, esto frenó el crecimiento que estaba experimentando la investigación de ésta área de la inteligencia artificial, hasta 1982. En 1982, John Hopfield presento su trabajo sobre redes neuronales en la academia nacional de las ciencias. En el trabajo, describe con claridad y rigor matemático una red a la que ha dado su nombre, que es una variación del asociador lineal, además mostró cómo tales redes pueden trabajar y de lo que son capaces de hacer.

2.3.1.1 Redes neuronales artificiales

Las redes neuronales, como su nombre lo indica, pretenden imitar en una pequeñísima escala la forma de funcionamiento del sistema nervioso central,

específicamente las neuronas que forman el cerebro humano, las cuales son elementos individuales de procesamiento, estas neuronas pueden tener contacto con el ambiente por medio de los sentidos, pueden hacer conexiones con ellas mismas, y también pueden actuar por medio de glándulas o impulsos nerviosos hacia el exterior. La información que viaja entre las neuronas, es modificada por las sinapsis, estas pueden ser excitadoras e inhibidoras, estas sinapsis dan el comportamiento de la red neuronal. Las redes neuronales artificiales son el resultado de la investigación del procesamiento en paralelo, aplicadas en sus inicios al reconocimiento de patrones alcanzado en la actualidad una infinidad de aplicaciones.

- Elementos de una neurona artificial.

Las redes neuronales son modelos basados en el cerebro humano, por lo tanto una adecuada elección de los elementos que componen este modelo ayudaran a obtener una mejor aproximación del modelo original, McCulloch y Pitts fueron los primeros en proponer un modelo de una neurona artificial, en la figura 2.5 se muestra dicho modelo, la ecuación 2.12 muestra la salida de la neurona.

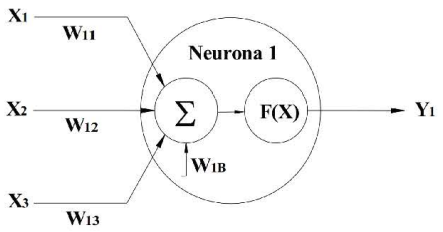

Figura 2.5: Neurona artificial.

$$y_1 = F(x_1 w_{11} + x_2 w_{12} + x_3 w_{13} + w_{1B}) \tag{2.12}$$

Donde x_1, x_2 y x_3 son las entradas, w_{11}, w_{12}, w_{13} y w_{1B} son los pesos o conexiones entre neuronas y $F(X)$ es una función de activación, lo anterior se describe a continuación.

La ecuación 2.12 para un número de entradas *n* puede ser descrita como:

$$y_1 = F\left(\sum_{i=1}^{n} x_i w_{1i} + w_{1B}\right) \tag{2.13}$$

Esencialmente una red neuronal está constituida por 3 elementos:

- Unidades de proceso.
- Conexión entre neuronas.
- Tipos de función de activación

✓ Unidad de proceso.

La unidad de proceso, consiste en recibir las entradas del ambiente o de células vecinas, calcular su valor de salida y enviarlas a neuronas vecinas o reenviarlas al ambiente.

En los modelos propuestos de las redes existen tres tipos de unidades de proceso: capa de entrada, capas ocultas y capa de salida. La capa de entrada recibe las señales del ambiente de algunos sensores. La capa de salida es la que envía las señales al ambiente para realizar alguna tarea. Las capas ocultas o intermedias son las que se encuentran en el interior de la red, su conexión es solo entre neuronas, no tienen contacto con el exterior.

✓ Conexión entre neuronas.

La conexión que une a las neuronas de una red neuronal tiene asociado un peso en el cual está almacenado el aprendizaje.

Una neurona recibe un conjunto de señales de sus neuronas vecinas las cuales le dan información del estado en que se encuentran las neuronas con las que se está conectada. Cada conexión tiene un peso el cual puede ser positivo o negativo. Así como en el cerebro existen conexiones excitadoras y conexiones inhibidoras, los pesos positivos corresponden a una excitación y los pesos negativos a una inhibición, por lo tanto, un peso igual a cero significa que no hay conexión entre ellas.
La regla de propagación dice que el procedimiento a seguir para combinar los valores de entrada con los pesos de la conexión: se considera que el efecto de cada señal es aditivo, de tal forma que la entrada total o neta recibe la neurona es la suma del producto de cada señal individual por el peso que conecta ambas neuronas.

✓ Tipos de función de activación.

Así como es necesario una regla que combine las entradas con los pesos de las conexiones, es necesario también que exista una regla para evaluar la entrada global de la neurona para determinar el estado en el que se encontrará la neurona para determinar un nuevo estado de activación.

Cualquier función definida en un intervalo de posibles valores de entradas, un incremento monotonico, y que tengan un límite superior y un límite inferior, podrán realizar la función de activación de forma satisfactoria. Al principio se empezaron a utilizar funciones sencillas de manejar como la función escalón en la cual solamente se utiliza cuando la salida de la red es binaria (dos posibles valores). Las funciones sigmoidales son las más

apropiadas cuando se procesa información analógica la cual toma infinidad de valores dentro de un rango dado.

- Función escalón: Una de las formas más fáciles de definir una función de activación de una neurona es considerar que es binaria. En la función escalón es para las neuronas binarias para la cual la suma de las entradas puede ser mayor o menor a un umbral, si es mayor al umbral toma el valor de 1 y si es menor al umbral toma el valor de 0 o en otros casos -1. Este tipo de redes son sencillas para poder ser implementadas en hardware pero sus capacidades se reducen demasiado debido a que sus resultados solo pueden ser binarios.

- Función lineal: en esta función, si la suma de sus entradas es menor a un límite inferior, toma el valor de 0 o -1. Cuando la suma de sus entradas es mayor a un límite superior, toma el valor de 1. Si la suma de las entradas está comprendida entre los límites inferior y superior, entonces la función se define como una función lineal.

- Funciones Sigmoidales: Con la función sigmoidal o tangente hiperbólica, para la mayoría de los estímulos de entrada, el valor entregado por la función son cercanos a los valores asintóticos. Con esto la mayoría de los valores quedan cercanos a la parte alta o baja de la función sigmoidal. Por lo que esta función es tan importante, se debe a que su derivada es siempre positiva, es decir que siempre existen valores continuos, a diferencia del escalón, que en el valor del umbral, existe una discontinuidad. Esta derivada positiva en la función sigmoidal, hace que se puedan utilizar entrenamientos que utilizan derivadas los cuales no se podrían utilizar en la función escalón. La ecuación 2.14, describe el comportamiento de la función LogSig y en la figura 2.6 se puede observar esta función. La ecuación 2.15 describe el comportamiento de la función tangente hiperbólica y en la figura 2.7 se observa la función.

$$f(x) = \frac{1}{1 + e^{-x}} \tag{2.14}$$

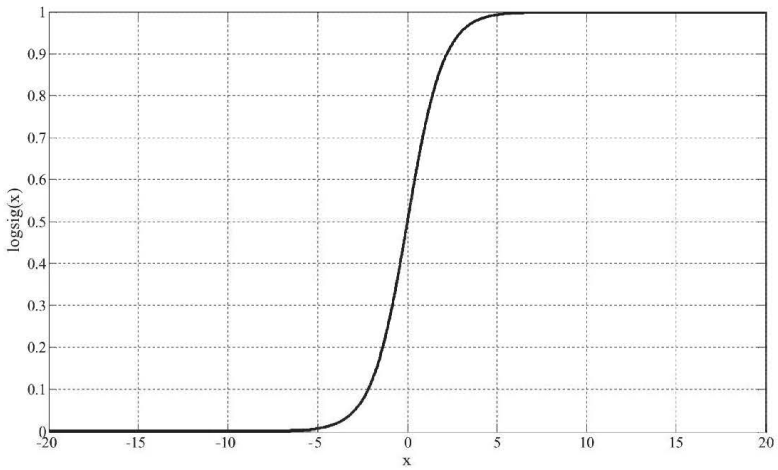

Figura 2.6: Función LogSig.

$$f(x) = \frac{e^{x} - e^{-x}}{e^{x} + e^{-x}} \tag{2.15}$$

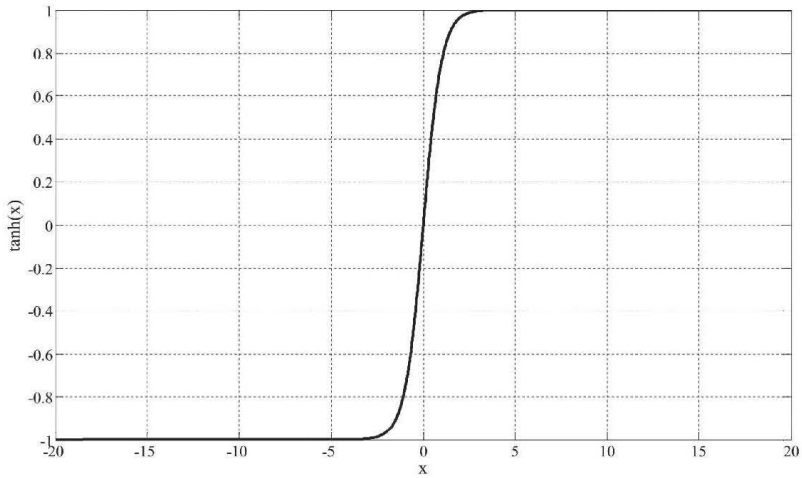

Figura 2.7: Función Tanh.

2.3.1.2 Topología

La topología de las redes neuronales es la forma en la que están estructuradas o en otros términos su arquitectura, esta consiste en la organización y disposición de las neuronas en forma de capas o agrupaciones que están alejadas de la entrada y la salida. Cuando se realiza una clasificación de este tipo de redes se hace la subdivisión entre las capas o niveles de neuronas. De aquí surgen la clasificación de las redes monocapa y multicapa.

- Redes monocapa.

La redes monocapa, como su nombre lo indica, solo poseen una capa o nivel de neuronas agrupadas entre la entrada y la salida (ver figura 2.8), la ecuación 2.16 muestra el valor de sus salidas, mientras que la ecuación 2.17 muestra el valor de salida para una red monocapa de *n* neuronas y *m* entradas, donde *m* puede ser igual a *n*.

En las redes monocapa, se establecen conexiones laterales entre las neuronas, esto significa que trabajan sin capa escondida utilizando su única capa para lograr su aprendizaje. También existen las conexiones auto-recurrentes que es la salida de una neurona conectada a su propia entrada. Una topología similar es la *crossbar*, la cual consiste en una matriz de terminales, ya sea de entrada o de salida, o de barras que se cruzan en puntos determinados a los que se les asocia un peso. Esta representación suele utilizarse como etapa de transición, puesto que es relativamente fácil desarrollar en hardware una estructura como la anterior. Las redes monocapa se utilizan normalmente en tareas relacionadas con lo que se conoce como auto asociación.

- Redes multicapa.

En este tipo de redes las capas exceden más de dos niveles (ver figura 2.9), la salida de este tipo de red está dada por el resultado secuencial de las capas anteriores tal y como muestra la ecuación 2.18, el resultado de una capa

siguiente no puede ser dado si antes no se ha calculado el resultado de la capa previa.

Una forma para distinguir la capa a la que pertenece una neurona cosiste en fijar la atención en el origen de las señales que recibe a la entrada y el destino de la señal de salida. Normalmente todas las neuronas reciben señales de entrada de la capa anterior y envían señales de salida a la capa superior. A estas conexiones se les llama conexiones hacia adelante o *feedforward*. Otra característica de las redes multicapa es que, además de enviar señales hacia adelante, también pueden enviar señales de salida a las entradas de las neuronas de la capa anterior. Estas características permiten distinguir entre las redes con conexiones hacia adelante o redes *feedforward*, y las redes con conexiones tanto para adelante como hacia atrás o redes *feedforward/feedback*.

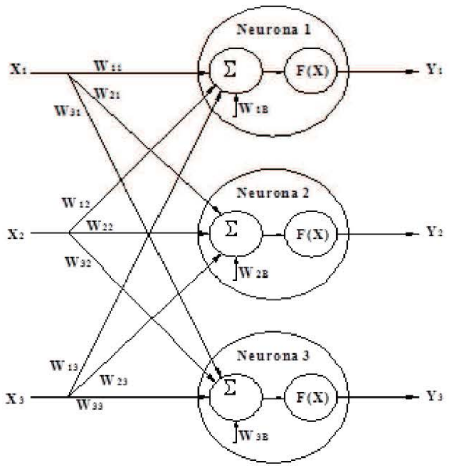

Figura 2.8: Red monocapa.

$$\begin{bmatrix} y_1 \\ y_2 \\ y_3 \end{bmatrix} = f\begin{pmatrix} x_1w_{11} + x_2w_{12} + x_3w_{13} + w_{1B} \\ x_1w_{21} + x_2w_{22} + x_3w_{23} + w_{2B} \\ x_1w_{31} + x_2w_{32} + x_3w_{33} + w_{3B} \end{pmatrix} \tag{2.14}$$

$$\begin{bmatrix} y_1 \\ y_2 \\ y_3 \\ \vdots \\ y_n \end{bmatrix} = f \begin{pmatrix} \sum_{i=1}^{m} x_i w_{1i} + w_{1B} \\ \sum_{i=1}^{m} x_i w_{2i} + w_{2B} \\ \sum_{i=1}^{m} x_i w_{3i} + w_{3B} \\ \vdots \\ \sum_{i=1}^{m} x_i w_{ni} + w_{nB} \end{pmatrix} \tag{2.15}$$

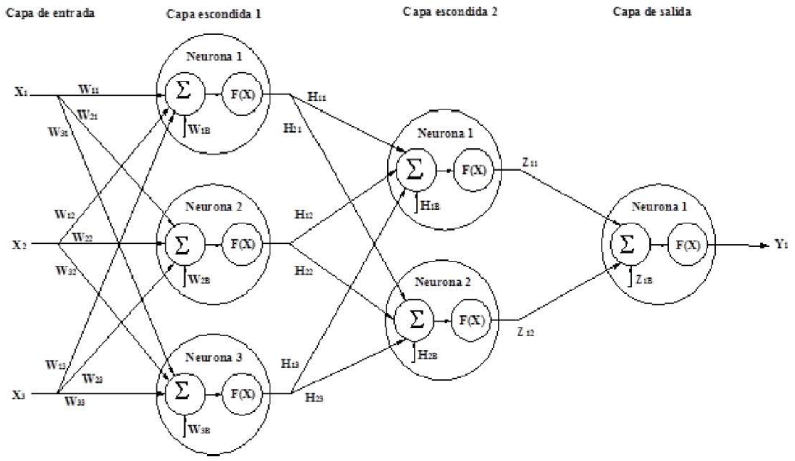

Figura 2.9: Red multicapa.

$$y_1 = f(S_1 z_{11} + S_2 z_{12} + z_{1B}) \tag{2.18}$$

Donde S_1 y S_2 son respectivamente las salidas de la capa escondida 2 y están definidas por:

$$\begin{bmatrix} S_1 \\ S_2 \end{bmatrix} = f \begin{pmatrix} P_1 H_{11} + P_2 H_{12} + P_3 H_{13} + H_{1B} \\ P_1 H_{21} + P_2 H_{22} + P_3 H_{23} + H_{2B} \end{pmatrix} \tag{2.19}$$

Donde P_1, P_2 y P_3 son respectivamente las salidas de la capa escondida 1 y están definidas por:

$$\begin{bmatrix} P_1 \\ P_2 \\ P_3 \end{bmatrix} = f\begin{pmatrix} x_1w_{11} + x_2w_{12} + x_3w_{13} + w_{1B} \\ x_1w_{21} + x_2w_{22} + x_3w_{23} + w_{2B} \\ x_1w_{31} + x_2w_{32} + x_3w_{33} + w_{3B} \end{pmatrix} \tag{2.20}$$

2.3.1.3 Tipos de aprendizaje

El aprendizaje o entrenamiento de las redes neuronales es el proceso mediante el cual se modifica la respuesta de una información entrante por medio de la modificación de los pesos. Estos cambios no son más que, la destrucción, modificación y creación de las conexiones entre las neuronas de las redes neuronales. En los sistemas biológicos este proceso es constante. En los modelos artificiales, la creación de una nueva conexión implica que el peso tenga un valor diferente de cero y la destrucción de una conexión sucede cuando un peso pasa a ser cero. Se debe tomar en cuenta que, cuando se desea que la red aprenda una nueva información, se debe conocer cómo se tienen que modificar el valor asignado a las conexiones cuando estas ya han aprendido. Estos criterios determinan las reglas de aprendizaje de la red. Generalmente solo se utilizan dos: las que responden al aprendizaje supervisado y las que pertenecen al aprendizaje no supervisado. La diferencia existente entre estos dos tipos de entrenamiento es, la presencia o ausencia de un agente externo o supervisor que controle el proceso de aprendizaje de la red neuronal.

- Aprendizaje supervisado.

El aprendizaje supervisado se caracteriza porque el proceso de aprendizaje se realiza mediante un entrenamiento controlado por un agente externo que determina la respuesta que debería generar la red a partir de una entrada determinada. El supervisor comprueba la salida de la red y en caso de que esta no coincida con la deseada, se procederá a modificar los pesos de las conexiones, con el fin de conseguir que la salida obtenida se aproxime a la deseada, en la figura 2.10 se muestra el entrenamiento supervisado.

Este tipo de aprendizaje se suele considerar, a su vez, tres formas de llevarlo a cabo que dan lugar a los siguientes tipos de aprendizaje supervisado.

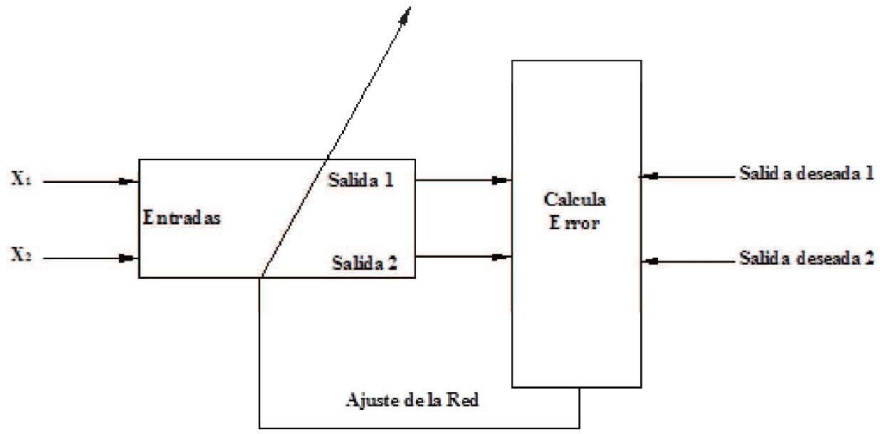

Figura 2.10: Aprendizaje supervisado.

- *Aprendizaje por corrección de error:* consiste en ajustar los pesos de las conexiones de la red en función de la diferencia entre los valores deseados y los obtenidos en la red, es decir, en función del error cometido en la salida.

- *Aprendizaje por refuerzo:* este aprendizaje supervisado, es más lento que el anterior, que se basa en la idea de no disponer de un ejemplo completo del comportamiento deseado, es decir, de no indicar en el entrenamiento exactamente la salida que se desea que proporcione la red ante una determinada entrada.

- *Aprendizaje estocástico:* este tipo consiste básicamente en realizar cambios aleatorios en los valores de los pesos de las conexiones de la red y evaluar su efecto a partir del objeto deseado y de las distribuciones de probabilidad. Si el error es menor del cambio, es decir se acerca la salida al valor

deseado, se acepta el cambio, si el error no es menor, se aceptaría el cambio en función de una determinada y preestablecida distribución de probabilidad.

- Aprendizaje no supervisado.

El aprendizaje no supervisado se caracteriza, a diferencia del supervisado en el cual el proceso de aprendizaje se realiza mediante un entrenamiento controlado por un agente externo, este tipo de aprendizaje no cuenta con un agente externo que enseñe a la red las salidas deseadas con ciertas entradas. Existen dos tipos de entrenamiento no supervisado, en el primer caso, normalmente se pretende medir la familiaridad o extraer características de los datos de entrada, mientras que el segundo suele orientarse hacia la clusterización o clasificación de dicho datos en la figura 2.11.

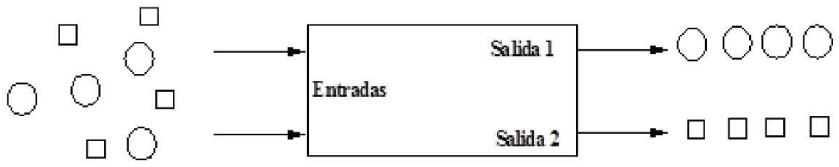

Figura 2.11: Aprendizaje no supervisado.

- Aprendizaje Hebbiano: Hebb entiende un conjunto de neuronas fuertemente conexionadas a través de una estructura compleja. La eficiencia podría identificarse con la identidad o magnitud de la conexión, es decir, con el peso. Se puede decir, por tanto, que el aprendizaje consiste básicamente en el ajuste de los pesos de la conexión de acuerdo con la correlación (multiplicación en el caso de los valores binarios +1 y -1) de los valores de activación (salidas) de las dos neuronas conectadas. Si las dos conexiones son activas (positivas) la conexión entre ellas se refuerza, si una es activa y otra pasiva, la conexión entre ellas se debilita.

- Aprendizaje competitivo y cooperativo: este tipo de aprendizaje, suele decirse que las neuronas compiten y cooperan unas con otras con el fin de llegar a cabo una tarea dada. Con este tipo de aprendizajes, se pretende que cuando se presente a la red cierta información en la entrada, solo una de las neuronas de salida de la red, se active, esto quiero decir, que alcance se valor de respuesta máximo. Por tanto, las neuronas compiten por activarse quedando finalmente una, o una por grupo, como neurona vencedora quedando anuladas el resto las cuales son forzadas a sus valores de respuesta mínimo.

2.3.1.4 Desarrollo de una red neuronal

El desarrollo típico de la red neuronal sigue los siguientes pasos:

- Crear un conjunto de datos de entrenamiento.
- Crear un conjunto de datos de validación.
- Crear la red.
- Entrenar la red (usar el conjunto datos de entrenamiento).
- Validar la red para averiguar si aprendió y generalizó (usar el conjunto de datos de validación).
- Usar la red aplicando datos nuevos, posiblemente diferentes a los de entrenamiento y validación.

Para el diseño del conjunto de datos de entrenamiento y validación se siguen los siguientes puntos y conceptos de diseño:

- El conjunto de datos de entrenamiento y de validación debe representar de forma apropiada el experimento.
- No se puede usar el conjunto de validación para el entrenamiento.

- El conjunto de entrenamiento debe contener los distintos tipos de lecciones que represente la totalidad del problema real.
- El conjunto de entrenamiento no debe de ser demasiado grande, ya que se provocaría un sobre entrenamiento.
- Las redes más grandes requieren un conjunto de entrenamiento más grande.
- El conjunto de entrenamiento puede obtenerse de una colección muy grande de datos y un generador de datos aleatorios, para seleccionar solo algunos datos del conjunto original.

Un síntoma de sobre entrenamiento es que la red trabaja muy bien con el conjunto de entrenamiento pero produce malos resultados con el conjunto de validación.

2.4 LÓGICA PROGRAMABLE

Valtierra (2014), menciona que los dispositivos de lógica programable se pueden clasificar en dos tipos: volátiles y no volátiles. Los primeros dependen de la alimentación para conservar la información del programa y los no volátiles no mantienen la información del programa si no se encuentran alimentados.

Los primeros dispositivos lógicos programables fueron las memorias de solo lectura (ROM, *Read Only Memory*) la desventajas de estas es que solo podían programarse una sola vez ya sea por el fabricante o el usuario, posteriormente surgió la ROM borrable y programable (EPROM, *Eraseable Programmable ROM*) y la ROM programable y borrable eléctricamente (EEPROM, *Electrically Eraseable Programmable ROM*), la principal característica de estas fue que el usuario podía borra y volver a programar estos dispositivos. Debido a la necesidad de contar con circuitos integrados en los cuales se pudieran sintetizar funciones combinacionales y funciones secuenciales, surgió el dispositivo lógico programable (PLD, *Programmable Logic Device*) a diferencia de las ROM, estos circuitos están

hechos por muchas macro-celdas que cuentan con flip-flops y lógica adicional que permiten la realización de funciones más complejas, también se puede encontrar el dispositivo lógico programable complejo (CPLD, *Complex Programmable Logic Device*), la característica de este es que podían integran varios PLDs en el mismo circuito. Otro dispositivo que cuenta con mejores características que los anteriores es el arreglo de compuertas programables en campo (FPGA, *Field Programmable Gate Array*) la característica de estos dispositivos es que están construidos por muchas celdas lógicas que tienen una mejor interconexión entre ellas.

La forma de programar este tipo de tecnología es mediante lenguaje de descripción de hardware (HDL, *Hardware Description Language*), donde, entre los más usados se encuentra VHDL, debido principalmente a que es un lenguaje estándar definido por la IEEE, con lo que se logra la portabilidad de los diseños lo que los hace independientes del fabricante de los dispositivos.

3. METODOLOGÍA

En este capítulo se describe la metodología seguida, para la prueba y validación de la hipótesis planteada, así como se describe cada uno de los experimentos e instrumentos utilizados. Primero, se muestra la descripción general de la metodología; segundo, se describen las especificaciones y características de los instrumentos utilizados para la implementación de los sensores inteligentes y colaborativo, así como el banco de prueba para la validación de cada uno de los sensores inteligentes y colaborativo. Finalmente, se describe el uso de las metodologías planteadas para la detección de fallas en máquinas eléctricas.

3.1 DESCRIPCIÓN GENERAL DE LA METODOLOGÍA

La figura 3.1 muestra el diagrama general de la metodología seguida en este trabajo para la realización y alcance de los objetivos planteados en el capítulo 1. A continuación se describe cada una de las etapas que conforman la metodología propuesta.

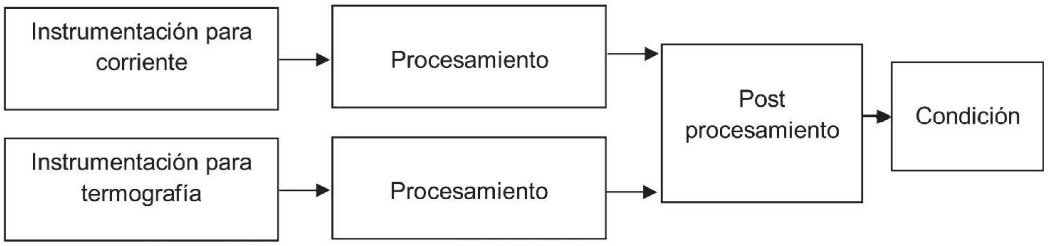

Figura 3.1: Planteamiento general de la metodología.

Instrumentación para corriente: Esta etapa consiste en el acondicionamiento y adquisición de datos de corriente para posteriormente realizar un análisis en su procesamiento, para este caso se proponen dos metodologías las cuales se describen a continuación:

1.- Metodología basada en la transformada Park, la cual convierte de un sistema de corriente trifásico *ABC* a un sistema de corriente de dos dimensiones en cuadratura *DQ*, el cual si es graficado en un plano X-Y se puede obtener una figura de Lissajous y se puede observar de manera intuitiva haciendo una comparativa, cuando se tiene un motor sano (figura 3.2a) se puede observar que tiene una forma redonda muy similar a un circulo perfecto y un motor con fallo (figura 3.2b) se observa un circulo deformado a causa del mismo fallo.

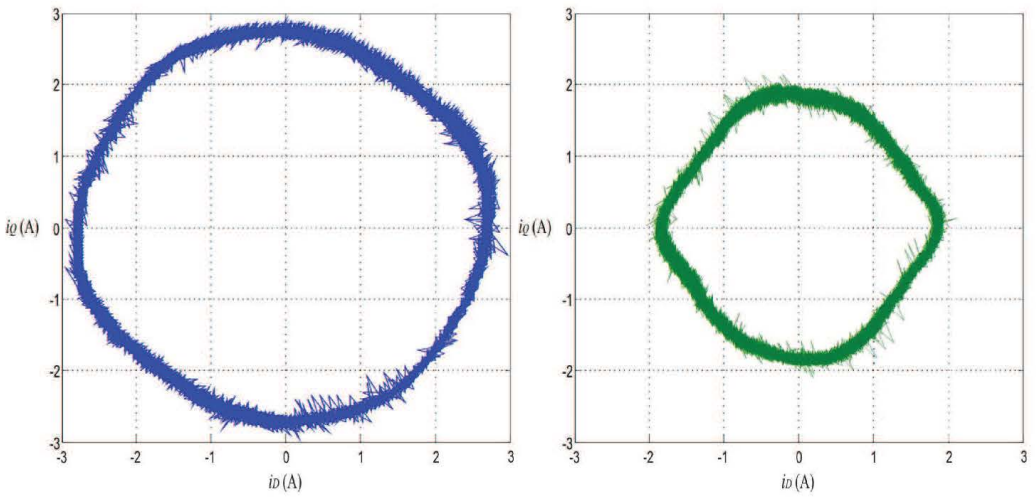

(a) (b)

Figura 3.2: Figuras de Lissajous de un sistema de corriente *DQ* de: (a) motor sano y (b) motor con fallo.

Esta metodología permite una detección automática y en línea para detectar tres tipos de fallas en motores de inducción (barra rota, desalineamiento y desbalance) alimentados por variador de velocidad desde frecuencias bajas como 3 Hz hasta la frecuencia nominal de 60 Hz. Después a través de la ecuación 3.1 aplicada como se muestra en la figura 3.3, se puede obtener un único vector i_{DQ} (figura 3.14), el cual es la resultante de la figura de Lissajous. Una vez obtenido el vector i_{DQ}, se obtiene la media para así obtener un único valor como entrada a una red neuronal artificial (ANN) que será la que arroje a su salida la condición del motor de inducción.

$$i_{DQ} = \sqrt{i_D^2 + i_Q^2} \tag{3.1}$$

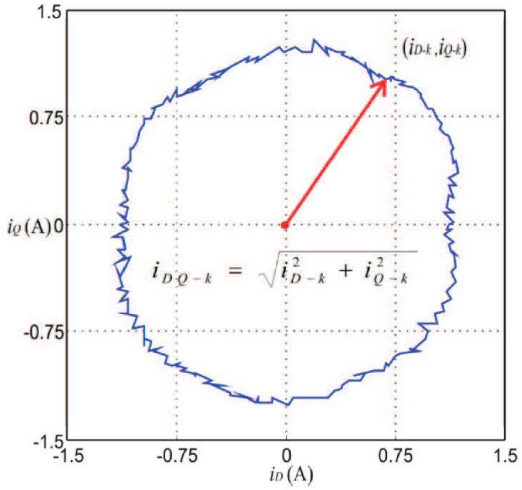

Figura 3.3: Figura de Lissajous y vector i_{DQ} obtenidos de la transformada Park.

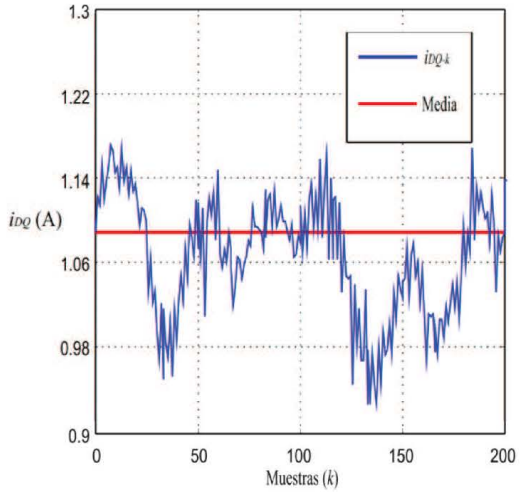

Figura 3.4: Representación de la figura de Lissajous por el vector i_{DQ}.

2.- Metodología basada en la transformada rápida de Fourier, esta metodología comienza con la aplicación de la FFT a la señal de corriente, para posteriormente hacer una selección de bandas de interés para los diferentes tipos de fallo los cuales son barras rotas (ecuación 3.2) y excentricidades cubriendo desalineamiento y desbalance (ecuación 3.3). La Figura 3.5a-b muestra la selección de las bandas en las frecuencias de interés y una comparativa entre un motor sano y uno con fallo.

$$f_{brb} = f(1 \pm 2ks) \tag{3.2}$$

$$f_{ecc} = f\left[1 \pm k\left(\frac{1-s}{p}\right)\right] \tag{3.3}$$

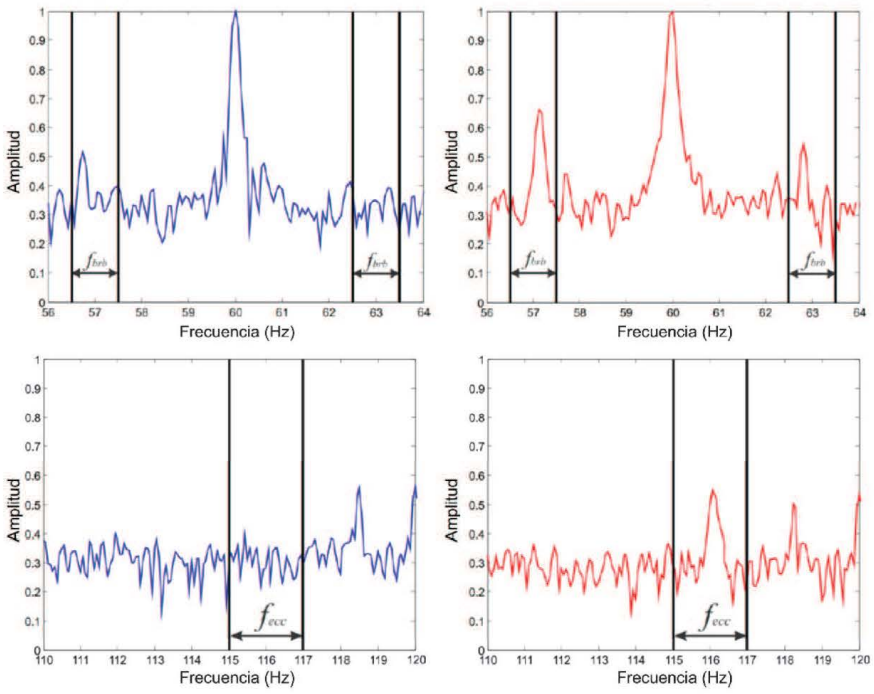

(a) (b)

Figura 3.5: Selección de las bandas en las frecuencias de interés de: (a) motor sano y (b) motor con fallo.

Su combinación con ANN, permite una detección automática y en línea para detectar fallas múltiples y múltiples-combinadas en motores de inducción alimentados por variador de velocidad desde frecuencias bajas como 3 Hz hasta la frecuencia nominal de 60 Hz.

Instrumentación para termografía: Esta etapa consiste en la toma de imágenes termográficas calibradas por un sistema de instrumentación RTD para posteriormente realizar un análisis en su procesamiento. La calibración consiste en comparar la salida de un instrumento bajo prueba en este caso la cámara termográfica contra la salida de un instrumento donde su exactitud (sistema de instrumentación RTD) es conocida cuando la cantidad de medición es aplicada a ambos instrumentos. Esta calibración asegura la exactitud de todos los instrumentos y sensores utilizados en condiciones ambientales que son los mismos bajo los cuales fueron calibrados. Para este caso se describe a continuación la metodología termográfica propuesta:

1.- Metodología basada en termografía, la cual se presenta en la figura 3.6 donde primeramente se realiza la calibración y validación de las imágenes termográficas entregadas por la cámara a través de sensores RTD, después las imágenes termográficas son segmentadas en las regiones de interés y finalmente se presenta como la segmentación puede ser interpretada para dar un diagnóstico.

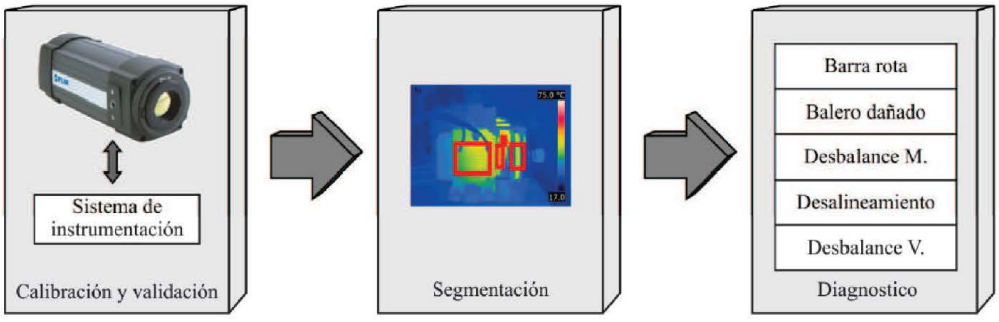

Figura 3.6: Metodología basada en termografía.

Por otro lado, la segmentación que se realiza de manera manual se realizó en cuatro secciones como lo muestra la figura 3.7a (imagen) y b (termografía) donde S1, S2, S3 y S4 corresponden a: carcasa del motor, balero, polea de carga y polea del motor respectivamente.

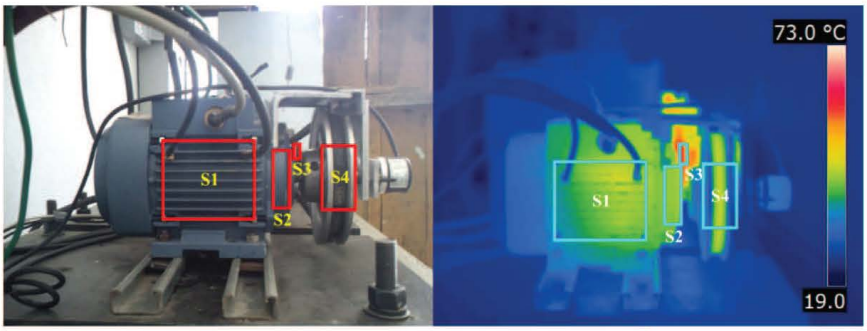

Figura 3.7: Segmentación en: (a) imagen y (b) termografía.

Al desarrollar dicha segmentación se tiene la posibilidad de un amplio análisis sobre el motor de inducción y su cadena cinemática, ya que ésta permite conocer una firma térmica del motor de inducción en buen estado a través de imágenes termográficas tomadas durante el funcionamiento del motor de inducción; dando un punto de referencia para el diagnóstico. La detección de fallas del motor de inducción es bastante intuitivo después de conocer las temperaturas normales de operación, ya que cuando una alteración en las condiciones térmicas en la firma del motor aparece en la imagen termográfica, significa que un fallo está presente. La metodología para el diagnóstico se presenta en la ecuación 3.4, donde *i* es el índice del segmento termográfico a analizar. Por lo tanto, para este diagnóstico: primero se obtiene la firma del motor con sus temperaturas máximas de cada segmento (TH_i), después se obtiene la temperatura máxima de cada segmento termográfica con condición de fallo (TF_i) con el fin de otorgar el índice de coeficiente térmico (TC_i).

$$TC_i = TF_i - TH_i \tag{3.4}$$

Post-procesamiento y condición: Esta etapa consiste en la fusión de los sensores inteligentes por medio de un árbol de decisiones para posteriormente entregar la condición actual del motor. La integración de los sensores inteligentes a este árbol de decisiones se realizó por medio de sus salidas de las redes neuronales (indicadores de fallo), donde su conjunto hace que el sistema entregue la condición actual del motor de una manera confiable.

3.2 SISTEMAS DE MONITOREO DE MÁQUINAS ELÉCTRICAS

3.2.1 Monitoreo de variables eléctricas

El monitoreo de variables eléctricas en los sistemas de potencia constituye una necesidad esencial para diversas aplicaciones industriales y científicas, tales como el diagnóstico y monitoreo de máquinas eléctricas, monitoreo de la calidad de la energía, sistemas de protección y control entre otros. Los equipos existentes en el mercado desarrollados para este fin, realizan la interpretación de las variables eléctricas por medio de diversos algoritmos con el fin de cubrir las necesidades para cada aplicación; sin embargo, en muchas ocasiones cuentan con funciones que no son explotadas o no son usadas en su totalidad, lo cual por una parte contribuye a elevar su costo. Debido a la gran diversidad de aplicaciones existentes en el monitoreo de variables eléctricas, es de gran ayuda contar con sistemas de adquisición y procesamiento de señales eléctricas que permitan la reconfiguración en su arquitectura para poder adecuarse de manera específica a las diversas tareas a un bajo costo. En este trabajo se presenta un sistema reconfigurable para el monitoreo de variables eléctricas basado en tecnología FPGA de bajo costo. Este sistema es capaz de adquirir las señales de voltaje y corriente en los sistemas trifásicos, además de contar con una capacidad de reconfigurabilidad para así poder utilizarse e integrarse con diversos algoritmos acorde a las necesidades particulares de cada aplicación.

En la figura 3.8 y 3.9 se muestran los instrumentos utilizados en este trabajo. El mostrado en la figura 3.8 es un instrumento realizado por Granados (2012) como elemento clave para su tesis doctoral; por otro lado, el sistema

mostrado en la figura 3.9 es un sistema desarrollado por Valtierra (2014) con un enfoque mayor hacia la calidad de la energía y monitoreo de máquinas eléctricas con características similares a un equipo comercial, como se puede apreciar por el uso de ganchos amperímetros i200 de la marca Fluke y las pinzas de voltaje. Al primer instrumento (figura 3.8) se le agregó gracias a su reconfigurabilidad una interfaz VGA para el desplegado de resultados, mientras que al mostrado en la figura 3.3 se le diseñó una interfaz a través de la pantalla táctil TRDLB de Terasic.

Figura 3.8: Sistema de monitoreo eléctrico basado en FPGA.

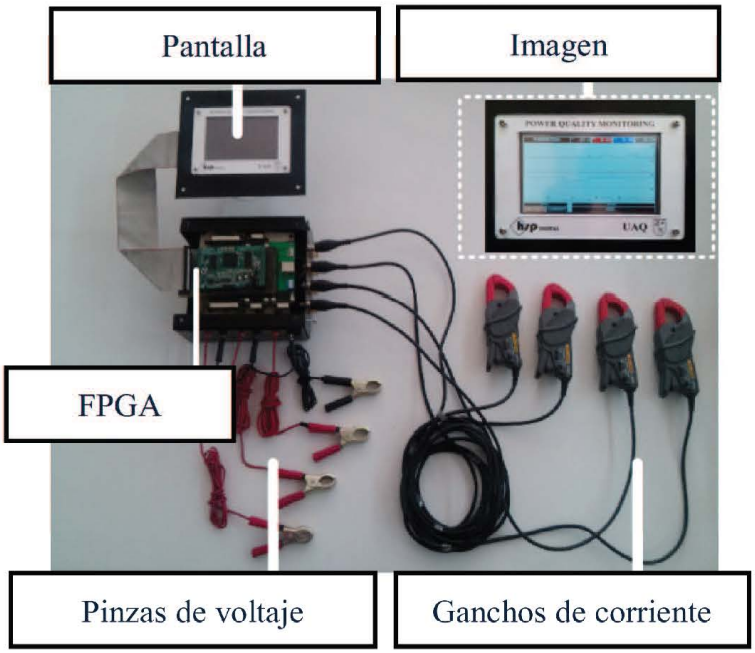

Figura 3.9: Sistema de monitoreo de la calidad de la energía y máquinas eléctricas basado en FPGA.

Ambos sistemas están compuestos por el diagrama a bloques que se muestra en la figura 3.10. Los sistemas de monitoreo constan de 4 sensores de efecto hall para el monitoreo de las corrientes de fase y la corriente del neutro o 4 ganchos Fluke de corriente, respectivamente. Los sensores de efecto hall presentan excelentes características de precisión, un ancho de banda grande así como la capacidad de sensado para corrientes tanto de AC como de DC. Por otra parte, se monitorea las 3 señales de voltaje del sistema eléctrico utilizando un divisor de voltaje y un amplificador de aislamiento para obtener aislamiento galvánico entre el sistema eléctrico y el instrumento de medición, la señal es obtenida de forma diferencial por medio de un convertidor DC-DC para el desacople entre las referencias. Esto permite la medición de voltajes entre fases $V_{fase\text{-}fase}$ o voltajes de fase a neutro $V_{fase\text{-}neutro}$. La ganancia utilizada para compensar la diferencia de magnitudes entre $V_{fase\text{-}fase}$ y $V_{fase\text{-}neutro}$ es seleccionada mediante un jumper de forma que se obtiene la mitad del voltaje en el rango dinámico del convertidor, tal y como establece la norma Std. IEEE 1159.

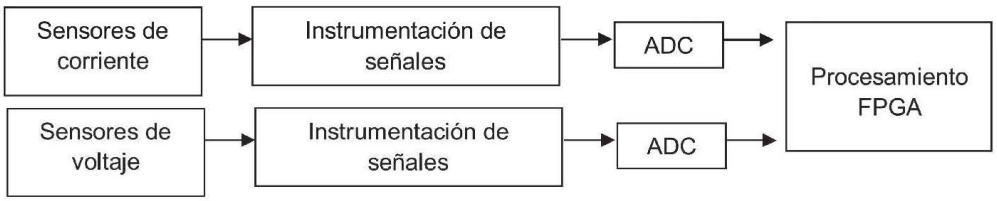

Figura 3.10: Diagrama a bloques de los sistemas de monitoreo.

3.2.1.1 Sensores e instrumentación.

La figura 3.11 y 3.12 muestran respectivamente los diagramas de los circuitos utilizados para las etapas de sensado y acondicionamiento de las corrientes y voltajes.

La instrumentación de los sensores de corriente es conformada por una etapa de ganancia con selección y un filtro antialiasing. De manera similar las señales de voltaje son filtradas por medio de un filtro antialising. Los filtros

antialiasing son filtros butterworth de segundo orden con una frecuencia de corte de 3 KHz. La figura 3.13 se muestra una fotografía de la tarjeta diseñada para el acondicionamiento de las señales de voltajes y corrientes.

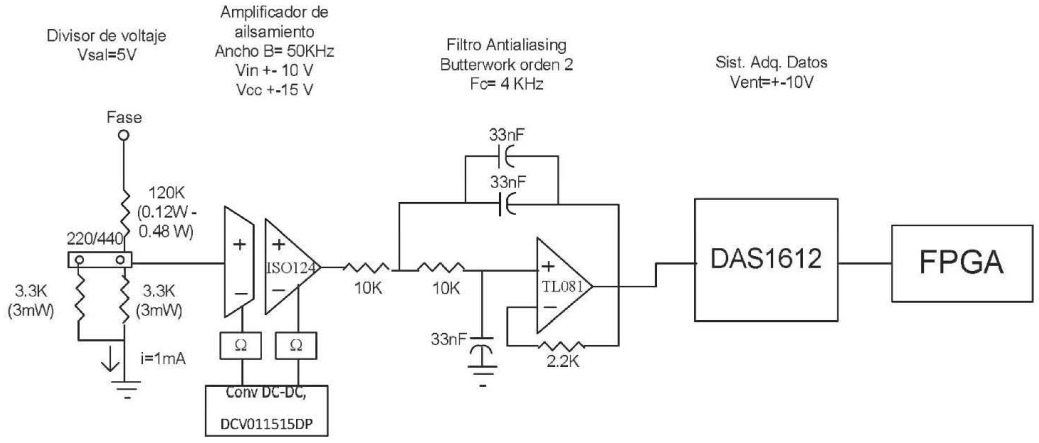

Figura 3.11: Instrumentación de sensores de voltaje.

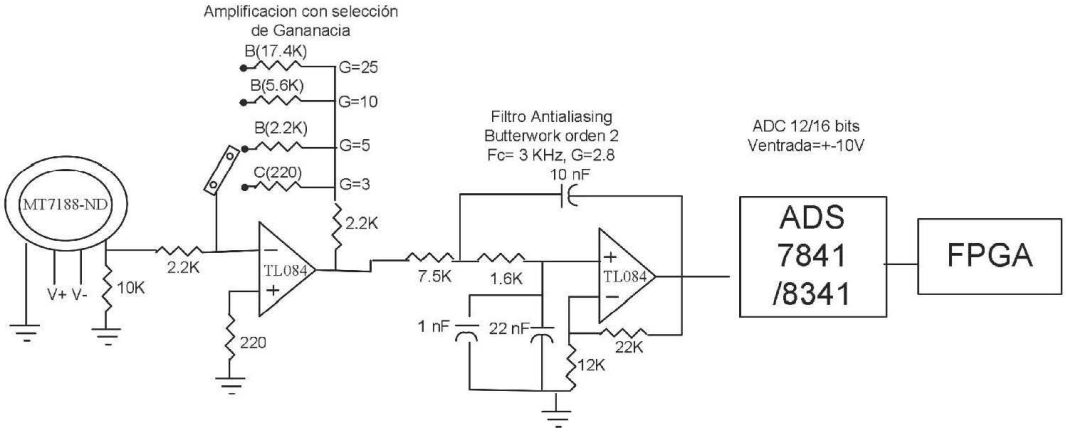

Figura 3.12: Instrumentación de sensores de corriente.

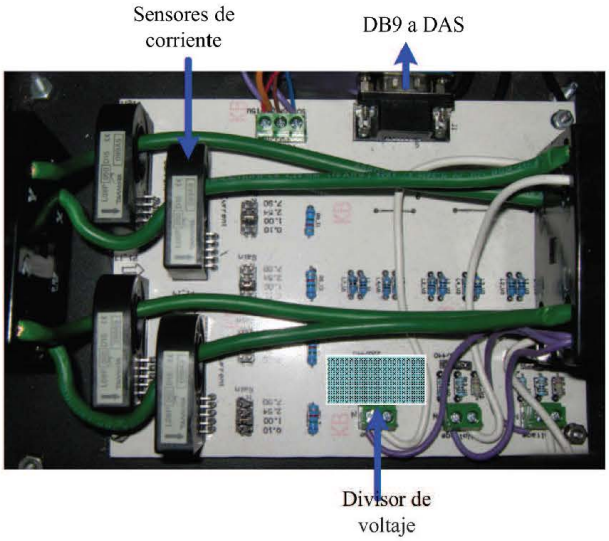

Figura 3.13: Tarjeta para la etapa de acondicionamiento de señales.

3.2.1.2 Adquisición de las señales.

La etapa de conversión digital analógica puede utilizar un convertidor analógico digital ADS7886 con una resolución de 12 bits o puede ser reemplazado por un ADS8341 de 16 bits. Este sistema es diseñado para obtener una tasa máxima de muestreo de 6000 muestra/s y cuenta con 20 MHz de transmisión serial para su procesamiento en una PC. El sistema de adquisición de datos (ADS) recibe una señal que determina la frecuencia de muestreo deseada, esta señal es proveniente de un controlador embebido en el FPGA. Posteriormente las señales digitales son multiplexadas y pueden ser almacenadas en memorias externas localizadas en la tarjeta que contiene el FPGA.

3.2.1.3 Procesamiento de las señales.

De acuerdo a los diferentes casos de estudios realizados el procesamiento de la señal varía de acuerdo a los estudios realizados, en los cuales se hace uso de los herramientas de procesamiento digital de señales como filtros y diezmado, así como el empleo de transformadas de espacio. La descripción detallada de los algoritmos y técnicas empleadas se presentan en la descripción de cada uno de los frentes del trabajo realizado.

3.2.2 Monitoreo por termografía

La termografía es el arte de transformar una imagen de infrarrojos en una imagen radiométrica que permita leer los valores de temperatura. Por tanto, cada píxel de la imagen radiométrica es, de hecho, una medición de temperatura. Para ello, se incorporan complejos algoritmos a la cámara termográfica. La tecnología termográfica se ha convertido en una de las herramientas de diagnóstico más valiosas para el mantenimiento predictivo, al detectar anomalías que suelen ser invisibles a simple vista. Esto hace de la cámara termográfica una herramienta perfecta para el monitoreo y mantenimiento predictivo. Las cámaras termográficas son potentes herramientas no invasivas para la supervisión y el diagnóstico del estado de máquinas eléctricas, instalaciones eléctricas y mecánicas. Los equipos existentes en el mercado desarrollados para este fin, capturan las imágenes termográficas con el fin de cubrir las necesidades para cada aplicación; sin embargo, en muchas ocasiones estos equipos no son calibrados para la aplicación en la cual serán utilizados. Debido a la gran diversidad de aplicaciones existentes en el monitoreo de máquinas eléctricas, es de gran ayuda contar con sistemas de monitoreo de temperatura con el fin de calibrar los sistemas termográficos que permitan la calibración de manera específica a las diversas tareas.

En la figura 3.14 se muestra la cámara termográfica FLIR A310, utilizada en este trabajo, la cual es una herramienta de la facultad de ingeniería, campus San Juan del Río y es utilizada para la captura de termogramas para atacar diferentes frentes de investigación que se tratan dentro de la misma facultad. Esta cámara termográfica es de montaje fijo y puede instalarse casi en cualquier sitio, ésta ayuda a proteger las instalaciones y miden diferencias de temperatura para valorar cuán crítica es la situación, lo que le permite detectar los problemas antes de que se produzcan fallos costosos, evitar periodos de inactividad y mejorar la seguridad de los trabajadores.

Figura 3.14: Cámara termográfica FLIR A310.

3.3 CASOS DE ESTUDIO

A continuación se describen los casos de estudio realizados para la validación y prueba de las metodologías desarrolladas así como de los sensores que lo integran. Es conveniente mencionar que los casos de estudio se aplicaron solamente a motores de inducción utilizando el banco de pruebas de la figura 3.15 y para las fallas de: barra rota del rotor (BRB) con diferentes severidades ½ BRB, 1 BRB y 2 BRB, desbalance mecánico (UNB), desalineamiento (MAL) y balero dañado (BD) como se muestra en la figura 3.16. Este trabajo se divide en tres casos de estudio diferentes, donde el primero hace uso de una cámara termográfica y sensores resistivos detectores de temperatura (RTD, *Resistance Temperature Detector*) para la calibración de la misma y los dos restantes están basados en sensores inteligentes. En estos casos de estudio, se proponen metodologías para la predicción y detección de fallas múltiples y detección de fallas múltiples combinadas en motores de inducción alimentados por variador de velocidad y por la línea directa como ha sido reportado en la literatura. El primer caso de estudio propone una metodología a través de termografía calibrada para la detección de fallas y el impacto que tienen sobre la cadena cinemática. En el segundo, parte de la detección de fallas múltiples en motores de inducción. Para finalizar, en el tercero, parte de la detección de fallas múltiples en motores de inducción y se propone una metodología que detecte fallas múltiples-combinadas y esto reducirlo a un único sensor primario.

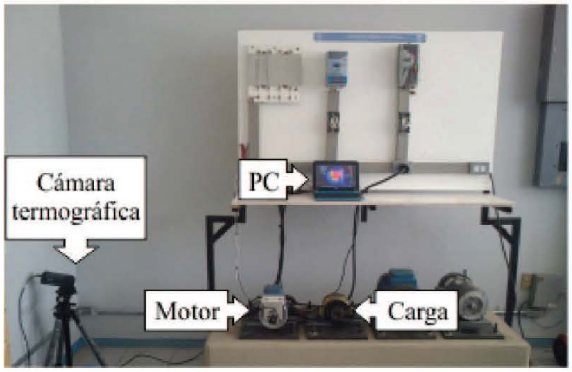

Figura 3.15: Banco de pruebas utilizado.

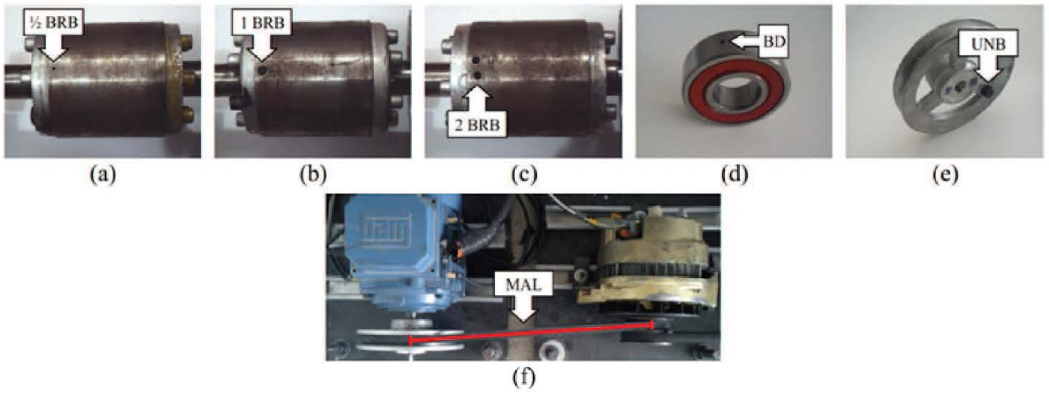

Figura 3.16: Fallas tratadas en este trabajo (a) ½ BRB, (b) 1 BRB, (c) 2 BRB, (d) BD, (e) UNB y (f) MAL.

3.3.1 Termografía: Monitoreo de fallas en motores de inducción y su impacto en la cadena cinemática.

El primer caso de estudio se basa en el desarrollo y planteamiento de una metodología basada en termografía calibrada para el monitoreo de fallas en motores de inducción y su impacto en la cadena cinemática, ya que en el monitoreo de máquinas eléctricas la termografía es una de las herramientas más utilizadas debido a que es una herramienta no invasiva y a que es una forma efectiva para el mantenimiento predictivo.

La cámara termográfica fue calibrada tomando 60 muestras de temperatura en un mismo punto con las RTD que se instalaron en el motor de inducción a analizar (figura 3.17), obteniendo una precisión del ±1.5%.

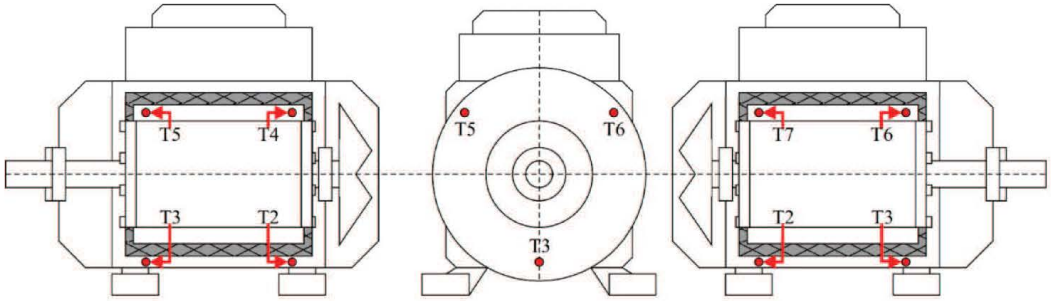

Figura 3.17: Puntos de instalación de los RTDs.

El objeto de usar una cámara termográfica calibrada con un sistema conocido es que permite conocer la precisión y la exactitud de las imágenes termográficas a analizar y así tener una firma térmica del motor en estado sano confiable la cual se obtiene hasta alcanzar su estado estable térmico, como se muestra en la figura 3.18.

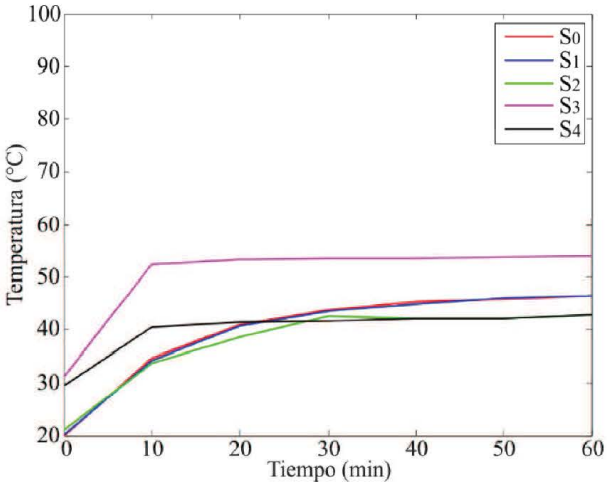

Figura 3.18: Firma térmica del motor en estado sano.

Una vez que la firma térmica del motor en estado sano es tomada, se puede observar que a partir del minuto 40, se alcanza un estado térmico estable y a desde ahí tomar los índices *TH* para cada segmento termográfico (S1-S4) y el promedio de las temperaturas de los sensores RTD (S0) colocados sobre el motor de inducción. Basado en este análisis previo, se determina que a partir del minuto 40 después del arranque, se pueden capturar las imágenes termográficas para cualquier análisis sobre el motor de inducción, esto es tomar las imágenes termográficas de las fallas en el estado térmico estable para así obtener los índices *TF* y aplicar la ecuación 3.1.

3.3.2 Sensor inteligente: Detección de fallas múltiples en motores de inducción.

En el caso de estudio número dos, una vez analizadas las fallas por medio de termografía el usuario inicia el primer sensor inteligente que detecta fallas múltiples en motores de inducción para corroborar la falla que está presente. El sensor inteligente cuenta con un procesador inteligente, así nombrado ya que utiliza un sistema inteligente para otorgar una condición de fallo, este procesador está desarrollado dentro de un FPGA. Principalmente este sensor inteligente (figura 3.19) está basado en la transformada Park como se mencionó al inicio de este capítulo, la cual permite pasar de un sistema *ABC* a un sistema *DQ* y de éste obtener una figura de Lissajous.

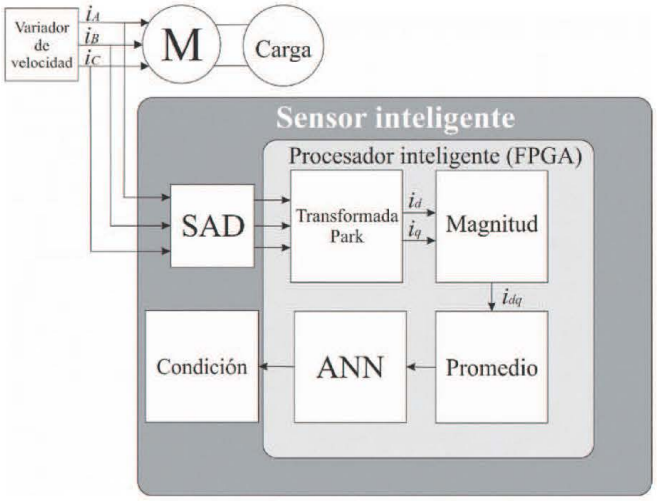

Figura 3.19: Sensor inteligente para detección de fallas múltiples.

3.3.3 Sensor inteligente: Detección de fallas múltiples combinadas en motores de inducción.

Una vez analizadas las fallas por medio de las metodologías anteriores el sistema pone en marcha el segundo sensor inteligente que detecta fallas múltiples y múltiples combinadas en motores de inducción para acertar la falla que está presente o saber si se trata de esta misma falla en combinación con alguna otra (figura 3.20). Este sensor cuenta con un procesador inteligente desarrollado dentro de un FPGA y basado en el análisis espectral bajo FFT en combinación con ANN. Este sensor inteligente (figura 3.21) lleva a cabo el siguiente esquema donde primeramente, se adquiere una señal de corriente del variador de velocidad que alimenta al motor de inducción por medio de un sensor de efecto Hall, para después hacer el acondicionamiento de la señal y poderla leer el sistema de adquisición de datos. Después, esta señal entra al procesador inteligente dentro del FPGA para finalmente entregar la condición del motor.

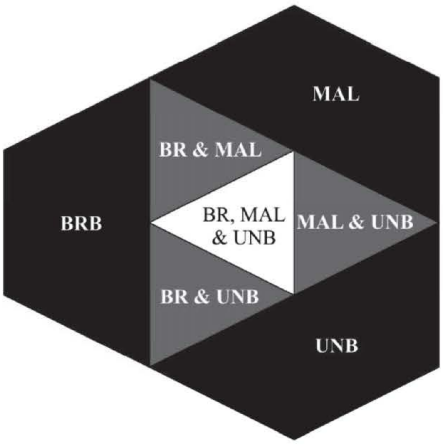

Figura 3.20: Representación de fallas múltiples-combinadas.

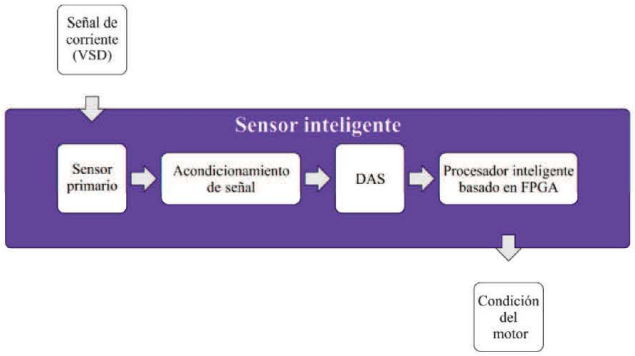

Figura 3.21: Sensor inteligente para detección de fallas múltiples y múltiples combinadas.

La metodología de este sensor inteligente está embebida principalmente en el FPGA donde el procesamiento se realiza como se describe a continuación y se muestra en la figura 3.22.

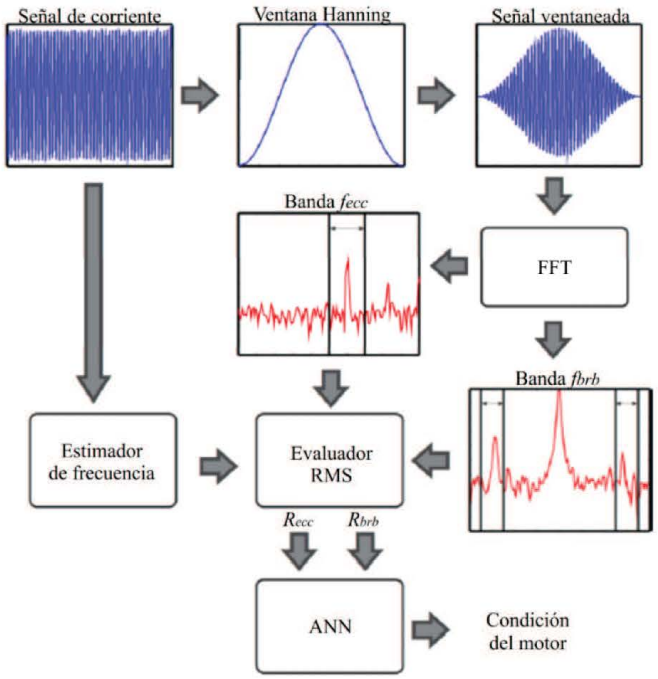

Figura 3.22: Diagrama de flujo de la metodología implementada en el procesador inteligente.

Primeramente, los datos salientes del convertidor analógico digital, son pasados por una ventana Hanning para reducir el chorreo (Leakage) en el dominio de la frecuencia y la frecuencia de operación del variador de velocidad, es calculado por un estimador de frecuencia. Después, la FFT es aplicada para obtener el espectro de la corriente; después se seleccionan las bandas de interés para las diferentes fallas las cuales son evaluadas a través de la estimación de un valor RMS están expresadas en las ecuaciones 3.5 y 3.6.

$$R_{brb} = \sum_{s=0.01}^{0.2} f(1 \pm 2ks) \tag{3.5}$$

$$R_{ecc} = \sum_{s=0.01}^{0.2} f\left[1 \pm k\left(\frac{1-s}{p}\right)\right] \tag{3.6}$$

Dónde *f* es la frecuencia de operación, *s* es el deslizamiento del motor, *p* es el número par de polos y *k* es el número del armónico a analizar.

Las bandas de interés están basadas en intervalos entre un mínimo y máximo deslizamiento del motor el cual va desde el 1% hasta el 20%, esto para cumplir el estándar NEMA de diseño de motores A, B, C y D. Estos porcentajes de deslizamiento garantizan una carga del motor entre 25 al 100%. Finalmente, la salida de cada evaluador RMS son entradas de la ANN para conceder una condición del motor de inducción.

4. RESULTADOS

En este capítulo se analizan y discuten los resultados obtenidos en cada uno de los casos de estudio abordados en este trabajo para la detección de fallas en los motores de inducción así como su conjunto para evaluar la condición del motor de inducción.

4.1 ANÁLISIS TERMOGRÁFICO DE FALLAS MÚLTIPLES EN MOTORES DE INDUCCIÓN Y SU IMPACTO EN LA CADENA CINEMÁTICA.

La figura 4.1 muestra las imágenes termográficas en estado térmico estable del motor de inducción bajo su estado sano y las diferentes condiciones de falla.

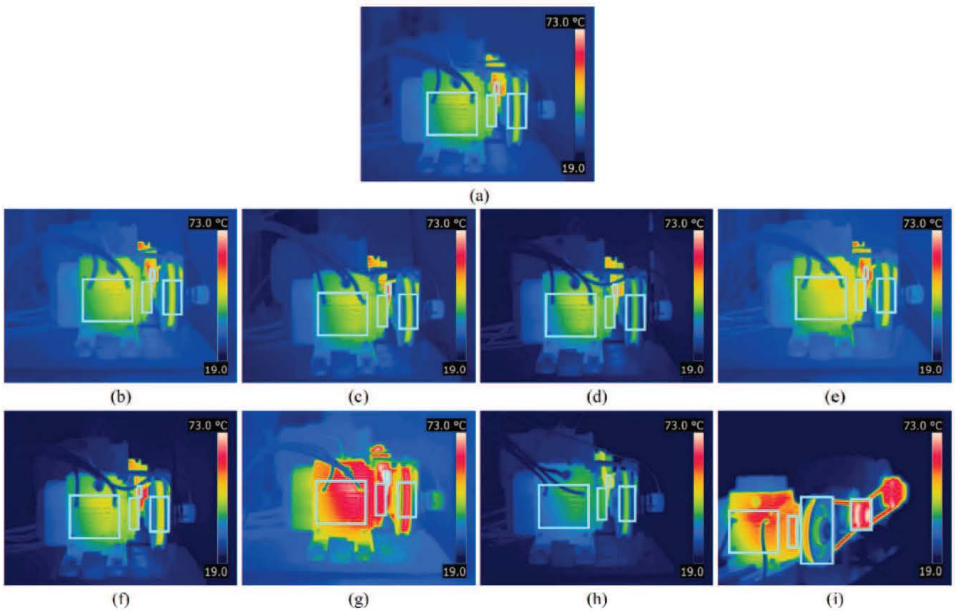

Figura 4.1: Termogramas en estado térmico estable: (a) Motor sano, (b) ½ BRB, (c) 1 BRB, (d) 2 BRB, (e) BD, (f) UNB, (g) MAL, (h) VUNB e (i) otra perspectiva con MAL

Por otro lado, la Tabla 4.1 muestra los resultados de las temperaturas obtenidas de cada segmento bajo cada condición de fallo así como sus coeficientes térmicos. Tomando estos resultados como referencia, se puede observar que la falla de desalineamiento es la de mayor impacto en el motor y su cadena cinemática y puede traer consecuencias severas. Por consecuencia, es importante aplicar acciones o dar un diagnóstico sobre qué es lo que está pasando, partiendo de esto se puede aplicar el estándar ASTM E1934-99[a] donde indica un cierto criterio y relevancia que tiene la temperatura en el coeficiente térmico a analizar para poder dar un diagnóstico y corroborarlo con los siguientes sensores colaboradores. La Tabla 4.2 muestra la relevancia del daño para los coeficientes térmicos.

Tabla 4.1. Resultados de las temperaturas obtenidas de cada segmento bajo cada condición de fallo y sus coeficientes térmicos.

Condición	Segmentos termográficos y TC_i (°C)							
	S_1	S_2	S_3	S_4	TC_1	TC_2	TC_3	TC_4
HLT	45	42.2	53.5	42	- [a]	- [a]	- [a]	- [a]
1/2 BRB	51.03	47.83	58.33	47.33	6.03	5.63	4.83	5.33
1BRB	48.43	45.27	58.53	45.67	3.43	3.07	5.03	3.67
2BRB	49.5	44.93	56.37	43.4	4.5	2.73	2.87	1.4
BD	50.3	51.17	53.03	49.3	5.3	8.97	0 [b]	7.3
UNB	53.03	48.15	65.53	51.5	8.03	5.95	12.03	9.5
VUNB	42.13	41.1	40.1	48	0 [b]	0 [b]	0 [b]	6
MAL	77.73	70.4	93.27	67.93	32.73	28.2	39.77	25.93

[a] Índices de coeficientes térmicos *TCi* no están definidos para el caso sano (HLT).

[b] $TC_i = 0$ significa que el gradiente de la condición relacionada es despreciable.

Tabla 4.2. Relevancia de daño.

Criterio	Relevancia
$TC_i \leq 5$	Ordinaria
$5 < TC_i \leq 15$	Ligera
$15 < TC_i \leq 30$	Mayor
$TC_i > 30$	Crítica

4.2 ANÁLISIS DE FALLAS MÚLTIPLES EN MOTORES DE INDUCCIÓN ALIMENTADOS POR VARIADOR DE VELOCIDAD.

Como continuación de este trabajo se realizó el análisis de fallas múltiples en motores de inducción a partir de la transformada Park en conjunto con una red neuronal artificial lo cual hace a esto un análisis inteligente, ya que a partir de estas dos herramientas, la detección de las fallas se hace de manera automática. Para hacer un análisis estadísticamente confiable fue necesario llevar a cabo 40 corridas del experimento bajo todas las condiciones de fallo y bajo las velocidades tratadas: 3, 30 y 60 Hz (figura 4.2a-c).

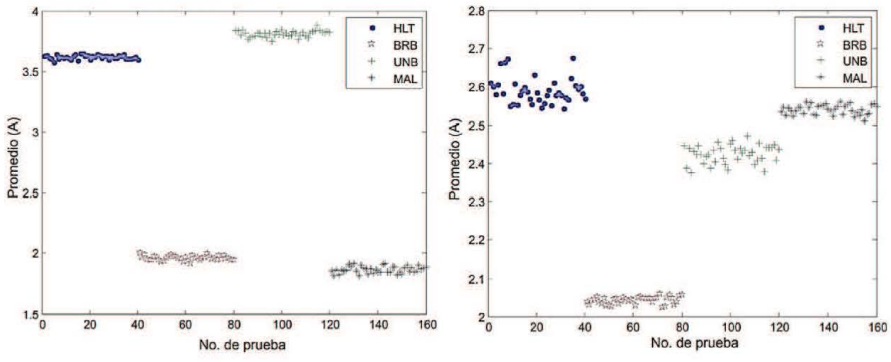

(a) (b)

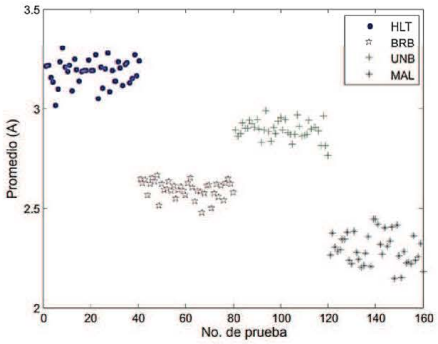

(c)

Figura 4.2: Cálculo del promedio del vector IDQ obtenido de cada condición de fallo en: (a) 3 Hz, (b) 30 Hz y (c) 60 Hz.

Continuando con el análisis de los resultados, en la Tabla 4.3 se muestra la efectividad que tuvo el sensor inteligente a la hora de detectar la falla, esto es: si de mis 40 pruebas que son el 100 %, ¿Qué porcentaje el sensor acertó la condición? Por ejemplo, para la condición sana (HLT) la detección fue de un 100 % corriendo a 3 y 60 Hz, y de un 90 % para 30 Hz. Para barra rota (BRB), en 30 y 60 Hz se obtuvo un 100 % de efectividad y para 3 Hz un 97 %. Por otro lado, para la condición de desbalance (UNB) la efectividad del sensor fue de un 100 % en todo el rango de frecuencias y finalmente para la condición de desalineamiento (MAL) se obtuvo un 100 % de efectividad en 3 Hz y 60 Hz, y un 95 % para 30 Hz.

Tabla 4.3. Efectividad del sensor inteligente para identificar la condición del motor de inducción.

Condición	3Hz Efectividad	30Hz Efectividad	60Hz Efectividad
HLT	100%	90%	100%
BRB	97%	100%	100%
UNB	100%	100%	100%
MAL	100%	95%	100%

4.3 ANÁLISIS DE FALLAS MÚLTIPLES EN MOTORES DE INDUCCIÓN ALIMENTADOS POR VARIADOR DE VELOCIDAD.

En este caso de estudio se abordan, al igual que en los casos anteriores, las mismas fallas pero ahora con la combinación entre ellas, donde por medio de un sensor de corriente y un procesador inteligente (sensor inteligente) se pueden detectar. La Tabla 4.4 muestra los resultados de clasificación para cada falla.

Tabla 4.4: Resultados de clasificación para identificar la condición del motor de inducción.

Condición	3Hz Efectividad	30Hz Efectividad	60Hz Efectividad
HLT	100%	100%	80%
BRB	80%	100%	100%
UNB	100%	100%	100%
MAL	100%	100%	100%
BRB-UNB	80%	100%	100%
BRB-MAL	90%	100%	100%
UNB-MAL	100%	100%	100%
BRB-MAL-UNB	100%	80%	90%

4.4 ANÁLISIS FALLAS EN MOTORES DE INDUCCIÓN CON SENSORES COLABORATIVOS

En este caso de estudio se aborda el conjunto de los sensores colaborando entre sí, donde por medio de un árbol de decisiones los sensores son capaces de entregar la condición del motor de manera intuitiva al usuario. Este árbol de

decisiones fue implementado dentro del FPGA utilizando las salidas de las redes neuronales artificiales (ANN) de los sensores inteligentes donde se pusieron en marcha 40 pruebas por cada condición en cada una de las velocidades estudiadas. La Tabla 4.5 muestra los resultados de los sensores colaborativos para cada falla.

Tabla 4.5: Resultados de los sensores colaborativos para identificar la condición del motor de inducción.

Condición	3Hz Efectividad	30Hz Efectividad	60Hz Efectividad
HLT	100%	100%	100%
BRB	97%	100%	100%
UNB	100%	100%	100%
MAL	100%	100%	100%
BRB-UNB	97%	100%	100%
BRB-MAL	97%	100%	100%
UNB-MAL	100%	100%	100%
BRB-MAL-UNB	97%	100%	100%

5. CONCLUSIONES

Del desarrollo de esta tesis se obtuvo un prototipo de sistema de monitoreo en red con diferentes sensores (sensores colaborativos) de fallas en motores de inducción, el cual permite analizar diferentes tipos condiciones individuales así como la combinación de éstas.

Referente a los diferentes casos de estudio por los cuales se atacó la problemática: el primero, partiendo de la calibración de la cámara termográfica podemos concluir que es un método importante para colaborar con diversas técnicas y sensores utilizados ampliamente en la industria (corriente y vibraciones) lo cual nos lleva a una mejor interpretación de los resultados y un mejor diagnóstico para el mantenimiento preventivo y correctivo.

Del caso dos, la detección de fallas a través del sensor inteligente basado en transformada Park pudo satisfacer los requerimientos de un sensor colaborativo al hacer uso de tres sensores de corriente, también cumplió con la característica de una baja carga computacional en comparación con otras técnicas, así como detectar múltiples fallas.

Finalmente, partiendo del sensor inteligente anterior cambiando su metodología a un análisis espectral, pero permaneciendo la clasificación inteligente (redes neuronales) se pudo realizar una mejor estimación para detectar fallas múltiples-combinadas, así como reducir el uso de sensores de corriente a uno solo.

Se puede decir que cada metodología independiente para cada caso de estudio es buena a la hora de detectar fallas en motores de inducción, pero el conjunto de estas tres con la metodología propuesta hacen de la red de sensores un sistema colaborativo, el cual alcanza los objetivos planteados, así como el cumplimiento de la hipótesis.

REFERENCIAS

Amezquita-Sanchez J.P., Cabal-Yepez E., Romero-Troncoso R.J., Osornio-Rios R.A., Garcia-Perez A., (2010) Determination of system frequencies in mechanical systems during shutdown transient. Journal of Scientific & Industrial Research, Vol 69, 415-421.

Benbouzid M.E.H., Vieira M., Theys C., (1999) Induction motors faults detection and localization using stator current advanced signal processing techniques, IEEE Transactions Power Electronic, Vol. 14(1), 14-22.

Betta G., Liguori C., Paolillo A., Pietrosanto A., (2002) A DSP-Based FFT-Analyzer for the Fault Diagnosis of Rotating Machine Based on Vibration Analysis, IEEE Transactions on industrial Electronics. Vol.51(6). 1316-1322.

Bollen M. H. J. 2003. What is power quality? , Electric Power Systems Research, Elsevier. Vol.66 (1).5-14.

Botha M., (1997) M. Electrical Machines Failure, Causes and Cures, Electrical Machines and Drives. 8va conferencia anual de IEEE, Nº 444, 114-117.

Cabal-Yepez E., Romero-Troncoso R.J., Garcia-Perez A., Rodriguez-Donate C., (2010) Novel hardware processing unit for dynamic on-line entropy estimation of discrete information. Digital Signal Processing, Elsevier, Vol. 20. 337-346.

Cabal-Yepez E., Valtierra-Rodriguez M., Saucedo-Gallaga R., Garcia-Ramirez A.G., Fernandez-Jaramillo A.A., Pena-Anaya M., (2010) FPGA-Based Online Detection of Multiple-Combined Faults through Information Entropy and Neural Networks. ReConFig 2010, International Conference on Reconfigurable Computing and FPGAs. 3-4.

Chapman S.J., (2005) Máquinas eléctricas, McGraw Hill, 4ta Edición, página 1.

Comisión Federal de Electricidad, (1999) Estadística de fallas de transformadores de potencia 1983-1998.

Contreras-Medina L.M., Romero-Troncoso R.J., Rangel-Magdaleno J.J., Millan-Almaraz J.R., (2008) FPGA Based Multiple-Channel Vibration Analyzer for Industrial Applications with Reconfigurable Post-processing Capabilities for Automatic Failure Detection on Machinery, FPGA '08 Proceedings of the 16th international ACM/SIGDA symposium on Field programmable gate arrays, 263-263.

Didier G., Ternisien E., Caspary O., Razik H., (2007) A new approach to detect broken rotor bars in induction machines by current spectrum analysis. Mechanical Systems and Signal Processing, Elsevier. Vol.21. 1127-1142.

European Standard EN 50160, (2002) Voltage characteristics of electricity supplied by public distribution systems.

Franco-Gasca L.A., Herrera-Ruiz G., Peniche-Vera R., Romero-Troncoso R.J., Leal-Tafolla W., (2006) Sensorless tool failure monitoring system for drilling machines. International Journal of Machine Tools & Manufacture, Elsevier, Vol.46. 3281-386.

Franco-Gasca L. A., Romero-Troncoso R. de J., Herrera-Ruiz G., Peniche-Vera R., (2008) FPGA based failure monitoring system for machining processes, FPGA based failure monitoring system for machining processes, Vol. 40(7-8). 676-686.

Granados-Lieberman D., Romero-Troncoso R.J., Osornio-Rios R.A., Garcia-Perez A., Cabal-Yepez E., (2010) Techiniques and methodologies for power quality analysis and disturbances classification in power systems: a review. IET Generation, Transmission & Distribution, Vol. 5. 519-529.

IEC 61000–4-30, (2003) Testing and measurement techniques power quality measurement methods.

IEEE Std 1159, (1995) IEEE recommended practices for monitoring electric power quality.

IEEE Std 1451.2, (1997) IEEE Smart Transducer Interface Module.

IEEE Standard 519. (1999) Recommended Practices and Requirements for Harmonic Control in Electrical Power Systems.

Jong-Duk Son. Gang Niu, Bo-Suk Yang, Don-Ha Hwang, Dong-Sik Kang, (2009) Development of smart sensors system for machine fault diagnosis, Expert Systems with Applications, Elsevier. Vol.36. 11981-11991.

Korkua, Suratsavadee Koonlaboon, Wei-Jen Lee, (2009) Wireless sensor network for performance monitoring of electrical machine. North American Power Symposium (NAPS). P1.

Mekid S., (2006) Further Structural Intelligent for Sensors Cluster Technology in Manufacturing. Sensors, MDPI. Vol. 6. 557-577.

Morales-Velazquez L., Romero-Troncoso R.J., Osornio-Rios R.A., Herrera-Ruiz G. and Cabal-Yepez E., (2010) Open architecture system based on a reconfigurable hardware–software multi-agent platform for CNC machines. Journal of Systems Architecture. Vol. 56(9). 407-418.

Moreno-Tapia S.V., Vera-Salas L.A., Osornio-Rios R.A., Dominguez-Gonzalez A., Ion Stiharu, Romero-Troncoso R.J., (2010) A Field Programmable Gate Array-Based Reconfigurable Smart-Sensor Network for Wireless Monitoring of New Generation Computer Numerically Controlled Machines. Sensors, MDPI. Vol. 10. 7263-7286.

Morgan, V.T., Effectos of frequency, temperature, compression and air pressure on the dielectric propierties of a multilayer stack of dry kraft paper. IEEE Transactions on Dielectrics and Elec. Insul, Vol. 5, 125-131.

Nelson-Saavedra Pedro. "La medición y análisis de las vibraciones como técnica de inspección de equipos y componentes, aplicaciones, normativas y certificación". U. A. ENDE- Comisión Nacional de Energía Atómica. Disponible en: http://www.aaende.org.ar/sitio/biblioteca/material/CONFCHILE.pdf

Ordaz-Moreno A., Romero-Troncoso R.J., Vite-Frias J.A., Rivera-Gillen J.R., Garcia-Perez A., (2008) Automatic Online Diagnosis Algorithm for Broken-Bar Detection on Induction Motors Base on Discrete Wavelet Transform for FPGA Implementation. IEEE Transactions on industrial Electronics. Vol.55 (5). 2193-2202.

Osornio-Rios R.A., Romero-Troncoso R.J., Morales-Velazquez L., Santiago-Perez J.J., Rivera-Guillen R.J., Rangel-Magdaleno J.J., (2008) A Real-Time FPGA Based Platform for Applications in Mechatronics. ReConFig 2008,

International Conference on Reconfigurable Computing and FPGAs. 289-294.

Peng Z. K., Chu F.L., (2004) Application of the wavelet transform in machine condition monitoring and fault diagnostics: a review with bibliography. Mechanical Systems and Signal Processing, Elsevier. Vol.18. 199-221.

Rivera J., Herrera G., Chacon M., Acosta P., Carrillo M., (2008) Improved Progressive Polynomial Algorithm for Self-Adjustment and Optimal Response in Intelligent Sensors. Sensors, MDPI. Vol. 8. 7410-7427.

Rodriguez-Donate C., Morales-Velazquez L., Osornio-Rios R.A., Herrera-Ruiz G., Romero-Troncoso R.R., (2010) FPGA-Based Fused Smart Sensor for Dynamic and vibration Parameter Extraction in Industrial Robot Links. Sensors, MDPI. Vol.10. 4114-4129.

Romero-Troncoso R. de J., Herrera-Ruiz G., Terol-Villalobos I., Jáuregui-Correa J. C.,(2004) FPGA based on-line tool breakage detection system for CNC milling machines, Mechatronics, Elsevier. Vol. 14(4). 439-454.

Shannon C.E., (1948) A mathematical theory of communication. Bell Syst. Tech. J. 27 379–423, 623–656.

Sheng J.L., (2007) Fault diagnosis for transformer based on fuzzy entropy, in: IEEE Annu. Rep. Conf. Electr. Insul. Dielectr. Phenom. 759–762.

Stones, J., Collinson A., (2001) Power quality. IET Power Engineering, Vol. 15(2). 58-64.

Tandon N, Choudhury A. A review of vibration and acoustic measurement methods for the detection of defects in rolling element bearings. J Tribol Int 1999;32(8):469–80.

Trejo-Hernandez M., Osornio-Rios R.A., Romero-Troncoso R.J., Rodriguez-Donate C., Dominguez-Gonzalez A., Herrera-Ruiz G., (2010) FPGA-Based Fused Smart-Sensor for Tool-Wear Area Quantitative Estimation in CNC Machine Inserts. Sensors, MDPI. Vol.10. 3373-3388.

Vite-Frias J.A., Romero-Troncoso R.J., Ordaz-Moreno A., (2005) VHDL Core for 1024-Point Radix-4 FFT Computation. ReConFig 2005, International Conference on Reconfigurable Computing and FPGAs. 4 pp. - 24.

Vite-Frias, J.A., Romero-Troncoso, R.J., Ordaz-Moreno, A., Rivera-Guillen, J.R., Garcia-Perez, A., (2007) Special Purpose Multi-processor for On-line Fault Detection on Induction Motors during Steady State. In ReCoSoC2007. 171-176.

Yen G. G., Lin Kuo-Chung, (2000) Wavelet packet feature extraction for vibration monitoring. IEEE Transactions on Industrial Electronics. Vol. 47. 650-667.

Zhang S., Yu D., Sheng S., (2006) A Discrete STFT Processor for Real-time Spectrum Analysis. IEEE Circuits and Systems. IEEE Asia Pacific Conference. 1943-1946.

Zhang YanPing, Huang ShuHong, Hou JingHong, Shen Tao, Liu Wei, (2006) Continuous wavelet grey moment approach for vibration analysis of rotating machinery. Mechanical Systems and Signal Processing, Elsevier. Vol.20. 1202-1220.

Zhu Kunpeng, Wong Yoke San, Hong Geok Soon, (2009) Wavelet analysis of sensor signals for tool condition monitoring: A review and some new results. International Journal of Machine Tools & Manufacture.

ANEXO A

Thermographic technique as a complement for MCSA in induction motor fault detection

A.G. Garcia-Ramirez, L.A. Morales-Hernandez, R.A. Osornio-Rios, *Member, IEEE*, A. Garcia-Perez, *Member, IEEE*, R.J. Romero-Troncoso, *Senior Member, IEEE*.

***Abstract* — Recently, mechanical condition monitoring in induction motors has become an important research area because of its relevance in different industrial applications. Infrared thermography has been considered for improving the monitoring of induction motors with the advantage of being a non-invasive technique and having a wide range of analysis. In this work, infrared thermography is used as complementary tool for motor current signature analysis (MCSA) under three common mechanical faults: bearing defects, unbalanced mass and misalignment, based on thermographic image segmentation and statistical feature extraction under the segments of interest. Results show the overall performance of the proposed technique as a complement in induction motor monitoring of mechanical faults.**

***Index Terms*—Induction motors, Infrared imaging, Temperature, Thermal analysis.**

I. Introduction

MECHANICAL faults is one of the most important topics in induction motor condition monitoring, due to they cover around 53% of the faults [1]. In general, mechanical faults are related the eccentricities such as misalignment, mass unbalance [2-6], and bearing defects [6-10]. Nowadays, for monitoring induction motor faults, motor current signature analysis (MCSA) is one of the most used techniques. In [1, 11-14] the MCSA technique is used to detect specific electrical and mechanical induction motor faults, with different digital signal processing techniques. Recently, infrared thermography (IRT) has become a widely accepted condition monitoring tool where the temperature is measured online in a non-contact manner [15]. Therefore, IRT analysis is currently applied to machine condition monitoring and diagnosis field [6]. For instance, in [6] it is proposed a fault diagnosis system for rotating machinery using IRT by extracting features of the enhanced image, with a support vector machine (SVM) for diagnosis, where four conditions are considered: healthy (HLT), misalignment (MAL), bearing defect (BD) and mass unbalance (UNB). Tran *et al.* [16] proposed a diagnosis system with residue gray-scale transformation and enhanced image to classify shaft faults attached to the induction motor. Picazo-Rodenas *et al.* [17] proposed a methodology based on the combination between the heat transfer theory and infrared data to build a thermal model of the induction motor and comparing the results with faulty machines. Eftekhari *et al.* [18] proposed an algorithm to extract features and predict failures in the stator winding. Recently, the IRT analysis has become more attractive due to the low cost of infrared cameras. All the research works mentioned above focus on the detection of the specific faults in the induction motor with hot-spots and the region of the motor frame which are specific in single points and regions of the induction motor and that only grants one temperature of it, leaving aside the thermal behavior of the whole induction motor with different segments of it to improve the monitoring and complement other techniques such as MCSA. The presence of a specific fault affects in the induction motor, which also increases its temperature, and this effect can be identified using IRT.

The contribution of this work is to present the thermography technique as a helpful complement for other techniques such as MCSA under different mechanical faults. An IRT camera is located aside the induction motor to acquire the thermogram. The proposed methodology is based on the segmentation of thermograms to extract the mean ($T\mu$) and the standard deviation (σ) of the temperature in each segment under different mechanical conditions and to extract the frequencies of interest of the faulty conditions through MCSA. The methodology is proposed in order to observe the affection points of the faults with thermography and complement the MCSA analysis. In this paper, three different faults in an induction motor are studied: BD, MAL, UNB and their thermal behavior on the induction motor.

II. Theoretical Background

A. Infrared Thermography

Infrared detectors are the principal components of IRT cameras, which absorb the infrared radiation emitted by a body in a non-contact way, and using Stefan-Boltzmann's law, the temperature of the body is obtained [15]. The IRT cameras can capture an image of thermal pattern called thermogram, where each pixel of the thermogram has a temperature value and a pseudo-color assigned according a palette of colors [19]. The IRT analysis has the advantage to offer a two-dimensional signal, which through segmentation is able to analyze specific areas, allowing the possibility of a broader analysis of the induction motor and its thermal behavior from the start-up up to thermal steady-state, which is important for establishing the maximum temperature that the induction motor can reach.

B. Motor current signature analysis

MCSA is a recognized technique used in the industry due to is a non-invasive method to induction motor condition monitoring. This technique allows distinguishing the effects of mechanical and electrical faults. For this analysis is

This work was supported by CONACyT under Scholarship 229736 and SEP PIFI-2013 Universidad de Guanajuato grant.

R.J. Romero-Troncoso is with HSPdigital CA-Telematica at DICIS, University of Guanajuato, Salamanca, Gto. 36885 Mexico (corresponding author; e-mail: troncoso@hspdigital.org).

A.G. Garcia-Ramirez is with HSPdigital CA-Mecatronica at Facultad de Ingenieria, Campus San Juan del Rio, Universidad Autonoma de Queretaro, San Juan del Rio, Qro. 76807 Mexico (e-mail: aggarcia@hspdigital.org).

L.A. Morales-Hernandez is with HSPdigital CA-Mecatronica at Facultad de Ingenieria, Campus San Juan del Rio, Universidad Autonoma de Queretaro, San Juan del Rio, Qro. 76807 Mexico (e-mail: lamorales@hspdigital.org).

R.A. Osornio-Rios is with HSPdigital CA-Mecatronica at Facultad de Ingenieria, Campus San Juan del Rio, Universidad Autonoma de Queretaro, San Juan del Rio, Qro. 76807 Mexico (e-mail: raosornio@hspdigital.org).

A. Garcia-Perez is with HSPdigital CA-Telematica at DICIS, University of Guanajuato, Salamanca, Gto. 36885 Mexico (e-mail: arturo@salamanca.ugto.mx).

necessary to set a sensor (current clamp or hall-effect sensor) in single current phase of the induction motor. In this work three mechanical faults are studied: bearing defects, mass unbalance and misalignment. The bearing defect (BD) condition corresponds to 40-50% of faults in induction motors [20], producing a deterioration in the lubricant of the bearing and an irregular friction in the bearing housing. Due to this irregular friction an increase in temperature is reflected, being propagated through the induction motor body [21]. Unbalanced mass (UNB) is present when the mechanical load is not uniformly distributed in the rotor, whereas the misalignment condition (MAL) occurs when the pulleys of the load and the motor are not correctly aligned. These faults generate more mechanical stress and excessive rubbing and fatigue of the ball bearings, which can be reflected into an efficiency decrease, demands more load and consequently an increase of slip and also the torque is increased with a consequent temperature rising in the induction motor and its parts [22]. This fault can be detected through MCSA because this faults have characteristic frequencies in the current spectrum whether the faults are: In the case of bearings with 6 to 12 rolling elements, the fundamental outer race frequency (f_o) is calculated approximately as given in (1), where f_r is the rotor frequency, N the number of ball bearings and f is the line supply frequency. This way, it is possible to determine the bearing race frequencies for all seven ball combinations without having explicit knowledge of the bearing configuration [23]. Otherwise, misalignment and unbalance mass creates air-gap eccentricities changing the frequency spectrum of the supply current, due to these affects the inductances of the motor resulting in harmonics (f_{ecc}) at rotating frequency sidebands of the supply frequency predicted by (2).

$$f_o = f \pm f_r \cdot N \cdot 0.4 \tag{1}$$

$$f_{ecc} = f\left[1 \pm k\left(\frac{1-s}{p}\right)\right] \tag{2}$$

Where f is the line supply frequency, k is the harmonic index, s is the slip and p is the number of pole pairs [1].

III. METHODOLOGY

A. *Proposed methodology*

The proposed methodology consists on the MCSA through spectral analysis to extract the frequencies of interest of the faults and on image segmentation of thermograms and a statistical feature extraction which permits a full analysis of the induction motor thermal behavior for complementing the MCSA.

B. *Spectral analysis trough MCSA*

With the objective to use the thermographic technique as a complement for techniques of induction motor fault detection, the MCSA analysis was used. The current data were obtained from a hall-effect sensor placed on a single current phase, captured during the operation of the motor in steady-state in each treated fault. Then, the fast Fourier transform (FFT) is applied to get the current spectrum. Afterward, the frequencies of interest for the different faults are evaluated in order to detect the fault that has been carried out. The frequency of interest for bearing defect is computed through (1), where the tested induction motor has a rotor frequency f_r = 55 Hz, a line supply frequency f = 60 Hz and the test bearing has eight balls; thus the ball pass outer raceway frequency defect is found in f_o = 116 Hz. On the other hand, the frequency of interest for misalignment and unbalance mass is computed by (2), where the tested induction motor has one pole pairs and the slip selection for MAL is s = 13.27 % giving a f_{ecc} = 112 Hz and for UNB is s = 7.41 % with a f_{ecc} = 115.5 Hz, but in order to have a better analysis of all the treated faults the band of analysis is in a range from 1% to 20% in order to fulfill the NEMA standard of A, B, C and D designs [24] giving a band of interest from 108 -119.4 Hz. Finally, making a comparative of amplitude between each frequency band of the faults a detection can be done.

C. *Segmentation*

This segmentation is manually done in the thermograms taken by a calibrated IRT camera through resistance temperature detectors (RTDs) as well as in [25]. Then, these thermograms are divided in two principal segments (*S1* – motor frame and *S2* – bearing). Fig 1a shows the motor under test where the segments are located in a visual image and Fig 1b shows those segments in the thermogram.

D. *Statistical features*

In this methodology two statistical features are extracted: the mean ($T\mu$) and the standard deviation (σ) of the temperature in each segment to analyze the thermal behavior of the induction motor, where $T\mu$ grants the average temperature of each segment of the induction motor under each thermogram and σ is an indicator for the temperature homogeneity of each segment. This mean ($T\mu$) allows establishing a healthy motor signature on thermal steady-state conditions, through captured thermograms during the operation of the motor under the analyzed condition to give the reference point of analysis. Therefore, it is important to know the standard deviation (σ) of the induction motor, because this value gives a reference on how the temperature is behaving and distributed, when the induction motor reach its thermal steady-state or its thermal balance, due to the temperature values are less dispersed and consequently the temperature is homogeneous.

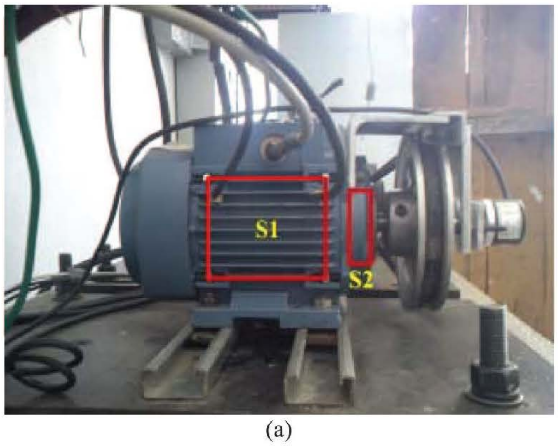

(a)

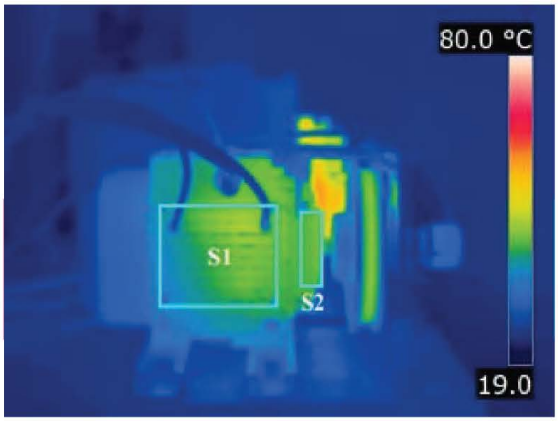

(b)

Fig. 1. Segmentation: (a) Digital image and (b) Thermographic image.

IV. EXPERIMENT

A. Experimental Setup

Fig. 2 shows the experimental setup, consisting in a thermographic camera FLIR A310 at a distance of 1.2 m. The IRT camera is set to a temperature range of 19-80°C for each thermogram. A 1-hp three-phase induction motor (WEG 00136AP3E48T) used for testing the fault conditions treated in this work. This induction motor has 2 poles, 28 bars and receives a power supply of 220 V AC. The applied mechanical load embraces around 100% represented by an ordinary alternator. The current signal is acquired using a hall-effect sensor model L08P050D15, from Tamura Corporation. A 12-bit 4-channel serial-output sampling analog-to-digital converter ADS7841 from Texas Instrument Incorporated is used in the data acquisition system (DAS) with an fs = 4 kHz obtaining 4096 samples during 1.024 seconds of the induction motor in steady-state. The IRT camera takes a thermogram every minute of the induction motor from start-up to thermal steady-state during 50 minutes. The acquired data is stored in a personal computer (PC) and analyzed in Matlab which provides the $T\mu$ and the σ of each segment under each thermogram and the spectrum of the current signal.

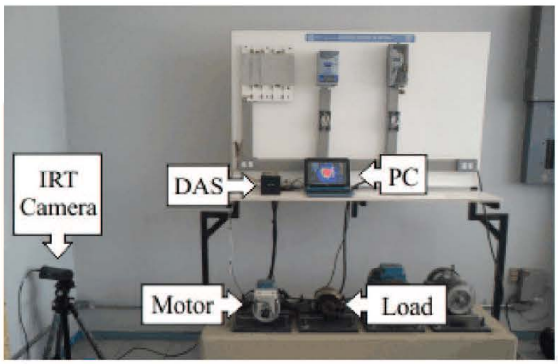

Fig. 2. Experimental setup.

B. Treated faults

In this work three different induction motor mechanical faults are studied: bearing defects (BD), mass unbalance (UNB) and misalignment condition (MAL).

The bearing defect was made drilling a 2.0 mm hole in the outer race as shown in Fig. 3a. The unbalance mass was made by attaching a bolt in an arm of the rotor pulley as Fig. 3b shows, and finally for the misalignment condition was produced by shifting backward the belt in the load pulley, so the transverse axes of rotation for the induction motor and its load were not aligned as shown in Fig 3c.

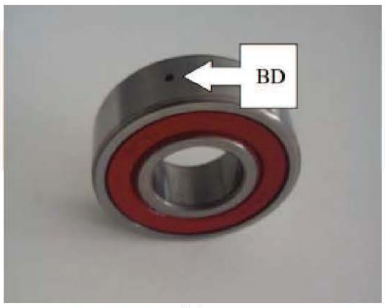

(a)

(b)

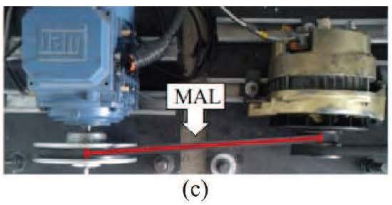

(c)

Fig. 3. Treated faults: (a) BD, (b) UNB and (c) MAL.

V. RESULTS AND DISCUSSION

Three different mechanical fault condition cases are studied through MCSA and thermography. In order to obtain statistically significant results, 5 tests were performed to acquire the thermograms and the current signals from the induction motor in all treated cases. Otherwise, Fig 4 shows that after 40 minutes from the startup of the induction motor, the thermal steady-state is reached in each thermographic segments (S_1 and S_2) and the dispersion σ is around the 8% for *S1* due to the cooling air of the fan in this area, and 2% for *S2* where the dispersion is less due to it is the farthest segment in respect to the fan. Therefore, after meeting the thermal steady-state of the healthy induction motor, the thermograms and the current signal of the motor with each treated fault are taken after 50 minutes from the start-up to evaluate the faults. Fig. 5a-d depict the thermograms for each condition of the induction motor (HLT, BD, UNB, MAL, respectively) in the minute 50, where the thermal steady-state is reached. Based on the thermograms the $T\mu$ value of each segment under the different conditions can be extracted as well as the standard deviation σ in order to evaluate the homogeneity in the thermal steady-state for each condition, where for BD has a σ of 7.81% for S1 and

2.36% for S2. Then, for UNB σ is 7.65% and 1.36% for S1 and S2, respectively. Finally, for MAL, σ for S1 is 10.42% and 3.34% for S2. These results depend on the construction of the induction motor and can be used for describing its thermal behavior. As it can be observed, the standard deviation in S1 is greater than in S2; consequently, the temperature in S2 is more homogeneous. On the other hand, for the current signal the FFT was applied, based on this, the band of interest was extracted as shown in Fig. 5e-h in order to assess the faults, where is quietly visible the amplitude of the fault frequencies. According to these results, with BD shows with MCSA the frequency of interest f_o = 116 Hz has an amplitude of -53.66 dB this show an increase of amplitude compared with HLT condition, then through IRT the fault can be asserted analyzing the segments of interest where, for *S1* show a temperature of 46.6 °C and for *S2* an increase in temperature up to 50.73 °C for BD because the analyzed segment corresponds to the location of the bearing where they show an increase of temperature in comparison with HLT. This behavior is due to the abnormal friction in the bearing. On the other hand, for UNB the results for MCSA show an amplitude difference with HLT of 16.46 dB in 115.5 Hz, which sometimes if the slip is unknown is difficult to find the frequency of the fault. Hence, the IRT is used to ensure the fault analyzing the segments of interest: in segment *S1* the temperature is about 46.6 °C and for segment *S2* = 48 °C, due to the UNB condition produces a slight eccentricity because of the mechanical load is not uniformly distributed, showing a considerable impact stress in the bearing due to this condition has indirect effects on it. Finally, for MAL condition the results for MCSA present an amplitude of -60.13 dB in 112 Hz where the frequency of interest is displaced -3.5 Hz due to the slip that produces the fault, due to these, sometimes the analysis through MCSA is difficult to interpret. For this condition using IRT is quietly visible that produces a higher increase in temperature up to 67 °C in *S1* and *S2* because there is more mechanical stress in this condition. Using IRT is easy to notice that MAL is the most critical condition due to the excessive rubbing and fatigue generated at the ball bearings, with a temperature increase of up to 67 °C in the thermal steady-state.

A meaningful characteristic of this work is the capacity of the thermographic analysis as a complementary technique for MCSA used in fault diagnosis. Although, with the MCSA technique the fault can be detected, sometimes is difficult due to appears spurious harmonics that can be seen like faults and the different slips that the faults generate displacing the frequency of interest. Consequently, the thermographic technique is helpful, since after knowing the healthy motor signature, it is fairly intuitive to find the fault, because the thermal conditions when a fault is present are different from the signature when the motor is healthy, due to the thermal energy is focused in the fault of interest and its closest components.

VI. Conclusions

This work proposes a complementary technique for induction motor fault detection using IRT and MCSA. The proposed technique focuses on the extraction of frequencies of interest through MCSA and on the average temperature and the standard deviation of two thermal segments.

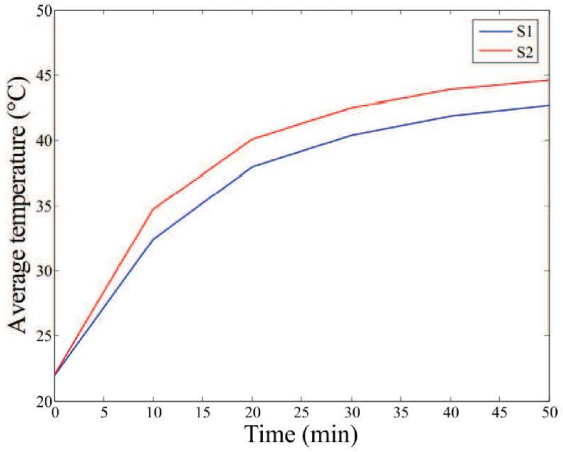

Fig. 4. Healthy motor thermal behavior of segments *S1* and *S2*.

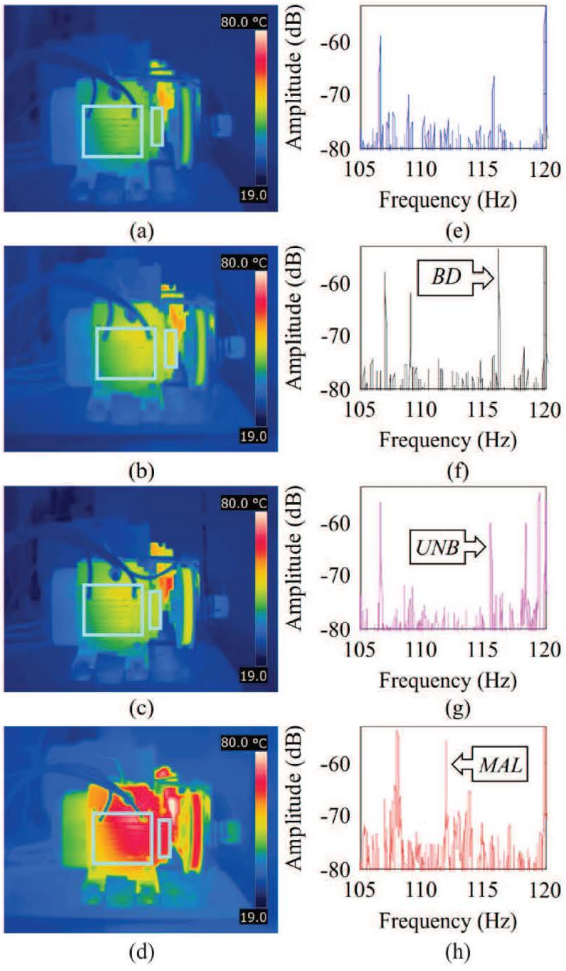

Fig. 5. Thermograms for the conditions: (a) HLT, (b) BD, (c) UNB and (d) MAL. Frequency band of interest: (e) HLT, (f) BD, (g) UNB and (h) MAL.

The frequency spectra show the localization of the faults in the frequencies of interest computed through (1) and (2) where sometimes spurious harmonics appears and the detection can be difficult. Therefore, using the average temperature depicts that for each fault the increase of temperature is different due to the nature of each fault the thermal energy is focused in the fault of interest and its closest components. These, give a rise to apply the IRT

technique as a complementary tool for MCSA in induction motor fault detection.

The proposed methodology can be used for industrial applications in motor fault diagnosis due to its simplicity. For future work, it is proposed to develop the methodology for different fault severities and to develop a smart instrument for automatic fault identification through IRT.

VII. References

[1] J. Cusido, L. Romeral, J.A. Ortega, A. Garcia and J. Riba, "Signal ingection as a fault detection technique," *Sensors*, vol. 11, pp. 3356-3380, Mar. 2011.

[2] C. Kral, T.G. Habetler and R.G. Harley, "Detection of mechanical imbalances of induction machines without spectral analysis of time-domain signals," *IEEE Trans. Industrial Applications*, vol. 40, pp. 1101-1106, July-Aug. 2004.

[3] J.M. Bossio, G.R. Bossio and C.H. De Angelo, "Angular misalignment in induction motors with flexible coupling," in *Annual Conference of Industrial Electronics (IECON 2009),* pp. 1033-1038, 2009.

[4] T.H. Patel and A.K. Darpe, "Experimental investigations on vibration response of misaligned rotors," *Elsevier Mechanical systems and signal processing,* vol. 23, pp. 2239-2252, May. 2009.

[5] L.M. Contreras-Medina, R.J. Romero-Troncoso, E. Cabal-Yepez, J.J. Rangel-Magdaleno and J.R. Millan-Almaraz, "FPGA-Based multiple-channel vibration analyzer for industrial applications in induction motor failure detection," *IEEE Trans. Instrumentation and Measurement*, vol. 59, pp. 63-72, Jan. 2010.

[6] A.MD. Younus and B. Yang, "Intelligent fault diagnosis of rotating machinery using infrared thermal image," *Elsevier Expert Systems with Applications,* vol. 39, pp. 2082-2091, Feb. 2012.

[7] M. Delgado-Prieto, G. Cirrincione, A. Garcia-Espinosa, J.A. Ortega and H. Henao, "Bearing fault detection by a novel condition-monitoring scheme based on statistical-time features and neural networks," *IEEE Trans. Industrial Electronics*, vol. 30, pp. 3398-3407, Aug. 2013.

[8] H.S. Kumar, P. Srinivasa Pai, N.S. Sriram and G.S. Vijay, "ANN based evaluation of performance of wavelet transform for condition monitoring of rolling element bearing," *Elsevier Procedia Engineering,* vol. 64, pp. 805-814, 2013.

[9] M.A. Abu-Zeid and S.M. Abdel-Rahman, "Bearing problems' effects on the dynamic performance off pumping stations," *Elsevier Alexandria Engineering Journal,* vol. 52, pp. 241-248, Mar. 2013.

[10] M. Barakat, M. El Badaoui, and F. Guillet, "Hard competitive growing neural network for the diagnosis of small bearing faults," *Elsevier Mechanical Systems and Signal Processing,* vol. 37, pp. 276-292, Feb. 2013.

[11] L. Frosini and E. Bassi, "Stator current and motor efficiency as indicators for different types of bearing faults in induction motors," *IEEE Trans. Industrial Electronics,* vol. 57, pp. 244-251, Jan. 2010.

[12] I.Y. Onel, M.E.H. Benbouzid, "Induction motor bearing failure detection and diagnosis: Park and Concordia transform approaches comparative study," *IEEE International Electric Machines & Drives Conference (IEMDC 2007),* pp. 1073-1078, (2007).

[13] M. Riera-Guasp, J. Pons-Llinares, F. Vedreno-Santos, J.A. Antonino-Daviu, M. Fernandez-Cabanas, "Evaluation of the amplitudes of high order fault related components in double bar faults," *IEEE International Symposium on Diagnosis for Electrical Machines Power Electronics and Drives (SDEMPED 2011),* pp. 307-315, 2011.

[14] P. Gardel, D. Morinigo-Sotelo, O. Duque-Perez, M. Perez-Alonso, L.A. Garcia-Escudero, "Neural network broken bar detection using time domain and current spectrum data," *20th International Conference on Electrical Machines (ICEM 2012),* pp. 2492-2497, 2012.

[15] S. Bagavathiappan, B.B. Lahiri, T. Saravanan, J. Philip and T. Jayakumar, "Infrared thermography for condition monitoring – A review," *Elsevier Infrared Physics & Technology,* vol. 60, pp. 35-55, Mar. 2013.

[16] V.T. Tran, B.S. Yang, F. Gu, A. Ball, "Thermal image enhancement using bi-dimensional empirical mode decomposition in combination with relevance vector machine for rotating machinery fault diagnosis", *Elsevier Mechanical Systems and Signal Processing,* vol. 38, pp. 601-614, Jul. 2013.

[17] M.J. Picazo-Rodenas, R. Royo, J. Antonino-Daviu and J. Roger-Folch, "Use of the infrared data for heating curve computation in induction motors: Application to fault diagnosis," *Elsevier Engineering Failure Analysis,* vol. 35, pp. 178-192, Dec. 2013.

[18] M. Eftekhari, M. Moallem, S. Sadri and M.-F. Hsieh, "A novel indicator of stator winding inter-turn fault in induction motor using infrared thermal imaging," *Elsevier Infrared Physics & Technology,* vol. 61, pp. 330-336, 2013.

[19] S. Taib, M.S. Jadin and S. Kabir, "Thermal imaging for enhancing inspection reliability detection and characterization," Dr. Raghu V. Prakash, Ed. InTech, 2012, pp. 209-236. Available: http://www.intechopen.com/books/infrared-thermography/thermal-imaging-for-enhancing-inspection-reliability-detection-and-characterization

[20] A. Garcia-Perez, R.J. Romero-Troncoso, E. Cabal-Yepez and R.A. Osornio-Rios, "The application of high-resolution spectral analysis for identifying multiple combined faults in induction motors," *IEEE Trans. Industrial Applications,* vol. 47, pp. 34-46, Jan.-Feb. 2011.

[21] P. Zhang, Y. Du, T.G. Habetler and B. Lu, "A survey of condition monitoring and protection methods for medium voltage induction motors," *IEEE Trans. Industrial Elextronics,* vol. 58, pp. 2002-2010, May 2011.

[22] J. Faiz and M. Ojaghi, "Different indexes for eccentricity faults diagnosis in three-phase squirrel-cage induction motors: A review," *Elsevier Mechatronics,* vol. 60, pp. 35-55, Mar. 2013.

[23] E.C.C. Lau and H.W. Ngan, "Detection of motor bearing outer raceway defect by wavelet packet transformed motor current signature analysis," *IEEE Trans. Instrumentation and Measurement*, vol. 59, pp. 2683-2690, 2010.

[24] Motors and Generators, "ANSI/NEMA MG 1-2003 (R2004) Standards Publication," *National Electrical Manufacturers Association,* Rosslyn, VA, USA, 2011.

[25] A.G. Garcia-Ramirez, L.A. Morales-Hernandez, R.A. Osornio-Rios, J.P. Benitez-Rangel, A. Garcia-Perez and R.J. Romero-Troncoso, "Fault detection in induction motors and the impact on the kinematic chain," *Elsevier Electric Power System Research,* vol. 114, pp. 1-9, 2014.

VIII. Biographies

Armando G. Garcia-Ramirez received the B. E. degree from the Mazatlan Institute of Technology, Mazatlan, Mexico, and the M.E. degree (Hons.) from the University of Guanajuato, Salamanca, Mexico in 2011, where he did research work at the HSPdigital group. Currently, he is a Ph.D. student at the Autonomous University of Queretaro, Queretaro, Mexico. His research interest includes hardware signal processing on field-programmable gate arrays, smart sensors and thermography analysis for applications in mechatronics.

Luis Alberto Morales-Hernandez received the Ph. D. degree in image processing from the Autonomous University of Queretaro, Queretaro, Mexico, in 2009. He is currently a Professor with the department of Electromechanical Engineering, in the University of Queretaro. He is a National Researcher with the Consejo Nacional de Ciencia y Tecnologia level 1. He has more than 20 publications in international journals and conferences. His fields of interest include image processing, computer vision for applications in mechatronics.

Roque A. Osornio-Rios (M'10) received the B.E. degree from the Instituto Tecnologico de Queretaro, Queretaro, Mexico, and the M.E. and the Ph.D. degrees from the University of Queretaro, Queretaro, Mexico, in 2007. He is a National Researcher with CONACYT. He is currently Professor with the University of Queretaro. He was an Advisor of over 30 theses, and a coauthor of over 40 technical papers in international journals and conferences His fields of interest include hardware signal processing and mechatronics. Dr. Osornio-Rios received the "2004 ADIAT National Award on Innovation" for his works in applied mechatronics.

Arturo Garcia-Perez (M'10) received the B.E. and M.E. degrees in electronics from the University of Guanajuato, Salamanca, Mexico, in 1992 and 1994, respectively, and the Ph.D. degree in electrical engineering from the University of Texas at Dallas, Richardson, in 2005. He is currently a Titular Professor with the Department of Electronic Engineering, University of Guanajuato. He is a National Researcher with the Consejo Nacional de Ciencia y Tecnología level 2. He was an Advisor of over 50 theses. His fields of interest include digital signal processing for applications in mechatronics.

Rene de J. Romero-Troncoso (M'07–SM'12) received the Ph.D. degree in mechatronics from the Autonomous University of Queretaro, Queretaro, Mexico, in 2004. He is a National Researcher level 2 with the Mexican Council of Science and Technology, CONACYT. He is currently a Head Professor with the University of Guanajuato and an Invited Researcher with the Autonomous University of Queretaro, Mexico. He has been an advisor for more than 190 theses, an author of two books on digital systems (in Spanish), and a coauthor of more than 100 technical papers published in international journals and conferences. His fields of interest include

hardware signal processing and mechatronics. Dr. Romero–Troncoso was a recipient of the 2004 Asociación Mexicana de Directivos de la Investigación Aplicada y el Desarrollo Tecnológico Nacional Award on Innovation for his work in applied mechatronics, and the 2005 IEEE ReConFig Award for his work in digital systems. He is part of the editorial board of Hindawi's The Scientific World Journal and the International Journal of Manufacturing Engineering.

ANEXO B

Electric Power Systems Research 114 (2014) 1–9

Contents lists available at ScienceDirect

Electric Power Systems Research

journal homepage: www.elsevier.com/locate/epsr

Fault detection in induction motors and the impact on the kinematic chain through thermographic analysis

Armando Guadalupe Garcia-Ramirez [a], Luis Alberto Morales-Hernandez [a], Roque Alfredo Osornio-Rios [a], Juan Primo Benitez-Rangel [a], Arturo Garcia-Perez [b], Rene de Jesus Romero-Troncoso [b,*]

[a] HSPdigital-CA Mecatronica/Facultad de Ingenieria, Campus San Juan del Rio, Universidad Autónoma de Querétaro, Rio Moctezuma 249, Col. San Cayetano, 76807 San Juan del Rio, Queretaro, Mexico

[b] HSPdigital-CA Telematica/Procesamiento Digital de Senales, DICIS, Universidad de Guanajuato, Carr., Salamanca-Valle km 3.5+1.8, Comunidad de Palo Blanco, 36885 Salamanca, Guanajuato, Mexico

ARTICLE INFO

Article history:
Received 14 July 2013
Received in revised form 28 March 2014
Accepted 30 March 2014

Keywords:
Fault diagnosis
Induction motors
Infrared thermography
Kinematic chain
Thermographic analysis

ABSTRACT

Thermographic analysis has been considered a technique that can be used in fault diagnosis with the advantage of being non-invasive and having a wide range of analysis. Nevertheless, other techniques such as motor current signature analysis (MCSA) and vibration analyses are still preferred. Regrettably, these techniques focus only on the detection of specific faults dismissing the repercussion of the induction motor parts and the elements of their kinematic chain. This work presents a methodology based on thermographic image segmentation for fault detection in induction motors, and the repercussion of these faults along the kinematic chain.

1. Introduction

Condition monitoring and fault detection in induction motors have become an important research area due to their widespread use in different industrial applications [1] for instance, induction motor faults are mainly associated with bearing defects [2–8], rotor faults such as broken rotor bars [9–14], mechanical unbalance [15–17], misalignment [18,19] and voltage unbalance [20–22]. However, the methodologies to diagnose these faults are becoming complex and specific, dismissing that the induction motor is always connected to a kinematic chain (pulleys, belts or couplings) [23]. Therefore, a fault in the induction motor has repercussions throughout the linked chain. At present, the most common techniques to monitor and diagnose the induction motor fault conditions are MCSA, vibration and thermography.

MCSA is one of the most used techniques because it is simple, non-invasive and can be automated. In [5–17], MCSA is used for detecting specific electrical and mechanical induction motor faults, using different digital signal processing methodologies. Otherwise, in [24–26] the MCSA technique is used to detect multiple-combined faults. Several signal processing methodologies which use this technique have a heavy computational load only used for detecting the treated faults, ignoring the implication on other links of the kinematic chain, or even other parts of the induction motor. Regarding vibration analysis, it has the advantage of being more sensitive than the MCSA technique for certain faults [15], but it has the disadvantage of being invasive, requiring the installation of an external sensor. Signal processing methodologies for vibration analysis are similar in complexity to those used in the MCSA technique, and they can be automated aiming at fault detection. Despite this, vibration analysis indicates only the presence or the absence of a fault, without considering the collateral effects of faults in the kinematic chain. Currently, these techniques are used to identify specific faults in induction motors. For instance, the fault diagnosis of bearing defects is a widely studied problem [2–6]. The effects of misalignment and unbalance are commonly established for frequency components of the electrical current [18]. Besides, the presence of broken rotor bars is one of the most studied conditions in research literature [9–14]. However, there are no studies on how these faults affect the elements of the kinematic chain.

* Corresponding author. Tel.: +52 464 647 9940; fax: +52 (464) 6479940 ext. 2311.
E-mail addresses: aggarcia@hspdigital.org (A.G. Garcia-Ramirez), lamorales@hspdigital.org (L.A. Morales-Hernandez), raosornio@hspdigital.org (R.A. Osornio-Rios), benitez@uaq.mx (J.P. Benitez-Rangel), agarcia@hspdigital.org (A. Garcia-Perez), troncoso@hspdigital.org (R.d.J. Romero-Troncoso).

http://dx.doi.org/10.1016/j.epsr.2014.03.031
0378-7796/

An induction motor fault is identified by the increment of temperature in the affected component [27]. At the same time, the fault affects other components of the kinematic chain that also increases the temperature which could be identified with the use of thermographic imaging. Hence, infrared thermography has been considered a new technique that can be used in fault diagnosis, because of its capability to measure the temperature on the surface of an induction motor with the advantages of, on one hand, being non-invasive [28]; and on the other hand, being able to globally monitor the induction motor and its kinematic chain by locating hot spots where temperature has been increased. Tran et al. in [29] proposed a diagnosis system with residue using gray-scale transformation and image enhancement to classify faults on the shaft attached to the induction motor. Picazo-Rodenas et al. in [27] used the thermographic analysis to build the thermal model of the induction motor by comparing the results with those corresponding to faulty machines. All the aforementioned works use thermal analysis taking the thermal image without calibration, focusing on induction motor fault detection or local hot spots of the induction motor and where the fault is held, disregarding the impact of these faults in the induction motor and in the whole kinematic chain. Thermographic analysis can be expensive because of the camera, though. Recently, these cameras have become more commercially available at lower prices [30,31], making it possible to enliven this analysis. The presence of faults in the induction motor can damage other parts of the motor and the kinematic chain, these faults may not be considered when a corrective maintenance is done. That is why, it is necessary to develop a methodology based on thermographic analysis which may be capable of identifying the thermal repercussions on the whole kinematic chain under the presence of faults in the induction motor.

This work proposes a thermographic-based methodology using both image segmentation for fault detection and diagnosis in induction motors, as well as the impact of these conditions in the kinematic chain. The contribution of this work is the identification of faults and the study of how the different induction motor conditions affect other elements in an induction motor and its kinematic chain, through the use of thermographic images. These images are thermally calibrated by means of six resistance temperature detectors (RTD) located on the induction motor, and another one is used to measure environmental temperature. The thermographic camera is strategically placed to fully cover in its image field the induction motor and the associated kinematic chain. Although the proposed methodology uses more sensors and a thermographic camera; this technique complements and is capable of improving the MCSA and the vibration methodologies, not only in the induction motor but in its kinematic chain as well. Experimental validation of the proposed methodology is done in two different kinematic chains under five different conditions in an induction motor: bearing defects, broken rotor bar, misalignment, mechanical unbalance, and voltage unbalance. Results show the feasibility of fault detection, as well as the thermal impact of the conditions on the induction motor and the associated kinematic chain.

2. Theoretical background

In this section, three different topics for the induction motor and their kinematic chain analysis through thermographic images are presented: First, the infrared thermography; second, the image segmentation topic and finally, the motor faults and their thermal relationship.

2.1. Infrared thermography

The thermographic camera sensor is an infrared detector whose objectives are to absorb both the energy emitted by the object and the temperature of the surface to be measured, and convert it into a signal. Relying on the Stefan–Boltzmann law, it says that any object emits proportional energy to the surface temperature [27], however, the energy actually detected by the infrared sensor depends on the emissivity coefficient of the surface to be measured, using the concept of Planck law [32]. The infrared thermographic camera can capture an image of the thermal pattern and can be used in several temperature ranges depending on the emissivity of the surface. The thermographic digital image captured by the camera is called a thermogram. Each pixel of a thermogram has a specific temperature value, and the contrast of the image is derived from the differences in temperature of the object surface [33]. It can occur in levels of gray. The colour assignment for each degree of temperature is based on a palette of colours with which it is allowed to view the object temperature. The infrared thermographic analysis has the advantage of offering a two-dimensional signal, through which segmentation is capable of analysing a specific hot spot or small areas [33].

2.2. Image segmentation

Image segmentation is usually defined as the partitioning of an image into non-overlapping constituent regions, which are homogeneous with respect to some characteristics, such as intensity, texture or feature [34–36]. The segmentation can be done manually or automatically. If the domain of the image is given by I, then the segmentation problem is to determine the sets $S_i \in I$ whose union is the entire image I. Thus, the sets that make up segmentation must satisfy Eq. (1).

$$I = \bigcup_{i=1}^{M} S_i \tag{1}$$

where $Si \cap Sj = 0$ for $i \neq j$, and each S_i is connected.

2.3. Motor faults and thermal relationship

Five of the most studied fault conditions are: bearing defects, broken rotor bars, misalignment, mechanical unbalance and voltage unbalance. Bearing defect (BD) is a very common failure in induction motors, producing deterioration in the bearing lubrication and an abnormal friction in the bearing housing. This abnormal friction is reflected in an increase of temperature [37], which propagates into the induction motor and other parts of the kinematic chain. Broken rotor bars consist of a total or partial breakage of bars inside the rotor armour. This fault appears because of welding defects, high strength joints, hot spots and mechanical stresses [27]. When a joint resistance appears in a bar, heat dissipation takes place around that point. On the other hand, broken rotor bar (BRB) is a fault which the detection is important because of its progressiveness. This fault propagates to adjacent bars due to the increment of current and temperature, accelerating the damage in the induction motor [27] and consequently to other elements in the kinematic chain. Misalignment (MAL) is presented when the motor and the load pulleys are not aligned and a mechanical unbalance (UNB) occurs when the mechanical load in the induction motor is not uniformly distributed. These faults can be expressed as an eccentricity in the induction motor, which generates more mechanical stress and excessive rubbing and fatigue of the ball-bearings, causing an increase of torque, decrease of average torque, a decrease of efficiency and a rise of temperature in the induction motor [38]. Consequently, an eccentricity is completely related to the kinematic chain, where the increment of temperature due to this condition is also reflected. Otherwise, voltage unbalance (VUNB) occurs when one or two phases of the line supply are out of phase and a thermal overloading can occur due to voltage variations; as a thumb rule, for every 3.5% voltage unbalance per phase,

the winding temperature increases by 25% in the phase with the highest current [39].

3. Methodology

This section shows the proposed methodology for the diagnosis in three steps as shown in Fig. 1: Firstly, the calibration and validation of the thermographic images through RTD sensors is presented, then the image segmentation of the thermographic images and finally, how this segmentation is interpreted to give a diagnosis.

3.1. Calibration and validation

Calibration consists in comparing the output of the instrument under test against the output of an instrument from known accuracy when the measured quantity is applied to both instruments. The calibration ensures the accuracy of all the instruments and sensors used in environmental conditions that are the same as those under which they were calibrated [40]. First, the RTDs are installed outside the induction motor in several places (T2–T7) as shown in Fig. 2, and another RTD is used to measure the ambient temperature (T1). Then, the calibration of the thermographic camera is performed, taking the instrumentation system of the RTD sensors as reference, with about 60 temperature samples of the motor frame at the thermal steady-state with HLT condition, giving $\mu = 45.4\,^{\circ}C$ and $\sigma = 0.72\,^{\circ}C$, where μ is the mean and σ the standard deviation of the temperature samples. Once the calibration is done, the validation in the induction motor in healthy condition is performed. This validation is based on a difference between the measured temperatures of the thermographic camera and the average of the measured temperatures by the RTDs. The difference between the thermographic camera and the RTDs produces a result of $\pm 1\,^{\circ}C$, due to the standard deviation of the temperature samples.

3.2. Segmentation

The segmentation of thermographic images allows the possibility of a wide analysis of the induction motor and the kinematic chain components. This segmentation is manually done in the thermographic images taken by an infrared camera FLIR A310, with lens of 25 × 19 at a distance of 1.2 m and focused to take into the field of view the complete kinematic chain. The thermographic camera is configured to take thermograms in a temperature range of 19–73 °C for the first kinematic chain and 19–70 °C for the second. It is worthy to notice that when the camera is displaced it produces a displacement in the segmentation regions of interest or in a defocus of the lens. That is why, it is important that when the segmentation and the diagnosis are carried out, the thermographic camera needs to be static. The manual segmentation of the regions of interest on the thermogram allows circumventing further image processing, which is beyond the scope of this research. The thermograms are divided into four thermographic segments to focus the analysis on the useful information.

Two kinematic chains are used for experimentation as shown in Fig. 3. In order to make the segmentation manually; it is necessary to find a hot spot, usually the hottest spot in the thermogram, to establish the conditions for the thermal signature of the motor and the kinematic chain. The first kinematic chain is segmented as shown in Fig. 3a (image) and b (thermogram) with the segments S_1 for the motor frame, S_2 corresponding to the bearing, S_3 to the load pulley, and S_4 to the motor pulley. Fig. 3c (image) and d (thermogram) depict the segmentation of the second kinematic chain where S_1 corresponds to the motor frame, S_2 to the bearing, S_3 to the coupling, and S_4 to the mechanical load.

3.3. Diagnosis

The image segmentation allows a healthy motor signature of thermal conditions to establish at each section, through thermographic images taken during operation of the induction motor under the analysed condition; giving a reference point to a diagnosis. Induction motor fault detection after meeting normal operation temperatures is fairly intuitive without requiring an expert interpretation; because, when an alteration of the thermal conditions in the motor signature appears in the thermographic image, it means that a fault is present. The methodology for the diagnosis is presented in Eq. (2), where i is the index of the thermographic segment to be analysed. Therefore, for this diagnosis: first, the motor signature is acquired with the maximum temperature of each thermographic segment of the induction motor in healthy condition (TH_i), then the maximum temperature of each thermographic segment in faulty condition (TF_i) is obtained in order to grant the thermal coefficient index (TC_i).

$$TC_i = TF_i - TH_i \tag{2}$$

Finally, for each coefficient index TC_i a diagnosis can be obtained, according to the standards in condition monitoring [41]. When there is no defect in the analysed thermographic segment, the coefficient has an approximate value to zero. Moreover, when a fault is presented, the TC_i of the induction motor and the kinematic chain is increased. The objective of TC_i is to identify probable defective parts, even further; it is possible to determine how the fault changes the operating conditions of other parts of the induction motor and the kinematic chain.

4. Experimentation and results

In this section, the experimental setup, treated faults and the results are presented.

4.1. Experimental setup

The experimental setup consists of using the thermal images provided by the thermographic camera and the temperature signals granted by the RTDs located outside the induction motor, and another RTD to measure the environmental temperature in two different kinematic chains. These experimental setups are tested by the diagnostic of the fault conditions mentioned in this work and for asserting the performance of the proposed methodology in the identification of these faults; as well as for identifying the consequent repercussions on the kinematic chain. Fig. 4a shows the experiment setup of the first kinematic chain, where a 1-hp three-phase induction motor (WEG 00136AP3E48T) is used. The kinematic chain in this experiment has two pulleys and a belt as shown in Fig. 4b. The tested motor has two poles, 28 bars and receives a power supply of 220 V AC. The applied mechanical load is of the 100% represented by an ordinary alternator. The external temperature signals are acquired using seven RTDs PT100 model DM-301, from Labfacility LTD. The second kinematic chain has a 2-hp three phase induction motor (WEG 00236ET3E145T-W22), a rigid coupling, and the applied mechanical is a DC generator (BALDOR CDP3604) as depicted in Fig. 4c, comprising around 50% of the mechanical load. A 12-bit 4-channel serial-output sampling analog-to-digital converter ADS7841 from Texas Instrument Incorporated is used in the data acquisition system (DAS). The instrumentation system uses a sampling frequency $f_s = 4$ kHz obtaining 14.4 MS during 60 min of the induction motor from start-up to the thermal steady-state. On the other hand, the thermal images are acquired using a thermographic camera model FLIR A310, from FLIR Systems Incorporated. The thermographic camera takes an image every

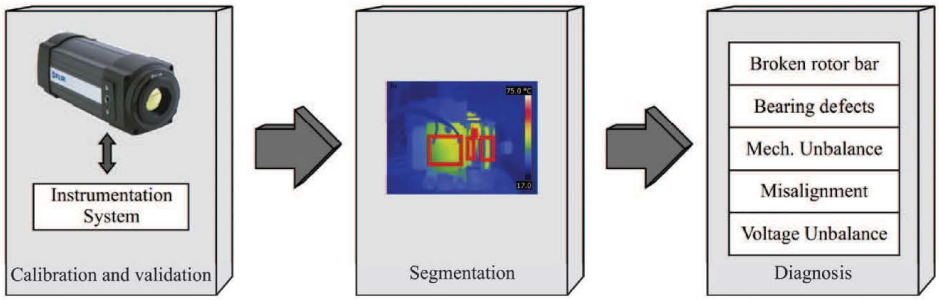

Fig. 1. Proposed methodology.

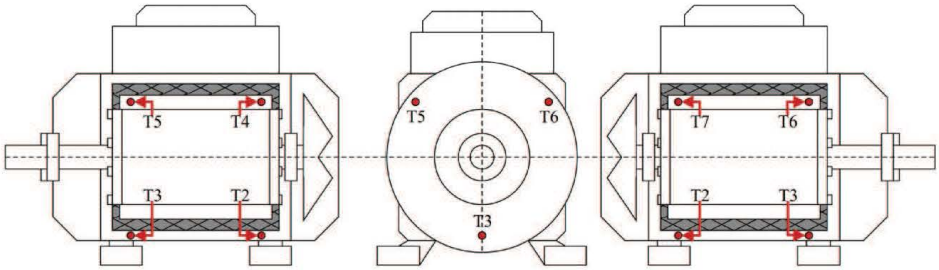

Fig. 2. RTD localization points.

minute during 60 min of the induction motor and their kinematic chain from start-up to the thermal steady-state. The acquired information is stored in a personal computer (PC) and analysed in Matlab which provides the TC_i and the induction motor condition.

4.2. Treated faults

In this work, five different induction motor conditions are studied: BRB at three severities (half-broken rotor bar,

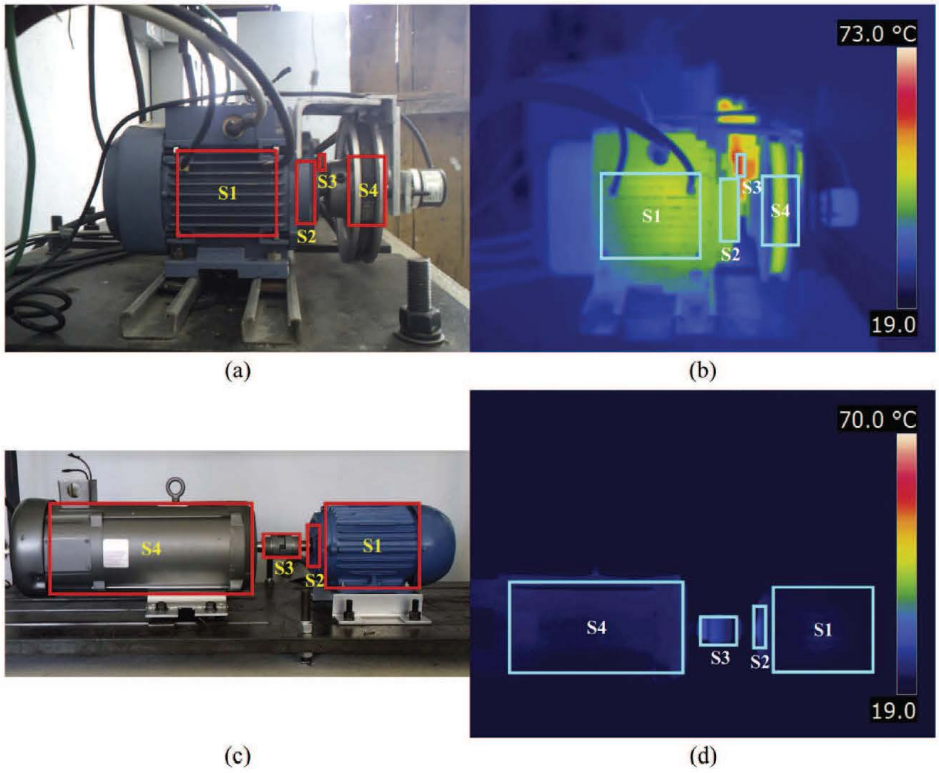

Fig. 3. Thermographic segments: (a) first experimental setup and its (b) thermographic image, (c) second experimental setup and its (d) thermographic image.

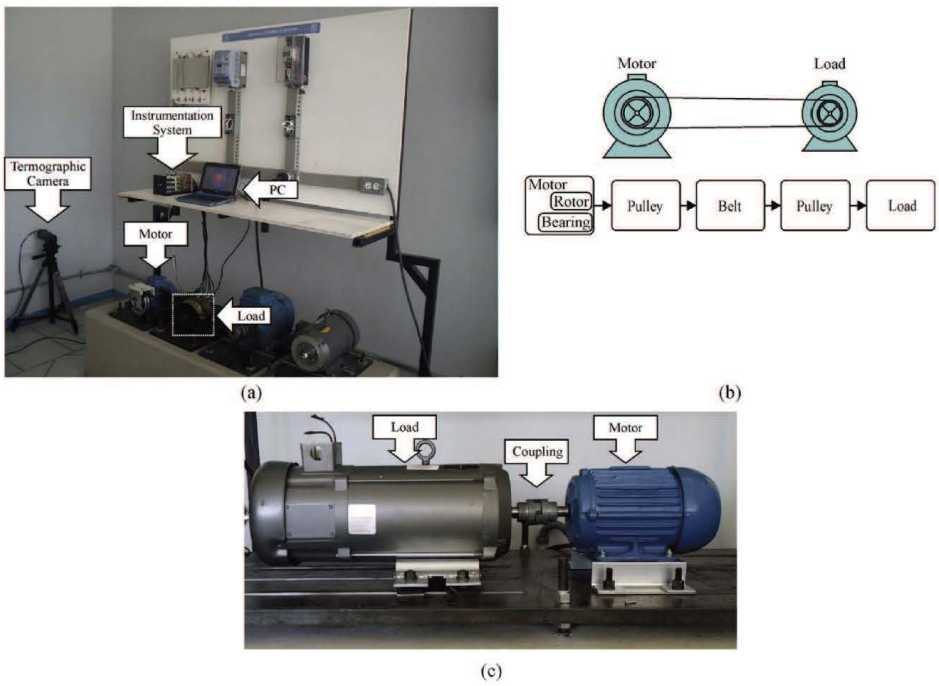

Fig. 4. Experiment: (a) first experimental setup, (b) first experimental kinematic chain, (c) second experimental setup and kinematic chain.

one-broken rotor bar and two-broken rotor bars), BD, UNB, VUNB and MAL.

For the first kinematic chain under test, the half-broken rotor bar (½ BRB) and one-broken rotor bar (1 BRB) conditions were artificially produced by drilling a 2.0 mm, 7.938 mm diameter hole in a rotor bar, respectively, and the two-broken rotor bar (2 BRB) condition was produced by drilling a 7.938 mm diameter hole in a rotor bar and another one in an adjacent rotor bar without harming the shaft of the rotor. Fig. 5a–c show the rotors with ½ BRB, 1 BRB and 2 BRB, respectively, used in the test. The BD condition was made on purpose for the experiment by drilling a 2.0 mm hole in the outer race as shown in Fig. 5d. The UNB condition was produced by attaching a bolt in an arm of the rotor pulley as shown in Fig. 5e. The VUNB of 5% was produced by the connection of a monophasic motor in one of the line supply phases of the induction motor. Finally, the MAL condition was carried out by shifting the band backward in the load pulley, so that the transverse rotation axes for the motor and its load were not aligned. Fig. 5f shows the misaligned motor.

For the second kinematic chain under test, two fault conditions are studied. Firstly, the 1 BRB condition that was artificially produced by drilling a 7.938 mm diameter hole in a rotor bar, without harming the shaft of the rotor, as shown in Fig. 6a. The second tested fault is the BD condition, which was also made on purpose for the experiment by drilling a 2.0 mm hole in the outer race as shown in Fig. 6b.

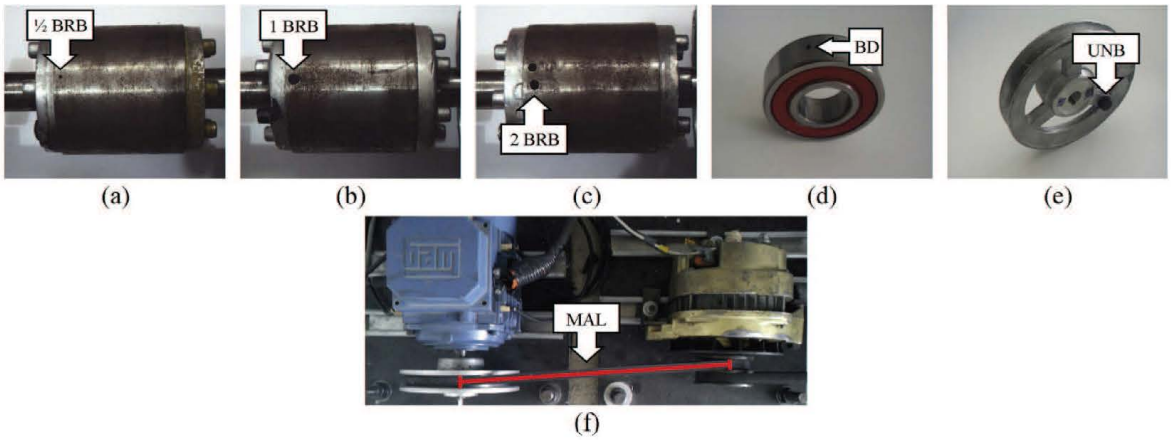

Fig. 5. Treated faults on the first kinematic chain: (a) ½ BRB, (b) 1 BRB, (c) 2 BRB, (d) BD, (e) UNB and (f) MAL.

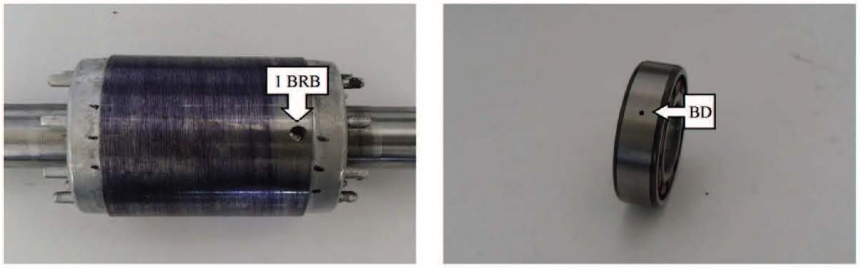

Fig. 6. Treated faults on the second kinematic chain: (a) 1 BRB and (b) BD.

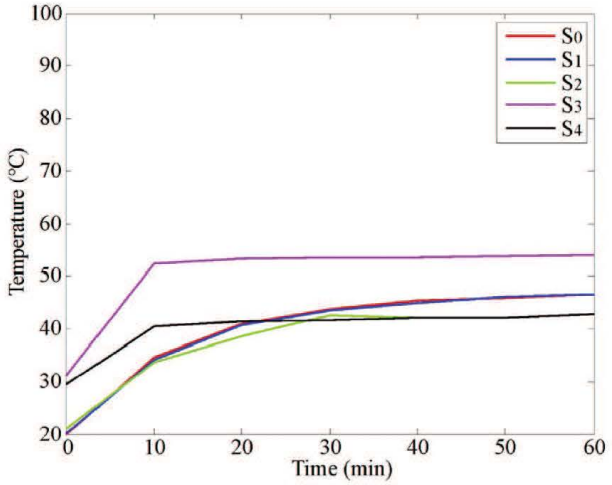

Fig. 7. Healthy motor thermal signature.

4.3. Results

Fig. 7 shows the thermal motor signature of the first kinematic chain acquired during 60 min through thermographic images, with the TH_i of each thermographic segment (S_1–S_4) of the induction motor in healthy condition, and the average of the measured temperatures by the RTDs (S_0) located on the induction motor . It is important to notice that regardless of the induction motor working load, it is necessary to know the reaching time of the thermal steady-state of the kinematic chain in order to determine when to take the thermographic image. Fig. 7 shows that the thermal steady-state is reached after 40 min from the induction motor start-up transient. Based on this analysis, after being determined the healthy motor signature, the faulty motor thermographic images for each study condition with the TF_i of each thermographic segment were taken in the thermal steady-state at minute 40 from the start-up transient as Fig. 8a–i shows for the first kinematic chain and Fig. 9a–c depicts on the second kinematic chain.

In order to evaluate that the thermal analysis can be performed from different perspectives of the camera, Fig. 8i depicts the segmentation of the thermogram under the MAL condition from a different position of the camera than in Fig. 8g. As it can be seen, both thermograms properly cover the induction motor and the whole kinematic chain, where the thermal signatures show the same values for both perspectives in the camera.

For assessing the behaviour of the induction motor and the kinematic chain in the different operating conditions, Eq. (2) is applied to calculate TC_i.

Table 1 shows the temperatures of the thermographic segments and the TC_i results of the first kinematic chain for each induction motor condition. Table 2 shows the temperatures of the thermographic segments and the TC_i results of the first kinematic chain for each induction motor condition with the second perspective where the MAL condition has similar values in the two different perspectives and Table 3 shows the temperature of the thermographic segments and the TC_i results of the second kinematic chain for the treated faults in this experimental setup.

4.4. Analysis and discussion

According to the results of the thermographic segments in the thermographic images, it is possible to propose a criterion of TC_i based on the widely accepted ASTM E1934-99a recommendation [42] to establish a damage relevance criterion that occurs in the induction motor and its kinematic chain as shown in Table 4, where the relevance refers to the action to perform. In the ordinary relevance, there are no anomalies. For slight relevance, it is important to pay attention to the affected areas and to consider a predictive maintenance. On the other hand, for major relevance, it is necessary to consider a preventive maintenance. Finally, for the critical

Table 1
Temperatures of the thermographic segments and TC_i results for each induction motor condition at thermal steady-state on the first kinematic chain.

Condition	Thermographic segments and TC_i (°C)							
	S_1	S_2	S_3	S_4	TC_1	TC_2	TC_3	TC_4
HLT	45	42.2	53.5	42	–[a]	–[a]	–[a]	–[a]
1/2 BRB	51.03	47.83	58.33	47.33	6.03	5.63	4.83	5.33
1BRB	48.43	45.27	58.53	45.67	3.43	3.07	5.03	3.67
2BRB	49.5	44.93	56.37	43.4	4.5	2.73	2.87	1.4
BD	50.3	51.17	53.03	49.3	5.3	8.97	0[b]	7.3
UNB	53.03	48.15	65.53	51.5	8.03	5.95	12.03	9.5
VUNB	42.13	41.1	40.1	48	0[b]	0[b]	0[b]	6
MAL	77.73	70.4	93.27	67.93	32.73	28.2	39.77	25.93

[a] Thermal coefficient indexes TC_i are not defined for the healthy case.
[b] $TC_i = 0$ means that the gradient under the related condition is negligible.

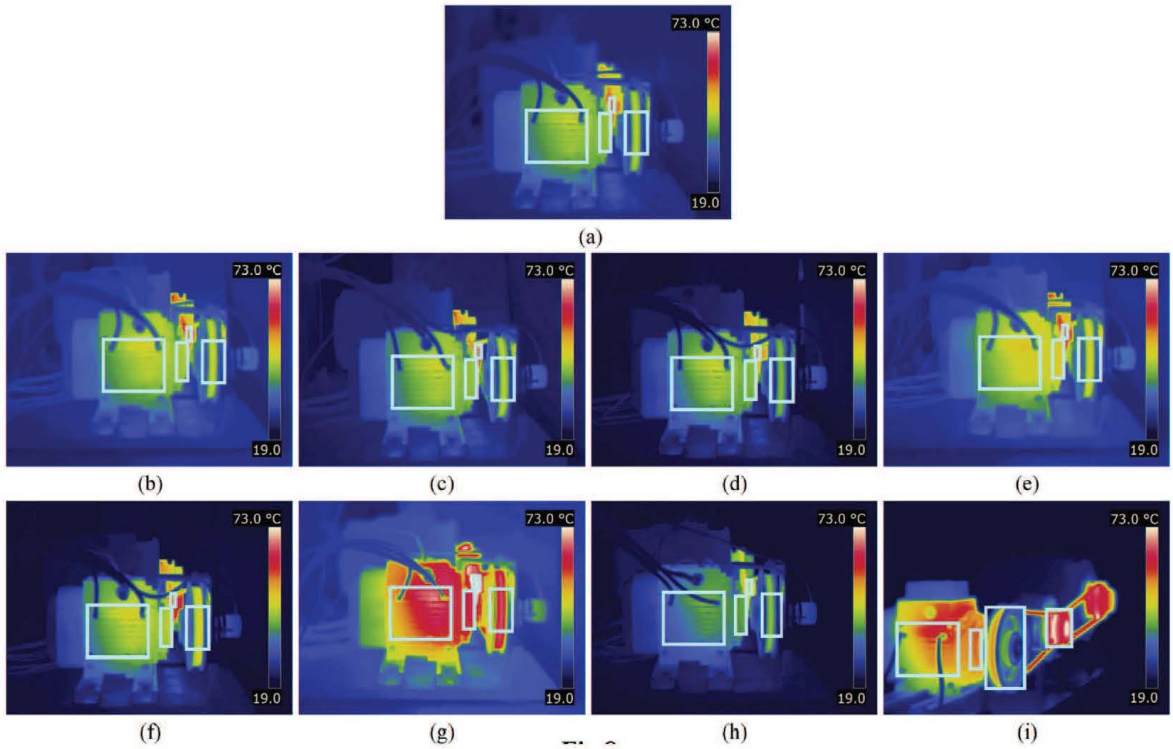

Fig. 8. Thermographic images on the first kinematic chain: (a) HLT, (b) ½ BRB, (c) 1 BRB, (d) 2 BRB, (e) BD, (f) UNB, (g) MAL, (h) VUNB and (i) another perspective of MAL.

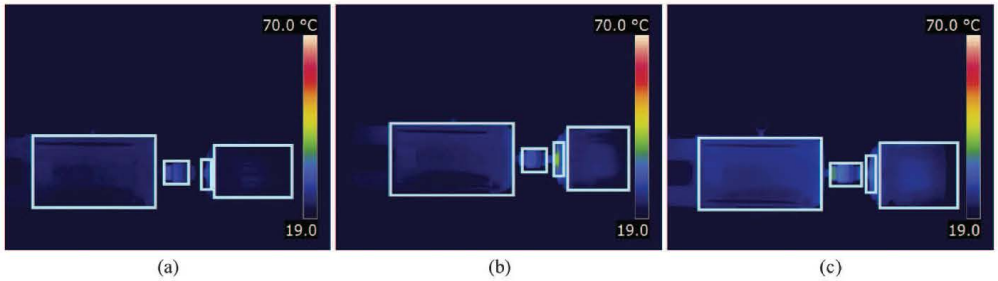

Fig. 9. Thermographic images on the second kinematic chain: (a) HLT, (b) 1 BRB and (c) BD.

Table 2
Temperatures of the thermographic segments and TC_i results for each induction motor condition at thermal steady-state on the first kinematic chain with the second perspective.

Condition	Thermographic segments and TC_i (°C)							
	S_1	S_2	S_3	S_4	TC_1	TC_2	TC_3	TC_4
HLT	45	42.2	53.5	42	–[a]	–[a]	–[a]	–[a]
MAL	75.41	65	77.5	65.45	22.8	24	39.77	23.45

[a] Thermal coefficient indexes TC_i are not defined for the healthy case.

Table 3
Temperatures of the thermographic segments and TC_i results for each induction motor condition at thermal steady-state on the second kinematic chain.

Condition	Thermographic segments and TC_i (°C)							
	S_1	S_2	S_3	S_4	TC_1	TC_2	TC_3	TC_4
HLT	24	30.6	31	25.2	–[a]	–[a]	–[a]	–[a]
BRB	27.7	41.1	35.6	27.2	3.7	10.5	4.6	2
BD	27.8	36.1	37.7	29.1	3.8	5.5	6.7	3.9

[a] Thermal coefficient indexes TC_i are not defined for the healthy case.

Table 4
Damage relevance.

Criterion	Relevance
$TC_i \leq 5$	Ordinary
$5 < TC_i \leq 15$	Slight
$15 < TC_i \leq 30$	Major
$TC_i > 30$	Critical

relevance the process must stop immediately and proceed to a corrective maintenance.

Therefore, it is important to analyse how each fault affects the induction motor, its components and the kinematic chain. In the first kinematic chain, for different severities of broken rotor bars, the TC_i for each thermographic segment shows a non-monotonic behaviour from ½ BRB and up to 2 BRB. This non-monotonic behaviour means that the value of TC_i does not reflect the severity in a proportional relationship with the broken rotor bar fault. However, TC_i permits to establish a general diagnosis methodology for broken rotor bars because TC_i shows that from ½ BRB and up, significant differences in the thermal behaviour at the induction motor and its kinematic chain are observed. This condition has an ordinary relevance on S_3 and slight relevance for S_1, whereas S_2 and S_4 are the most affected components under this condition. These results suggest a predictive maintenance on the induction motor. For BD, results show that the most affected areas are S_2 and S_4; where, due to the abnormal friction on the bearing, it increases its temperature as well as its closest component S_4, affecting their TC_i. S_1 and S_3 under BD condition which have an ordinary relevance. These results mean that it is mandatory to make a bearing replacement during the next programmed maintenance cycle. On the other hand, UNB results show slight relevance in all the motor and the kinematic chain, being S_3 and S_4 the most affected components, without leaving aside S_2 due to an increment in S_4 temperature that is transmitted to S_2. In this condition the induction motor has an abnormal behaviour, due to a slight eccentricity and it is important to attend the affected components in the next maintenance cycle. For VUNB, results show an ordinary relevance in S_1, S_2 and S_3, being S_4 the component with a slight relevance. Under this condition, it is worthy to notice that the TC_is show an ordinary and a slight relevance. Then, at this point it is important to schedule a predictive maintenance including the monitoring of the voltage balance to assess whether the TC_is are due to VUNB or to a faulty condition. Finally, MAL is the most critical condition where results show a major relevance in S_2 and S_4, and a critical relevance in S_1 and S_3, which can potentially damage the kinematic chain, the bearings, and most critically, the induction motor. For this condition, the process must stop immediately to proceed to a corrective maintenance of each part of the induction motor and their kinematic chain: stator windings, rotor, bearings, pulleys, belts and consider a realignment of the kinematic chain.

Otherwise, in the second kinematic chain for 1 BRB the TC_i indicates that this condition has an ordinary relevance on all the parts except in S_2 with a slight relevance. Based on the results of the TC_i, the suggestion is to consider a predictive maintenance on the induction motor. For BD, results show that as well as the first kinematic chain, the most affected areas are S_2 and S_3. Due to the abnormal friction on the bearing, its temperature increases, affecting the TC_i of its closest component S_3. Regarding the S_1 and S_4, under BD condition they have an ordinary relevance. In this condition, it is important to consider replacing the bearing.

Furthermore, to apply this methodology it is important to know the thermal signature at the healthy condition of the induction motor and its kinematic chain with the applied working load. Because within any test bench these parameters are different as well as the TC_i; although, the proposed methodology can be applied in order to analyse the segments of interest with their TC_i and diagnose the fault with the damage relevance criterion.

A meaningful characteristic of the proposed methodology is the advantage of indicating the action to take in the affected components and the capability of monitoring the whole kinematic chain. Therefore, this method provides a rise to evaluate multiple combined faults in further works with the combination of different TC_i in the induction motor and its kinematic chain. Another characteristic is the maximum temperature extraction for each thermographic segment, due to the simplicity to analyse single data, different from the reviewed literature which focuses on hot-spots [18,27]. The instrumentation system helps to verify this characteristic, because the behaviour of the average temperature provided by the RTDs is similar to the temperatures given by the thermographic camera.

Care must be taken to choose the spatial resolution of a thermal imaging system, detector size, distance to the object, lens system and a pinpoint calibration of the thermographic camera. When analysing the kinematic chain, other factors can affect measurements such as the environmental temperature, the distance from the thermographic camera to the objects, the colour of the objects and set of signature values for objects previously obtained without any fault.

5. Conclusions

This work proposes a methodology based on thermographic image segmentation for fault detection in induction motors, and the repercussion of these conditions in the critical components of the kinematic chain. The proposed methodology is based on the widely accepted ASTM E1934-99a recommendation, establishing a criterion of the thermal coefficient index TC_i of each thermographic segment, contrary to other reviewed works that do not mention it. This methodology is based on thermal calibration of the thermographic camera through RTDs which, despite the use of more sensors than MCSA and vibrations, the proposed methodology complements the standard techniques and could help to improve the overall diagnosis. The functionality of the methodology has been tested in five typical conditions for an induction motor, using criteria which indicate the relevance and the action to perform under the different conditions. Otherwise, based on the analysis and discussion of the results when maintenance is performed, a voltage balance monitoring is recommended to discard the voltage unbalance as the source of the thermal disturbance in the thermographic image. Furthermore, it is important to highlight that this criterion can be applied on any induction motor at the thermal steady-state, after having the healthy condition thermal signature with its working load.

Finally, the simplicity of this methodology for industrial applications allows the fault detection as well as a wide analysis of the induction motor and its kinematic chain, benefiting in maintenance time and it can be used in the analysis of other electrical machines establishing their own criteria. However, for future development, it is proposed to design a tool for automatic segmentation as well as a smart instrument for fault identification.

References

[1] D.J. Siyambalapitiva, P.G. Mclaren, Reliability improvement and economic benefits of on-line monitoring systems for large induction machines, IEEE Trans. Ind. Electron. 26 (1990) 1018–1025.
[2] M.D. Prieto, G. Cirrincione, A.G. Espinosa, J.A. Ortega, H. Henao, Bearing fault detection by a novel condition-monitoring scheme based on statistical-time features and neural networks, IEEE Trans. Ind. Electron. 66 (2013) 3398–3407.

[3] A. Bellini, F. Filippetti, C. Tassoni, G.A. Capolino, Advances in diagnostic techniques for induction machines, IEEE Trans. Ind. Electron. 55 (2008) 4109–4126.
[4] B. Zhang, C. Sconyers, C. Byington, C. Patrick, M.E. Orchad, G. Vachtsevanos, A probabilistic fault detection approach: application to bearing fault detection, IEEE Trans. Ind. Electron. 58 (2011) 2011–2018.
[5] L. Frosini, E. Bassi, Stator current and motor efficiency as indicators for different types of bearing faults in induction motors, IEEE Trans. Ind. Electron. 57 (2010) 244–251.
[6] J.R. Stack, T.G. Habetler, R.G. Harley, Fault classification and fault signature production for rolling element bearings in electric machines, IEEE Trans. Ind. Appl. 40 (2004) 735–739.
[7] I.Y. Onel, M.E.H. Benbouzid, Induction motor bearing failure detection and diagnosis: Park and Concordia transform approaches comparative study, IEEE/ASME Trans. Mechatron. 13 (2008) 257–262.
[8] V.K. Rai, A.R. Mohanty, Bearing fault diagnosis using FFT of intrinsic mode functions in Hilbert–Huang transform, Mech. Syst. Signal Process. 21 (2007) 2607–2615.
[9] S.H. Kia, H. Henao, G.A. Capolino, Diagnosis of broken-bar fault in induction machines using discrete wavelet transform without slip estimation, IEEE Trans. Ind. Appl. 45 (2009) 1395–1404.
[10] M. Riera-Guasp, J. Pons-Llinares, F. Vedreno-Santos, J.A. Antonino-Daviu, M. Fernandez-Cabanas, Evaluation of the amplitudes of high order fault related components in double bar faults, IEEE Inter. Symp. Diagn. Electr. Mach. Power Electron. Drives (2011) 307–315.
[11] J.A. Antonino-Daviu, S. Aviyente, E.G. Strangas, M. Riera-Guasp, J. Roger-Folch, R.B. Perez, An EMD-based invariant feature extraction algorithm for rotor bar condition monitoring, IEEE Inter. Symp. Diagn. Electr. Mach. Power Electron. Drives (2011) 669–675.
[12] P. Gardel, D. Morinigo-Sotelo, O. Duque-Perez, M. Perez-Alonso, L.A. Garcia-Escudero, Neural network broken bar detection using time domain and current spectrum data, in: Proc. 20th Inter. Conf. of Electr. Mach. Drives., 2012, pp. 2492–2497.
[13] M. Pineda-Sanchez, M. Riera-Guasp, J.A. Antonino-Daviu, J. Roger-Folch, J. Perez-Cruz, R. Puche-Panadero, Instantaneous frequency of the left sideband harmonic during the start-up transient: a new method for diagnosis of broken bars, IEEE Trans. Ind. Electron. 56 (2009) 4557–4570.
[14] L.M. Rabelo-Baccarani, J.P. Braga-Tavares, B. Rodrigues-Menezes, W. Matos-Caminhas, Sliding mode observer for on-line broken rotor bar detection, Electr. Power Syst. Res. 80 (2010) 1085–1089.
[15] C. Kral, T.G. Habetler, Detection of mechanical imbalances of induction machines without spectral analysis of time-domain signals, IEEE Trans. Ind. Appl. 40 (2004) 1101–1106.
[16] S.K. Ahamed, S. Karmakar, M. Mitra, S. Sengupta, Novel diagnosis technique of mass unbalance in rotor of induction motor by the analysis of motor starting current at no load through wavelet transform, Int. Conf. Electr. Comput. Eng. (2009) 474–477.
[17] C. Kral, H. Kapeller, J.V. Gragger, F. Pirker, G. Pascoli, Detection of mechanical imbalances during transient torque operating conditions, IEEE Inter. Symp. Diagn. Electr. Mach. Power Electron. Drives (2005) 1–4.
[18] J.M. Bossio, G.R. Bossio, C.H. De Angelo, Angular misalignment in induction motors with flexible with flexible coupling, in: IEEE 35th Annu. Conf. of Ind. Electron, 2009, pp. 1033–1038.
[19] T.H. Patel, A.K. Darpe, Experimental investigations on vibration response of misaligned rotors, Mech. Syst. Signal Process. 23 (2009) 2236–2252.
[20] M.E.H. Benbouzid, M. Vieira, C. Theys, Induction motors' faults detection and localization using stator current advanced signal processing, IEEE Trans. Power Electron. 14 (1999) 14–22.
[21] H. Nejjari, M.E.H. Benbouzid, Monitoring and diagnosis of induction motors electrical faults using a current Park's vector pattern learning approach, IEEE Trans. Energy Convers. 19 (2004) 657–662.
[22] J. Faiz, H. Ebrahimpour, P. Pillay, Influence of unbalanced voltage on the steady-state performance of a three-phase squirrel-cage induction motor, MDPI-Sens. 12 (2012) 11989–12005.
[23] W.M. Hwang, Y.W. Hwang, An algorithm for the detection of degenerate kinematic chains, Math. Comput. Model. 11 (1991) 9–15.
[24] A. Garcia-Perez, R.J. Romero-Troncoso, E. Cabal-Yepez, R.A. Osornio-Rios, The application of high-resolution spectral analysis for identifying multiple combined faults in induction motors, IEEE Trans. Ind. Electron. 58 (2011) 2002–2010.
[25] A.G. Garcia-Ramirez, R.A. Osornio-Rios, D. Granados-Lieberman, A. Garcia-Perez, R.J. Romero-Troncoso, Smart sensor for online detection of multiple-combined faults in VSD-fed induction motors, MDPI-Sens. 12 (2012) 11989–12005.
[26] A. Lebaroud, G. Clerc, Classification of induction machine faults by optimal time-frequency representations, IEEE Trans. Ind. Electron. 55 (2008) 4290–4298.
[27] M.J. Picazo-Rodenas, R. Royo, J. Antonino-Daviu, J. Roger-Folch, Use of the infrared data for heating curve computation in induction motors: application to fault diagnosis, Eng. Fail. Anal. 35 (2013) 178–192.
[28] B.S. Yang, A. MD, Intelligent fault diagnosis of rotating machinery using infrared thermal image, Expert Syst. Res. 39 (2012) 2082–2091.
[29] V.T. Tran, B.S. Yang, F. Gu, A. Ball, Thermal image enhancement using bi-dimensional empirical mode decomposition in combination with relevance vector machine for rotating machinery fault diagnosis, Mech. Syst. Signal Process. 38 (2013) 601–614.
[30] http://www.fluke.com/fluke/m3en/Ti105.htm?PID=74966, (27.03.14).
[31] http://www.flir-webshop.com/en/electrical-mechanical/flir-i3-130.html, (27.03.14).
[32] G.C. Holst, Common Sense Approach to Thermal Imaging, PM86, SPIE press monograph, Winter Park, Florida, 2000.
[33] S. Taib, M.S. Jadin, S. Kabir, in: R.V. Prakash (Ed.), Thermal Imaging for Enhancing Inspection Reliability: Detection and Characterization, InTech, Rijeka, Croatia, 2012, pp. 209–236.
[34] R.C. Gonzalez, R.E. Woods, Digital Image Processing, 3rd ed., Prentice Hall, New Jersey, 2008.
[35] R.M. Haralick, L.G. Shapiro, Image segmentation techniques, Comput. Vis. Graph. Image Process. 29 (1985) 100–132.
[36] N.R. Pal, S.K. Pal, A review on image segmentation techniques, Pattern Recognit. 26 (1993) 1277–1294.
[37] P. Zhang, Y. Du, T.G. Habetler, B. Lu, A survey of condition monitoring and protection methods for medium-voltage induction motors, IEEE Trans. Ind. Appl. 47 (2011) 34–46.
[38] J. Faiz, M. Ojaghi, Different indexes for eccentricity fault diagnosis in three-phase squirrel-cage induction motors: a review, Mechatronics 19 (2009) 2–13.
[39] A. Siddique, G.S. Yadava, B. Singh, A review of stator fault monitoring techniques of induction motors, IEEE Trans. Energy Convers. 20 (2005) 106–114.
[40] A.S. Morris, R. Langari, in: Butterworth Heinemann (Ed.), Measurement and Instrumentation. Theory and Application, Academic Press, California, 2012, pp. 103–114.
[41] S. Bagavathiappan, B.B. Lahiri, T. Saravanan, J. Philip, T. Jayakumar, Infrared thermography for condition monitoring – a review, Infrared Phys. Technol. 60 (2013) 35–55.
[42] Standard Guide for Examining Electrical and Mechanical Equipment with Infrared Thermography, ASTM E1934-99a, 2010.

ANEXO C

FPGA-based Smart-sensor for Fault Detection in VSD-fed Induction Motors

A.G. Garcia-Ramirez, R.A. Osornio-Rios, *Member*, *IEEE*, A. Garcia-Perez, *Member*, *IEEE*, R.J. Romero-Troncoso, *Senior Member*, *IEEE*.

***Abstract* – Nowadays, different industrial processes use induction motors fed through variable speed drives (VSD). In order to improve these processes, the industry demands the use of smart sensors to detect the faults, reduce the cost of maintenance, and decrease power consumption. In this work, broken rotor bars, unbalance and misalignment are automatically detected in induction motors fed by a VSD using the three current phases online, with a smart sensor. The proposed smart sensor is implemented in a field programmable gate array offering a low computational load methodology, low-cost, and portable solution for fault detection in induction motors VSD-fed. Results show a high effectiveness detection of the treated faults.**

***Index Terms*--Fault detection; Field programmable gate arrays; Induction motors; Variable speed drives.**

I. INTRODUCTION

INDUCTION motors are key elements in industry due to their robustness, easy construction, low cost and versatility, representing 85% of power consumption worldwide. Consequently, early fault detection in induction motors is one of the most important subjects for industry [1], because these faults may produce unanticipated interruptions on product lines, with severe consequences in product quality, such as safety and cost. Therefore, the detection of incipient faults has attracted the interest of many researchers in recent years [2]. Around 40% to 50% of induction motor faults are bearing related, rotor faults represent 5% to 10% and unbalance and misalignment faults are about 12% [3]. Furthermore, connection of induction motors through variable speed drives (VSD), allows extending their useful life, and saving energy, but making the detection of faults more difficult due to the spurious harmonics induced by the VSD operation [4]. Moreover, the extensive use of VSD allows new possibilities for the on-line detection of faults [5]. Concerning to fault detection in induction motors, a number of techniques had been proposed. For instance, in [6] Shahin *et al.* investigate the recent advances on digital signal processing techniques for induction motors diagnosis. These techniques cover the frequency domain as the fast Fourier transform (FFT), the zoom-FFT, the chirp Z-transform, and the time-frequency domain such as multiple signal classification (MUSIC), short time Fourier transform, wavelet transform, etc. The best technique is chosen depending on the physical phenomena to observe. Garcia-Perez *et al.* [3] proposed a methodology which combines a filter bank of finite impulse response (FIR) filters with high resolution spectral analysis based on MUSIC for detecting multiple combined faults, with current and vibration signals. The results show the analytical predetermined fault frequency location for single, two or three combined faults (broken rotor bars, unbalance and bearings damage). In [7], it is proposed an artificial neural network (ANN) methodology to detect broken rotor bars (BRB) with statistical patterns of time-domain data, current spectrum and the combination of two ANN inputs to classify the motor condition. Riera-Guasp *et al.* [8] studies the relation between the amplitude of the components of the air-gap fault field produced by a double bar breakage and the relative position of the broken bars. Otherwise, [9] describes a method for the diagnosis and detection of BRB and bearing damage in induction motors by motor current signal analysis and multiple features extracted from transformations on current and voltage signals, using the hidden Markov model as classifier. Regarding the unbalance condition (UNB), Kral *et al.* in [10] proposed a technique to sense the specific modulation of the electric power of faults such as eccentricities as well as load torque perturbation without using the frequency spectrum. Otherwise, in [11] the misalignment condition (MAL) is computed by the FFT extracting the unique vibration features exhibited in the full spectrum. All the aforementioned works, need a heavy computational load and can be difficult to implement on hardware for online operation because most of these techniques requires offline processing and an expert technician for interpreting results. In [12], two techniques namely Park transform approach and Concordia transform are presented and compared for the detection of bearing damage in induction motors. The results of this work show that these techniques are valid to identify faulty patterns making suitable for hardware implementation, such as a smart sensor.

A smart sensor is a device that includes primary sensors,

This work was supported in part by FOFIUAQ2012, under ACAEC188088 CONACyT-2012 and by CONACyT under Scholarship 229736.

R. J. Romero-Troncoso is with HSPdigital CA-Telematica at DICIS, University of Guanajuato, Salamanca, Gto. 36885 Mexico (corresponding author; e-mail: troncoso@hspdigital.org).

A.G. Garcia-Ramirez is with HSPdigital CA-Mecatronica at Facultad de Ingenieria, Campus San Juan del Rio, Universidad Autonoma de Queretaro, San Juan del Rio, Qro. 76807 Mexico (e-mail: aggarcia@hspdigital.org).

R.A. Osornio-Rios is with HSPdigital CA-Mecatronica at Facultad de Ingenieria, Campus San Juan del Rio, Universidad Autonoma de Queretaro, San Juan del Rio, Qro. 76807 Mexico (e-mail: raosornio@hspdigital.org).

A. Garcia-Perez is with HSPdigital CA-Procesamiento Digital de Señales at DICIS, University of Guanajuato, Salamanca, Gto. 36885 Mexico (e-mail: arturo@salamanca.ugto.mx).

978-1-4799-0025-1/13/$31.00 ©2013 IEEE

signal processing, communication, and integration capabilities. The term "smart sensor" is employed according to the functionality classification. Nowadays the use of smart sensors improves the monitoring system demands due to their features in communication and data processing functionalities, and their versatility and ability to work in environments where the access for field workers is limited [13].

In this work the development of a smart sensor, based on a field-programmable gate array (FPGA), for automatic and online detection of faults in induction motor fed through VSD is presented, covering operating frequencies from as low as 3 Hz and up to 60 Hz. The methodology used in this work is based on the Park transform that converts the *ABC* current system to the *D-Q* current system, having the advantage of a lower computational load than the FFT and other spectrum-based methodologies; then the magnitude of the *DQ* current system and the mean are calculated to be the inputs of an artificial neural network, which gives the identification of the fault. Three different faults on induction motor: broken rotor bars, unbalance and misalignment are investigated, and the results show the potentiality of the smart sensor to classify the induction motor faults, automatically and online.

II. THEORETICAL BACKGROUND

A. *Park Transform*

The Park transform, permits to express the three current phases of an induction motor through a two-axis system in quadrature. The components of this system: direct and quadrature (i_D and i_Q), are given by (1) and (2), respectively:

$$i_D = \sqrt{\frac{2}{3}} i_A - \sqrt{\frac{1}{6}} i_B - \sqrt{\frac{1}{6}} i_C \quad (1)$$

$$i_Q = \sqrt{\frac{1}{6}} i_B - \sqrt{\frac{1}{6}} i_C \quad (2)$$

Where, i_A, i_B and i_C are the stator current phases [14]. Using (1) and (2) the transformation of the stator current phases *ABC* to the *D-Q* system is very simple. Fig. 1 shows the Lissajous figures of the current in *D-Q* system for a healthy motor (Fig. 1a) and a faulty motor (Fig. 1b).

B. *Induction Motor Faults*

This work focuses on three different faulty conditions: broken rotor bars (BRB), misalignment (MAL) and unbalance (UNB).

The BRB fault appears because of welding defects, high strength joints, expansion and mechanical stresses [15]. The presence of BRB in induction motors produces several problems, such as power quality degradation [16]. On the other hand, MAL is presented when the motor and the load pulleys are not aligned. The MAL fault can cause over 70% of the rotating machinery vibration problems, and it is the second most commonly fault in rotating machines [11]. Finally, the UNB condition is presented when the rotor weight is not uniformly distributed around its geometrical center, which means that the center of mass is not on the center of rotation. The UNB condition is the most observed fault in induction motors, and if is not attended, the results for the machinery can be catastrophic [10].

C. *Artificial Neural Networks*

An Artificial Neural Network (ANN) is a computational model that provides a method to characterize synthetic neurons to solve problems in the same way as the human brain [1]. The most popular architecture for ANN is the multilayer feed-forward networks (MFN), which has an input layer, one or more hidden layers and an output layer. In this architecture, the data goes in one direction, from the input layer through the hidden layer to the output layer, as shown in Fig. 2.

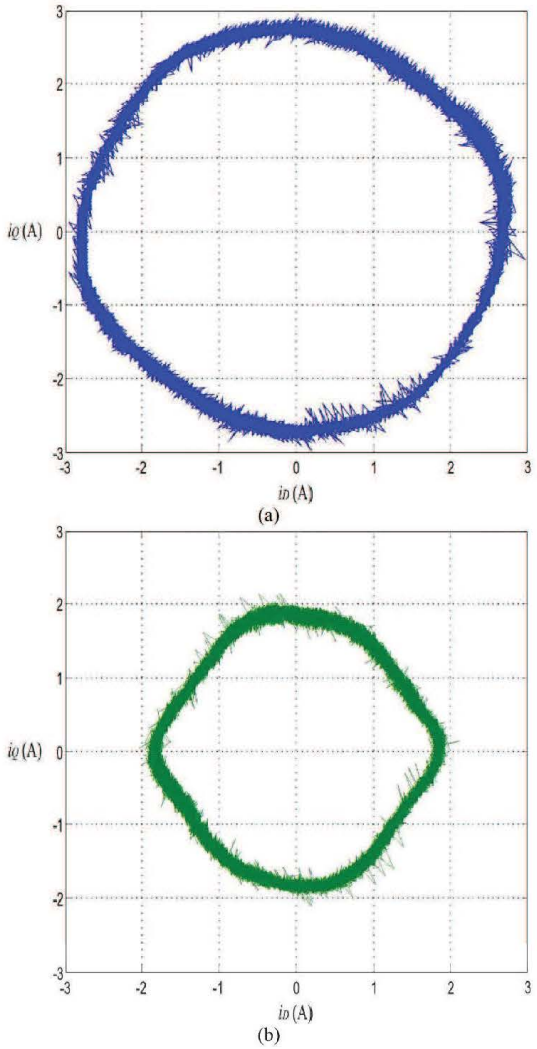

Fig. 1. Lissajous figures of the *D-Q* system current of (a) Healthy motor, and (b) Faulty motor.

Where, X_i (i = 1,2,3,...,n) are inputs and Y_i (i = 1,2,3,...,m) are outputs. The back-propagation algorithm (BPA), is the most conventional method to train an MFN, which is a supervised learning method, that consists on mapping the process inputs to the desired outputs by minimizing the error between the desired outputs and the calculated outputs [17]. The MFN is an excellent candidate to be implemented in FPGA, due to its simplicity, practicality and low computational load [18].

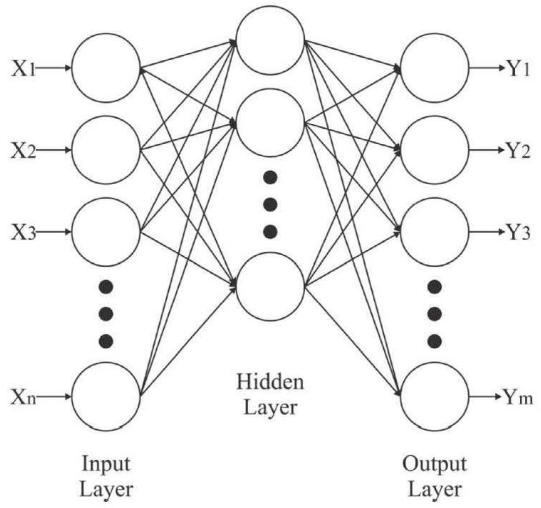

Fig. 2. Multilayer feed-forward network architecture.

III. METHODOLOGY

The methodology is based on the Park transform that allows representing the three current phases of an induction motor in a two-dimensional system. Fig. 3 shows the Lissajous figure obtained from the Park transform. Then, through a magnitude calculation (3) of each k sample, as shown also in Fig. 3, the D-Q system is translated to a vector $i_{DQ\text{-}k}$ that is the resultant representation of the Lissajous figure. In Fig. 4 the $i_{DQ\text{-}k}$ vector is presented. Afterward, by a mean computation (4) of the $i_{DQ\text{-}k}$ vector, the average radius of the Lissajous figure can be taken. This mean value of the $i_{DQ\text{-}k}$ vector is also presented in Fig. 4. Finally, the data from the mean computation is an input of the proposed ANN which delivers the motor condition.

$$i_{DQ-k} = \sqrt{i_{D-k}^2 + i_{Q-k}^2} \tag{3}$$

$$Mean = \frac{1}{L}\sum_{k} i_{DQ-k} \tag{4}$$

Where, L is the length of the $i_{DQ\text{-}k}$ vector.

A. Proposed Artificial Neural Network

The proposed ANN implements an MFN with three inputs nodes that receive the mean calculation of the i_{DQ} vector in each treated frequency, thirty nodes in the hidden layer and four output nodes for the detection of: healthy condition (HLT), broken rotor bars (BRB), unbalance (UNB) and misalignment (MAL). The output nodes correspond to each fault condition.

IV. EXPERIMENT

A. Experimental Setup

The steady-state current signal provided by a VSD (model WEG CFW08) connected to the induction motor is used for detecting the faults and to classify them. The VSD has an operation range from 0 Hz to 100 Hz using a frequency resolution of 0.01 Hz. In Fig. 5(a) the experimental setup is shown, where one 1-hp three-phase induction motors (model WEG 00136APE48T) is used to test the performance of the proposed methodology to identify the fault conditions considered in this work. The rotational speed of the motor is controlled by a VSD at 3Hz, 30Hz and 60Hz. The tested motors have two poles, twenty eight bars and receive a power supply of 220 V AC. The applied mechanical load is from an ordinary alternator, which represents a quarter of load for the motor. The three-phase current signals are acquired using three hall-effect sensors model L08P050D15, from Tamura Corporation. A 16-bit 4-channerl serial-output sampling analog-to-digital converter ADS8341 from Texas Instrument Incorporated is used in the data acquisition system (DAS). The instrumentation system which was calibrated through the Fluke 435 that uses a sampling frequency f_s = 12 KHz obtains 120,000 samples of each current phase during 10 seconds of the induction motor steady-state. The motor start-up is controlled by a relay to automate the test run. Fig. 5(b) shows the proposed smart sensor for induction motor fault detection. The three current phases of the induction motor fed by VSD are acquired by the hall-effect sensors; then it is conditioned and analog-to-digital (A/D) converted in the DAS. Afterwards, in a smart unit implemented into a proprietary Spartan 3E XC3S1600 FPGA platform running at 48 MHz, the three digital current phases are transformed in i_D and i_Q phases by the Park transform. Then, the magnitude (3) and the mean of this magnitude (4) are calculated to be a single data for an input of an ANN which gives the induction motor condition. However, the current magnitude depends on the load and the motor power; then, to minimize the undesired effects of magnitude variation that could modify the diagnosis, the ABC current signals are normalized before the Park transform is applied. Fig. 6 shows the mean calculation of the i_{DQ} vector obtained by each fault condition in the three studied frequencies Table I summarizes the resource usage of the FPGA.

B. Investigated Faults

The BRB condition was artificially produced by drilling a 7.938mm diameter hole in a rotor bar without harming the

shaft of the rotor. Fig. 7(a) shows the rotor with the BRB condition used in the test. The misalignment condition (MAL) was carried out by shifting forward the band in the alternator pulley, so that the transverse axes of rotation for the motor and its load were not aligned. Fig. 7(b) shows the misaligned motor. The UNB test was produced by attaching a bolt in an arm of the rotor pulley as shown in Fig. 7(c).

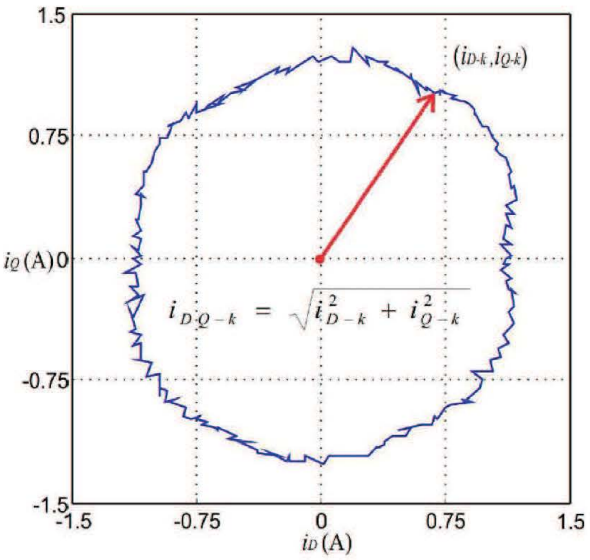

Fig. 3. Lissajous figure obtained from the Park transform.

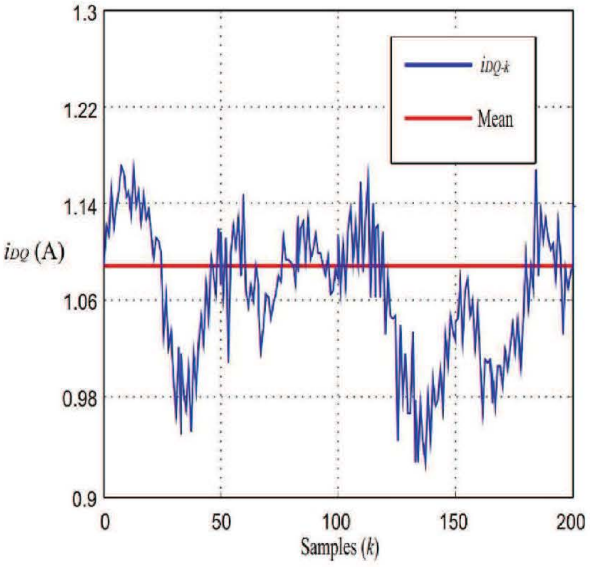

Fig. 4. Representation of the Lissajous figure by the $i_{DQ\text{-}k}$ vector.

C. *Network Training*

The training set for the ANN training was obtained with 500 random synthetic values for every condition in each treated frequency within the range $[\mu - \sigma, \mu + \sigma]$, where μ is the mean and σ the standard deviation of the mean values of the i_{DQ} vector on the first ten trials. Forty trials are carried out under each motor condition in every treated frequency; which were used as validation set for the diagnosis. Using Matlab neural network toolbox, the weights and the biases of each layer in the ANN were calculated for being implemented on the FPGA for the diagnosis. In some cases when the design of the motor is changed, a new training is required for adjusting the calibration of the smart sensor and improving the classification results. For future development, it is proposed to add an additional input to the ANN where the load value is given.

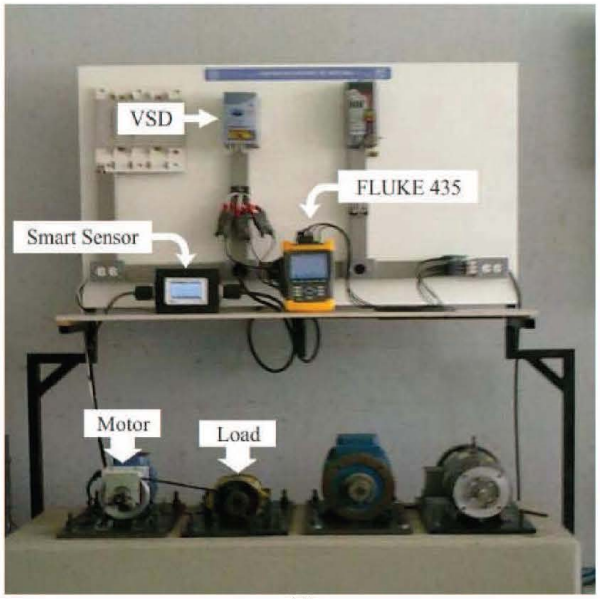

(a)

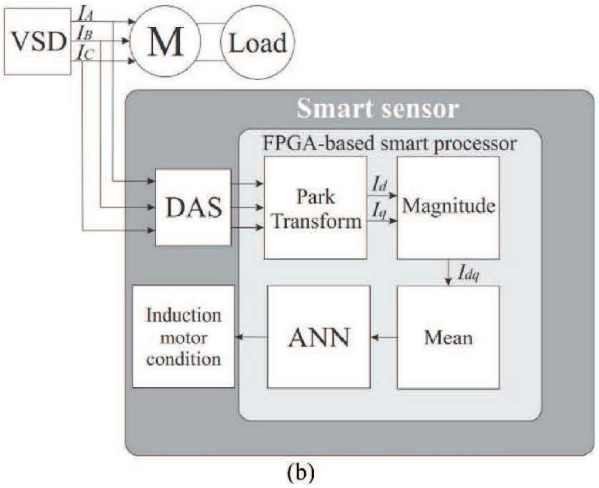

(b)

Fig. 5. (a) Experimental setup. (b) Block diagram of the proposed smart sensor for induction motor fault detection.

TABLE I
RESOURCE USAGE OF THE FPGA.

Resource utilization	Xilinx Spartan 3E XC3S1600E
Slices	1,495/14,752 (10%)
Flip-flops	979/29,504 (3%)
4-input LUTs	2,662/29,504 (9%)
Maximum operation frequency	58.28 MHz

V. RESULTS

A. *Fault Identification Results*

Table II shows the effectiveness by the proposed smart sensor during the induction motor condition classification of every frequency studied. The results include the identification of the healthy condition, broken rotor bar, unbalance and misalignment for each selected frequency. In Fig. 8 some examples of Lissajous figures are presented in order to observe the behavior of the faults in the D-Q system compared to the healthy condition. In order to obtain statistically significant results, forty tests were performed to acquire the three current phases from the induction motor in all treated cases for each selected frequency.

B. *Discussion*

Three different frequency cases of the VSD are studied in order to fulfill a range from low to high frequencies: 3Hz, 30Hz and 60Hz. Results of the smart sensor with motor running in healthy condition (HLT) show a detection effectiveness of 100% in 3Hz and 60Hz, while at 30Hz the detection effectiveness is 90%. Results at the broken rotor bars (BRB) condition present a detection effectiveness over 97% in 3Hz and 100% at 30Hz and 60Hz. In the unbalance (UNB) condition the 100% of effectiveness is present in each studied frequency. Finally, with the misalignment (MAL) condition the smart sensor delivers an effectiveness of 100% for 3Hz and 60Hz, and 95% at 30Hz. A characteristic of the proposed smart sensor is the automatic detection of multiple faults in VSD-fed induction motors using a simple methodology, different from other works that have a heavy computational load, requiring offline processing and an expert technician for interpreting results. For instance, as stated in Table I, the resources of the FPGA are around 10% with the proposed methodology. In [19], the implementation of a 1024-point FFT requires over 30% of FPGA resources, regardless the magnitude computation and an ANN. Otherwise, in [20] it is reported a 34% of resource usage of a reconfigurable FPGA-based system for wavelet analysis. On the other hand, [9-12] report offline methodologies for the detection of single isolated faults in induction motors connected through the power line supply. The FPGA implementation of the proposed smart sensor offers an online hardware implementation with a low computational load methodology, low-cost, and portable solution for fault detection in VSD-fed induction motors, different from other works that employ techniques with higher computational load, which are not suited for automatic online hardware/software implementation.

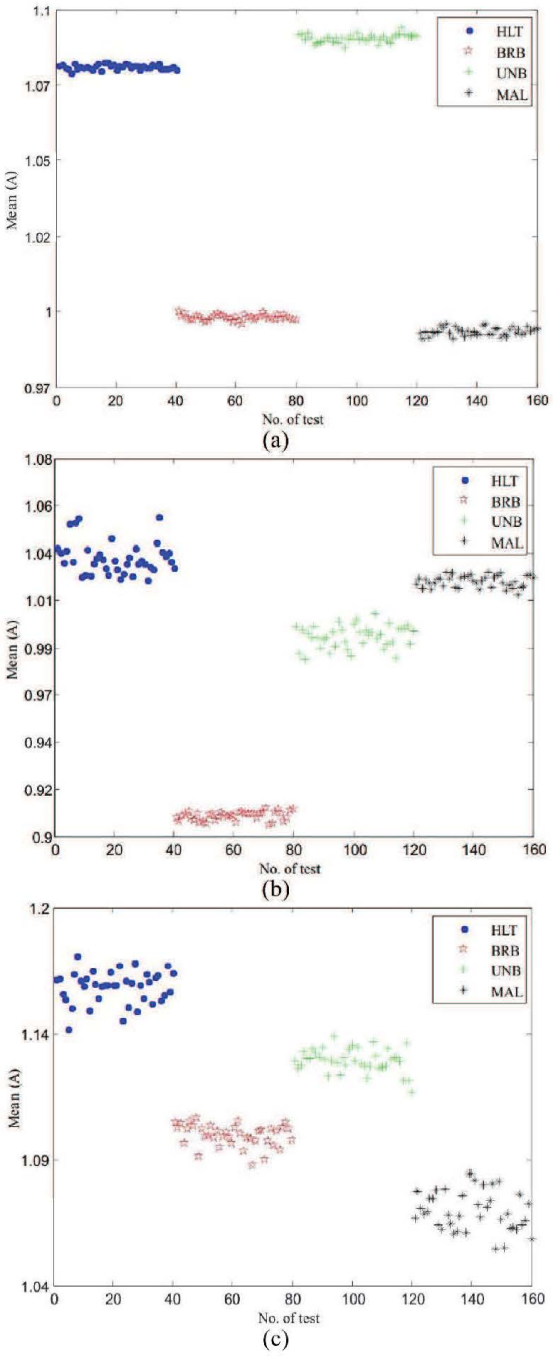

Fig. 6. Mean calculation of the i_{DQ} vector obtained of each fault condition in: (a) 3Hz, (b) 30 Hz and (c) 60 Hz.

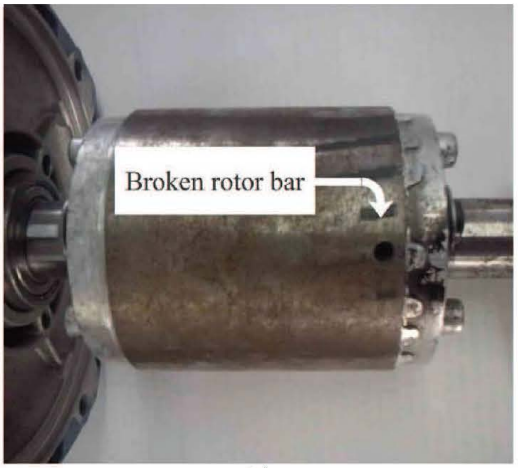

(a)

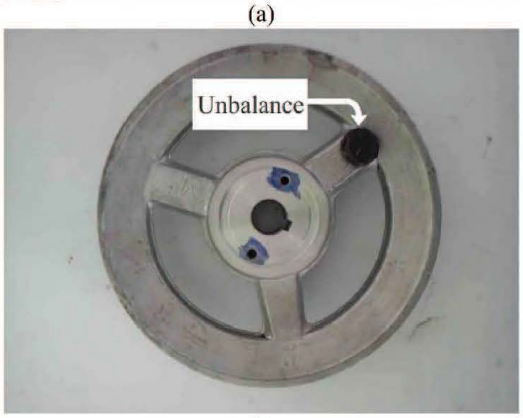

(b)

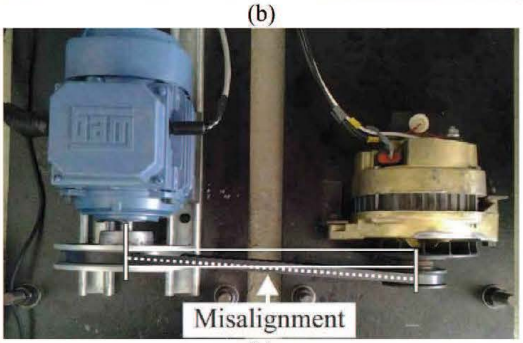

(c)

Fig. 7. (a) Broken rotor bar. (b) Unbalance. (c) Misalignment.

TABLE II
EFFECTIVENESS OF THE PROPOSED SMART SENSOR ON IDENTIFYING THE INDUCTION MOTOR CONDITION.

Induction motor condition	3Hz Effectiveness	30Hz Effectiveness	60Hz Effectiveness
HLT	100%	90%	100%
BRB	97%	100%	100%
UNB	100%	100%	100%
MAL	100%	95%	100%

VI. CONCLUSIONS

This work proposes a new smart sensor for detection of faults in VSD-fed induction motors using the three current phases. The proposed methodology is based on the Park transform and an MFN in order to determine the motor condition when is fed by a VSD, due to their simplicity and lower computational load different from other techniques, it is an excellent candidate to be implemented on hardware. The functionality of the smart sensor was successfully tested in forty tests of each category of the faults.

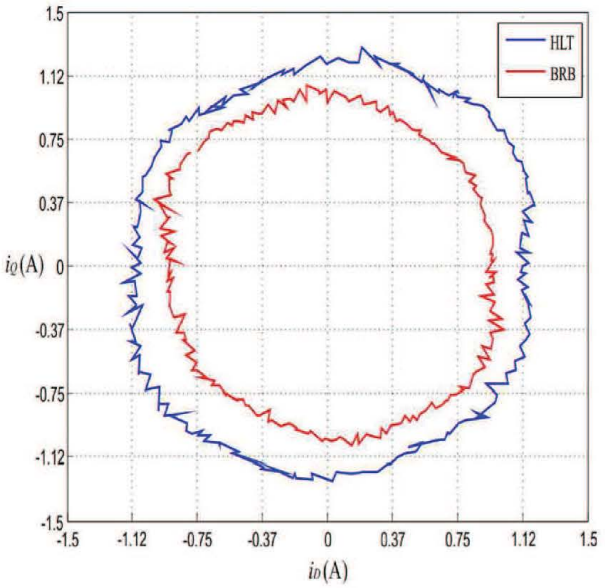

(a)

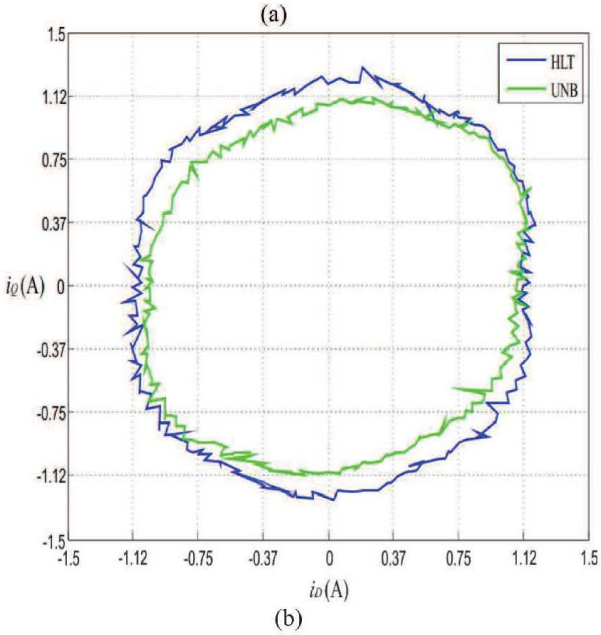

(b)

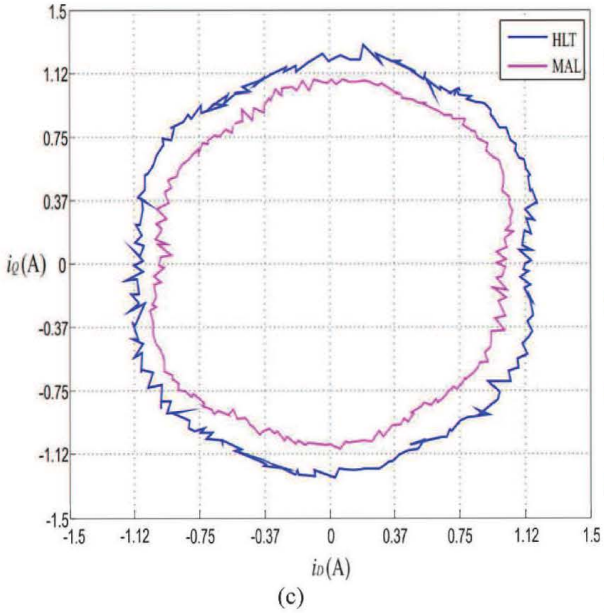

(c)

Fig. 8. Examples of Lissajous figures of the *D-Q* system current for comparing the healthy condition against (a) Broken rotor bar, (b) Unbalance and (c) Misalignment.

VII. REFERENCES

[1] A. Bellini, F. Fillipeti, C. Tassoni, G.A. Capolino, "Advances in diagnostic techniques for induction machines," *IEEE Trans. Industrial Elextronics,* vol. 55, pp. 4109-4126, Dec. 2008.

[2] D.J. Siyambalapitiya, P.G. Mclaren, "Reliability improvement and economic benefits of on-line monitoring systems for large induction machines," *IEEE Trans. Industrial Applications,* vol. 26, pp. 1018-1025, Nov-Dec. 1990.

[3] A. Garcia-Perez, R.J. Romero-Troncoso, E. Cabal-Yepez, R.A. Osornio-Rios, "The application of high-resolution spectral analysis for identifying multiple combined faults in induction motors," *IEEE Trans. Industrial Elextronics,* vol. 58, pp. 2002-2010, May 2011.

[4] O. Duque-Perez, L.A. Garcia-Escudero, D. Morinigo-Sotelo, P.E. Gardel, M. Perez-Alonso, "Condition monitoring of induction motors fed by voltage source inverters. Statistical Analysis of spectral data," in *Proc. Of the International Conference of Electric Machines and Drives (ICEM12)*, pp. 2479-2484, 2012.

[5] S.H. Kia, H. Henao, G.A. Capolino, "Some digital signal processing techniques for induction machines diagnosis," *IEEE International Symposium on Diagnostics for Electric Machines, Power Electronics & Drives (SDEMPED).* pp. 322-329, Sept. 5-8 2011.

[6] J. Urresty, J. Riba, H. Saavedra, J. Romeral, "Analysis of demagnetization faults in surface-mounted permanent magnet synchronous motors with symmetric windings," *IEEE International Symposium on Diagnostics for Electric Machines, Power Electronics & Drives (SDEMPED).* pp. 240-245, Sept. 5-8 2011.

[7] P. Gardel, D. Morinigo-Sotelo, O. Duque-Perez, M. Perez-Alonso, L.A. Garcia-Escudero, "Neural network broken bar detection using time domain and current spectrum data," in *Proc. Of the International Conference of Electric Machines and Drives (ICEM12)*, pp. 2492-2497, 2012.

[8] M. Riera-Guasp, J.Pons-Llinares, F. Vedreno-Santos, J.A. Antonino-Daviu, M. Fernandez-Cabanas, "Evaluation of the amplitudes of high-order fault related components in double bar faults," *IEEE International Symposium on Diagnostics for Electric Machines, Power Electronics & Drives (SDEMPED).* pp. 307-315, Sept. 5-8 2011.

[9] A. Soualhi, G. Clerc, H. Razik, A. Lebaroud, "Fault detection and diagnosis of induction motors based on hidden Markov model," in *Proc. Of the International Conference of Electric Machines and Drives (ICEM12)*, pp. 1693-1699, 2012.

[10] C. Kral, T.G. Habetler, R.G. Harley, "Detection of mechanical imbalances of induction machines without spectral analysis of time-domain signals," *IEEE Trans. Industrial Applications,* vol. 40, pp. 1101-1106, July-Aug. 2004.

[11] T. H. Patel, A.K. Darpe, "Experimental investigations on vibration response of misaligned rotors," *Elseiver Mechanical systems and signal processing,* vol. 23, pp. 2239-2252, May. 2009.

[12] I.Y. Onel, M.E.H. Benbouzid, "Induction motor bearing failure detection and diagnosis: Park and Concordia transform approaches comparative study," *IEEE Trans. Mechatronics,* vol. 13, pp. 257-262, April. 2008.

[13] J. Rivera, G. Herrera, M. Chacon, P.Acosta, M. Carrillo, "Improved progressive polynomial algorithm for self-adjustment and optimal response in intelligent sensors" *MDPI Sensors,* vol. 9, pp. 3767-3789, Nov. 2008.

[14] H. Nejjari, M.E.H. Benbouzid, "Monitoring and diagnosis of induction motors electrical faults using a current Park's vector pattern learning approach," *IEEE Trans. Industrial Applications,* vol. 36, pp. 730-735, May-June. 2000.

[15] M.J. Picazo-Rodenas, R. Royo, J. Antonino-Daviu, J. Roger-Folch, "Use of infrared thermography for computation of heating curves and preliminary failure detection in induction motors," in *Proc. Of the International Conference of Electric Machines and Drives (ICEM12)*, pp. 525-531, 2012.

[16] M.E.H. Benbouzid, "A review of induction motors signature analysis as a medium for faults detection," *IEEE Trans. Industrial Elextronics,* vol. 47, pp. 984-993, Oct. 2000.

[17] Y. Huang, "Advances in artificial networks – Methodological development and application" *MDPI Algorithms,* vol. 2, pp. 973-1007, Aug. 2009.

[18] L. Capocchi, G.A. Capolino, "An efficient architecture of multi-stage neural network for rotor induction generator short-circuit fault classification," in *Proc. Of the International Conference of Electric Machines and Drives (ICEM12)*, pp. 1565-1571, 2012.

[19] J. A. Vite-Frias, R. J. Romero-Troncoso, A. Ordaz-Moreno, "VHDL core for 1024-point radix-4 FFT computation," in *Proc. Int. Conf. Reconfigurable Computing and FPGAs ReConFig 2005*, pp. 26/1-4. 2005.

[20] R.J. Romero-Troncoso, M. Pena-Anaya, E. Cabal-Yepez, A. Garcia-Perez, R.A. Osornio-Rios, "Reconfigurable SoC-based smart sensor for wavelet and wavelet packet analysis," *IEEE Trans. Intrumentation and Measurement,* vol. 61, pp. 2458-2468, Sep. 2012.

VIII. BIOGRAPHIES

Armando G. Garcia-Ramirez received the B. E. degree from the Mazatlan Institute of Technology, Mazatlan, Mexico, and the M.E. degree (with Honors) from the University of Guanajuato, Salamanca, Mexico in 2011, where he did research work at the HSPdigital group. Currently, he is a Ph.D. student at the University of Queretaro, Queretaro, Mexico. His research interest includes hardware signal processing and smart sensors on a field-programmable gate arrays for applications on mechatronics.

Roque A. Osornio-Rios (M'10) received the B.E. degree from the Instituto Tecnologico de Queretaro, Queretaro, Mexico, and the M.E. and the Ph.D. degrees from the University of Queretaro, Queretaro, Mexico, in 2007. He is a National Researcher with CONACYT. He is currently Professor whit the University of Queretaro. He was an Advisor of over 30 theses, and a coauthor of over 40 technical papers in international journals and conferences His fields of interest include hardware signal processing and mechatronics. Dr. Osornio-Rios received the "2004 ADIAT National Award on Innovation" for his works in applied mechatronics.

Arturo Garcia-Perez (M'10) received the B.E. and M.E. degrees in electronics from the University of Guanajuato, Salamanca, Mexico, in 1992 and 1994, respectively, and the Ph.D. degree in electrical engineering from the University of Texas at Dallas, Richardson, in 2005. He is currently a Titular Professor with the Department of Electronic Engineering, University of Guanajuato. He is a National Researcher with the Consejo Nacional de

Ciencia y Tecnología level 1. He was an Advisor of over 50 theses. His fields of interest include digital signal processing for applications in mechatronics

Rene de J. Romero-Troncoso (M'07–SM'12) received the Ph.D. degree in mechatronics from the Autonomous University of Queretaro, Queretaro, Mexico, in 2004. He is a National Researcher level 2 with the Mexican Council of Science and Technology, CONACYT. He is currently a Head Professor with the University of Guanajuato and an Invited Researcher with the Autonomous University of Queretaro, Mexico. He has been an advisor for more than 180 theses, an author of two books on digital systems (in Spanish), and a coauthor of more than 90 technical papers published in international journals and conferences. His fields of interest include hardware signal processing and mechatronics. Dr. Romero–Troncoso was a recipient of the 2004 Asociación Mexicana de Directivos de la Investigación Aplicada y el Desarrollo Tecnológico Nacional Award on Innovation for his work in applied mechatronics, and the 2005 IEEE ReConFig Award for his work in digital systems.

ANEXO D

Sensors **2012**, *12*, 11989-12005; doi:10.3390/s120911989

OPEN ACCESS

sensors

ISSN 1424-8220

www.mdpi.com/journal/sensors

Article

Smart Sensor for Online Detection of Multiple-Combined Faults in VSD-Fed Induction Motors

Armando G. Garcia-Ramirez [1], Roque A. Osornio-Rios [1], David Granados-Lieberman [1], Arturo Garcia-Perez [2] and Rene J. Romero-Troncoso [2,*]

1 HSPdigital-CA Mecatronica, Facultad de Ingenieria, Universidad Autonoma de Queretaro, Campus San Juan del Rio, Rio Moctezuma 249, Col. San Cayetano, San Juan del Rio, Qro. 76807, Mexico; E-Mails: aggarcia@hspdigital.org (A.G.G.-R.); raosornio@hspdigital.org (R.A.O.-R.); granlieber@hspdigital.org (D.G.-L.)

2 HSPdigital-CA Telematica, DICIS, Universidad de Guanajuato, Carr. Salamanca-Valle km 3.5+1.8, Palo Blanco, Salamanca, Gto. 36885, Mexico; E-Mail: agarcia@hspdigital.org

* Author to whom correspondence should be addressed; E-Mail: troncoso@hspdigital.org; Tel./Fax: +52-464-647-9940.

Received: 27 July 2012; in revised form: 17 August 2012 / Accepted: 24 August 2012 / Published: 30 August 2012

Abstract: Induction motors fed through variable speed drives (VSD) are widely used in different industrial processes. Nowadays, the industry demands the integration of smart sensors to improve the fault detection in order to reduce cost, maintenance and power consumption. Induction motors can develop one or more faults at the same time that can be produce severe damages. The combined fault identification in induction motors is a demanding task, but it has been rarely considered in spite of being a common situation, because it is difficult to identify two or more faults simultaneously. This work presents a smart sensor for online detection of simple and multiple-combined faults in induction motors fed through a VSD in a wide frequency range covering low frequencies from 3 Hz and high frequencies up to 60 Hz based on a primary sensor being a commercially available current clamp or a hall-effect sensor. The proposed smart sensor implements a methodology based on the fast Fourier transform (FFT), RMS calculation and artificial neural networks (ANN), which are processed online using digital hardware signal processing based on field programmable gate array (FPGA).

Keywords: smart sensor; induction motors; multiple-combined faults; VSD; FPGA

1. Introduction

Induction motors are widely used in industry due to their robustness, low cost, easy maintenance and versatility; representing 85% of power consumption worldwide. Thus, when induction motors start developing incipient faults [1] it is important to detect the fault early because at this stage it is easier to repair, benefiting the industry in cost and maintenance time. Faults in induction motors may produce unanticipated interruptions on production lines, with severe consequences in product quality, safety and cost. For this reason, early fault detection in induction motors has attracted the interest of many researchers in recent years [2–5]. Induction motor faults are mainly associated to bearing defects (BD), rotor faults such as broken bars (BRB) [6–18], unbalance (UNB) [19] and misalignment (MAL) [20–23]. According to these faults, sometimes two or more of them may develop simultaneously, making it important to identify if they are alone or combined. Thus far, the combined fault identification in induction motors represents a big challenge, but it has been rarely considered in spite of being a common situation, because it is difficult to identify two or more faults simultaneously online through sensors [24–31]. Besides, the connection of induction motors through variable speed drives (VSD), which allow controlling their rotational speed, extending their useful life, and saving energy is a common practice in industry [32–35], but with the undesired effect of making the detection of faults more difficult because of the spurious harmonics induced by the VSD operation.

A number of vibration and current analysis-based techniques exist for identifying specific faults in induction motors. Regrettably, most of the condition-monitoring techniques for early fault detection focus on the detection of single specific faults. Broken rotor bar condition is one of the most difficult faults to detect because the induction motor works normally without perceivable anomalies, making this fault one of the most studied in research literature. For instance, in [6] the half broken bar condition is detected by combining the correlation of the vibration and current spectra. Then, a post processing technique is applied to improve the detectability and present a motor diagnosis. In a different case, in [7] the discrete wavelet transform (DWT) is applied to the instantaneous power signal to study the case of one and three broken bars for an induction motor. Otherwise, in [8] one broken bar is detected by applying the DWT to the induction motor current at the start-up transient, and through a weighting function granting the motor diagnosis. On the other hand, after unbalance, misalignment is the second most common fault causing life reduction in induction motors. For instance, in [20] misalignment is diagnosed through unique vibration features exhibited in the full spectrum computed by the fast Fourier transform (FFT). In [22] the misalignment behavior of the rotor in an induction machine is investigated with its vibration waveforms using orbit plots and conventional FFT to identify their unique vibration features. Unfortunately, few works are related to the diagnosis and the identification of multiple combined faults. Ballal *et al.* [25] develop a combined method with artificial neural networks (ANN) and fuzzy logic to detect stator inter-turn insulation and bearing wear faults in single-phase induction motor. They take five measurable parameters (motor intake current, speed, winding temperature, bearing temperature and the noise of the machine) for the input of the adaptive neural fuzzy inference system (ANFIS) to provide a diagnosis of the induction machine. Garcia-Perez *et al.* [28] proposed a method that combines a finite impulse response (FIR) filter bank with high resolution spectral analysis based on multiple signal classification (MUSIC) for detecting multiple combined faults, analyzing vibration and current signals. The results show concordance with

the analytical predetermined fault frequency for single and two or three combined faults (BRB, UNB, and BD). Romero-Troncoso *et al.* [29] performed a methodology using the information entropy and a fuzzy logic analysis in an FPGA device to identify faults like BD, UNB, BRB and their combinations by analyzing one phase of the induction motor steady-state current signal. Lebaroud *et al.* [31] presented a diagnosis method of multiple combined faults based on time-frequency classification of the current signals. All the aforementioned theoretical frameworks focus on fault detection of induction motors directly connected to the power line supply and do not consider the case of motors connected through a variable speed drive (VSD). Therefore, few works are related to faults in induction motors connected through VSDs. For instance Obaid *et al.* in [32] examined the effect of changing the input frequency in an induction motor fed through a VSD with faults such as unbalance and misalignment; the work highlighted that the harmonics induced by the VSD do not change the conditions of the frequencies of interest. Other research [34], reports a methodology for the detection of broken bars in induction motors connected through a VSD at different frequencies from 30 to 60Hz or directly to the power line supply and this methodology is based on electrical current transient analysis through DWT. The work of Cabal-Yepez *et al.* in [35] proposed the use of information entropy as a tool for multiple fault detection on induction motors controlled by a VSD obtaining results in different frequencies of operation from 30 to 50 Hz. Unfortunately, the aforementioned methodologies are based on an offline diagnosis, except for [34] that presents an online diagnosis for BRB. From an industrial point of view an online system that ensures the diagnosis of multiple-combined faults in a VSD-fed induction motor is nowadays a necessity for reducing power consumption and preventing any further damage.

From the technological point of view, smart sensors can be used to overcome the monitoring system demands due to their versatility and ability to work in environments where the access for field workers is limited, and their features in communication and data processing functionalities [36]. On the other hand, smart sensors based on field-programmable gate arrays (FPGA) are capable of performing the task due to their high-speed processing capabilities, reconfigurability, and system-on-a-chip (SoC) solutions. Smart sensors have being applied in different research areas [36–45]. For instance, Granados-Lieberman *et al.* [38] developed an FPGA-based smart sensor for real-time high-resolution frequency measurement in accordance with international standards of power quality monitoring, using a current clamp as primary sensor and the chirp z-transform (CZT) as signal processing for the diagnosis. Humin *et al.* [39] presented a smart sensor for medium-voltage dc power grid protection via current and voltage transformers. Otherwise, Rodriguez-Donate *et al.* [40] proposed a smart sensor to obtain several parameters related to motion dynamics using two primary sensors: an encoder and an accelerometer on a single link of industrial robots. In biology, Millan-Almaraz *et al.* [42] showed a smart sensor that can estimate plant transpiration. This smart sensor fuses five primary sensors: two temperature sensors, two relative humidity sensors and a light sensor. Depari *et al.* [44] presented a sensor network connected through a universal serial bus (USB)-to-Ethernet gateway for industrial applications. In [45] Son *et al.* developed a smart sensor system for machine fault diagnosis using three different sensors: vibration, current, and flux acquiring their signals, processing and diagnosing offline in a personal computer (PC). Due to their proven reliability in different research areas, smart sensors are the best suited candidates for induction motor fault monitoring systems with the presence of single or multiple-combined faults when the motor is fed through a VSD rather than having costly monitoring systems with several independent sensors and processing units connected through a computer network.

The contribution of this work is the development of a smart sensor for on-line detection of single or multiple-combined faults in induction motors connected through a VSD over a wide frequency range, covering low frequencies from 3 Hz and high frequencies up to 60 Hz, extending previously reported frequency ranges. The proposed smart sensor can use a commercially available current clamp or a Hall-effect sensor as the only primary sensor required, contrary to other works that use two or more sensors to identify a fault. The use of a current clamp as primary sensor provides additional benefits in portability, allowing one to perform the fault diagnosis in different motors without interrupting their operation. Another contribution of this work is the methodology, due to its simplicity and the theoretical foundation to analyze the frequencies of interest excited by the failure; this methodology is based on FFT fused with artificial neural networks, which is implemented into an FPGA due to its high-performance computational capabilities. In the proposed methodology, FFT provides the induction motor current spectrum normalized at steady-state, which allows covering motors with different power capabilities and a wide load range; then, specific frequency components are selected to compute their RMS to be inputs of the artificial neural network, which gives an online identification of single or combined faulty conditions. In this paper, three different faults in an induction motor: BRB, UNB, MAL and their combinations are investigated. Results confirm the potentiality of the smart sensor as an instrument for single and multiple-combined faults online detection.

2. Theoretical Background

2.1. Fault Effect on Stator Current Components

This article focuses on three different induction motor faults and their combinations: broken rotor bars (BRB), unbalance (UNB), and misalignment (MAL). The presence of BRB in induction motors produces several problems, such as power quality degradation [23]. On the other hand, UNB is the most observed fault in induction motors, and can cause catastrophic damages if not remedied. Finally, MAL is the second most commonly observed fault in rotating machines, and it is estimated to cause over 70% of the rotating machinery vibration problems [20].

2.1.1. Broken Rotor Bar

The detection of a broken bar fault can be done by the observation of the space harmonics f_{brb} components in the motor current as a fault indicator:

$$f_{brb} = f(1 \pm 2ks) \tag{1}$$

where f is the input frequency, k is the harmonic index, s is the slip. These components are known as left sideband component and right sideband component. When a bar is broken, the amplitude of these sideband components increases significantly, as shown in Figure 1, where the markers shown delimit the sideband component area [23].

2.1.2. Unbalance

The unbalance condition is presented when the mechanical load in the induction motor is not uniformly distributed, taking the center of mass out of the motor shaft. Unbalance in induction machines creates air-gap eccentricities, which change the frequency spectrum of the supply current [19].

Figure 1. Left and right sideband components. (**a**) Healthy motor; (**b**) Broken rotor bar fault.

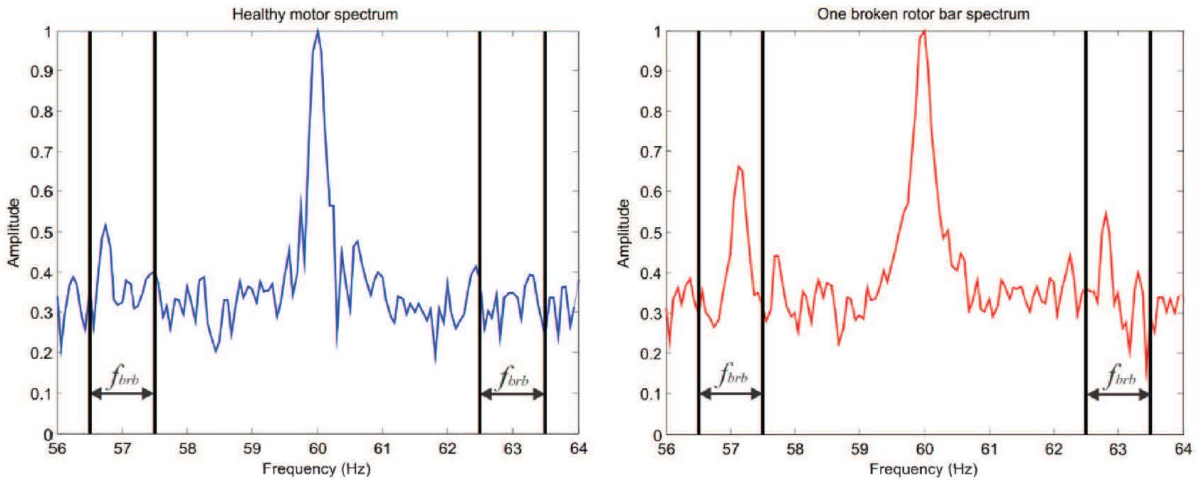

2.1.3. Misalignment

The misalignment in induction motors occurs when the motor and the load pulleys are not aligned. The misalignment condition, like unbalance, creates air-gap eccentricities changing the frequency spectrum of the supply current [19]. The air-gap eccentricity affects the inductances of the motor resulting in harmonics (f_{ecc}) at rotating frequency sidebands of the supply frequency predicted by Equation (2):

$$f_{ecc} = f\left[1 \pm k\left(\frac{1-s}{p}\right)\right] \tag{2}$$

where p is the number of pole pairs. Figure 2(a) shows the air-gap eccentricities in the healthy motor current spectrum and Figure 2(b) shows the air-gap eccentricities in a motor current spectrum with unbalance where the regions of interest are delimited.

2.2. Artificial Neural Networks

Artificial neural networks (ANN) are computational models that simulate the neurological structure of the human brain and its capability to learn and solve problems through pattern recognition. There are different ANN architectures, such as multilayer feed-forward networks (MFN), recurrent networks, feedback networks, radial basis function networks, and Kohonen self-organizing map networks. The most popular architecture for ANN is the MFN that has an input layer, an output layer and one or more hidden layers. In this ANN architecture the data moves in only one direction, from the input neurons

through the hidden neurons to the output neurons, as shown in Figure 3. Where X_i (i = *1,2,...,n*) are inputs and y_i (i = *1,2,...,m*) are outputs. An MFN is usually trained by the back-propagation algorithm (BPA), which is a supervised learning method, and consists on mapping the process inputs to the desired outputs by minimizing the error between the desired outputs and the calculated outputs [46]. The MFN architecture is simple and practical in terms of classifier and computational load, making it an excellent candidate to be implemented in the methodology.

Figure 2. Air-gap eccentricities. (**a**) Healthy motor current spectrum; (**b**) Motor current spectrum with air-gap eccentricities.

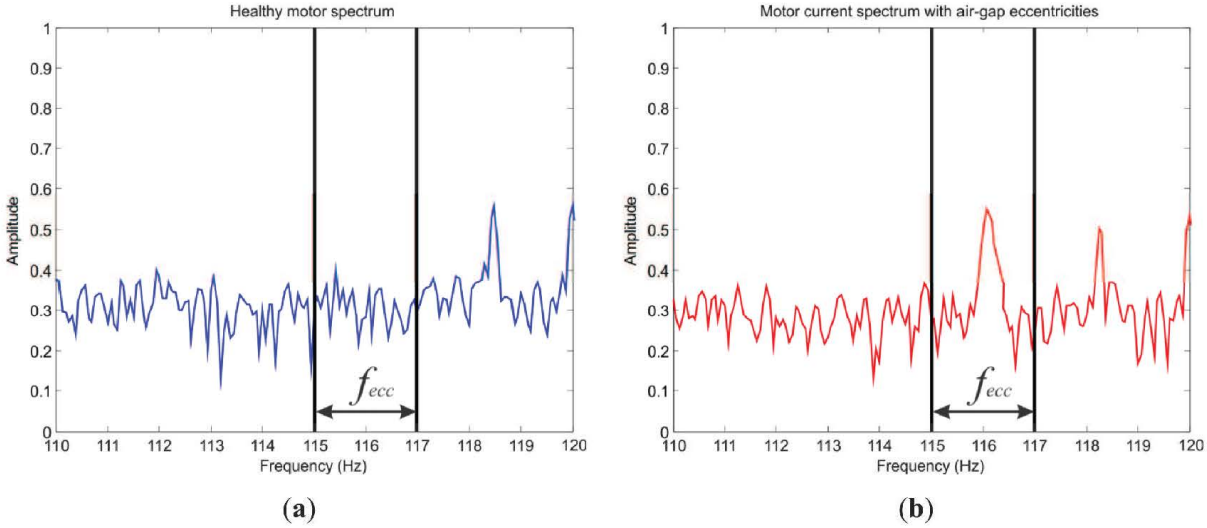

Figure 3. Multilayer feed-forward network architecture.

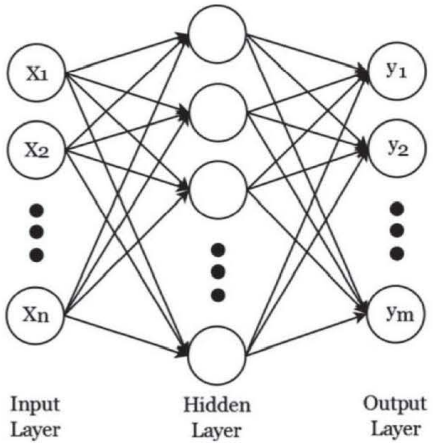

2.3. Variable Speed Drive

In industry the operation of induction motors through variable speed drives (VSDs) is very common, since it allows controlling their rotational speed, extending their useful life, and saving energy [32–35]. There are two different kinds of control in VSDs: Vector control drive and the Scalar control drive. The first one is an excellent driver to handle transients. It also enables fast control of

torque speed. Some disadvantages are the complexity and the high price of the circuit. This control is commonly used in high precision tasks. As for scalar control drives, they are widely used in the industry due to their low-cost, simple design and high immunity to feedback signal errors. That type of control is preferred for simple tasks like those of pumps and fans [47,48]. When the speed varies under vector control drives the frequency content of the monitoring signals are affected by the controller bandwidth. However, it is possible to extract the condition monitoring information from signals derived within the controller [49]. For instance, in [50] rotor failures in induction motors, fed by a vector and scalar control, are diagnosed with three different signals: voltage, current and speed. In scalar control drives the characteristic harmonics of broken rotor bars in current are clearly visible and generate the same speed ripples, contrary to vector control drive where these harmonics are not affected and the speed spectrum is perfect.

3. Methodology

This section shows the proposed methodology for the smart sensor development, the configuration and the block diagram of the FPGA-based smart processor. First, the general structure of the smart sensor is discussed, then the smart processor architecture with the processing stages and finally, the proposed ANN.

3.1. Smart Sensor

The block diagram of Figure 4 shows the proposed smart sensor for fault detection. The system uses a primary sensor (current clamp or Hall-effect sensor) to measure one phase of the stator current in the induction motor connected through a VSD; then, signal conditioning is applied. Subsequently, the conditioned signal is digitalized in the analog-to-digital converter block (ADC). Finally, the digital information is passed through the smart processor that is in charge to assert the motor diagnostic.

Figure 4. Block diagram of the fault detector smart sensor.

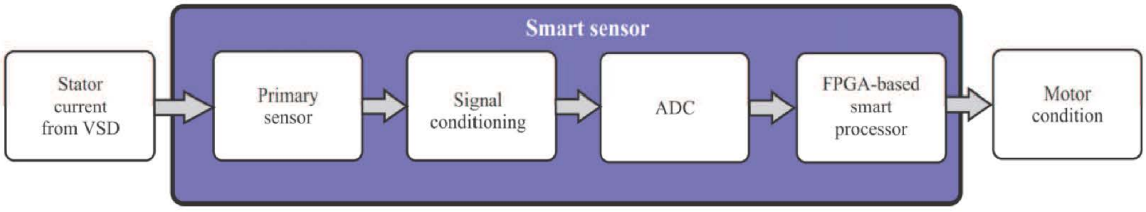

3.1.1. FPGA-Based Smart Processor

The block diagram of the FPGA-based smart processor internal structure to determine the condition of the motor is shown in Figure 5. The outgoing data from the ADC is time windowed with a Hanning window to reduce the leakage in the frequency domain and the frequency operation of the VSD is computed by a frequency estimator. Then, FFT is applied to get the current spectrum. In order to cover motors with different power capabilities and a wide load range the spectrum is normalized according to the magnitude of the fundamental frequency. Afterward, the bands of interest for the different faults are evaluated through the estimation of the RMS value of these selected bands

according to Equations (3) and (4). The selection of the bands of interest is based on intervals between a minimum and maximum slip from 1% to 20% in order to fulfill the NEMA standard of A, B, C and D designs [51]. These slip percentages guarantee a motor load range between 25 to 100%, nevertheless lower values of this range cannot be detected. Finally, the data from each RMS evaluator are inputs of the ANN to deliver the motor condition. Figure 6 shows the smart processing flow up to detect single and multiple-combined faults in induction motors.

Figure 5. Block diagram of the FPGA-based smart processor.

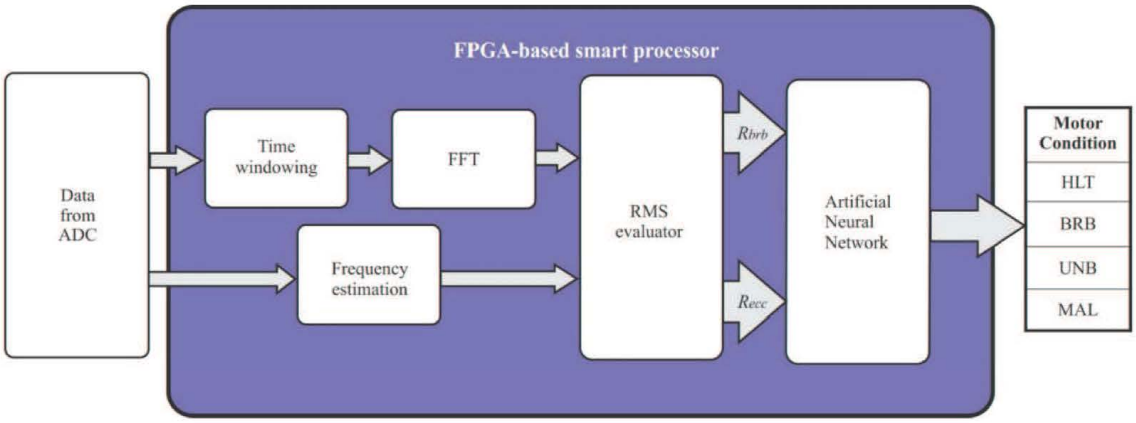

Figure 6. Smart processing flow up.

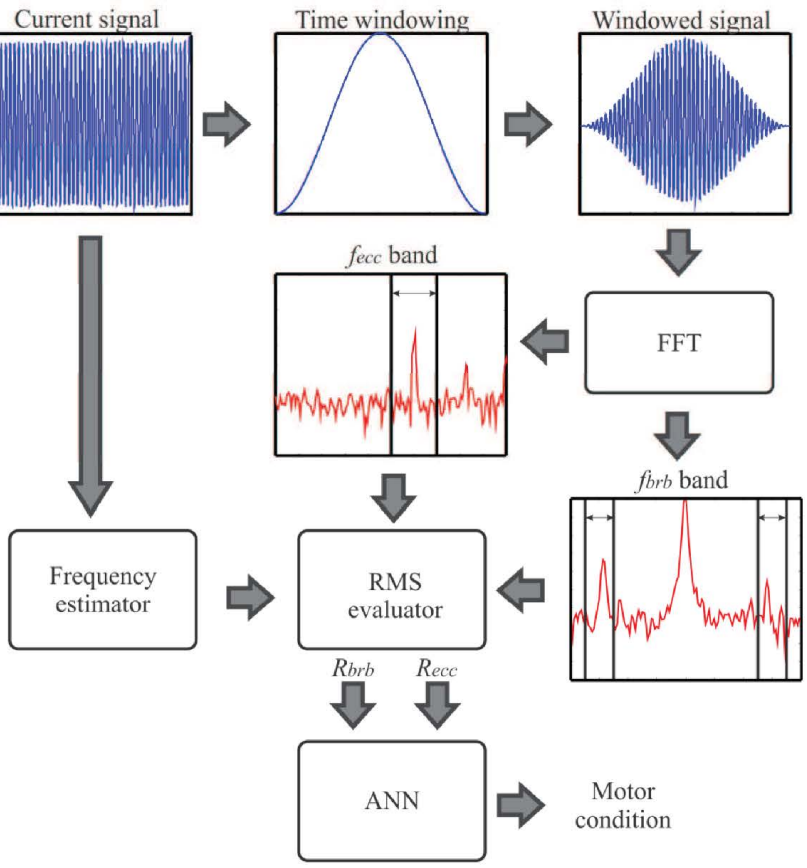

3.2. Proposed ANN

The proposed ANN implements an MFN with two input nodes that receive the RMS value of the left and right sideband components (R_{brb}) and the RMS value of air-gap eccentricities (R_{ecc}) of the stator current from VSD, ten nodes in the hidden layer and four output nodes to detect: healthy motor (HLT), broken rotor bars (BRB), unbalance (UNB), misalignment (MAL) and their combinations. The output nodes correspond to each single fault condition, and if two or more faults are presented at the same time, the corresponding output nodes will be triggered up. Figure 7 shows the proposed ANN.

$$R_{ecc} = \sum_{s=0.01}^{0.20} f\left[1 \pm k\left(\frac{1-s}{p}\right)\right] \tag{5}$$

$$R_{brb} = \sum_{s=0.01}^{0.20} f(1 \pm 2ks) \tag{6}$$

Figure 7. Proposed ANN.

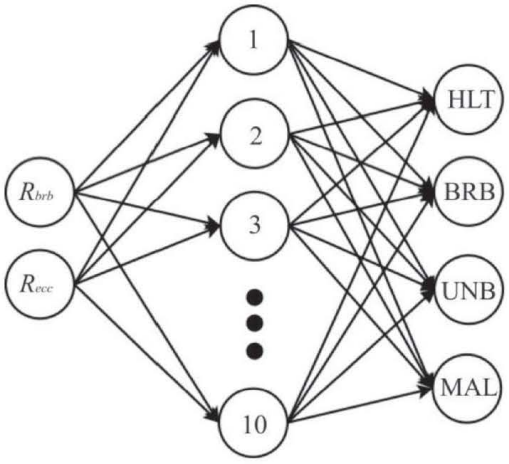

4. Experiments and Results

In this section, the experimental setup and the results are presented for validation the proposed smart sensor. The online fault detection was performed during the steady-state of the induction motor.

4.1. Experimental Setup

The experimental setup consists in using the steady-state current signal provided by a VSD (model WEG CFW08) to the motor under test for detecting the multiple-combined faults and to classify the conditions of the induction motor. The VSD has an operation range from 0 Hz up to 100 Hz using a frequency resolution of 0.01 Hz. Figure 8(a) shows the experiment setup where three different 1-hp three-phase induction motors (model WEG 00136APE48T) are used for testing the performance of the proposed methodology identifying the single and multiple combined fault conditions treated in this work. The tested motors have 2 poles, 28 bars and receive a power supply of 220 V AC. The motor rotational speed is controlled through a VSD at 3 Hz, 30 Hz and 60 Hz. The applied mechanical load is of an ordinary alternator, which represents a quarter (25%) of nominal load for the motor. The current

signal is acquired using a hall-effect sensor model L08P050D15, from Tamura Corporation. A 16-bit 4-channel serial-output sampling analog-to-digital converter ADS8341 from Texas Instrument Incorporated is used in the data acquisition system (DAS). The instrumentation system which was calibrated through the Fluke 435 uses a sampling frequency f_s = 256 Hz obtaining 4,096 samples during 16 seconds of the induction motor steady-state and has a bandwidth of 128 Hz, which covers the VSD operation range. The motor start-up is controlled by a relay in order to automatize the test run. The acquired information is analyzed by the proposed smart sensor that is implemented in a proprietary Spartan 3E XC3S1600 FPGA platform running at 48 MHz that provides the induction motor condition as shown in Figure 8(b). Table 1 summarizes the resource usage of the FPGA.

Figure 8. (**a**) Experiment setup; (**b**) Smart sensor.

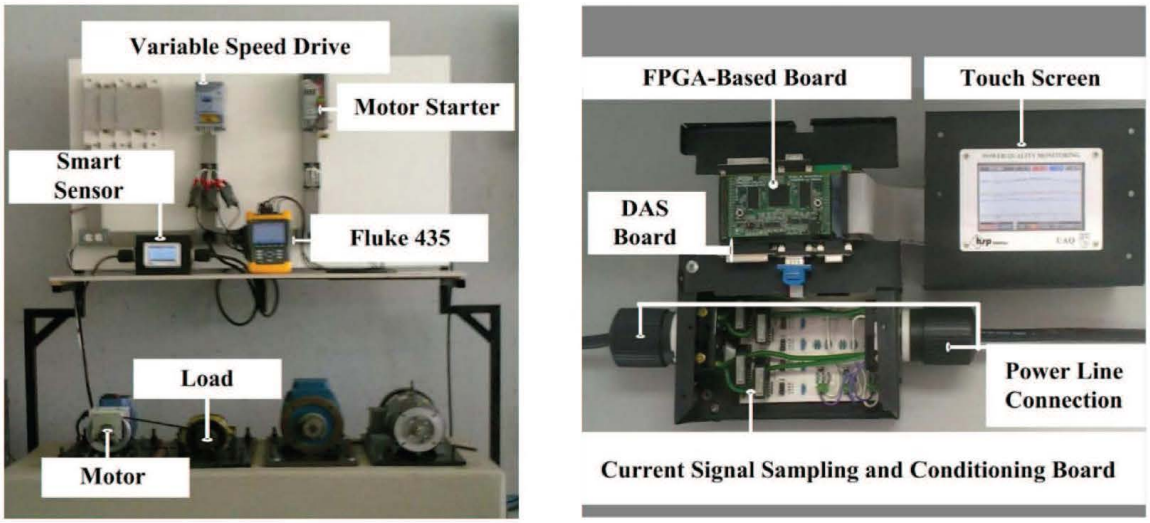

(**a**) (**b**)

Table 1. Resource usage of the FPGA.

Resource utilization	Xilinx Spartan 3E XC3S1600E
Slices	1,757/14,752 (12%)
Flip-flops	638/29,504 (2%)
4-input LUTs	3,270/29,504 (11%)
Maximum operation frequency	53.012 MHz

4.1.1. Single Faults

To produce an artificial broken rotor bar condition it was necessary to drill a 2.0 mm diameter hole in a bar of the rotor without harming the rotor shaft. Figure 9(a) shows the rotor with the broken bar used during the test. The unbalance condition was produced artificially by a bolt in the rotor pulley as shown in Figure 9(b). The misalignment test was carried out by shifting forward the band in the alternator pulley, so that the transverse axes of rotation for the motor and its load were not aligned. Figure 10(a) shows the aligned motor and the Figure 10(b) shows the misaligned motor.

Figure 9. (**a**) Broken rotor bar; (**b**) Unbalance.

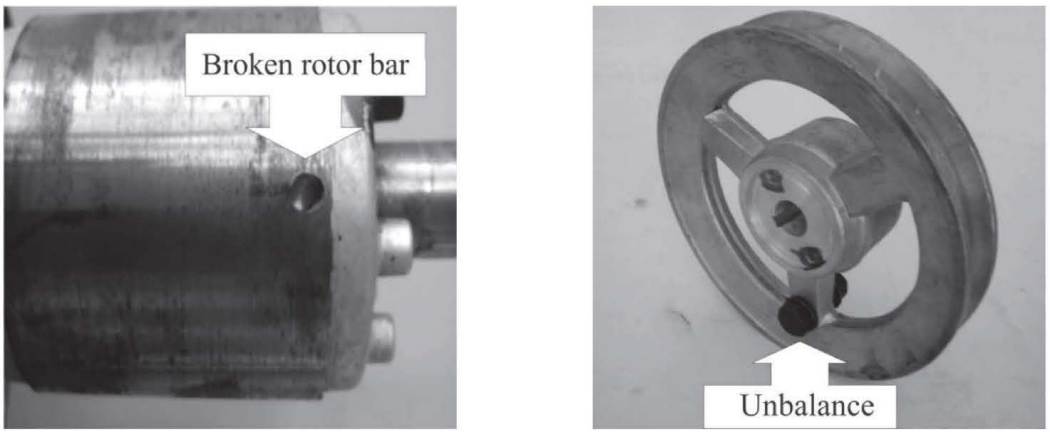

(**a**) (**b**)

Figure 10. (**a**) Motor aligned; (**b**) Motor misaligned.

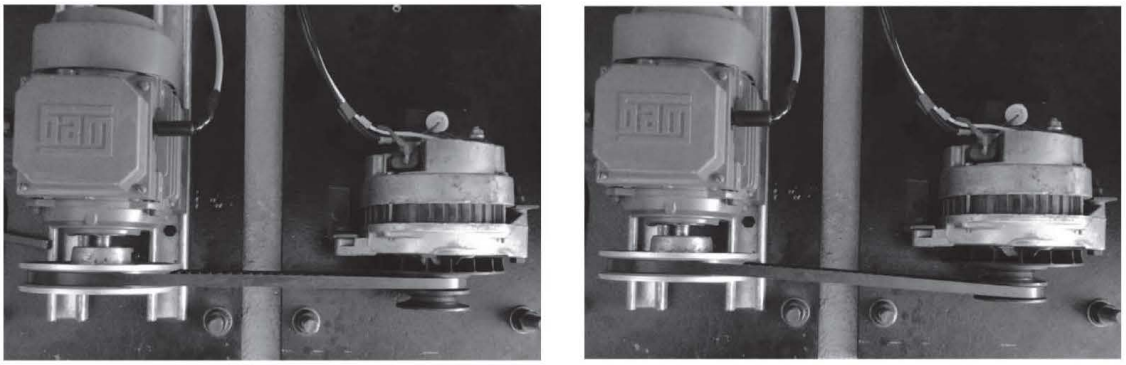

(**a**) (**b**)

4.1.2. Multiple-Combined Faults

The multiple-combined fault conditions were obtained by mixing each single fault with one or two of the remaining faults as shown in Figure 11.

Figure 11. Combination for multiple-combined fault analysis.

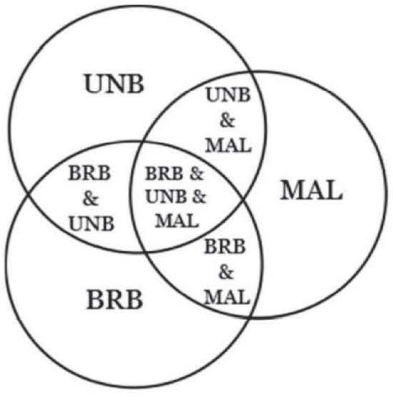

4.1.3. Network Training

The ANN is trained with the back-propagation algorithm to identify single or multiple-combined faults in induction motors. Forty trials are carried out under each motor condition for each study frequency. The training set was obtained with 1,000 random synthetic values for each study frequency within the range $[\mu - \sigma, \mu + \sigma]$, where μ is the mean and σ the standard deviation of the RMS values of spectral components of interest from steady-state of the induction motor on the first five trials. Real values of each fault were used as validation set for the diagnosis. The weights and the biases of each layer in the ANN were obtained offline, using the Matlab neural network toolbox for being implemented on the FPGA for the online diagnosis. The ANN is trained for motors with B NEMA design, since those are used in general applications [51]. The theoretical background shows that the frequency components of the faults do not depend of the power motor capability. Nevertheless, the current magnitude depends of the load and the motor power. So as to minimize those undesired effects that could modify the ANN output the spectrum is normalized before being applied to the ANN. This guarantees the same results in motors with similar characteristics. However, other NEMA designs have different relationship between the fundamental frequency and the fault components because of changes in the current flux density and the stator field [5]. In some of these cases a new training is required for adjusting the calibration of the smart sensor and improving the classification results.

4.2. Fault Identification Results

Table 2 presents the results delivered by the proposed smart sensor during the induction motor condition identification for each frequency studied in order to show the effectiveness of the system. The results include the identification of a healthy condition, a single isolated fault, and the combination of two or three faulty conditions for each study frequency. In order to obtain statistically significant results, 40 tests were performed to acquire the current signals from the induction motor in all treated cases for each study frequency.

Table 2. Effectiveness of the proposed smart sensor on identifying the induction motor condition with one or multiple combined faults.

Induction motor condition	03 Hz Effectiveness (%)	30 Hz Effectiveness (%)	60 Hz Effectiveness (%)
HLT	100	100	80
BRB	80	100	100
UNB	100	100	100
MAL	100	100	100
BRB-UNB	80	100	100
BRB-MAL	90	100	100
UNB-MAL	100	100	100
BRB-UNB-MAL	100	80	90

4.3. Discussion

Three different frequency cases are studied in order to fulfill a range from low to high frequencies: 3 Hz, 30 Hz and 60 Hz. Results of the smart sensor with the motor running at 3 Hz show an

effectiveness of 100% in health motor (HLT), unbalance (UNB), misalignment (MAL), the combination of unbalance and misalignment (UNB-MAL) and the combination of broken bars with unbalance and misalignment (BRB-UNB-MAL); the results for broken rotor bars (BRB), broken rotor bars in combination of unbalance (BRB-UNB) and broken rotor bars combined with misalignment (BRB-MAL) present an effectiveness over 80%. Due to the fact the sideband frequencies at 3 Hz were closer to the fundamental frequency, the conditions with broken bars were more difficult to diagnose. On the other hand, with the motor running at 30 Hz the smart sensor shows an effectiveness of 100% with the exception of BRB-UNB-MAL which presented an 80% effectiveness. Finally, at 60 Hz of the VSD, the smart sensor presents an effectiveness of 100% with the exception of HLT and BRB-UNB-MAL with effectiveness over 80%. A significant characteristic of the proposed smart sensor is the detection of single and multiple-combined faults in VSD-fed induction motors in an automatic way with only a primary sensor, different from the reviewed literature where the results are from single faults or multiple-combined faults interpreted offline by the user from current of the power supply or vibration signals of the induction motor with two or more primary sensors. Table 3 shows the faults detected by the proposed smart sensor (PSS), and the works that fulfill some of the faults detected and their combination. For instance, in [29,30] show online methodologies for the detection of multiple-combined faults of induction motors connected through the power line supply. On the other hand, in [32], reports an offline methodology for the detection of UNB and MAL at different operation frequencies. In a different case, [35] presents a methodology for the detection of different single isolated faults at different operation frequencies over 30 Hz. The PSS offers an online detection of single and multiple-combined faults at different operation frequencies in a wide range from 3 Hz to 60 Hz.

Table 3. Comparison between proposed smart sensor (PSS) and reviewed literature.

Induction motor condition	VSD-fed	Power line supply
BRB	[34], PSS	[7–19,27]
UNB	[32,33,35], PSS	[20]
MAL	[32,35], PSS	[21–23]
BRB-UNB	PSS	[28–31]
BRB-MAL	PSS	[24]
UNB-MAL	PSS	
BRB-UNB-MAL	PSS	

5. Conclusions

This work proposes a new smart sensor for online detection of multiple-combined faults in VSD-fed induction motors using only a Hall-effect current sensor as primary sensor in one-phase of the induction motor, which results in a high portability. The proposed methodology is based on the FFT and an ANN classifier in order to determine the motor condition according to the motor operation frequency controlled by the VSD, the simplicity of this methodology allows analyzing the frequencies of interest excited by the different failures. The FFT spectrum is normalized in order to cover different power motor capabilities and a wide load range. The functionality of the smart sensor was successfully tested in forty tests of each category of the faults and their combinations. Results demonstrate that the

proposed smart sensor is highly efficient in effecting a diagnosis of the induction motor operating over a wide frequency range of the VSD (3, 30 and 60 Hz), different from other works [7–31] that show results from motors fed by the power line supply only or [32–34] that present results from VSD-fed ones, but in a narrow frequency range without combining faults. The obtained results show the versatility of the proposed smart sensor for its use in diverse industrial applications that employ induction motors fed by a VSD. The proposed smart sensor allows the early fault detection benefiting the industry in cost and maintenance time. The proposed smart sensor for online detection of multiple-combined faults in VSD-fed induction motors is based on FPGA technology that provides high computation performance for the proposed methodology, as well as a low-cost, portable and efficient solution. This implementation shows that an FPGA platform is a suitable solution for smart processing units in developing smart sensors.

Acknowledgments

This project was partially supported by CONACyT scholarship (229736), FOFIUAQ-2012, SEP-PIFI (Integral Program of Institutional Support—Universidad de Guanajuato) 2011, and SEP-CONACyT 84723 projects.

References

1. Siyambalapitiya, D.J.; Mclaren, P.G. Reliability improvement and economic benefits of on-line monitoring systems for large induction machines. *IEEE Trans. Ind. Appl.* **1990**, *26*, 1018–1025.
2. Bellini, A.; Filipetti, F.; Tassoni, C.; Capolino, G.A. Advances in diagnostic techniques for induction machines. *IEEE Trans. Ind. Electron.* **2008**, *55*, 4109–4126.
3. Tallam, R.M.; Lee, S.B.; Stone, G.C.; Kliman, G.B.; Yoo, J.; Habetler, T.G.; Harley, R.G. A survey methods for detection of stator related faults in induction machines. *IEEE Trans. Ind. Appl.* **2007**, *43*, 920–933.
4. Nandi, S.; Toliyat, H.A.; Li, X. Condition monitoring and fault diagnosis of electrical motors—A review. *IEEE Trans. Energy Convers.* **2005**, *20*, 719–729.
5. Cusido, J.; Romeral, L.; Ortega, J.A.; Garcia, A.; Riba, J. Signal injection as a fault detection technique. *Sensors* **2011**, *11*, 3356–3380.
6. Rangel-Magdaleno, J.J.; Romero-Troncoso, R.J.; Osornio-Rios, R.A.; Cabal-Yepez, E.; Contreras-Medina, L.M. Novel methodology for online half-broken-bar detection on induction motors. *IEEE Trans. Instrum. Meas.* **2009**, *58*, 1690–1698.
7. Hedayati-Kia, S.; Henao, H.; Mpanda-Mabwe, A.; Capolino, G.A. Wavelet Based Instantaneous Power Analysis for Induction Machine Fault Diagnosis. In *Proceedings of 32nd Annual Conference on IEEE Industrial Electronics (IECON 2006)*, Paris, France, 6–10 November 2006; pp. 1229–1334.
8. Ordaz-Moreno, A.; Romero-Troncoso, R.J.; Vite-Frias, J.A.; Rivera-Gillen, J.R.; Garcia-Perez, A. Automatic online diagnosis algorithm for broken-bar detection on induction motors based on discrete wavelet transform for FPGA implementation. *IEEE Trans. Ind. Electron.* **2008**, *5*, 2193–2202.

9. Ayhan, B.; Chow, M.; Song, M. Multiple discriminant analysis and neural-network-based monolith and partition fault-detection schemes for broken rotor bar in induction motors. *IEEE Trans. Ind. Electron.* **2006**, *53*, 1298–1308.
10. Karami, F.; Poshtan, J.; Poshtan, M. Detection of broken rotor bars in induction motors using nonlinear Kalman filters. *ISA Trans.* **2010**, *49*, 189–195.
11. Jimenez, G.A.; Muñoz, A.O.; Duarte-Mermoud, M.A. Fault detection in induction motors using Hilbert and wavelet transforms. *Electr. Eng.* **2007**, *89*, 205–220.
12. Rabelo-Baccarani, L.M.; Braga-Tavares, J.P.; Rodrigues-Menezes, B.; Matos-Caminhas, W. Sliding mode observer for on-line broken rotor bar detection. *Electr. Pow. Syst. Res.* **2010**, *80*, 1085–1089.
13. Contreras-Medina, L.M.; Romero-Troncoso, R.J.; Cabal-Yepez, E.; Rangel-Magdaleno, J.J.; Millan-Almaraz, J.R. FPGA-based multiple-channel vibration analyzer for industrial applications in induction motor failure detection. *IEEE Trans. Instrum. Meas.* **2010**, *59*, 63–72.
14. Didier, G.; Ternisien, E.; Caspary, O.; Razik, H. A new approach to detect broken rotor bars in induction machines by current spectrum analysis. *Mech. Syst. Signal Process.* **2007**, *21*, 1127–1142.
15. Supangat, R.; Ertugrul, N.; Soong, W.L.; Gray, C.; Hansen, C.; Grieger, J. Detection of broken rotor bars in induction motor using starting-current analysis and effects of loading. *IEEE Proc. Electr. Power Appl.* **2006**, *153*, 848–855.
16. Hedayati-Kia, S.; Henao, H.; Capolino, G.A. Diagnosis of broken-bar fault in induction machines using discrete wavelet transform without slip estimation. *IEEE Trans. Ind. Appl.* **2009**, *45*, 1395–1404.
17. Bellini, A.; Yazidi, A.; Filippetti, F.; Rossi, C.; Capolino, G.A. High frequency resolution techniques for rotor fault detection of induction machines. *IEEE Trans. Ind. Electron.* **2008**, *55*, 4200–4209.
18. Yahia, K.; Cardoso, A.J.M.; Zouzou, S.E.; Gueddidi, S. Broken rotor bars diagnosis in an induction motor fed from a frequency converter: Experimental research. *Int. J. Syst. Assur. Eng. Manag.* **2012**, *3*, 40–46.
19. Kral, C.; Habetler, T.G.; Harley, R.G. Detection of mechanical imbalances of induction machines without spectral analysis of time-domain signals. *IEEE Trans. Ind. Appl.* **2004**, *40*, 1101–1106.
20. Patel, T.H.; Darpe, A.K. Experimental investigations on vibration response of misaligned rotors. *Mech. Syst. Signal Process.* **2009**, *23*, 2236–2252.
21. Salem, S.B.; Bacha, K.; Chaari, A. Support vector machine-based decision for induction motor fault diagnosis using air-gap torque frequency response. *Int. J. Comput. Appl.* **2012**, *38*, doi:10.5120/4686-6812.
22. Patel, T.H.; Darpe, A.K. Vibration response of misaligned rotors. *J. Sound Vib.* **2009**, *325*, 609–628.
23. Benbouzid, M.E.H. A review of induction motors signature analysis as a medium of fault detection. *IEEE Trans. Ind. Electron.* **2000**, *47*, 984–993.
24. Antonino-Daviu, P.; Jover-Rodriguez, M.; Riera-Guasp, M.; Pineda-Sanchez, M. Arkkio, A. Detection of combined faults in induction machines with stator parallel branches through the DWT of startup current. *Mech. Syst. Signal Process.* **2009**, *23*, 2336–2351.

25. Ballal, M.S.; Khan, H.M.; Suryawanshi, R.L.; Sonolikar, R.L. Adaptive neural fuzzy inference system for the detection of inter-turn instulation and bearing wear faults in induction motor. *IEEE Trans. Ind. Eletron.* **2007**, *54*, 250–258.
26. Wang, Y.; He, Z.; Zi, Y. Enhancement of signal denoising and multiple fault signatures detecting in rotating machinery using dual-tree complex wavelet transform. *Mech. Syst. Signal Process.* **2010**, *24*, 119–137.
27. Messaoudi, M.; Sbita, L. Multiple faults diagnosis in induction motor using the MCSA method. *Hyper Sci. Int. J. Signal Image Process.* **2010**, *1*, 190–195.
28. Garcia-Perez, A.; Romero-Troncoso, R.J.; Cabal-Yepez, E.; Osornio-Rios, R.A. The application of high-resolution spectral analysis for identifying multiple combined faults in induction motors. *IEEE Trans. Ind. Electron.* **2011**, *58*, 2002–2010.
29. Romero-Troncoso, R.J.; Saucedo-Gallaga, R.; Cabal-Yepez, E.; Garcia-Perez, A.; Osornio-Rios, R.A.; Alvarez-Salas, R.; Miranda-Vidales, H.; Huber, N. FPGA-based online detection of multiple combined faults in induction motors through information entropy and fuzzy inference. *IEEE Trans. Ind. Electron.* **2011**, *58*, 5263–5270.
30. Cabal-Yepez, E.; Valtierra-Rodriguez, M.; Romero-Troncoso, R.J.; Garcia-Perez, A.; Osornio-Rios, R.A.; Miranda-Vidales, H.; Alvares-Salas, R. FPGA-based entropy neural processor for online detection of multiple combined faults on induction motors. *Mech. Syst. Signal Process.* **2012**, *30*, 123–130.
31. Lebaroud, A.; Clerc, G. Classification of induction machine faults by optimal time-frequency representations. *IEEE Trans. Ind. Electron.* **2008**, *55*, 4290–4298.
32. Obaid, R.R.; Habetler, T.G.; Tallam, R.M. Detecting Load Unbalance and Shaft Misalignment Using Stator Current in Inverter-Driven Induction Motors. In *Proceedings of Electric Machines and Drives Conference (IEMDC 2003)*, Atlanta, GA, USA, 1–4 June 2003; pp. 1454–1458.
33. Blödt, M.; Bonacci, D.; Regnier, J.; Chabert, M.; Faucher, J. On-line monitoring of mechanical faults in variable-speed induction motor drives using the wigner distribution. *IEEE Trans. Ind. Electron.* **2008**, *55*, 522–533.
34. Millan-Almaraz, J.R.; Romero-Troncoso, R.J.; Osornio-Rios, R.A.; Garcia-Perez, A. Wavelet-based methodology for broken bar detection in induction motors with variable-speed drive. *Electr. Power Compon. Syst.* **2011**, *39*, 271–287.
35. Cabal-Yepez, E.; Romero-Troncoso, R.J.; Garcia-Perez, A.; Osornio-Rios, R.A.; Alvarez-Salas, R. Multiple Fault Detection through Information Entropy Analysis in ASD-Fed Induction Motors. In *Proceedings of 8th IEEE International Symposium on Diagnostics for Electrical Machines, Power Electronics & Drives (SDEMPED 2011)*, Bologna, Italy, 5–8 September 2011; pp. 391–396.
36. Rivera, J.; Herrera, G.; Chacon, M.; Acosta, P.; Carrillo, M. Improved progressive polynomial algorithm for self-adjustment and optimal response in intelligent sensors. *Sensors* **2008**, *8*, 7410–7427.
37. Rangel-Magdaleno, J.J.; Romero-Troncoso, R.J.; Osornio-Rios, R.A.; Cabal-Yepez, E. Novel oversampling technique for improving signal-to-quantization noise ratio on accelerometer-based smart jerk sensors in CNC applications. *Sensors* **2009**, *9*, 3767–3789.
38. Granados-Lieberman, D.; Romero-Troncoso, R.J.; Cabal-Yepez, E.; Osornio-Rios, R.A.; Franco-Gasca, L.A. A real-time smart sensor for high-resolution frequency estimation in power systems. *Sensors* **2009**, *9*, 7412–7429.

39. Humin, L.; Weilin, L.; Min, L.; Monti, A.; Ponci, F. Design of smart MVDC power grid protection. *IEEE Trans. Intrum. Meas.* **2011**, *60*, 3035–3046.
40. Rodriguez-Donate, C.; Morales-Velazquez, L.; Osornio-Rios, R.A.; Herrera-Ruiz, G.; Romero-Troncoso, R.J. FPGA-based fused smart-sensor for dynamic and vibration parameter extraction in industrial robot links. *Sensors* **2010**, *10*, 4114–4129.
41. Moreno-Tapia, S.V.; Vera-Salas, L.A.; Osornio-Rios, R.A.; Dominguez-Gonzalez, A.; Stiharu, I.; Romero-Troncoso, R.J. A field programmable gate array-based reconfigurable smart-sensor network for wireless monitoring of new generation computer numerically controlled machines. *Sensors* **2010**, *10*, 7263–7286.
42. Millan-Almaraz, J.R.; Romero-Troncoso, R.J.; Guevara-Gonzalez, R.G.; Contreras-Medina, L.M.; Carrillo-Serrano, R.V.; Osornio-Rios, R.A.; Duarte-Galvan, C.; Rios-Alcaraz, M.A.; Torres-Pacheco, I. FPGA-based fused smart sensor for real-time plant-transpiration dynamic estimation. *Sensors* **2010**, *10*, 8316–8331.
43. Rodriguez-Donate, C.; Osornio-Rios, R.A.; Rivera-Guillen, J.R.; Romero-Troncoso, R.J. Fused smart sensor network for multi-axis forward kinematics estimation in industrial robots. *Sensors* **2011**, *11*, 4335–4357.
44. Depari, A.; Flammini, A.; Marioli, D.; Taroni, A. USB sensor network for industrial applications. *IEEE Trans. Instrum. Meas.* **2008**, *57*, 1344–1349.
45. Son, J.-D.; Niu, G.; Yang, B.-S.; Hwang, D.-H.; Kang, D.-S. Development of smart sensors system for machine fault diagnosis. *Expert Syst. Appl.* **2009**, *9*, 11981–11991.
46. Huang, Y. Advances in artificial neural networks—Methodological development and application. *Algorithms* **2009**, *2*, 973–1007.
47. Holtz, J. Sensorless of induction motor drives. *Proc. IEEE* **2002**, *90*, 1359–1394.
48. *WEG-CFW-08 Frequency Inverter Manual*; WEG Corporation: Jaraguá do Sul, Santa Catarina, Brazil, 2006.
49. Bellini, A.; Filippetti, F.; Franceschini, G.; Tassoni, C. Closed-loop control impact on the diagnosis of induction motors faults. *IEEE Trans. Ind. Appl.* **2000**, *36*, 1318–1329.
50. Menacer, A.; Champenois, G.; Nait-Said, M.S.; Benakcha, A.; Moreau, S.; Hassaine, S. Rotor failures diagnosis of squirrel cage induction motors with different supplying sources. *J. Electr. Eng. Technol.* **2009**, *4*, 219–228.
51. *Motors and Generators*; ANSI/NEMA MG 1-2003 (R2004) Standards Publication; National Electrical Manufacturers Association: Rosslyn, VA, USA, 2011.

Thermographic technique as a complement for MCSA in induction motor fault detection

A.G. Garcia-Ramirez, L.A. Morales-Hernandez, R.A. Osornio-Rios, *Member*, *IEEE*, A. Garcia-Perez, *Member*, *IEEE*, R.J. Romero-Troncoso, *Senior Member*, *IEEE*.

***Abstract* -- Recently, mechanical condition monitoring in induction motors has become an important research area because of its relevance in different industrial applications. Infrared thermography has been considered for improving the monitoring of induction motors with the advantage of being a non-invasive technique and having a wide range of analysis. In this work, infrared thermography is used as complementary tool for motor current signature analysis (MCSA) under three common mechanical faults: bearing defects, unbalanced mass and misalignment, based on thermographic image segmentation and statistical feature extraction under the segments of interest. Results show the overall performance of the proposed technique as a complement in induction motor monitoring of mechanical faults.**

***Index Terms*—Induction motors, Infrared imaging, Temperature, Thermal analysis.**

I. Introduction

MECHANICAL faults is one of the most important topics in induction motor condition monitoring, due to they cover around 53% of the faults [1]. In general, mechanical faults are related the eccentricities such as misalignment, mass unbalance [2-6], and bearing defects [6-10]. Nowadays, for monitoring induction motor faults, motor current signature analysis (MCSA) is one of the most used techniques. In [1, 11-14] the MCSA technique is used to detect specific electrical and mechanical induction motor faults, with different digital signal processing techniques. Recently, infrared thermography (IRT) has become a widely accepted condition monitoring tool where the temperature is measured online in a non-contact manner [15]. Therefore, IRT analysis is currently applied to machine condition monitoring and diagnosis field [6]. For instance, in [6] it is proposed a fault diagnosis system for rotating machinery using IRT by extracting features of the enhanced image, with a support vector machine (SVM) for diagnosis, where four conditions are considered: healthy (HLT), misalignment (MAL), bearing defect (BD) and mass unbalance (UNB). Tran *et al*. [16] proposed a diagnosis system with residue gray-scale transformation and enhanced image to classify shaft faults attached to the induction motor. Picazo-Rodenas *et al.* [17] proposed a methodology based on the combination between the heat transfer theory and infrared data to build a thermal model of the induction motor and comparing the results with faulty machines. Eftekhari *et al.* [18] proposed an algorithm to extract features and predict failures in the stator winding. Recently, the IRT analysis has become more attractive due to the low cost of infrared cameras. All the research works mentioned above focus on the detection of the specific faults in the induction motor with hot-spots and the region of the motor frame which are specific in single points and regions of the induction motor and that only grants one temperature of it, leaving aside the thermal behavior of the whole induction motor with different segments of it to improve the monitoring and complement other techniques such as MCSA. The presence of a specific fault affects in the induction motor, which also increases its temperature, and this effect can be identified using IRT.

The contribution of this work is to present the thermography technique as a helpful complement for other techniques such as MCSA under different mechanical faults. An IRT camera is located aside the induction motor to acquire the thermogram. The proposed methodology is based on the segmentation of thermograms to extract the mean ($T\mu$) and the standard deviation (σ) of the temperature in each segment under different mechanical conditions and to extract the frequencies of interest of the faulty conditions through MCSA. The methodology is proposed in order to observe the affection points of the faults with thermography and complement the MCSA analysis. In this paper, three different faults in an induction motor are studied: BD, MAL, UNB and their thermal behavior on the induction motor.

II. Theoretical Background

A. Infrared Thermography

Infrared detectors are the principal components of IRT cameras, which absorb the infrared radiation emitted by a body in a non-contact way, and using Stefan-Boltzmann's law, the temperature of the body is obtained [15]. The IRT cameras can capture an image of thermal pattern called thermogram, where each pixel of the thermogram has a temperature value and a pseudo-color assigned according a palette of colors [19]. The IRT analysis has the advantage to offer a two-dimensional signal, which through segmentation is able to analyze specific areas, allowing the possibility of a broader analysis of the induction motor and its thermal behavior from the start-up up to thermal steady-state, which is important for establishing the maximum temperature that the induction motor can reach.

B. Motor current signature analysis

MCSA is a recognized technique used in the industry due to is a non-invasive method to induction motor condition monitoring. This technique allows distinguishing the effects of mechanical and electrical faults. For this analysis is

This work was supported by CONACyT under Scholarship 229736 and SEP PIFI-2013 Universidad de Guanajuato grant.

R.J. Romero-Troncoso is with HSPdigital CA-Telematica at DICIS, University of Guanajuato, Salamanca, Gto. 36885 Mexico (corresponding author; e-mail: troncoso@hspdigital.org).

A.G. Garcia-Ramirez is with HSPdigital CA-Mecatronica at Facultad de Ingenieria, Campus San Juan del Rio, Universidad Autonoma de Queretaro, San Juan del Rio, Qro. 76807 Mexico (e-mail: aggarcia@hspdigital.org).

L.A. Morales-Hernandez is with HSPdigital CA-Mecatronica at Facultad de Ingenieria, Campus San Juan del Rio, Universidad Autonoma de Queretaro, San Juan del Rio, Qro. 76807 Mexico (e-mail: lamorales@hspdigital.org).

R.A. Osornio-Rios is with HSPdigital CA-Mecatronica at Facultad de Ingenieria, Campus San Juan del Rio, Universidad Autonoma de Queretaro, San Juan del Rio, Qro. 76807 Mexico (e-mail: raosornio@hspdigital.org).

A. Garcia-Perez is with HSPdigital CA-Telematica at DICIS, University of Guanajuato, Salamanca, Gto. 36885 Mexico (e-mail: arturo@salamanca.ugto.mx).

necessary to set a sensor (current clamp or hall-effect sensor) in single current phase of the induction motor. In this work three mechanical faults are studied: bearing defects, mass unbalance and misalignment. The bearing defect (BD) condition corresponds to 40-50% of faults in induction motors [20], producing a deterioration in the lubricant of the bearing and an irregular friction in the bearing housing. Due to this irregular friction an increase in temperature is reflected, being propagated through the induction motor body [21]. Unbalanced mass (UNB) is present when the mechanical load is not uniformly distributed in the rotor, whereas the misalignment condition (MAL) occurs when the pulleys of the load and the motor are not correctly aligned. These faults generate more mechanical stress and excessive rubbing and fatigue of the ball bearings, which can be reflected into an efficiency decrease, demands more load and consequently an increase of slip and also the torque is increased with a consequent temperature rising in the induction motor and its parts [22]. This fault can be detected through MCSA because this faults have characteristic frequencies in the current spectrum whether the faults are: In the case of bearings with 6 to 12 rolling elements, the fundamental outer race frequency (f_o) is calculated approximately as given in (1), where f_r is the rotor frequency, N the number of ball bearings and f is the line supply frequency. This way, it is possible to determine the bearing race frequencies for all seven ball combinations without having explicit knowledge of the bearing configuration [23]. Otherwise, misalignment and unbalance mass creates air-gap eccentricities changing the frequency spectrum of the supply current, due to these affects the inductances of the motor resulting in harmonics (f_{ecc}) at rotating frequency sidebands of the supply frequency predicted by (2).

$$f_o = f \pm f_r \cdot N \cdot 0.4 \tag{1}$$

$$f_{ecc} = f\left[1 \pm k\left(\frac{1-s}{p}\right)\right] \tag{2}$$

Where f is the line supply frequency, k is the harmonic index, s is the slip and p is the number of pole pairs [1].

III. METHODOLOGY

A. Proposed methodology

The proposed methodology consists on the MCSA through spectral analysis to extract the frequencies of interest of the faults and on image segmentation of thermograms and a statistical feature extraction which permits a full analysis of the induction motor thermal behavior for complementing the MCSA.

B. Spectral analysis trough MCSA

With the objective to use the thermographic technique as a complement for techniques of induction motor fault detection, the MCSA analysis was used. The current data were obtained from a hall-effect sensor placed on a single current phase, captured during the operation of the motor in steady-state in each treated fault. Then, the fast Fourier transform (FFT) is applied to get the current spectrum. Afterward, the frequencies of interest for the different faults are evaluated in order to detect the fault that has been carried out. The frequency of interest for bearing defect is computed through (1), where the tested induction motor has a rotor frequency f_r = 55 Hz, a line supply frequency f = 60 Hz and the test bearing has eight balls; thus the ball pass outer raceway frequency defect is found in f_o = 116 Hz. On the other hand, the frequency of interest for misalignment and unbalance mass is computed by (2), where the tested induction motor has one pole pairs and the slip selection for MAL is s = 13.27 % giving a f_{ecc} = 112 Hz and for UNB is s = 7.41 % with a f_{ecc} = 115.5 Hz, but in order to have a better analysis of all the treated faults the band of analysis is in a range from 1% to 20% in order to fulfill the NEMA standard of A, B, C and D designs [24] giving a band of interest from 108 -119.4 Hz. Finally, making a comparative of amplitude between each frequency band of the faults a detection can be done.

C. Segmentation

This segmentation is manually done in the thermograms taken by a calibrated IRT camera through resistance temperature detectors (RTDs) as well as in [25]. Then, these thermograms are divided in two principal segments (*S1* – motor frame and *S2* – bearing). Fig 1a shows the motor under test where the segments are located in a visual image and Fig 1b shows those segments in the thermogram.

D. Statistical features

In this methodology two statistical features are extracted: the mean ($T\mu$) and the standard deviation (σ) of the temperature in each segment to analyze the thermal behavior of the induction motor, where $T\mu$ grants the average temperature of each segment of the induction motor under each thermogram and σ is an indicator for the temperature homogeneity of each segment. This mean ($T\mu$) allows establishing a healthy motor signature on thermal steady-state conditions, through captured thermograms during the operation of the motor under the analyzed condition to give the reference point of analysis. Therefore, it is important to know the standard deviation (σ) of the induction motor, because this value gives a reference on how the temperature is behaving and distributed, when the induction motor reach its thermal steady-state or its thermal balance, due to the temperature values are less dispersed and consequently the temperature is homogeneous.

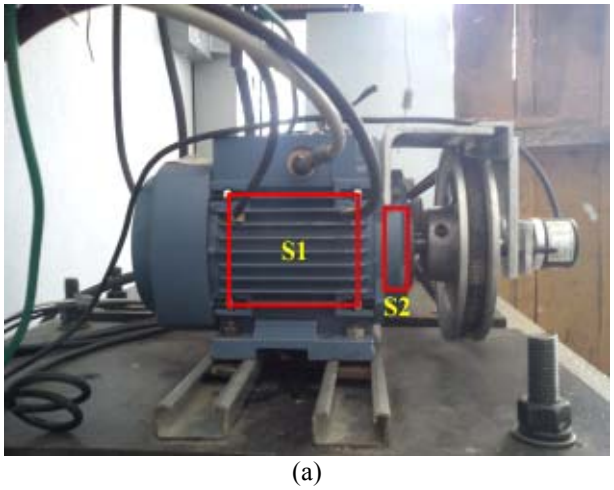

(a)

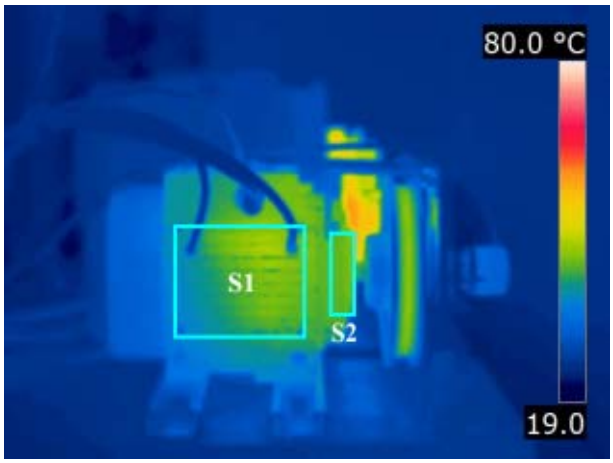

(b)

Fig. 1. Segmentation: (a) Digital image and (b) Thermographic image.

IV. Experiment

A. Experimental Setup

Fig. 2 shows the experimental setup, consisting in a thermographic camera FLIR A310 at a distance of 1.2 m. The IRT camera is set to a temperature range of 19-80°C for each thermogram. A 1-hp three-phase induction motor (WEG 00136AP3E48T) used for testing the fault conditions treated in this work. This induction motor has 2 poles, 28 bars and receives a power supply of 220 V AC. The applied mechanical load embraces around 100% represented by an ordinary alternator. The current signal is acquired using a hall-effect sensor model L08P050D15, from Tamura Corporation. A 12-bit 4-channel serial-output sampling analog-to-digital converter ADS7841 from Texas Instrument Incorporated is used in the data acquisition system (DAS) with an *fs* = 4 kHz obtaining 4096 samples during 1.024 seconds of the induction motor in steady-state. The IRT camera takes a thermogram every minute of the induction motor from start-up to thermal steady-state during 50 minutes. The acquired data is stored in a personal computer (PC) and analyzed in Matlab which provides the $T\mu$ and the σ of each segment under each thermogram and the spectrum of the current signal.

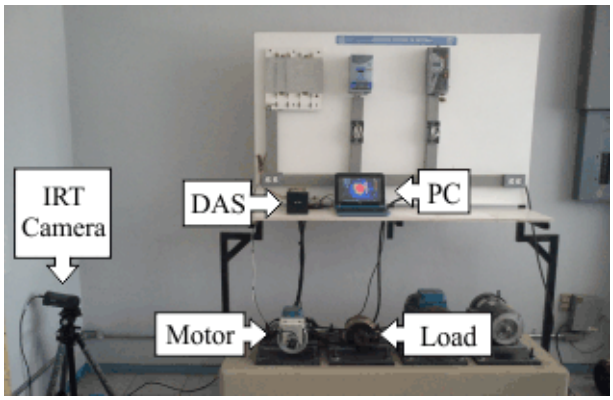

Fig. 2. Experimental setup.

B. Treated faults

In this work three different induction motor mechanical faults are studied: bearing defects (BD), mass unbalance (UNB) and misalignment condition (MAL).

The bearing defect was made drilling a 2.0 mm hole in the outer race as shown in Fig. 3a. The unbalance mass was made by attaching a bolt in an arm of the rotor pulley as Fig. 3b shows, and finally for the misalignment condition was produced by shifting backward the belt in the load pulley, so the transverse axes of rotation for the induction motor and its load were not aligned as shown in Fig 3c.

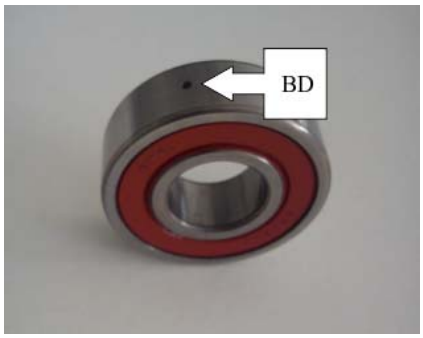

(a)

(b)

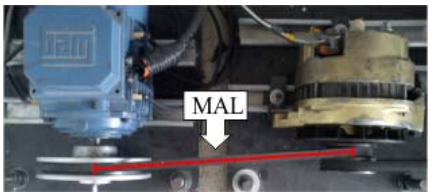

(c)

Fig. 3. Treated faults: (a) BD, (b) UNB and (c) MAL.

V. Results and Discussion

Three different mechanical fault condition cases are studied through MCSA and thermography. In order to obtain statistically significant results, 5 tests were performed to acquire the thermograms and the current signals from the induction motor in all treated cases. Otherwise, Fig 4 shows that after 40 minutes from the startup of the induction motor, the thermal steady-state is reached in each thermographic segments (S_1 and S_2) and the dispersion σ is around the 8% for *S1* due to the cooling air of the fan in this area, and 2% for *S2* where the dispersion is less due to it is the farthest segment in respect to the fan. Therefore, after meeting the thermal steady-state of the healthy induction motor, the thermograms and the current signal of the motor with each treated fault are taken after 50 minutes from the start-up to evaluate the faults. Fig. 5a-d depict the thermograms for each condition of the induction motor (HLT, BD, UNB, MAL, respectively) in the minute 50, where the thermal steady-state is reached. Based on the thermograms the $T\mu$ value of each segment under the different conditions can be extracted as well as the standard deviation σ in order to evaluate the homogeneity in the thermal steady-state for each condition, where for BD has a σ of 7.81% for S1 and

2.36% for S2. Then, for UNB σ is 7.65% and 1.36% for S1 and S2, respectively. Finally, for MAL, σ for S1 is 10.42% and 3.34% for S2. These results depend on the construction of the induction motor and can be used for describing its thermal behavior. As it can be observed, the standard deviation in S1 is greater than in S2; consequently, the temperature in S2 is more homogeneous. On the other hand, for the current signal the FFT was applied, based on this, the band of interest was extracted as shown in Fig. 5e-h in order to assess the faults, where is quietly visible the amplitude of the fault frequencies. According to these results, with BD shows with MCSA the frequency of interest f_o = 116 Hz has an amplitude of -53.66 dB this show an increase of amplitude compared with HLT condition, then through IRT the fault can be asserted analyzing the segments of interest where, for *S1* show a temperature of 46.6 °C and for *S2* an increase in temperature up to 50.73 °C for BD because the analyzed segment corresponds to the location of the bearing where they show an increase of temperature in comparison with HLT. This behavior is due to the abnormal friction in the bearing. On the other hand, for UNB the results for MCSA show an amplitude difference with HLT of 16.46 dB in 115.5 Hz, which sometimes if the slip is unknown is difficult to find the frequency of the fault. Hence, the IRT is used to ensure the fault analyzing the segments of interest: in segment *S1* the temperature is about 46.6 °C and for segment *S2* = 48 °C, due to the UNB condition produces a slight eccentricity because of the mechanical load is not uniformly distributed, showing a considerable impact stress in the bearing due to this condition has indirect effects on it. Finally, for MAL condition the results for MCSA present an amplitude of -60.13 dB in 112 Hz where the frequency of interest is displaced -3.5 Hz due to the slip that produces the fault, due to these, sometimes the analysis through MCSA is difficult to interpret. For this condition using IRT is quietly visible that produces a higher increase in temperature up to 67 °C in *S1* and *S2* because there is more mechanical stress in this condition. Using IRT is easy to notice that MAL is the most critical condition due to the excessive rubbing and fatigue generated at the ball bearings, with a temperature increase of up to 67 °C in the thermal steady-state.

A meaningful characteristic of this work is the capacity of the thermographic analysis as a complementary technique for MCSA used in fault diagnosis. Although, with the MCSA technique the fault can be detected, sometimes is difficult due to appears spurious harmonics that can be seen like faults and the different slips that the faults generate displacing the frequency of interest. Consequently, the thermographic technique is helpful, since after knowing the healthy motor signature, it is fairly intuitive to find the fault, because the thermal conditions when a fault is present are different from the signature when the motor is healthy, due to the thermal energy is focused in the fault of interest and its closest components.

VI. Conclusions

This work proposes a complementary technique for induction motor fault detection using IRT and MCSA. The proposed technique focuses on the extraction of frequencies of interest through MCSA and on the average temperature and the standard deviation of two thermal segments.

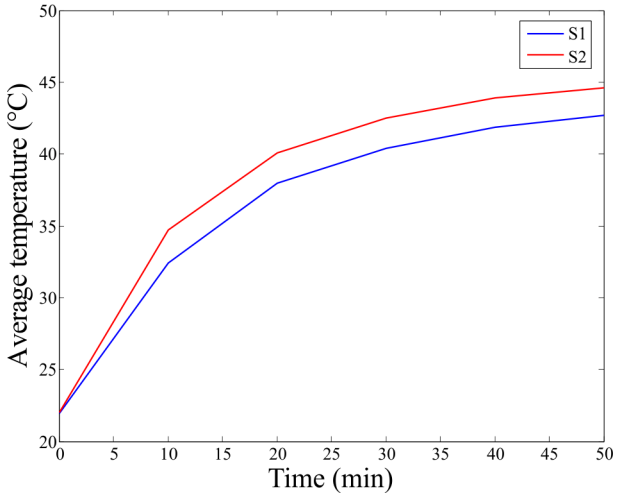

Fig. 4. Healthy motor thermal behavior of segments *S1* and *S2*.

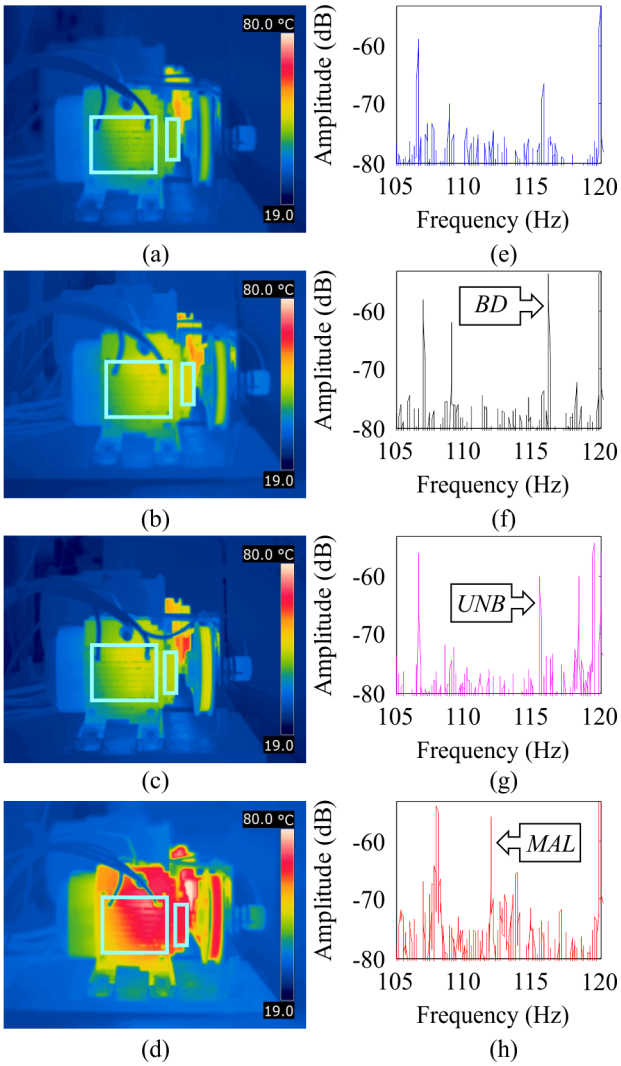

Fig. 5. Thermograms for the conditions: (a) HLT, (b) BD, (c) UNB and (d) MAL. Frequency band of interest: (e) HLT, (f) BD, (g) UNB and (h) MAL.

The frequency spectra show the localization of the faults in the frequencies of interest computed through (1) and (2) where sometimes spurious harmonics appears and the detection can be difficult. Therefore, using the average temperature depicts that for each fault the increase of temperature is different due to the nature of each fault the thermal energy is focused in the fault of interest and its closest components. These, give a rise to apply the IRT

technique as a complementary tool for MCSA in induction motor fault detection.

The proposed methodology can be used for industrial applications in motor fault diagnosis due to its simplicity. For future work, it is proposed to develop the methodology for different fault severities and to develop a smart instrument for automatic fault identification through IRT.

VII. REFERENCES

[1] J. Cusido, L. Romeral, J.A. Ortega, A. Garcia and J. Riba, "Signal ingection as a fault detection technique," *Sensors*, vol. 11, pp. 3356-3380, Mar. 2011.

[2] C. Kral, T.G. Habetler and R.G. Harley, "Detection of mechanical imbalances of induction machines without spectral analysis of time-domain signals," *IEEE Trans. Industrial Applications*, vol. 40, pp. 1101-1106, July-Aug. 2004.

[3] J.M. Bossio, G.R. Bossio and C.H. De Angelo, "Angular misalignment in induction motors with flexible coupling," in *Annual Conference of Industrial Electronics (IECON 2009),* pp. 1033-1038, 2009.

[4] T.H. Patel and A.K. Darpe, "Experimental investigations on vibration response of misaligned rotors," *Elsevier Mechanical systems and signal processing,* vol. 23, pp. 2239-2252, May. 2009.

[5] L.M. Contreras-Medina, R.J. Romero-Troncoso, E. Cabal-Yepez, J.J. Rangel-Magdaleno and J.R. Millan-Almaraz, "FPGA-Based multiple-channel vibration analyzer for industrial applications in induction motor failure detection," *IEEE Trans. Instrumentation and Measurement*, vol. 59, pp. 63-72, Jan. 2010.

[6] A.MD. Younus and B. Yang, "Intelligent fault diagnosis of rotating machinery using infrared thermal image," *Elsevier Expert Systems with Applications,* vol. 39, pp. 2082-2091, Feb. 2012.

[7] M. Delgado-Prieto, G. Cirrincione, A. Garcia-Espinosa, J.A. Ortega and H. Henao, "Bearing fault detection by a novel condition-monitoring scheme based on statistical-time features and neural networks," *IEEE Trans. Industrial Electronics*, vol. 30, pp. 3398-3407, Aug. 2013.

[8] H.S. Kumar, P. Srinivasa Pai, N.S. Sriram and G.S. Vijay, "ANN based evaluation of performance of wavelet transform for condition monitoring of rolling element bearing," *Elsevier Procedia Engineering,* vol. 64, pp. 805-814, 2013.

[9] M.A. Abu-Zeid and S.M. Abdel-Rahman, "Bearing problems' effects on the dynamic performance off pumping stations," *Elsevier Alexandria Engineering Journal,* vol. 52, pp. 241-248, Mar. 2013.

[10] M. Barakat, M. El Badaoui, and F. Guillet, "Hard competitive growing neural network for the diagnosis of small bearing faults," *Elsevier Mechanical Systems and Signal Processing,* vol. 37, pp. 276-292, Feb. 2013.

[11] L. Frosini and E. Bassi, "Stator current and motor efficiency as indicators for different types of bearing faults in induction motors," *IEEE Trans. Industrial Electronics,* vol. 57, pp. 244-251, Jan. 2010.

[12] I.Y. Onel, M.E.H. Benbouzid, "Induction motor bearing failure detection and diagnosis: Park and Concordia transform approaches comparative study," *IEEE International Electric Machines & Drives Conference (IEMDC 2007),* pp. 1073-1078, (2007).

[13] M. Riera-Guasp, J. Pons-Llinares, F. Vedreno-Santos, J.A. Antonino-Daviu, M. Fernandez-Cabanas, "Evaluation of the amplitudes of high order fault related components in double bar faults," *IEEE International Symposium on Diagnosis for Electrical Machines Power Electronics and Drives (SDEMPED 2011),* pp. 307-315, 2011.

[14] P. Gardel, D. Morinigo-Sotelo, O. Duque-Perez, M. Perez-Alonso, L.A. Garcia-Escudero, "Neural network broken bar detection using time domain and current spectrum data," *20th International Conference on Electrical Machines (ICEM 2012),* pp. 2492-2497, 2012.

[15] S. Bagavathiappan, B.B. Lahiri, T. Saravanan, J. Philip and T. Jayakumar, "Infrared thermography for condition monitoring – A review," *Elsevier Infrared Physics & Technology,* vol. 60, pp. 35-55, Mar. 2013.

[16] V.T. Tran, B.S. Yang, F. Gu, A. Ball, "Thermal image enhancement using bi-dimensional empirical mode decomposition in combination with relevance vector machine for rotating machinery fault diagnosis", *Elsevier Mechanical Systems and Signal Processing,* vol. 38, pp. 601-614, Jul. 2013.

[17] M.J. Picazo-Rodenas, R. Royo, J. Antonino-Daviu and J. Roger-Folch, "Use of the infrared data for heating curve computation in induction motors: Application to fault diagnosis," *Elsevier Engineering Failure Analysis,* vol. 35, pp. 178-192, Dec. 2013.

[18] M. Eftekhari, M. Moallem, S. Sadri and M.-F. Hsieh, "A novel indicator of stator winding inter-turn fault in induction motor using infrared thermal imaging," *Elsevier Infrared Physics & Technology,* vol. 61, pp. 330-336, 2013.

[19] S. Taib, M.S. Jadin and S. Kabir, "Thermal imaging for enhancing inspection reliability detection and characterization," Dr. Raghu V. Prakash, Ed. InTech, 2012, pp. 209-236. Available: http://www.intechopen.com/books/infrared-thermography/thermal-imaging-for-enhancing-inspection-reliability-detection-and-characterization

[20] A. Garcia-Perez, R.J. Romero-Troncoso, E. Cabal-Yepez and R.A. Osornio-Rios, "The application of high-resolution spectral analysis for identifying multiple combined faults in induction motors," *IEEE Trans. Industrial Applications,* vol. 47, pp. 34-46, Jan.-Feb. 2011.

[21] P. Zhang, Y. Du, T.G. Habetler and B. Lu, "A survey of condition monitoring and protection methods for medium voltage induction motors," *IEEE Trans. Industrial Elextronics,* vol. 58, pp. 2002-2010, May 2011.

[22] J. Faiz and M. Ojaghi, "Different indexes for eccentricity faults diagnosis in three-phase squirrel-cage induction motors: A review," *Elsevier Mechatronics,* vol. 60, pp. 35-55, Mar. 2013.

[23] E.C.C. Lau and H.W. Ngan, "Detection of motor bearing outer raceway defect by wavelet packet transformed motor current signature analysis," *IEEE Trans. Instrumentation and Measurement*, vol. 59, pp. 2683-2690, 2010.

[24] Motors and Generators, "ANSI/NEMA MG 1-2003 (R2004) Standards Publication," *National Electrical Manufacturers Association,* Rosslyn, VA, USA, 2011.

[25] A.G. Garcia-Ramirez, L.A. Morales-Hernandez, R.A. Osornio-Rios, J.P. Benitez-Rangel, A. Garcia-Perez and R.J. Romero-Troncoso, "Fault detection in induction motors and the impact on the kinematic chain," *Elsevier Electric Power System Research,* vol. 114, pp. 1-9, 2014.

VIII. BIOGRAPHIES

Armando G. Garcia-Ramirez received the B. E. degree from the Mazatlan Institute of Technology, Mazatlan, Mexico, and the M.E. degree (Hons.) from the University of Guanajuato, Salamanca, Mexico in 2011, where he did research work at the HSPdigital group. Currently, he is a Ph.D. student at the Autonomous University of Queretaro, Queretaro, Mexico. His research interest includes hardware signal processing on field-programmable gate arrays, smart sensors and thermography analysis for applications in mechatronics.

Luis Alberto Morales-Hernandez received the Ph. D. degree in image processing from the Autonomous University of Queretaro, Queretaro, Mexico, in 2009. He is currently a Professor with the department of Electromechanical Engineering, in the University of Queretaro. He is a National Researcher with the Consejo Nacional de Ciencia y Tecnologia level 1. He has more than 20 publications in international journals and conferences. His fields of interest include image processing, computer vision for applications in mechatronics.

Roque A. Osornio-Rios (M'10) received the B.E. degree from the Instituto Tecnologico de Queretaro, Queretaro, Mexico, and the M.E. and the Ph.D. degrees from the University of Queretaro, Queretaro, Mexico, in 2007. He is a National Researcher with CONACYT. He is currently Professor with the University of Queretaro. He was an Advisor of over 30 theses, and a coauthor of over 40 technical papers in international journals and conferences His fields of interest include hardware signal processing and mechatronics. Dr. Osornio-Rios received the "2004 ADIAT National Award on Innovation" for his works in applied mechatronics.

Arturo Garcia-Perez (M'10) received the B.E. and M.E. degrees in electronics from the University of Guanajuato, Salamanca, Mexico, in 1992 and 1994, respectively, and the Ph.D. degree in electrical engineering from the University of Texas at Dallas, Richardson, in 2005. He is currently a Titular Professor with the Department of Electronic Engineering, University of Guanajuato. He is a National Researcher with the Consejo Nacional de Ciencia y Tecnología level 2. He was an Advisor of over 50 theses. His fields of interest include digital signal processing for applications in mechatronics.

Rene de J. Romero-Troncoso (M'07–SM'12) received the Ph.D. degree in mechatronics from the Autonomous University of Queretaro, Queretaro, Mexico, in 2004. He is a National Researcher level 2 with the Mexican Council of Science and Technology, CONACYT. He is currently a Head Professor with the University of Guanajuato and an Invited Researcher with the Autonomous University of Queretaro, Mexico. He has been an advisor for more than 190 theses, an author of two books on digital systems (in Spanish), and a coauthor of more than 100 technical papers published in international journals and conferences. His fields of interest include

hardware signal processing and mechatronics. Dr. Romero–Troncoso was a recipient of the 2004 Asociación Mexicana de Directivos de la Investigación Aplicada y el Desarrollo Tecnológico Nacional Award on Innovation for his work in applied mechatronics, and the 2005 IEEE ReConFig Award for his work in digital systems. He is part of the editorial board of Hindawi's The Scientific World Journal and the International Journal of Manufacturing Engineering.

Electric Power Systems Research 114 (2014) 1–9

Contents lists available at ScienceDirect

Electric Power Systems Research

journal homepage: www.elsevier.com/locate/epsr

Fault detection in induction motors and the impact on the kinematic chain through thermographic analysis

Armando Guadalupe Garcia-Ramirez [a], Luis Alberto Morales-Hernandez [a], Roque Alfredo Osornio-Rios [a], Juan Primo Benitez-Rangel [a], Arturo Garcia-Perez [b], Rene de Jesus Romero-Troncoso [b,*]

[a] HSPdigital-CA Mecatronica/Facultad de Ingenieria, Campus San Juan del Rio, Universidad Autónoma de Querétaro, Rio Moctezuma 249, Col. San Cayetano, 76807 San Juan del Rio, Queretaro, Mexico
[b] HSPdigital-CA Telematica/Procesamiento Digital de Senales, DICIS, Universidad de Guanajuato, Carr., Salamanca-Valle km 3.5+1.8, Comunidad de Palo Blanco, 36885 Salamanca, Guanajuato, Mexico

ARTICLE INFO

Article history:
Received 14 July 2013
Received in revised form 28 March 2014
Accepted 30 March 2014

Keywords:
Fault diagnosis
Induction motors
Infrared thermography
Kinematic chain
Thermographic analysis

ABSTRACT

Thermographic analysis has been considered a technique that can be used in fault diagnosis with the advantage of being non-invasive and having a wide range of analysis. Nevertheless, other techniques such as motor current signature analysis (MCSA) and vibration analyses are still preferred. Regrettably, these techniques focus only on the detection of specific faults dismissing the repercussion of the induction motor parts and the elements of their kinematic chain. This work presents a methodology based on thermographic image segmentation for fault detection in induction motors, and the repercussion of these faults along the kinematic chain.

1. Introduction

Condition monitoring and fault detection in induction motors have become an important research area due to their widespread use in different industrial applications [1] for instance, induction motor faults are mainly associated with bearing defects [2–8], rotor faults such as broken rotor bars [9–14], mechanical unbalance [15–17], misalignment [18,19] and voltage unbalance [20–22]. However, the methodologies to diagnose these faults are becoming complex and specific, dismissing that the induction motor is always connected to a kinematic chain (pulleys, belts or couplings) [23]. Therefore, a fault in the induction motor has repercussions throughout the linked chain. At present, the most common techniques to monitor and diagnose the induction motor fault conditions are MCSA, vibration and thermography.

MCSA is one of the most used techniques because it is simple, non-invasive and can be automated. In [5–17], MCSA is used for detecting specific electrical and mechanical induction motor faults, using different digital signal processing methodologies. Otherwise, in [24–26] the MCSA technique is used to detect multiple-combined faults. Several signal processing methodologies which use this technique have a heavy computational load only used for detecting the treated faults, ignoring the implication on other links of the kinematic chain, or even other parts of the induction motor. Regarding vibration analysis, it has the advantage of being more sensitive than the MCSA technique for certain faults [15], but it has the disadvantage of being invasive, requiring the installation of an external sensor. Signal processing methodologies for vibration analysis are similar in complexity to those used in the MCSA technique, and they can be automated aiming at fault detection. Despite this, vibration analysis indicates only the presence or the absence of a fault, without considering the collateral effects of faults in the kinematic chain. Currently, these techniques are used to identify specific faults in induction motors. For instance, the fault diagnosis of bearing defects is a widely studied problem [2–6]. The effects of misalignment and unbalance are commonly established for frequency components of the electrical current [18]. Besides, the presence of broken rotor bars is one of the most studied conditions in research literature [9–14]. However, there are no studies on how these faults affect the elements of the kinematic chain.

* Corresponding author. Tel.: +52 464 647 9940; fax: +52 (464) 6479940 ext. 2311.
E-mail addresses: aggarcia@hspdigital.org (A.G. Garcia-Ramirez), lamorales@hspdigital.org (L.A. Morales-Hernandez), raosornio@hspdigital.org (R.A. Osornio-Rios), benitez@uaq.mx (J.P. Benitez-Rangel), agarcia@hspdigital.org (A. Garcia-Perez), troncoso@hspdigital.org (R.d.J. Romero-Troncoso).

http://dx.doi.org/10.1016/j.epsr.2014.03.031
0378-7796/

An induction motor fault is identified by the increment of temperature in the affected component [27]. At the same time, the fault affects other components of the kinematic chain that also increases the temperature which could be identified with the use of thermographic imaging. Hence, infrared thermography has been considered a new technique that can be used in fault diagnosis, because of its capability to measure the temperature on the surface of an induction motor with the advantages of, on one hand, being non-invasive [28]; and on the other hand, being able to globally monitor the induction motor and its kinematic chain by locating hot spots where temperature has been increased. Tran et al. in [29] proposed a diagnosis system with residue using gray-scale transformation and image enhancement to classify faults on the shaft attached to the induction motor. Picazo-Rodenas et al. in [27] used the thermographic analysis to build the thermal model of the induction motor by comparing the results with those corresponding to faulty machines. All the aforementioned works use thermal analysis taking the thermal image without calibration, focusing on induction motor fault detection or local hot spots of the induction motor and where the fault is held, disregarding the impact of these faults in the induction motor and in the whole kinematic chain. Thermographic analysis can be expensive because of the camera, though. Recently, these cameras have become more commercially available at lower prices [30,31], making it possible to enliven this analysis. The presence of faults in the induction motor can damage other parts of the motor and the kinematic chain, these faults may not be considered when a corrective maintenance is done. That is why, it is necessary to develop a methodology based on thermographic analysis which may be capable of identifying the thermal repercussions on the whole kinematic chain under the presence of faults in the induction motor.

This work proposes a thermographic-based methodology using both image segmentation for fault detection and diagnosis in induction motors, as well as the impact of these conditions in the kinematic chain. The contribution of this work is the identification of faults and the study of how the different induction motor conditions affect other elements in an induction motor and its kinematic chain, through the use of thermographic images. These images are thermally calibrated by means of six resistance temperature detectors (RTD) located on the induction motor, and another one is used to measure environmental temperature. The thermographic camera is strategically placed to fully cover in its image field the induction motor and the associated kinematic chain. Although the proposed methodology uses more sensors and a thermographic camera; this technique complements and is capable of improving the MCSA and the vibration methodologies, not only in the induction motor but in its kinematic chain as well. Experimental validation of the proposed methodology is done in two different kinematic chains under five different conditions in an induction motor: bearing defects, broken rotor bar, misalignment, mechanical unbalance, and voltage unbalance. Results show the feasibility of fault detection, as well as the thermal impact of the conditions on the induction motor and the associated kinematic chain.

2. Theoretical background

In this section, three different topics for the induction motor and their kinematic chain analysis through thermographic images are presented: First, the infrared thermography; second, the image segmentation topic and finally, the motor faults and their thermal relationship.

2.1. Infrared thermography

The thermographic camera sensor is an infrared detector whose objectives are to absorb both the energy emitted by the object and the temperature of the surface to be measured, and convert it into a signal. Relying on the Stefan–Boltzmann law, it says that any object emits proportional energy to the surface temperature [27], however, the energy actually detected by the infrared sensor depends on the emissivity coefficient of the surface to be measured, using the concept of Planck law [32]. The infrared thermographic camera can capture an image of the thermal pattern and can be used in several temperature ranges depending on the emissivity of the surface. The thermographic digital image captured by the camera is called a thermogram. Each pixel of a thermogram has a specific temperature value, and the contrast of the image is derived from the differences in temperature of the object surface [33]. It can occur in levels of gray. The colour assignment for each degree of temperature is based on a palette of colours with which it is allowed to view the object temperature. The infrared thermographic analysis has the advantage of offering a two-dimensional signal, through which segmentation is capable of analysing a specific hot spot or small areas [33].

2.2. Image segmentation

Image segmentation is usually defined as the partitioning of an image into non-overlapping constituent regions, which are homogeneous with respect to some characteristics, such as intensity, texture or feature [34–36]. The segmentation can be done manually or automatically. If the domain of the image is given by I, then the segmentation problem is to determine the sets $S_i \in I$ whose union is the entire image I. Thus, the sets that make up segmentation must satisfy Eq. (1).

$$I = \bigcup_{i=1}^{M} S_i \tag{1}$$

where $Si \cap Sj = 0$ for $i \neq j$, and each S_i is connected.

2.3. Motor faults and thermal relationship

Five of the most studied fault conditions are: bearing defects, broken rotor bars, misalignment, mechanical unbalance and voltage unbalance. Bearing defect (BD) is a very common failure in induction motors, producing deterioration in the bearing lubrication and an abnormal friction in the bearing housing. This abnormal friction is reflected in an increase of temperature [37], which propagates into the induction motor and other parts of the kinematic chain. Broken rotor bars consist of a total or partial breakage of bars inside the rotor armour. This fault appears because of welding defects, high strength joints, hot spots and mechanical stresses [27]. When a joint resistance appears in a bar, heat dissipation takes place around that point. On the other hand, broken rotor bar (BRB) is a fault which the detection is important because of its progressiveness. This fault propagates to adjacent bars due to the increment of current and temperature, accelerating the damage in the induction motor [27] and consequently to other elements in the kinematic chain. Misalignment (MAL) is presented when the motor and the load pulleys are not aligned and a mechanical unbalance (UNB) occurs when the mechanical load in the induction motor is not uniformly distributed. These faults can be expressed as an eccentricity in the induction motor, which generates more mechanical stress and excessive rubbing and fatigue of the ball-bearings, causing an increase of torque, decrease of average torque, a decrease of efficiency and a rise of temperature in the induction motor [38]. Consequently, an eccentricity is completely related to the kinematic chain, where the increment of temperature due to this condition is also reflected. Otherwise, voltage unbalance (VUNB) occurs when one or two phases of the line supply are out of phase and a thermal overloading can occur due to voltage variations; as a thumb rule, for every 3.5% voltage unbalance per phase,

the winding temperature increases by 25% in the phase with the highest current [39].

3. Methodology

This section shows the proposed methodology for the diagnosis in three steps as shown in Fig. 1: Firstly, the calibration and validation of the thermographic images through RTD sensors is presented, then the image segmentation of the thermographic images and finally, how this segmentation is interpreted to give a diagnosis.

3.1. Calibration and validation

Calibration consists in comparing the output of the instrument under test against the output of an instrument from known accuracy when the measured quantity is applied to both instruments. The calibration ensures the accuracy of all the instruments and sensors used in environmental conditions that are the same as those under which they were calibrated [40]. First, the RTDs are installed outside the induction motor in several places (T2–T7) as shown in Fig. 2, and another RTD is used to measure the ambient temperature (T1). Then, the calibration of the thermographic camera is performed, taking the instrumentation system of the RTD sensors as reference, with about 60 temperature samples of the motor frame at the thermal steady-state with HLT condition, giving $\mu = 45.4\,^{\circ}C$ and $\sigma = 0.72\,^{\circ}C$, where μ is the mean and σ the standard deviation of the temperature samples. Once the calibration is done, the validation in the induction motor in healthy condition is performed. This validation is based on a difference between the measured temperatures of the thermographic camera and the average of the measured temperatures by the RTDs. The difference between the thermographic camera and the RTDs produces a result of $\pm 1\,^{\circ}C$, due to the standard deviation of the temperature samples.

3.2. Segmentation

The segmentation of thermographic images allows the possibility of a wide analysis of the induction motor and the kinematic chain components. This segmentation is manually done in the thermographic images taken by an infrared camera FLIR A310, with lens of 25×19 at a distance of 1.2 m and focused to take into the field of view the complete kinematic chain. The thermographic camera is configured to take thermograms in a temperature range of 19–73 °C for the first kinematic chain and 19–70 °C for the second. It is worthy to notice that when the camera is displaced it produces a displacement in the segmentation regions of interest or in a defocus of the lens. That is why, it is important that when the segmentation and the diagnosis are carried out, the thermographic camera needs to be static. The manual segmentation of the regions of interest on the thermogram allows circumventing further image processing, which is beyond the scope of this research. The thermograms are divided into four thermographic segments to focus the analysis on the useful information.

Two kinematic chains are used for experimentation as shown in Fig. 3. In order to make the segmentation manually; it is necessary to find a hot spot, usually the hottest spot in the thermogram, to establish the conditions for the thermal signature of the motor and the kinematic chain. The first kinematic chain is segmented as shown in Fig. 3a (image) and b (thermogram) with the segments S_1 for the motor frame, S_2 corresponding to the bearing, S_3 to the load pulley, and S_4 to the motor pulley. Fig. 3c (image) and d (thermogram) depict the segmentation of the second kinematic chain where S_1 corresponds to the motor frame, S_2 to the bearing, S_3 to the coupling, and S_4 to the mechanical load.

3.3. Diagnosis

The image segmentation allows a healthy motor signature of thermal conditions to establish at each section, through thermographic images taken during operation of the induction motor under the analysed condition; giving a reference point to a diagnosis. Induction motor fault detection after meeting normal operation temperatures is fairly intuitive without requiring an expert interpretation; because, when an alteration of the thermal conditions in the motor signature appears in the thermographic image, it means that a fault is present. The methodology for the diagnosis is presented in Eq. (2), where i is the index of the thermographic segment to be analysed. Therefore, for this diagnosis: first, the motor signature is acquired with the maximum temperature of each thermographic segment of the induction motor in healthy condition (TH_i), then the maximum temperature of each thermographic segment in faulty condition (TF_i) is obtained in order to grant the thermal coefficient index (TC_i).

$$TC_i = TF_i - TH_i \tag{2}$$

Finally, for each coefficient index TC_i a diagnosis can be obtained, according to the standards in condition monitoring [41]. When there is no defect in the analysed thermographic segment, the coefficient has an approximate value to zero. Moreover, when a fault is presented, the TC_i of the induction motor and the kinematic chain is increased. The objective of TC_i is to identify probable defective parts, even further; it is possible to determine how the fault changes the operating conditions of other parts of the induction motor and the kinematic chain.

4. Experimentation and results

In this section, the experimental setup, treated faults and the results are presented.

4.1. Experimental setup

The experimental setup consists of using the thermal images provided by the thermographic camera and the temperature signals granted by the RTDs located outside the induction motor, and another RTD to measure the environmental temperature in two different kinematic chains. These experimental setups are tested by the diagnostic of the fault conditions mentioned in this work and for asserting the performance of the proposed methodology in the identification of these faults; as well as for identifying the consequent repercussions on the kinematic chain. Fig. 4a shows the experiment setup of the first kinematic chain, where a 1-hp three-phase induction motor (WEG 00136AP3E48T) is used. The kinematic chain in this experiment has two pulleys and a belt as shown in Fig. 4b. The tested motor has two poles, 28 bars and receives a power supply of 220 V AC. The applied mechanical load is of the 100% represented by an ordinary alternator. The external temperature signals are acquired using seven RTDs PT100 model DM-301, from Labfacility LTD. The second kinematic chain has a 2-hp three phase induction motor (WEG 00236ET3E145T-W22), a rigid coupling, and the applied mechanical is a DC generator (BALDOR CDP3604) as depicted in Fig. 4c, comprising around 50% of the mechanical load. A 12-bit 4-channel serial-output sampling analog-to-digital converter ADS7841 from Texas Instrument Incorporated is used in the data acquisition system (DAS). The instrumentation system uses a sampling frequency $f_s = 4$ kHz obtaining 14.4 MS during 60 min of the induction motor from start-up to the thermal steady-state. On the other hand, the thermal images are acquired using a thermographic camera model FLIR A310, from FLIR Systems Incorporated. The thermographic camera takes an image every

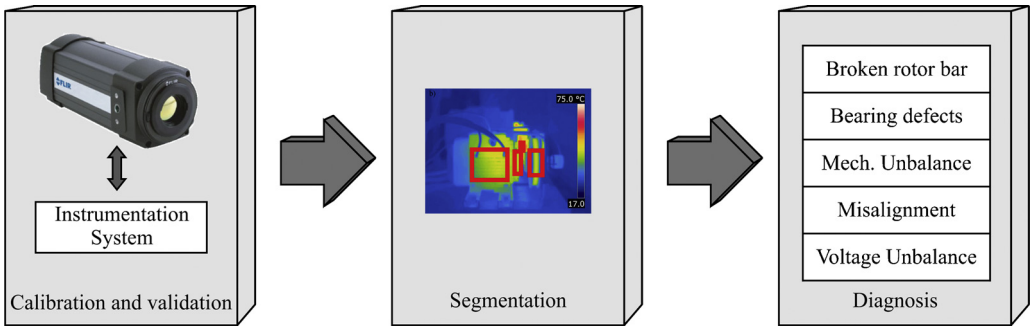

Fig. 1. Proposed methodology.

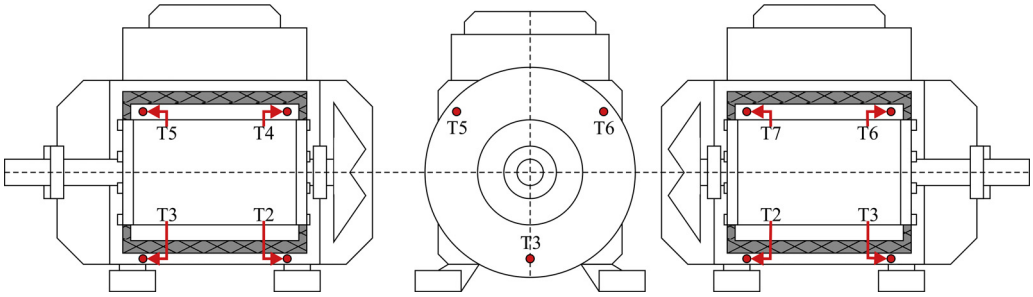

Fig. 2. RTD localization points.

minute during 60 min of the induction motor and their kinematic chain from start-up to the thermal steady-state. The acquired information is stored in a personal computer (PC) and analysed in Matlab which provides the TC_i and the induction motor condition.

4.2. Treated faults

In this work, five different induction motor conditions are studied: BRB at three severities (half-broken rotor bar,

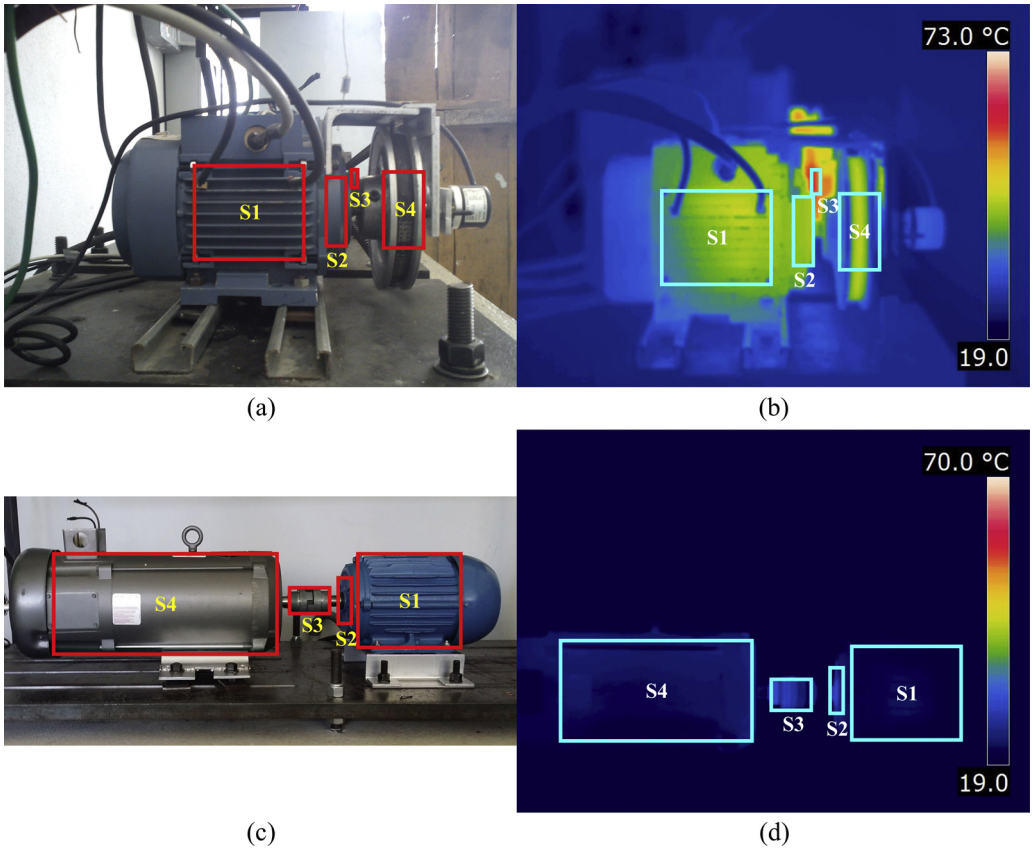

Fig. 3. Thermographic segments: (a) first experimental setup and its (b) thermographic image, (c) second experimental setup and its (d) thermographic image.

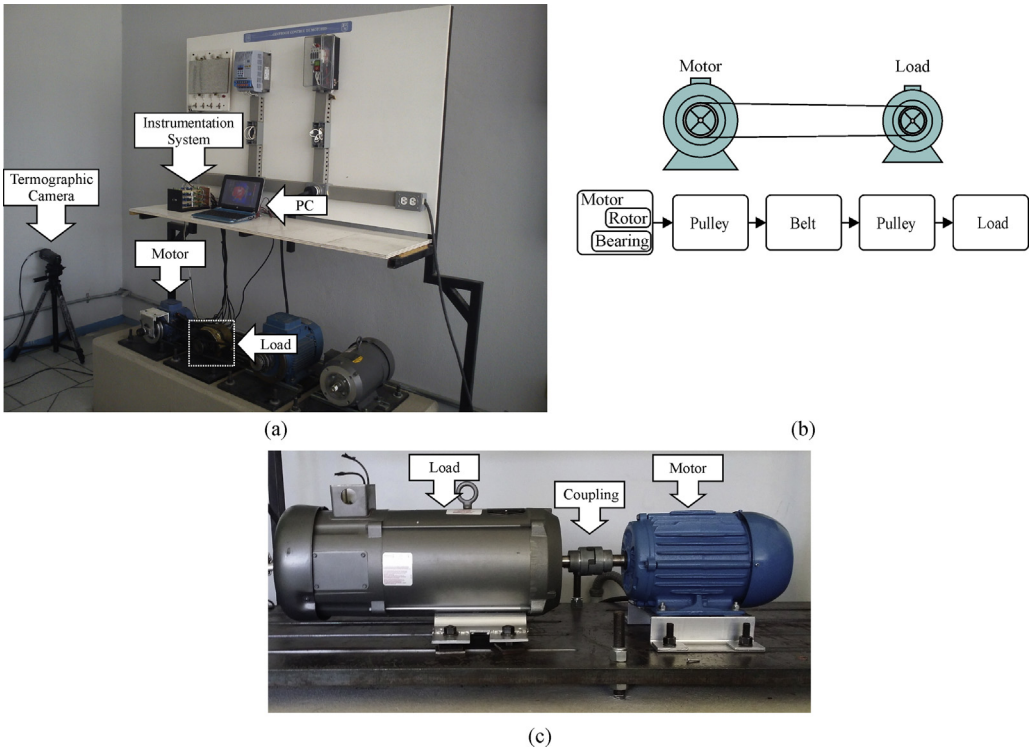

Fig. 4. Experiment: (a) first experimental setup, (b) first experimental kinematic chain, (c) second experimental setup and kinematic chain.

one-broken rotor bar and two-broken rotor bars), BD, UNB, VUNB and MAL.

For the first kinematic chain under test, the half-broken rotor bar (½ BRB) and one-broken rotor bar (1 BRB) conditions were artificially produced by drilling a 2.0 mm, 7.938 mm diameter hole in a rotor bar, respectively, and the two-broken rotor bar (2 BRB) condition was produced by drilling a 7.938 mm diameter hole in a rotor bar and another one in an adjacent rotor bar without harming the shaft of the rotor. Fig. 5a–c show the rotors with ½ BRB, 1 BRB and 2 BRB, respectively, used in the test. The BD condition was made on purpose for the experiment by drilling a 2.0 mm hole in the outer race as shown in Fig. 5d. The UNB condition was produced by attaching a bolt in an arm of the rotor pulley as shown in Fig. 5e. The VUNB of 5% was produced by the connection of a monophasic motor in one of the line supply phases of the induction motor. Finally, the MAL condition was carried out by shifting the band backward in the load pulley, so that the transverse rotation axes for the motor and its load were not aligned. Fig. 5f shows the misaligned motor.

For the second kinematic chain under test, two fault conditions are studied. Firstly, the 1 BRB condition that was artificially produced by drilling a 7.938 mm diameter hole in a rotor bar, without harming the shaft of the rotor, as shown in Fig. 6a. The second tested fault is the BD condition, which was also made on purpose for the experiment by drilling a 2.0 mm hole in the outer race as shown in Fig. 6b.

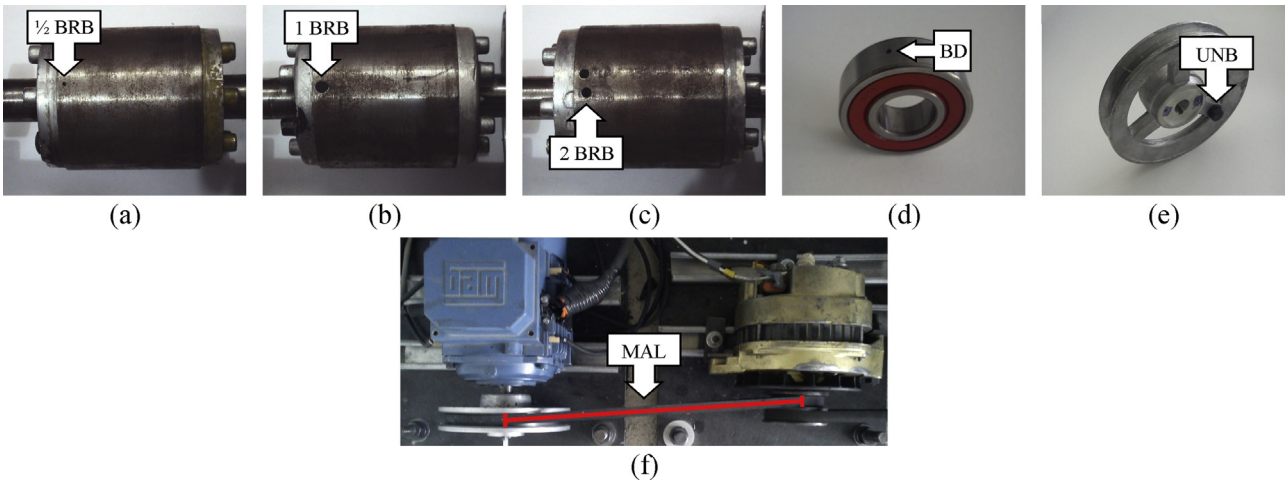

Fig. 5. Treated faults on the first kinematic chain: (a) ½ BRB, (b) 1 BRB, (c) 2 BRB, (d) BD, (e) UNB and (f) MAL.

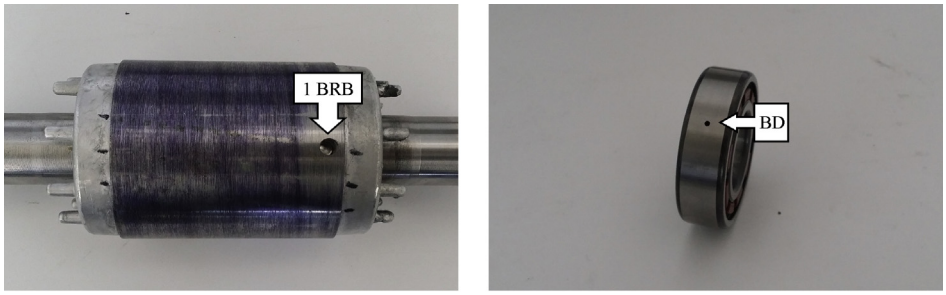

Fig. 6. Treated faults on the second kinematic chain: (a) 1 BRB and (b) BD.

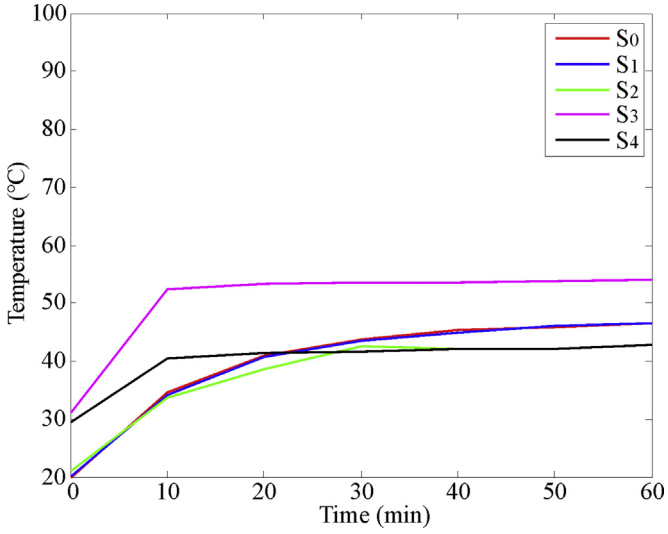

Fig. 7. Healthy motor thermal signature.

4.3. Results

Fig. 7 shows the thermal motor signature of the first kinematic chain acquired during 60 min through thermographic images, with the TH_i of each thermographic segment (S_1–S_4) of the induction motor in healthy condition, and the average of the measured temperatures by the RTDs (S_0) located on the induction motor . It is important to notice that regardless of the induction motor working load, it is necessary to know the reaching time of the thermal steady-state of the kinematic chain in order to determine when to take the thermographic image. Fig. 7 shows that the thermal steady-state is reached after 40 min from the induction motor start-up transient. Based on this analysis, after being determined the healthy motor signature, the faulty motor thermographic images for each study condition with the TF_i of each thermographic segment were taken in the thermal steady-state at minute 40 from the start-up transient as Fig. 8a–i shows for the first kinematic chain and Fig. 9a–c depicts on the second kinematic chain.

In order to evaluate that the thermal analysis can be performed from different perspectives of the camera, Fig. 8i depicts the segmentation of the thermogram under the MAL condition from a different position of the camera than in Fig. 8g. As it can be seen, both thermograms properly cover the induction motor and the whole kinematic chain, where the thermal signatures show the same values for both perspectives in the camera.

For assessing the behaviour of the induction motor and the kinematic chain in the different operating conditions, Eq. (2) is applied to calculate TC_i.

Table 1 shows the temperatures of the thermographic segments and the TC_i results of the first kinematic chain for each induction motor condition. Table 2 shows the temperatures of the thermographic segments and the TC_i results of the first kinematic chain for each induction motor condition with the second perspective where the MAL condition has similar values in the two different perspectives and Table 3 shows the temperature of the thermographic segments and the TC_i results of the second kinematic chain for the treated faults in this experimental setup.

4.4. Analysis and discussion

According to the results of the thermographic segments in the thermographic images, it is possible to propose a criterion of TC_i based on the widely accepted ASTM E1934-99a recommendation [42] to establish a damage relevance criterion that occurs in the induction motor and its kinematic chain as shown in Table 4, where the relevance refers to the action to perform. In the ordinary relevance, there are no anomalies. For slight relevance, it is important to pay attention to the affected areas and to consider a predictive maintenance. On the other hand, for major relevance, it is necessary to consider a preventive maintenance. Finally, for the critical

Table 1
Temperatures of the thermographic segments and TC_i results for each induction motor condition at thermal steady-state on the first kinematic chain.

Condition	Thermographic segments and TC_i (°C)							
	S_1	S_2	S_3	S_4	TC_1	TC_2	TC_3	TC_4
HLT	45	42.2	53.5	42	–[a]	–[a]	–[a]	–[a]
1/2 BRB	51.03	47.83	58.33	47.33	6.03	5.63	4.83	5.33
1BRB	48.43	45.27	58.53	45.67	3.43	3.07	5.03	3.67
2BRB	49.5	44.93	56.37	43.4	4.5	2.73	2.87	1.4
BD	50.3	51.17	53.03	49.3	5.3	8.97	0[b]	7.3
UNB	53.03	48.15	65.53	51.5	8.03	5.95	12.03	9.5
VUNB	42.13	41.1	40.1	48	0[b]	0[b]	0[b]	6
MAL	77.73	70.4	93.27	67.93	32.73	28.2	39.77	25.93

[a] Thermal coefficient indexes TC_i are not defined for the healthy case.
[b] $TC_i = 0$ means that the gradient under the related condition is negligible.

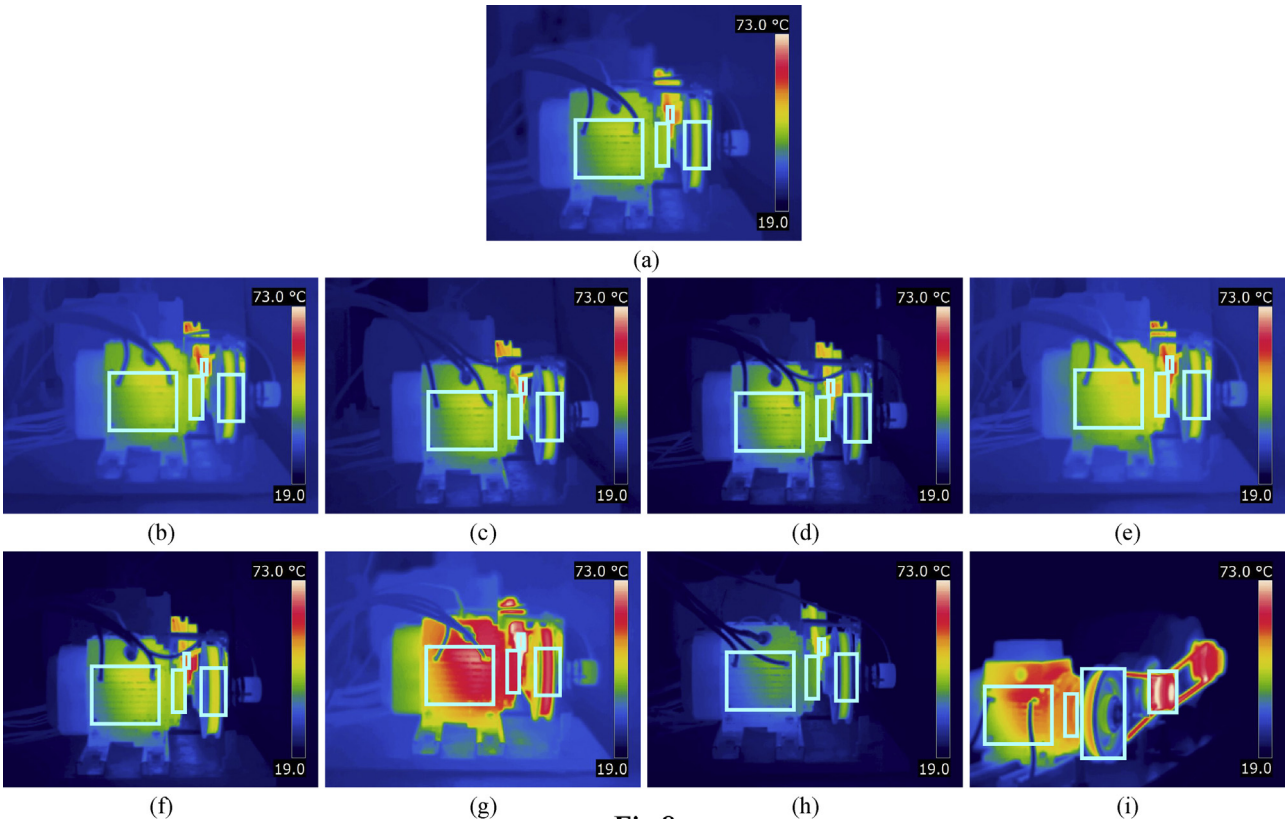

Fig. 8. Thermographic images on the first kinematic chain: (a) HLT, (b) ½ BRB, (c) 1 BRB, (d) 2 BRB, (e) BD, (f) UNB, (g) MAL, (h) VUNB and (i) another perspective of MAL.

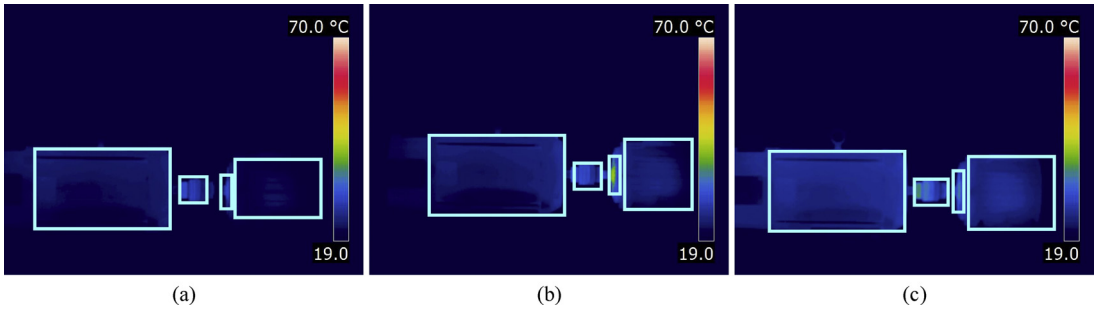

Fig. 9. Thermographic images on the second kinematic chain: (a) HLT, (b) 1 BRB and (c) BD.

Table 2
Temperatures of the thermographic segments and TC_i results for each induction motor condition at thermal steady-state on the first kinematic chain with the second perspective.

Condition	Thermographic segments and TC_i (°C)							
	S_1	S_2	S_3	S_4	TC_1	TC_2	TC_3	TC_4
HLT	45	42.2	53.5	42	–[a]	–[a]	–[a]	–[a]
MAL	75.41	65	77.5	65.45	22.8	24	39.77	23.45

[a] Thermal coefficient indexes TC_i are not defined for the healthy case.

Table 3
Temperatures of the thermographic segments and TC_i results for each induction motor condition at thermal steady-state on the second kinematic chain.

Condition	Thermographic segments and TC_i (°C)							
	S_1	S_2	S_3	S_4	TC_1	TC_2	TC_3	TC_4
HLT	24	30.6	31	25.2	–[a]	–[a]	–[a]	–[a]
BRB	27.7	41.1	35.6	27.2	3.7	10.5	4.6	2
BD	27.8	36.1	37.7	29.1	3.8	5.5	6.7	3.9

[a] Thermal coefficient indexes TC_i are not defined for the healthy case.

Table 4
Damage relevance.

Criterion	Relevance
$TC_i \leq 5$	Ordinary
$5 < TC_i \leq 15$	Slight
$15 < TC_i \leq 30$	Major
$TC_i > 30$	Critical

relevance the process must stop immediately and proceed to a corrective maintenance.

Therefore, it is important to analyse how each fault affects the induction motor, its components and the kinematic chain. In the first kinematic chain, for different severities of broken rotor bars, the TC_i for each thermographic segment shows a non-monotonic behaviour from ½ BRB and up to 2 BRB. This non-monotonic behaviour means that the value of TC_i does not reflect the severity in a proportional relationship with the broken rotor bar fault. However, TC_i permits to establish a general diagnosis methodology for broken rotor bars because TC_i shows that from ½ BRB and up, significant differences in the thermal behaviour at the induction motor and its kinematic chain are observed. This condition has an ordinary relevance on S_3 and slight relevance for S_1, whereas S_2 and S_4 are the most affected components under this condition. These results suggest a predictive maintenance on the induction motor. For BD, results show that the most affected areas are S_2 and S_4; where, due to the abnormal friction on the bearing, it increases its temperature as well as its closest component S_4, affecting their TC_i. S_1 and S_3 under BD condition which have an ordinary relevance. These results mean that it is mandatory to make a bearing replacement during the next programmed maintenance cycle. On the other hand, UNB results show slight relevance in all the motor and the kinematic chain, being S_3 and S_4 the most affected components, without leaving aside S_2 due to an increment in S_4 temperature that is transmitted to S_2. In this condition the induction motor has an abnormal behaviour, due to a slight eccentricity and it is important to attend the affected components in the next maintenance cycle. For VUNB, results show an ordinary relevance in S_1, S_2 and S_3, being S_4 the component with a slight relevance. Under this condition, it is worthy to notice that the TC_is show an ordinary and a slight relevance. Then, at this point it is important to schedule a predictive maintenance including the monitoring of the voltage balance to assess whether the TC_is are due to VUNB or to a faulty condition. Finally, MAL is the most critical condition where results show a major relevance in S_2 and S_4, and a critical relevance in S_1 and S_3, which can potentially damage the kinematic chain, the bearings, and most critically, the induction motor. For this condition, the process must stop immediately to proceed to a corrective maintenance of each part of the induction motor and their kinematic chain: stator windings, rotor, bearings, pulleys, belts and consider a realignment of the kinematic chain.

Otherwise, in the second kinematic chain for 1 BRB the TC_i indicates that this condition has an ordinary relevance on all the parts except in S_2 with a slight relevance. Based on the results of the TC_i, the suggestion is to consider a predictive maintenance on the induction motor. For BD, results show that as well as the first kinematic chain, the most affected areas are S_2 and S_3. Due to the abnormal friction on the bearing, its temperature increases, affecting the TC_i of its closest component S_3. Regarding the S_1 and S_4, under BD condition they have an ordinary relevance. In this condition, it is important to consider replacing the bearing.

Furthermore, to apply this methodology it is important to know the thermal signature at the healthy condition of the induction motor and its kinematic chain with the applied working load. Because within any test bench these parameters are different as well as the TC_i; although, the proposed methodology can be applied in order to analyse the segments of interest with their TC_i and diagnose the fault with the damage relevance criterion.

A meaningful characteristic of the proposed methodology is the advantage of indicating the action to take in the affected components and the capability of monitoring the whole kinematic chain. Therefore, this method provides a rise to evaluate multiple combined faults in further works with the combination of different TC_i in the induction motor and its kinematic chain. Another characteristic is the maximum temperature extraction for each thermographic segment, due to the simplicity to analyse single data, different from the reviewed literature which focuses on hotspots [18,27]. The instrumentation system helps to verify this characteristic, because the behaviour of the average temperature provided by the RTDs is similar to the temperatures given by the thermographic camera.

Care must be taken to choose the spatial resolution of a thermal imaging system, detector size, distance to the object, lens system and a pinpoint calibration of the thermographic camera. When analysing the kinematic chain, other factors can affect measurements such as the environmental temperature, the distance from the thermographic camera to the objects, the colour of the objects and set of signature values for objects previously obtained without any fault.

5. Conclusions

This work proposes a methodology based on thermographic image segmentation for fault detection in induction motors, and the repercussion of these conditions in the critical components of the kinematic chain. The proposed methodology is based on the widely accepted ASTM E1934-99a recommendation, establishing a criterion of the thermal coefficient index TC_i of each thermographic segment, contrary to other reviewed works that do not mention it. This methodology is based on thermal calibration of the thermographic camera through RTDs which, despite the use of more sensors than MCSA and vibrations, the proposed methodology complements the standard techniques and could help to improve the overall diagnosis. The functionality of the methodology has been tested in five typical conditions for an induction motor, using criteria which indicate the relevance and the action to perform under the different conditions. Otherwise, based on the analysis and discussion of the results when maintenance is performed, a voltage balance monitoring is recommended to discard the voltage unbalance as the source of the thermal disturbance in the thermographic image. Furthermore, it is important to highlight that this criterion can be applied on any induction motor at the thermal steady-state, after having the healthy condition thermal signature with its working load.

Finally, the simplicity of this methodology for industrial applications allows the fault detection as well as a wide analysis of the induction motor and its kinematic chain, benefiting in maintenance time and it can be used in the analysis of other electrical machines establishing their own criteria. However, for future development, it is proposed to design a tool for automatic segmentation as well as a smart instrument for fault identification.

References

[1] D.J. Siyambalapitiva, P.G. Mclaren, Reliability improvement and economic benefits of on-line monitoring systems for large induction machines, IEEE Trans. Ind. Electron. 26 (1990) 1018–1025.
[2] M.D. Prieto, G. Cirrincione, A.G. Espinosa, J.A. Ortega, H. Henao, Bearing fault detection by a novel condition-monitoring scheme based on statistical-time features and neural networks, IEEE Trans. Ind. Electron. 66 (2013) 3398–3407.

[3] A. Bellini, F. Filippetti, C. Tassoni, G.A. Capolino, Advances in diagnostic techniques for induction machines, IEEE Trans. Ind. Electron. 55 (2008) 4109–4126.
[4] B. Zhang, C. Sconyers, C. Byington, C. Patrick, M.E. Orchad, G. Vachtsevanos, A probabilistic fault detection approach: application to bearing fault detection, IEEE Trans. Ind. Electron. 58 (2011) 2011–2018.
[5] L. Frosini, E. Bassi, Stator current and motor efficiency as indicators for different types of bearing faults in induction motors, IEEE Trans. Ind. Electron. 57 (2010) 244–251.
[6] J.R. Stack, T.G. Habetler, R.G. Harley, Fault classification and fault signature production for rolling element bearings in electric machines, IEEE Trans. Ind. Appl. 40 (2004) 735–739.
[7] I.Y. Onel, M.E.H. Benbouzid, Induction motor bearing failure detection and diagnosis: Park and Concordia transform approaches comparative study, IEEE/ASME Trans. Mechatron. 13 (2008) 257–262.
[8] V.K. Rai, A.R. Mohanty, Bearing fault diagnosis using FFT of intrinsic mode functions in Hilbert–Huang transform, Mech. Syst. Signal Process. 21 (2007) 2607–2615.
[9] S.H. Kia, H. Henao, G.A. Capolino, Diagnosis of broken-bar fault in induction machines using discrete wavelet transform without slip estimation, IEEE Trans. Ind. Appl. 45 (2009) 1395–1404.
[10] M. Riera-Guasp, J. Pons-Llinares, F. Vedreno-Santos, J.A. Antonino-Daviu, M. Fernandez-Cabanas, Evaluation of the amplitudes of high order fault related components in double bar faults, IEEE Inter. Symp. Diagn. Electr. Mach. Power Electron. Drives (2011) 307–315.
[11] J.A. Antonino-Daviu, S. Aviyente, E.G. Strangas, M. Riera-Guasp, J. Roger-Folch, R.B. Perez, An EMD-based invariant feature extraction algorithm for rotor bar condition monitoring, IEEE Inter. Symp. Diagn. Electr. Mach. Power Electron. Drives (2011) 669–675.
[12] P. Gardel, D. Morinigo-Sotelo, O. Duque-Perez, M. Perez-Alonso, L.A. Garcia-Escudero, Neural network broken bar detection using time domain and current spectrum data, in: Proc. 20th Inter. Conf. of Electr. Mach. Drives., 2012, pp. 2492–2497.
[13] M. Pineda-Sanchez, M. Riera-Guasp, J.A. Antonino-Daviu, J. Roger-Folch, J. Perez-Cruz, R. Puche-Panadero, Instantaneous frequency of the left sideband harmonic during the start-up transient: a new method for diagnosis of broken bars, IEEE Trans. Ind. Electron. 56 (2009) 4557–4570.
[14] L.M. Rabelo-Baccarani, J.P. Braga-Tavares, B. Rodrigues-Menezes, W. Matos-Caminhas, Sliding mode observer for on-line broken rotor bar detection, Electr. Power Syst. Res. 80 (2010) 1085–1089.
[15] C. Kral, T.G. Habetler, Detection of mechanical imbalances of induction machines without spectral analysis of time-domain signals, IEEE Trans. Ind. Appl. 40 (2004) 1101–1106.
[16] S.K. Ahamed, S. Karmakar, M. Mitra, S. Sengupta, Novel diagnosis technique of mass unbalance in rotor of induction motor by the analysis of motor starting current at no load through wavelet transform, Int. Conf. Electr. Comput. Eng. (2009) 474–477.
[17] C. Kral, H. Kapeller, J.V. Gragger, F. Pirker, G. Pascoli, Detection of mechanical imbalances during transient torque operating conditions, IEEE Inter. Symp. Diagn. Electr. Mach. Power Electron. Drives (2005) 1–4.
[18] J.M. Bossio, G.R. Bossio, C.H. De Angelo, Angular misalignment in induction motors with flexible with flexible coupling, in: IEEE 35th Annu. Conf. of Ind. Electron, 2009, pp. 1033–1038.
[19] T.H. Patel, A.K. Darpe, Experimental investigations on vibration response of misaligned rotors, Mech. Syst. Signal Process. 23 (2009) 2236–2252.
[20] M.E.H. Benbouzid, M. Vieira, C. Theys, Induction motors' faults detection and localization using stator current advanced signal processing, IEEE Trans. Power Electron. 14 (1999) 14–22.
[21] H. Nejjari, M.E.H. Benbouzid, Monitoring and diagnosis of induction motors electrical faults using a current Park's vector pattern learning approach, IEEE Trans. Energy Convers. 19 (2004) 657–662.
[22] J. Faiz, H. Ebrahimpour, P. Pillay, Influence of unbalanced voltage on the steady-state performance of a three-phase squirrel-cage induction motor, MDPI-Sens. 12 (2012) 11989–12005.
[23] W.M. Hwang, Y.W. Hwang, An algorithm for the detection of degenerate kinematic chains, Math. Comput. Model. 11 (1991) 9–15.
[24] A. Garcia-Perez, R.J. Romero-Troncoso, E. Cabal-Yepez, R.A. Osornio-Rios, The application of high-resolution spectral analysis for identifying multiple combined faults in induction motors, IEEE Trans. Ind. Electron. 58 (2011) 2002–2010.
[25] A.G. Garcia-Ramirez, R.A. Osornio-Rios, D. Granados-Lieberman, A. Garcia-Perez, R.J. Romero-Troncoso, Smart sensor for online detection of multiple-combined faults in VSD-fed induction motors, MDPI-Sens. 12 (2012) 11989–12005.
[26] A. Lebaroud, G. Clerc, Classification of induction machine faults by optimal time-frequency representations, IEEE Trans. Ind. Electron. 55 (2008) 4290–4298.
[27] M.J. Picazo-Rodenas, R. Royo, J. Antonino-Daviu, J. Roger-Folch, Use of the infrared data for heating curve computation in induction motors: application to fault diagnosis, Eng. Fail. Anal. 35 (2013) 178–192.
[28] B.S. Yang, A. MD, Intelligent fault diagnosis of rotating machinery using infrared thermal image, Expert Syst. Res. 39 (2012) 2082–2091.
[29] V.T. Tran, B.S. Yang, F. Gu, A. Ball, Thermal image enhancement using bi-dimensional empirical mode decomposition in combination with relevance vector machine for rotating machinery fault diagnosis, Mech. Syst. Signal Process. 38 (2013) 601–614.
[30] http://www.fluke.com/fluke/m3en/Ti105.htm?PID=74966, (27.03.14).
[31] http://www.flir-webshop.com/en/electrical-mechanical/flir-i3-130.html, (27.03.14).
[32] G.C. Holst, Common Sense Approach to Thermal Imaging, PM86, SPIE press monograph, Winter Park, Florida, 2000.
[33] S. Taib, M.S. Jadin, S. Kabir, in: R.V. Prakash (Ed.), Thermal Imaging for Enhancing Inspection Reliability: Detection and Characterization, InTech, Rijeka, Croatia, 2012, pp. 209–236.
[34] R.C. Gonzalez, R.E. Woods, Digital Image Processing, 3rd ed., Prentice Hall, New Jersey, 2008.
[35] R.M. Haralick, L.G. Shapiro, Image segmentation techniques, Comput. Vis. Graph. Image Process. 29 (1985) 100–132.
[36] N.R. Pal, S.K. Pal, A review on image segmentation techniques, Pattern Recognit. 26 (1993) 1277–1294.
[37] P. Zhang, Y. Du, T.G. Habetler, B. Lu, A survey of condition monitoring and protection methods for medium-voltage induction motors, IEEE Trans. Ind. Appl. 47 (2011) 34–46.
[38] J. Faiz, M. Ojaghi, Different indexes for eccentricity fault diagnosis in three-phase squirrel-cage induction motors: a review, Mechatronics 19 (2009) 2–13.
[39] A. Siddique, G.S. Yadava, B. Singh, A review of stator fault monitoring techniques of induction motors, IEEE Trans. Energy Convers. 20 (2005) 106–114.
[40] A.S. Morris, R. Langari, in: Butterworth Heinemann (Ed.), Measurement and Instrumentation. Theory and Application, Academic Press, California, 2012, pp. 103–114.
[41] S. Bagavathiappan, B.B. Lahiri, T. Saravanan, J. Philip, T. Jayakumar, Infrared thermography for condition monitoring – a review, Infrared Phys. Technol. 60 (2013) 35–55.
[42] Standard Guide for Examining Electrical and Mechanical Equipment with Infrared Thermography, ASTM E1934-99a, 2010.

FPGA-based Smart-sensor for Fault Detection in VSD-fed Induction Motors

A.G. Garcia-Ramirez, R.A. Osornio-Rios, *Member*, *IEEE*, A. Garcia-Perez, *Member*, *IEEE*, R.J. Romero-Troncoso, *Senior Member*, *IEEE*.

***Abstract* – Nowadays, different industrial processes use induction motors fed through variable speed drives (VSD). In order to improve these processes, the industry demands the use of smart sensors to detect the faults, reduce the cost of maintenance, and decrease power consumption. In this work, broken rotor bars, unbalance and misalignment are automatically detected in induction motors fed by a VSD using the three current phases online, with a smart sensor. The proposed smart sensor is implemented in a field programmable gate array offering a low computational load methodology, low-cost, and portable solution for fault detection in induction motors VSD-fed. Results show a high effectiveness detection of the treated faults.**

***Index Terms*--Fault detection; Field programmable gate arrays; Induction motors; Variable speed drives.**

I. INTRODUCTION

INDUCTION motors are key elements in industry due to their robustness, easy construction, low cost and versatility, representing 85% of power consumption worldwide. Consequently, early fault detection in induction motors is one of the most important subjects for industry [1], because these faults may produce unanticipated interruptions on product lines, with severe consequences in product quality, such as safety and cost. Therefore, the detection of incipient faults has attracted the interest of many researchers in recent years [2]. Around 40% to 50% of induction motor faults are bearing related, rotor faults represent 5% to 10% and unbalance and misalignment faults are about 12% [3]. Furthermore, connection of induction motors through variable speed drives (VSD), allows extending their useful life, and saving energy, but making the detection of faults more difficult due to the spurious harmonics induced by the VSD operation [4]. Moreover, the extensive use of VSD allows new possibilities for the on-line detection of faults [5]. Concerning to fault detection in induction motors, a number of techniques had been proposed. For instance, in [6] Shahin *et al.* investigate the recent advances on digital signal processing techniques for induction motors diagnosis. These techniques cover the frequency domain as the fast Fourier transform (FFT), the zoom-FFT, the chirp Z-transform, and the time-frequency domain such as multiple signal classification (MUSIC), short time Fourier transform, wavelet transform, etc. The best technique is chosen depending on the physical phenomena to observe. Garcia-Perez *et al.* [3] proposed a methodology which combines a filter bank of finite impulse response (FIR) filters with high resolution spectral analysis based on MUSIC for detecting multiple combined faults, with current and vibration signals. The results show the analytical predetermined fault frequency location for single, two or three combined faults (broken rotor bars, unbalance and bearings damage). In [7], it is proposed an artificial neural network (ANN) methodology to detect broken rotor bars (BRB) with statistical patterns of time-domain data, current spectrum and the combination of two ANN inputs to classify the motor condition. Riera-Guasp *et al.* [8] studies the relation between the amplitude of the components of the air-gap fault field produced by a double bar breakage and the relative position of the broken bars. Otherwise, [9] describes a method for the diagnosis and detection of BRB and bearing damage in induction motors by motor current signal analysis and multiple features extracted from transformations on current and voltage signals, using the hidden Markov model as classifier. Regarding the unbalance condition (UNB), Kral *et al.* in [10] proposed a technique to sense the specific modulation of the electric power of faults such as eccentricities as well as load torque perturbation without using the frequency spectrum. Otherwise, in [11] the misalignment condition (MAL) is computed by the FFT extracting the unique vibration features exhibited in the full spectrum. All the aforementioned works, need a heavy computational load and can be difficult to implement on hardware for online operation because most of these techniques requires offline processing and an expert technician for interpreting results. In [12], two techniques namely Park transform approach and Concordia transform are presented and compared for the detection of bearing damage in induction motors. The results of this work show that these techniques are valid to identify faulty patterns making suitable for hardware implementation, such as a smart sensor.

A smart sensor is a device that includes primary sensors,

This work was supported in part by FOFIUAQ2012, under ACAEC188088 CONACyT-2012 and by CONACyT under Scholarship 229736.

R. J. Romero-Troncoso is with HSPdigital CA-Telematica at DICIS, University of Guanajuato, Salamanca, Gto. 36885 Mexico (corresponding author; e-mail: troncoso@hspdigital.org).

A.G. Garcia-Ramirez is with HSPdigital CA-Mecatronica at Facultad de Ingenieria, Campus San Juan del Rio, Universidad Autonoma de Queretaro, San Juan del Rio, Qro. 76807 Mexico (e-mail: aggarcia@hspdigital.org).

R.A. Osornio-Rios is with HSPdigital CA-Mecatronica at Facultad de Ingenieria, Campus San Juan del Rio, Universidad Autonoma de Queretaro, San Juan del Rio, Qro. 76807 Mexico (e-mail: raosornio@hspdigital.org).

A. Garcia-Perez is with HSPdigital CA-Procesamiento Digital de Señales at DICIS, University of Guanajuato, Salamanca, Gto. 36885 Mexico (e-mail: arturo@salamanca.ugto.mx).

978-1-4799-0025-1/13/$31.00 ©2013 IEEE

signal processing, communication, and integration capabilities. The term "smart sensor" is employed according to the functionality classification. Nowadays the use of smart sensors improves the monitoring system demands due to their features in communication and data processing functionalities, and their versatility and ability to work in environments where the access for field workers is limited [13].

In this work the development of a smart sensor, based on a field-programmable gate array (FPGA), for automatic and online detection of faults in induction motor fed through VSD is presented, covering operating frequencies from as low as 3 Hz and up to 60 Hz. The methodology used in this work is based on the Park transform that converts the *ABC* current system to the *D-Q* current system, having the advantage of a lower computational load than the FFT and other spectrum-based methodologies; then the magnitude of the *DQ* current system and the mean are calculated to be the inputs of an artificial neural network, which gives the identification of the fault. Three different faults on induction motor: broken rotor bars, unbalance and misalignment are investigated, and the results show the potentiality of the smart sensor to classify the induction motor faults, automatically and online.

II. THEORETICAL BACKGROUND

A. Park Transform

The Park transform, permits to express the three current phases of an induction motor through a two-axis system in quadrature. The components of this system: direct and quadrature (i_D and i_Q), are given by (1) and (2), respectively:

$$i_D = \sqrt{\frac{2}{3}} i_A - \sqrt{\frac{1}{6}} i_B - \sqrt{\frac{1}{6}} i_C \quad (1)$$

$$i_Q = \sqrt{\frac{1}{6}} i_B - \sqrt{\frac{1}{6}} i_C \quad (2)$$

Where, i_A, i_B and i_C are the stator current phases [14]. Using (1) and (2) the transformation of the stator current phases *ABC* to the *D-Q* system is very simple. Fig. 1 shows the Lissajous figures of the current in *D-Q* system for a healthy motor (Fig. 1a) and a faulty motor (Fig. 1b).

B. Induction Motor Faults

This work focuses on three different faulty conditions: broken rotor bars (BRB), misalignment (MAL) and unbalance (UNB).

The BRB fault appears because of welding defects, high strength joints, expansion and mechanical stresses [15]. The presence of BRB in induction motors produces several problems, such as power quality degradation [16]. On the other hand, MAL is presented when the motor and the load pulleys are not aligned. The MAL fault can cause over 70% of the rotating machinery vibration problems, and it is the second most commonly fault in rotating machines [11]. Finally, the UNB condition is presented when the rotor weight is not uniformly distributed around its geometrical center, which means that the center of mass is not on the center of rotation. The UNB condition is the most observed fault in induction motors, and if is not attended, the results for the machinery can be catastrophic [10].

C. Artificial Neural Networks

An Artificial Neural Network (ANN) is a computational model that provides a method to characterize synthetic neurons to solve problems in the same way as the human brain [1]. The most popular architecture for ANN is the multilayer feed-forward networks (MFN), which has an input layer, one or more hidden layers and an output layer. In this architecture, the data goes in one direction, from the input layer through the hidden layer to the output layer, as shown in Fig. 2.

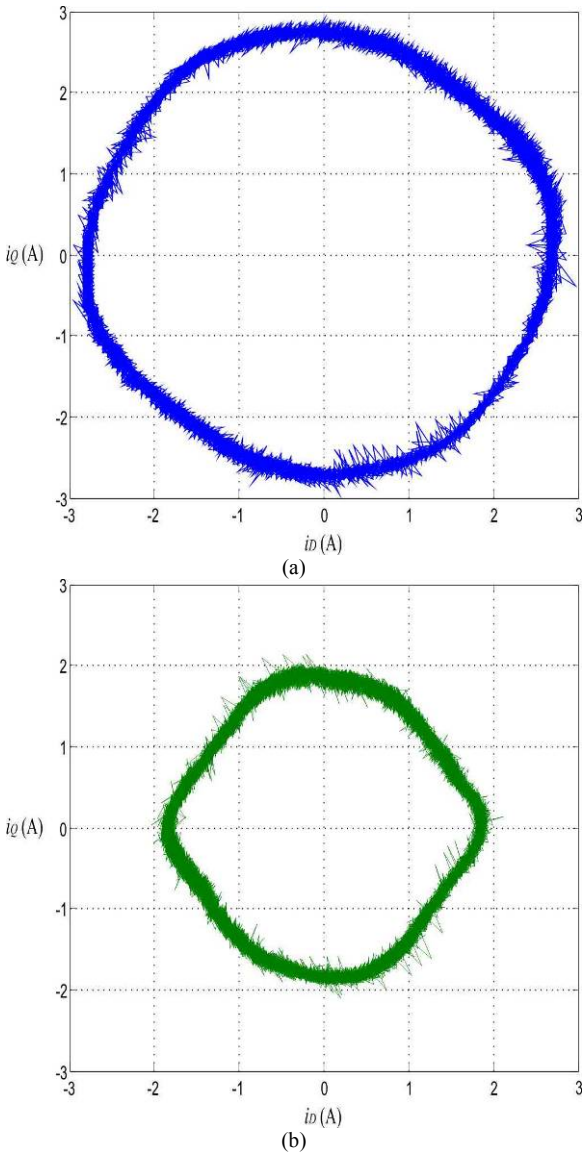

Fig. 1. Lissajous figures of the *D-Q* system current of (a) Healthy motor, and (b) Faulty motor.

Where, X_i ($i = 1,2,3,...,n$) are inputs and Y_i ($i = 1,2,3,...,m$) are outputs. The back-propagation algorithm (BPA), is the most conventional method to train an MFN, which is a supervised learning method, that consists on mapping the process inputs to the desired outputs by minimizing the error between the desired outputs and the calculated outputs [17]. The MFN is an excellent candidate to be implemented in FPGA, due to its simplicity, practicality and low computational load [18].

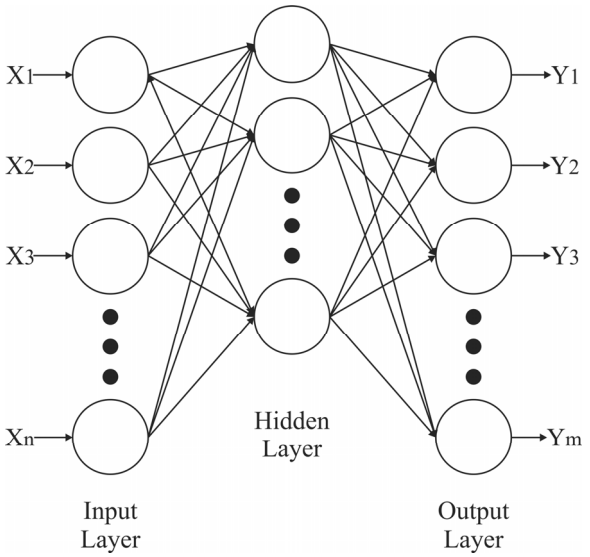

Fig. 2. Multilayer feed-forward network architecture.

III. METHODOLOGY

The methodology is based on the Park transform that allows representing the three current phases of an induction motor in a two-dimensional system. Fig. 3 shows the Lissajous figure obtained from the Park transform. Then, through a magnitude calculation (3) of each k sample, as shown also in Fig. 3, the D-Q system is translated to a vector $i_{DQ\text{-}k}$ that is the resultant representation of the Lissajous figure. In Fig. 4 the $i_{DQ\text{-}k}$ vector is presented. Afterward, by a mean computation (4) of the $i_{DQ\text{-}k}$ vector, the average radius of the Lissajous figure can be taken. This mean value of the $i_{DQ\text{-}k}$ vector is also presented in Fig. 4. Finally, the data from the mean computation is an input of the proposed ANN which delivers the motor condition.

$$i_{DQ-k} = \sqrt{i_{D-k}^2 + i_{Q-k}^2} \tag{3}$$

$$Mean = \frac{1}{L}\sum_{k} i_{DQ-k} \tag{4}$$

Where, L is the length of the $i_{DQ\text{-}k}$ vector.

A. Proposed Artificial Neural Network

The proposed ANN implements an MFN with three inputs nodes that receive the mean calculation of the i_{DQ} vector in each treated frequency, thirty nodes in the hidden layer and four output nodes for the detection of: healthy condition (HLT), broken rotor bars (BRB), unbalance (UNB) and misalignment (MAL). The output nodes correspond to each fault condition.

IV. EXPERIMENT

A. Experimental Setup

The steady-state current signal provided by a VSD (model WEG CFW08) connected to the induction motor is used for detecting the faults and to classify them. The VSD has an operation range from 0 Hz to 100 Hz using a frequency resolution of 0.01 Hz. In Fig. 5(a) the experimental setup is shown, where one 1-hp three-phase induction motors (model WEG 00136APE48T) is used to test the performance of the proposed methodology to identify the fault conditions considered in this work. The rotational speed of the motor is controlled by a VSD at 3Hz, 30Hz and 60Hz. The tested motors have two poles, twenty eight bars and receive a power supply of 220 V AC. The applied mechanical load is from an ordinary alternator, which represents a quarter of load for the motor. The three-phase current signals are acquired using three hall-effect sensors model L08P050D15, from Tamura Corporation. A 16-bit 4-channerl serial-output sampling analog-to-digital converter ADS8341 from Texas Instrument Incorporated is used in the data acquisition system (DAS). The instrumentation system which was calibrated through the Fluke 435 that uses a sampling frequency f_s = 12 KHz obtains 120,000 samples of each current phase during 10 seconds of the induction motor steady-state. The motor start-up is controlled by a relay to automate the test run. Fig. 5(b) shows the proposed smart sensor for induction motor fault detection. The three current phases of the induction motor fed by VSD are acquired by the hall-effect sensors; then it is conditioned and analog-to-digital (A/D) converted in the DAS. Afterwards, in a smart unit implemented into a proprietary Spartan 3E XC3S1600 FPGA platform running at 48 MHz, the three digital current phases are transformed in i_D and i_Q phases by the Park transform. Then, the magnitude (3) and the mean of this magnitude (4) are calculated to be a single data for an input of an ANN which gives the induction motor condition. However, the current magnitude depends on the load and the motor power; then, to minimize the undesired effects of magnitude variation that could modify the diagnosis, the ABC current signals are normalized before the Park transform is applied. Fig. 6 shows the mean calculation of the i_{DQ} vector obtained by each fault condition in the three studied frequencies Table I summarizes the resource usage of the FPGA.

B. Investigated Faults

The BRB condition was artificially produced by drilling a 7.938mm diameter hole in a rotor bar without harming the

shaft of the rotor. Fig. 7(a) shows the rotor with the BRB condition used in the test. The misalignment condition (MAL) was carried out by shifting forward the band in the alternator pulley, so that the transverse axes of rotation for the motor and its load were not aligned. Fig. 7(b) shows the misaligned motor. The UNB test was produced by attaching a bolt in an arm of the rotor pulley as shown in Fig. 7(c).

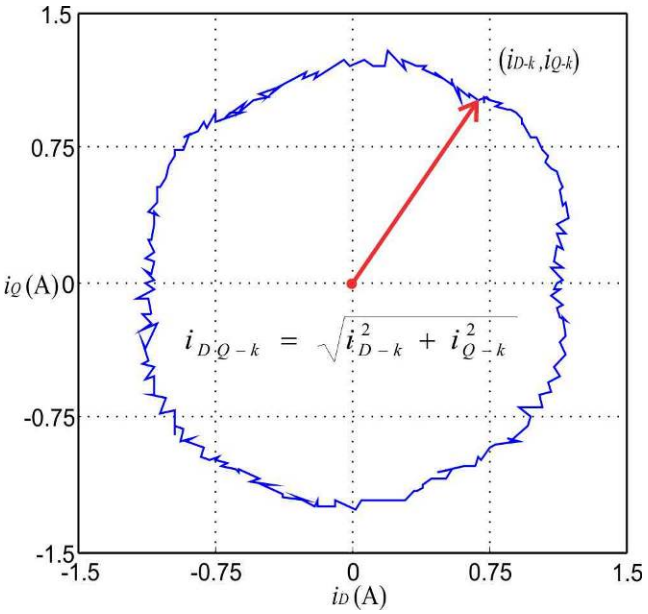

Fig. 3. Lissajous figure obtained from the Park transform.

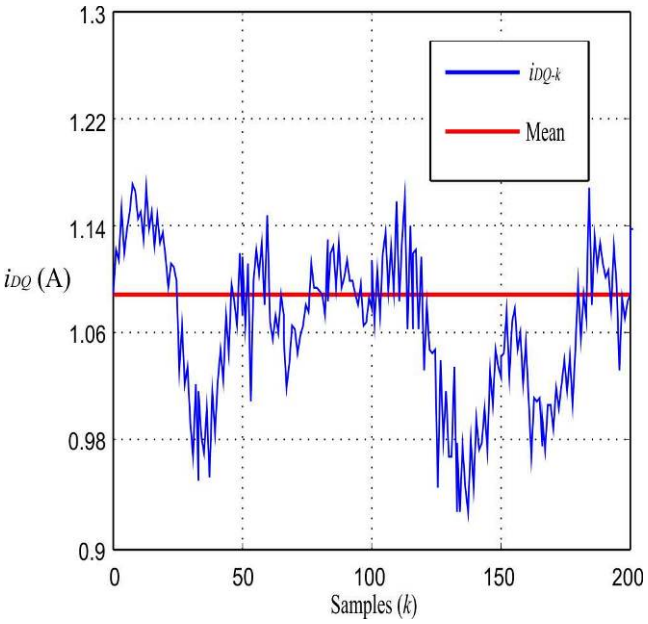

Fig. 4. Representation of the Lissajous figure by the $i_{DQ\text{-}k}$ vector.

C. Network Training

The training set for the ANN training was obtained with 500 random synthetic values for every condition in each treated frequency within the range $[\mu - \sigma, \mu + \sigma]$, where μ is the mean and σ the standard deviation of the mean values of the i_{DQ} vector on the first ten trials. Forty trials are carried out under each motor condition in every treated frequency; which were used as validation set for the diagnosis. Using Matlab neural network toolbox, the weights and the biases of each layer in the ANN were calculated for being implemented on the FPGA for the diagnosis. In some cases when the design of the motor is changed, a new training is required for adjusting the calibration of the smart sensor and improving the classification results. For future development, it is proposed to add an additional input to the ANN where the load value is given.

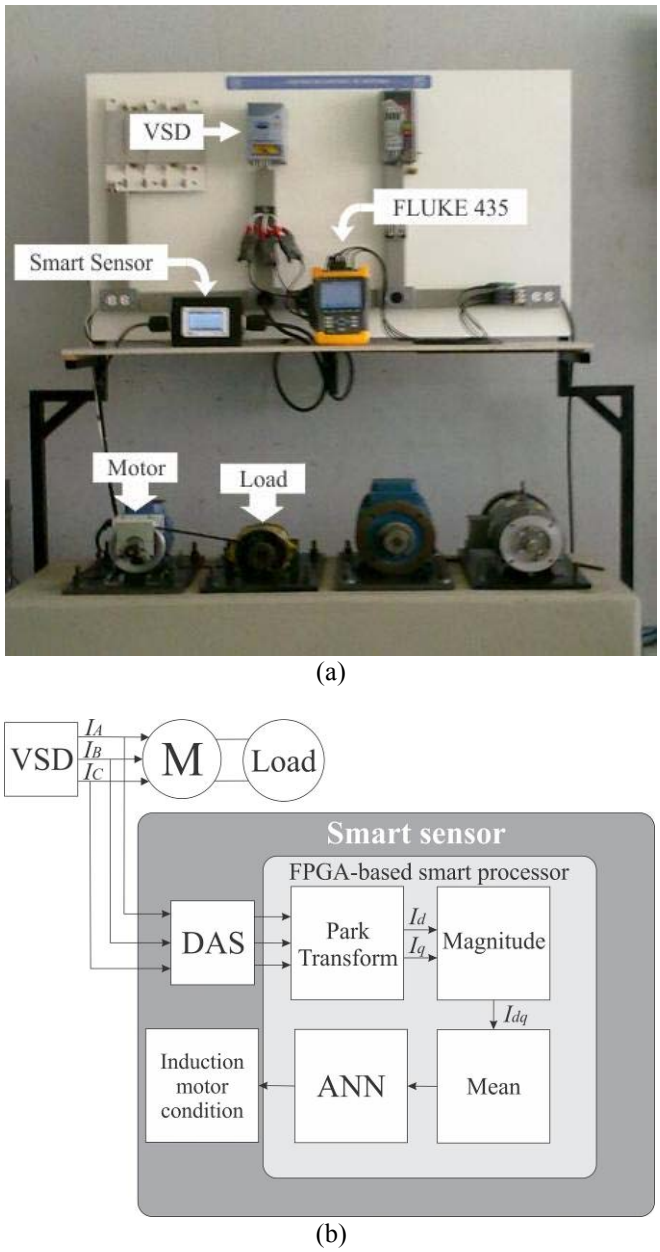

Fig. 5. (a) Experimental setup. (b) Block diagram of the proposed smart sensor for induction motor fault detection.

TABLE I
RESOURCE USAGE OF THE FPGA.

Resource utilization	Xilinx Spartan 3E XC3S1600E
Slices	1,495/14,752 (10%)
Flip-flops	979/29,504 (3%)
4-input LUTs	2,662/29,504 (9%)
Maximum operation frequency	58.28 MHz

V. RESULTS

A. Fault Identification Results

Table II shows the effectiveness by the proposed smart sensor during the induction motor condition classification of every frequency studied. The results include the identification of the healthy condition, broken rotor bar, unbalance and misalignment for each selected frequency. In Fig. 8 some examples of Lissajous figures are presented in order to observe the behavior of the faults in the D-Q system compared to the healthy condition. In order to obtain statistically significant results, forty tests were performed to acquire the three current phases from the induction motor in all treated cases for each selected frequency.

B. Discussion

Three different frequency cases of the VSD are studied in order to fulfill a range from low to high frequencies: 3Hz, 30Hz and 60Hz. Results of the smart sensor with motor running in healthy condition (HLT) show a detection effectiveness of 100% in 3Hz and 60Hz, while at 30Hz the detection effectiveness is 90%. Results at the broken rotor bars (BRB) condition present a detection effectiveness over 97% in 3Hz and 100% at 30Hz and 60Hz. In the unbalance (UNB) condition the 100% of effectiveness is present in each studied frequency. Finally, with the misalignment (MAL) condition the smart sensor delivers an effectiveness of 100% for 3Hz and 60Hz, and 95% at 30Hz. A characteristic of the proposed smart sensor is the automatic detection of multiple faults in VSD-fed induction motors using a simple methodology, different from other works that have a heavy computational load, requiring offline processing and an expert technician for interpreting results. For instance, as stated in Table I, the resources of the FPGA are around 10% with the proposed methodology. In [19], the implementation of a 1024-point FFT requires over 30% of FPGA resources, regardless the magnitude computation and an ANN. Otherwise, in [20] it is reported a 34% of resource usage of a reconfigurable FPGA-based system for wavelet analysis. On the other hand, [9-12] report offline methodologies for the detection of single isolated faults in induction motors connected through the power line supply. The FPGA implementation of the proposed smart sensor offers an online hardware implementation with a low computational load methodology, low-cost, and portable solution for fault detection in VSD-fed induction motors, different from other works that employ techniques with higher computational load, which are not suited for automatic online hardware/software implementation.

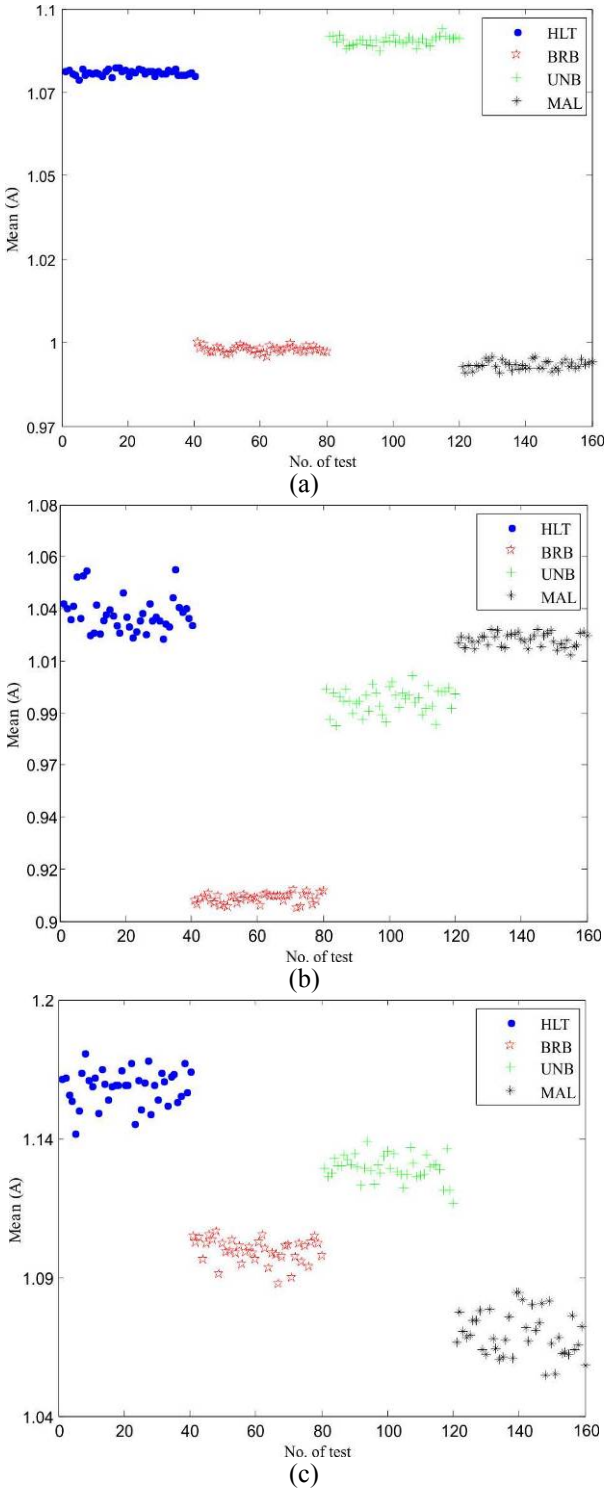

Fig. 6. Mean calculation of the i_{DQ} vector obtained of each fault condition in: (a) 3Hz, (b) 30 Hz and (c) 60 Hz.

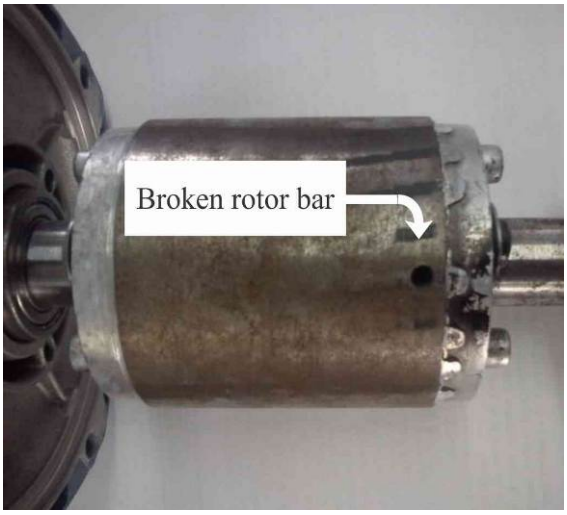

(a)

(b)

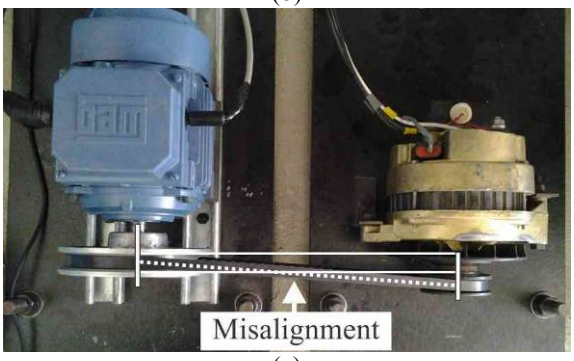

(c)

Fig. 7. (a) Broken rotor bar. (b) Unbalance. (c) Misalignment.

TABLE II
EFFECTIVENESS OF THE PROPOSED SMART SENSOR ON IDENTIFYING THE INDUCTION MOTOR CONDITION.

Induction motor condition	3Hz Effectiveness	30Hz Effectiveness	60Hz Effectiveness
HLT	100%	90%	100%
BRB	97%	100%	100%
UNB	100%	100%	100%
MAL	100%	95%	100%

VI. CONCLUSIONS

This work proposes a new smart sensor for detection of faults in VSD-fed induction motors using the three current phases. The proposed methodology is based on the Park transform and an MFN in order to determine the motor condition when is fed by a VSD, due to their simplicity and lower computational load different from other techniques, it is an excellent candidate to be implemented on hardware. The functionality of the smart sensor was successfully tested in forty tests of each category of the faults.

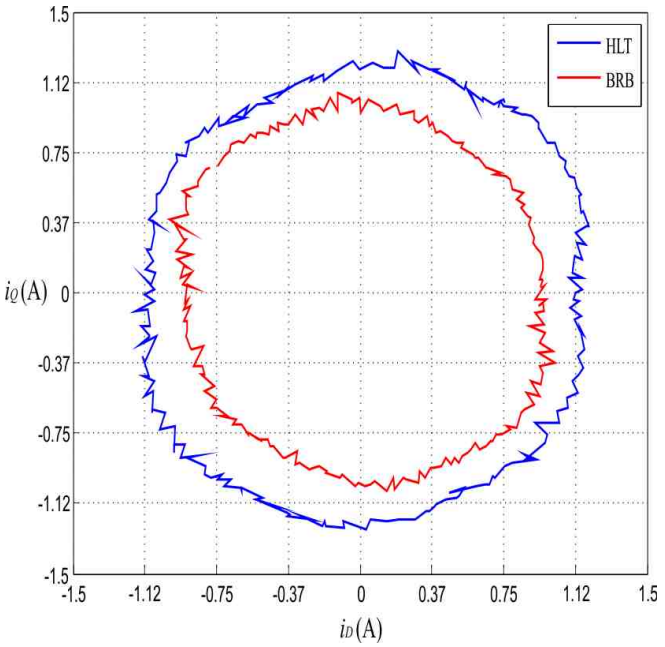

(a)

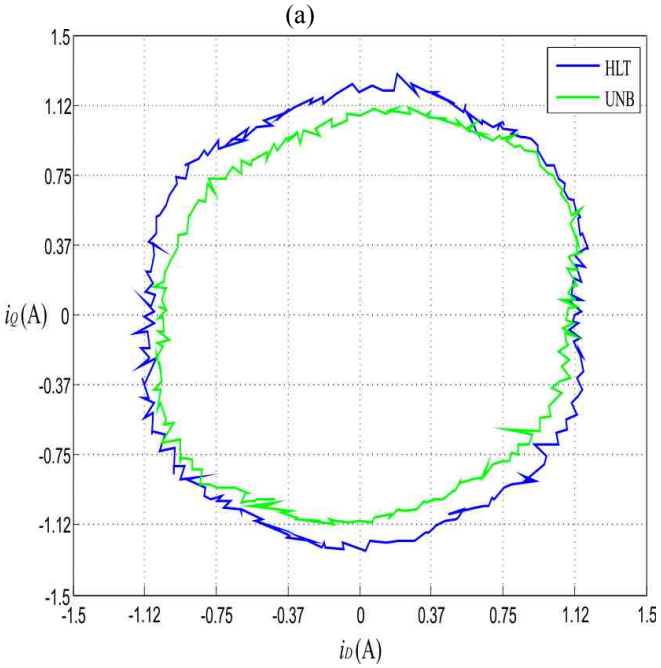

(b)

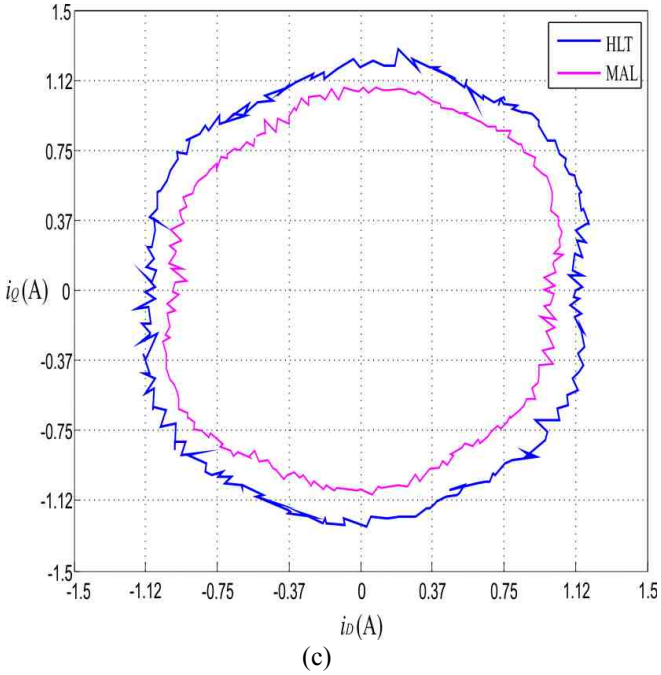

(c)

Fig. 8. Examples of Lissajous figures of the *D-Q* system current for comparing the healthy condition against (a) Broken rotor bar, (b) Unbalance and (c) Misalignment.

VII. REFERENCES

[1] A. Bellini, F. Fillipeti, C. Tassoni, G.A. Capolino, "Advances in diagnostic techniques for induction machines," *IEEE Trans. Industrial Elextronics,* vol. 55, pp. 4109-4126, Dec. 2008.

[2] D.J. Siyambalapitiya, P.G. Mclaren, "Reliability improvement and economic benefits of on-line monitoring systems for large induction machines," *IEEE Trans. Industrial Applications,* vol. 26, pp. 1018-1025, Nov-Dec. 1990.

[3] A. Garcia-Perez, R.J. Romero-Troncoso, E. Cabal-Yepez, R.A. Osornio-Rios, "The application of high-resolution spectral analysis for identifying multiple combined faults in induction motors," *IEEE Trans. Industrial Elextronics,* vol. 58, pp. 2002-2010, May 2011.

[4] O. Duque-Perez, L.A. Garcia-Escudero, D. Morinigo-Sotelo, P.E. Gardel, M. Perez-Alonso, "Condition monitoring of induction motors fed by voltage source inverters. Statistical Analysis of spectral data," in *Proc. Of the International Conference of Electric Machines and Drives (ICEM12)*, pp. 2479-2484, 2012.

[5] S.H. Kia, H. Henao, G.A. Capolino, "Some digital signal processing techniques for induction machines diagnosis," *IEEE International Symposium on Diagnostics for Electric Machines, Power Electronics & Drives (SDEMPED).* pp. 322-329, Sept. 5-8 2011.

[6] J. Urresty, J. Riba, H. Saavedra, J. Romeral, "Analysis of demagnetization faults in surface-mounted permanent magnet synchronous motors with symmetric windings," *IEEE International Symposium on Diagnostics for Electric Machines, Power Electronics & Drives (SDEMPED).* pp. 240-245, Sept. 5-8 2011.

[7] P. Gardel, D. Morinigo-Sotelo, O. Duque-Perez, M. Perez-Alonso, L.A. Garcia-Escudero, "Neural network broken bar detection using time domain and current spectrum data," in *Proc. Of the International Conference of Electric Machines and Drives (ICEM12)*, pp. 2492-2497, 2012.

[8] M. Riera-Guasp, J.Pons-Llinares, F. Vedreno-Santos, J.A. Antonino-Daviu, M. Fernandez-Cabanas, "Evaluation of the amplitudes of high-order fault related components in double bar faults," *IEEE International Symposium on Diagnostics for Electric Machines, Power Electronics & Drives (SDEMPED).* pp. 307-315, Sept. 5-8 2011.

[9] A. Soualhi, G. Clerc, H. Razik, A. Lebaroud, "Fault detection and diagnosis of induction motors based on hidden Markov model," in *Proc. Of the International Conference of Electric Machines and Drives (ICEM12)*, pp. 1693-1699, 2012.

[10] C. Kral, T.G. Habetler, R.G. Harley, "Detection of mechanical imbalances of induction machines without spectral analysis of time-domain signals," *IEEE Trans. Industrial Applications,* vol. 40, pp. 1101-1106, July-Aug. 2004.

[11] T. H. Patel, A.K. Darpe, "Experimental investigations on vibration response of misaligned rotors," *Elseiver Mechanical systems and signal processing,* vol. 23, pp. 2239-2252, May. 2009.

[12] I.Y. Onel, M.E.H. Benbouzid, "Induction motor bearing failure detection and diagnosis: Park and Concordia transform approaches comparative study," *IEEE Trans. Mechatronics,* vol. 13, pp. 257-262, April. 2008.

[13] J. Rivera, G. Herrera, M. Chacon, P.Acosta, M. Carrillo, "Improved progressive polynomial algorithm for self-adjustment and optimal response in intelligent sensors" *MDPI Sensors,* vol. 9, pp. 3767-3789, Nov. 2008.

[14] H. Nejjari, M.E.H. Benbouzid, "Monitoring and diagnosis of induction motors electrical faults using a current Park's vector pattern learning approach," *IEEE Trans. Industrial Applications,* vol. 36, pp. 730-735, May-June. 2000.

[15] M.J. Picazo-Rodenas, R. Royo, J. Antonino-Daviu, J. Roger-Folch, "Use of infrared thermography for computation of heating curves and preliminary failure detection in induction motors," in *Proc. Of the International Conference of Electric Machines and Drives (ICEM12)*, pp. 525-531, 2012.

[16] M.E.H. Benbouzid, "A review of induction motors signature analysis as a medium for faults detection," *IEEE Trans. Industrial Elextronics,* vol. 47, pp. 984-993, Oct. 2000.

[17] Y. Huang, "Advances in artificial networks – Methodological development and application" *MDPI Algorithms,* vol. 2, pp. 973-1007, Aug. 2009.

[18] L. Capocchi, G.A. Capolino, "An efficient architecture of multi-stage neural network for rotor induction generator short-circuit fault classification," in *Proc. Of the International Conference of Electric Machines and Drives (ICEM12)*, pp. 1565-1571, 2012.

[19] J. A. Vite-Frias, R. J. Romero-Troncoso, A. Ordaz-Moreno, "VHDL core for 1024-point radix-4 FFT computation," in *Proc. Int. Conf. Reconfigurable Computing and FPGAs ReConFig 2005*, pp. 26/1-4. 2005.

[20] R.J. Romero-Troncoso, M. Pena-Anaya, E. Cabal-Yepez, A. Garcia-Perez, R.A. Osornio-Rios, "Reconfigurable SoC-based smart sensor for wavelet and wavelet packet analysis," *IEEE Trans. Intrumentation and Measurement,* vol. 61, pp. 2458-2468, Sep. 2012.

VIII. BIOGRAPHIES

Armando G. Garcia-Ramirez received the B. E. degree from the Mazatlan Institute of Technology, Mazatlan, Mexico, and the M.E. degree (with Honors) from the University of Guanajuato, Salamanca, Mexico in 2011, where he did research work at the HSPdigital group. Currently, he is a Ph.D. student at the University of Queretaro, Queretaro, Mexico. His research interest includes hardware signal processing and smart sensors on a field-programmable gate arrays for applications on mechatronics.

Roque A. Osornio-Rios (M'10) received the B.E. degree from the Instituto Tecnologico de Queretaro, Queretaro, Mexico, and the M.E. and the Ph.D. degrees from the University of Queretaro, Queretaro, Mexico, in 2007. He is a National Researcher with CONACYT. He is currently Professor whit the University of Queretaro. He was an Advisor of over 30 theses, and a coauthor of over 40 technical papers in international journals and conferences His fields of interest include hardware signal processing and mechatronics. Dr. Osornio-Rios received the "2004 ADIAT National Award on Innovation" for his works in applied mechatronics.

Arturo Garcia-Perez (M'10) received the B.E. and M.E. degrees in electronics from the University of Guanajuato, Salamanca, Mexico, in 1992 and 1994, respectively, and the Ph.D. degree in electrical engineering from the University of Texas at Dallas, Richardson, in 2005. He is currently a Titular Professor with the Department of Electronic Engineering, University of Guanajuato. He is a National Researcher with the Consejo Nacional de

Ciencia y Tecnología level 1. He was an Advisor of over 50 theses. His fields of interest include digital signal processing for applications in mechatronics

Rene de J. Romero-Troncoso (M'07–SM'12) received the Ph.D. degree in mechatronics from the Autonomous University of Queretaro, Queretaro, Mexico, in 2004. He is a National Researcher level 2 with the Mexican Council of Science and Technology, CONACYT. He is currently a Head Professor with the University of Guanajuato and an Invited Researcher with the Autonomous University of Queretaro, Mexico. He has been an advisor for more than 180 theses, an author of two books on digital systems (in Spanish), and a coauthor of more than 90 technical papers published in international journals and conferences. His fields of interest include hardware signal processing and mechatronics. Dr. Romero–Troncoso was a recipient of the 2004 Asociación Mexicana de Directivos de la Investigación Aplicada y el Desarrollo Tecnológico Nacional Award on Innovation for his work in applied mechatronics, and the 2005 IEEE ReConFig Award for his work in digital systems.

Sensors **2012**, *12*, 11989-12005; doi:10.3390/s120911989

OPEN ACCESS

sensors

ISSN 1424-8220

www.mdpi.com/journal/sensors

Article

Smart Sensor for Online Detection of Multiple-Combined Faults in VSD-Fed Induction Motors

Armando G. Garcia-Ramirez [1], Roque A. Osornio-Rios [1], David Granados-Lieberman [1], Arturo Garcia-Perez [2] and Rene J. Romero-Troncoso [2,*]

[1] HSPdigital-CA Mecatronica, Facultad de Ingenieria, Universidad Autonoma de Queretaro, Campus San Juan del Rio, Rio Moctezuma 249, Col. San Cayetano, San Juan del Rio, Qro. 76807, Mexico; E-Mails: aggarcia@hspdigital.org (A.G.G.-R.); raosornio@hspdigital.org (R.A.O.-R.); granlieber@hspdigital.org (D.G.-L.)

[2] HSPdigital-CA Telematica, DICIS, Universidad de Guanajuato, Carr. Salamanca-Valle km 3.5+1.8, Palo Blanco, Salamanca, Gto. 36885, Mexico; E-Mail: agarcia@hspdigital.org

***** Author to whom correspondence should be addressed; E-Mail: troncoso@hspdigital.org; Tel./Fax: +52-464-647-9940.

Received: 27 July 2012; in revised form: 17 August 2012 / Accepted: 24 August 2012 / Published: 30 August 2012

Abstract: Induction motors fed through variable speed drives (VSD) are widely used in different industrial processes. Nowadays, the industry demands the integration of smart sensors to improve the fault detection in order to reduce cost, maintenance and power consumption. Induction motors can develop one or more faults at the same time that can be produce severe damages. The combined fault identification in induction motors is a demanding task, but it has been rarely considered in spite of being a common situation, because it is difficult to identify two or more faults simultaneously. This work presents a smart sensor for online detection of simple and multiple-combined faults in induction motors fed through a VSD in a wide frequency range covering low frequencies from 3 Hz and high frequencies up to 60 Hz based on a primary sensor being a commercially available current clamp or a hall-effect sensor. The proposed smart sensor implements a methodology based on the fast Fourier transform (FFT), RMS calculation and artificial neural networks (ANN), which are processed online using digital hardware signal processing based on field programmable gate array (FPGA).

Keywords: smart sensor; induction motors; multiple-combined faults; VSD; FPGA

1. Introduction

Induction motors are widely used in industry due to their robustness, low cost, easy maintenance and versatility; representing 85% of power consumption worldwide. Thus, when induction motors start developing incipient faults [1] it is important to detect the fault early because at this stage it is easier to repair, benefiting the industry in cost and maintenance time. Faults in induction motors may produce unanticipated interruptions on production lines, with severe consequences in product quality, safety and cost. For this reason, early fault detection in induction motors has attracted the interest of many researchers in recent years [2–5]. Induction motor faults are mainly associated to bearing defects (BD), rotor faults such as broken bars (BRB) [6–18], unbalance (UNB) [19] and misalignment (MAL) [20–23]. According to these faults, sometimes two or more of them may develop simultaneously, making it important to identify if they are alone or combined. Thus far, the combined fault identification in induction motors represents a big challenge, but it has been rarely considered in spite of being a common situation, because it is difficult to identify two or more faults simultaneously online through sensors [24–31]. Besides, the connection of induction motors through variable speed drives (VSD), which allow controlling their rotational speed, extending their useful life, and saving energy is a common practice in industry [32–35], but with the undesired effect of making the detection of faults more difficult because of the spurious harmonics induced by the VSD operation.

A number of vibration and current analysis-based techniques exist for identifying specific faults in induction motors. Regrettably, most of the condition-monitoring techniques for early fault detection focus on the detection of single specific faults. Broken rotor bar condition is one of the most difficult faults to detect because the induction motor works normally without perceivable anomalies, making this fault one of the most studied in research literature. For instance, in [6] the half broken bar condition is detected by combining the correlation of the vibration and current spectra. Then, a post processing technique is applied to improve the detectability and present a motor diagnosis. In a different case, in [7] the discrete wavelet transform (DWT) is applied to the instantaneous power signal to study the case of one and three broken bars for an induction motor. Otherwise, in [8] one broken bar is detected by applying the DWT to the induction motor current at the start-up transient, and through a weighting function granting the motor diagnosis. On the other hand, after unbalance, misalignment is the second most common fault causing life reduction in induction motors. For instance, in [20] misalignment is diagnosed through unique vibration features exhibited in the full spectrum computed by the fast Fourier transform (FFT). In [22] the misalignment behavior of the rotor in an induction machine is investigated with its vibration waveforms using orbit plots and conventional FFT to identify their unique vibration features. Unfortunately, few works are related to the diagnosis and the identification of multiple combined faults. Ballal *et al.* [25] develop a combined method with artificial neural networks (ANN) and fuzzy logic to detect stator inter-turn insulation and bearing wear faults in single-phase induction motor. They take five measurable parameters (motor intake current, speed, winding temperature, bearing temperature and the noise of the machine) for the input of the adaptive neural fuzzy inference system (ANFIS) to provide a diagnosis of the induction machine. Garcia-Perez *et al.* [28] proposed a method that combines a finite impulse response (FIR) filter bank with high resolution spectral analysis based on multiple signal classification (MUSIC) for detecting multiple combined faults, analyzing vibration and current signals. The results show concordance with

the analytical predetermined fault frequency for single and two or three combined faults (BRB, UNB, and BD). Romero-Troncoso *et al.* [29] performed a methodology using the information entropy and a fuzzy logic analysis in an FPGA device to identify faults like BD, UNB, BRB and their combinations by analyzing one phase of the induction motor steady-state current signal. Lebaroud *et al.* [31] presented a diagnosis method of multiple combined faults based on time-frequency classification of the current signals. All the aforementioned theoretical frameworks focus on fault detection of induction motors directly connected to the power line supply and do not consider the case of motors connected through a variable speed drive (VSD). Therefore, few works are related to faults in induction motors connected through VSDs. For instance Obaid *et al.* in [32] examined the effect of changing the input frequency in an induction motor fed through a VSD with faults such as unbalance and misalignment; the work highlighted that the harmonics induced by the VSD do not change the conditions of the frequencies of interest. Other research [34], reports a methodology for the detection of broken bars in induction motors connected through a VSD at different frequencies from 30 to 60Hz or directly to the power line supply and this methodology is based on electrical current transient analysis through DWT. The work of Cabal-Yepez *et al.* in [35] proposed the use of information entropy as a tool for multiple fault detection on induction motors controlled by a VSD obtaining results in different frequencies of operation from 30 to 50 Hz. Unfortunately, the aforementioned methodologies are based on an offline diagnosis, except for [34] that presents an online diagnosis for BRB. From an industrial point of view an online system that ensures the diagnosis of multiple-combined faults in a VSD-fed induction motor is nowadays a necessity for reducing power consumption and preventing any further damage.

From the technological point of view, smart sensors can be used to overcome the monitoring system demands due to their versatility and ability to work in environments where the access for field workers is limited, and their features in communication and data processing functionalities [36]. On the other hand, smart sensors based on field-programmable gate arrays (FPGA) are capable of performing the task due to their high-speed processing capabilities, reconfigurability, and system-on-a-chip (SoC) solutions. Smart sensors have being applied in different research areas [36–45]. For instance, Granados-Lieberman *et al.* [38] developed an FPGA-based smart sensor for real-time high-resolution frequency measurement in accordance with international standards of power quality monitoring, using a current clamp as primary sensor and the chirp z-transform (CZT) as signal processing for the diagnosis. Humin *et al.* [39] presented a smart sensor for medium-voltage dc power grid protection via current and voltage transformers. Otherwise, Rodriguez-Donate *et al.* [40] proposed a smart sensor to obtain several parameters related to motion dynamics using two primary sensors: an encoder and an accelerometer on a single link of industrial robots. In biology, Millan-Almaraz *et al.* [42] showed a smart sensor that can estimate plant transpiration. This smart sensor fuses five primary sensors: two temperature sensors, two relative humidity sensors and a light sensor. Depari *et al.* [44] presented a sensor network connected through a universal serial bus (USB)-to-Ethernet gateway for industrial applications. In [45] Son *et al.* developed a smart sensor system for machine fault diagnosis using three different sensors: vibration, current, and flux acquiring their signals, processing and diagnosing offline in a personal computer (PC). Due to their proven reliability in different research areas, smart sensors are the best suited candidates for induction motor fault monitoring systems with the presence of single or multiple-combined faults when the motor is fed through a VSD rather than having costly monitoring systems with several independent sensors and processing units connected through a computer network.

The contribution of this work is the development of a smart sensor for on-line detection of single or multiple-combined faults in induction motors connected through a VSD over a wide frequency range, covering low frequencies from 3 Hz and high frequencies up to 60 Hz, extending previously reported frequency ranges. The proposed smart sensor can use a commercially available current clamp or a Hall-effect sensor as the only primary sensor required, contrary to other works that use two or more sensors to identify a fault. The use of a current clamp as primary sensor provides additional benefits in portability, allowing one to perform the fault diagnosis in different motors without interrupting their operation. Another contribution of this work is the methodology, due to its simplicity and the theoretical foundation to analyze the frequencies of interest excited by the failure; this methodology is based on FFT fused with artificial neural networks, which is implemented into an FPGA due to its high-performance computational capabilities. In the proposed methodology, FFT provides the induction motor current spectrum normalized at steady-state, which allows covering motors with different power capabilities and a wide load range; then, specific frequency components are selected to compute their RMS to be inputs of the artificial neural network, which gives an online identification of single or combined faulty conditions. In this paper, three different faults in an induction motor: BRB, UNB, MAL and their combinations are investigated. Results confirm the potentiality of the smart sensor as an instrument for single and multiple-combined faults online detection.

2. Theoretical Background

2.1. Fault Effect on Stator Current Components

This article focuses on three different induction motor faults and their combinations: broken rotor bars (BRB), unbalance (UNB), and misalignment (MAL). The presence of BRB in induction motors produces several problems, such as power quality degradation [23]. On the other hand, UNB is the most observed fault in induction motors, and can cause catastrophic damages if not remedied. Finally, MAL is the second most commonly observed fault in rotating machines, and it is estimated to cause over 70% of the rotating machinery vibration problems [20].

2.1.1. Broken Rotor Bar

The detection of a broken bar fault can be done by the observation of the space harmonics f_{brb} components in the motor current as a fault indicator:

$$f_{brb} = f(1 \pm 2ks) \tag{1}$$

where f is the input frequency, k is the harmonic index, s is the slip. These components are known as left sideband component and right sideband component. When a bar is broken, the amplitude of these sideband components increases significantly, as shown in Figure 1, where the markers shown delimit the sideband component area [23].

2.1.2. Unbalance

The unbalance condition is presented when the mechanical load in the induction motor is not uniformly distributed, taking the center of mass out of the motor shaft. Unbalance in induction machines creates air-gap eccentricities, which change the frequency spectrum of the supply current [19].

Figure 1. Left and right sideband components. (**a**) Healthy motor; (**b**) Broken rotor bar fault.

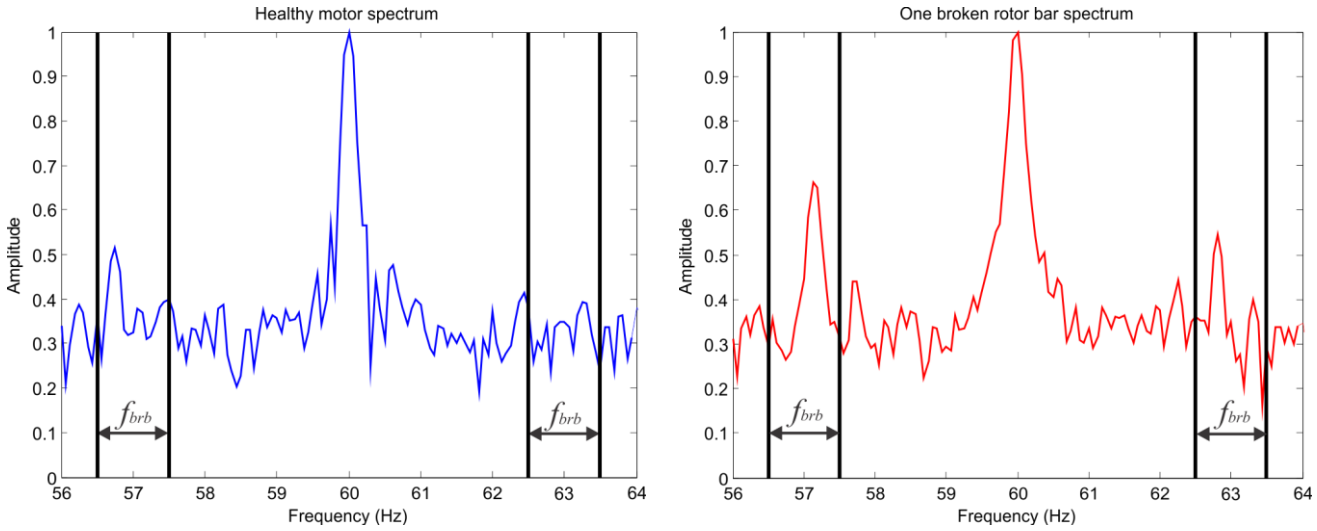

(**a**) (**b**)

2.1.3. Misalignment

The misalignment in induction motors occurs when the motor and the load pulleys are not aligned. The misalignment condition, like unbalance, creates air-gap eccentricities changing the frequency spectrum of the supply current [19]. The air-gap eccentricity affects the inductances of the motor resulting in harmonics (f_{ecc}) at rotating frequency sidebands of the supply frequency predicted by Equation (2):

$$f_{ecc} = f\left[1 \pm k\left(\frac{1-s}{p}\right)\right] \tag{2}$$

where p is the number of pole pairs. Figure 2(a) shows the air-gap eccentricities in the healthy motor current spectrum and Figure 2(b) shows the air-gap eccentricities in a motor current spectrum with unbalance where the regions of interest are delimited.

2.2. Artificial Neural Networks

Artificial neural networks (ANN) are computational models that simulate the neurological structure of the human brain and its capability to learn and solve problems through pattern recognition. There are different ANN architectures, such as multilayer feed-forward networks (MFN), recurrent networks, feedback networks, radial basis function networks, and Kohonen self-organizing map networks. The most popular architecture for ANN is the MFN that has an input layer, an output layer and one or more hidden layers. In this ANN architecture the data moves in only one direction, from the input neurons

through the hidden neurons to the output neurons, as shown in Figure 3. Where X_i ($i = 1,2,...,n$) are inputs and y_i ($i = 1,2,...,m$) are outputs. An MFN is usually trained by the back-propagation algorithm (BPA), which is a supervised learning method, and consists on mapping the process inputs to the desired outputs by minimizing the error between the desired outputs and the calculated outputs [46]. The MFN architecture is simple and practical in terms of classifier and computational load, making it an excellent candidate to be implemented in the methodology.

Figure 2. Air-gap eccentricities. (**a**) Healthy motor current spectrum; (**b**) Motor current spectrum with air-gap eccentricities.

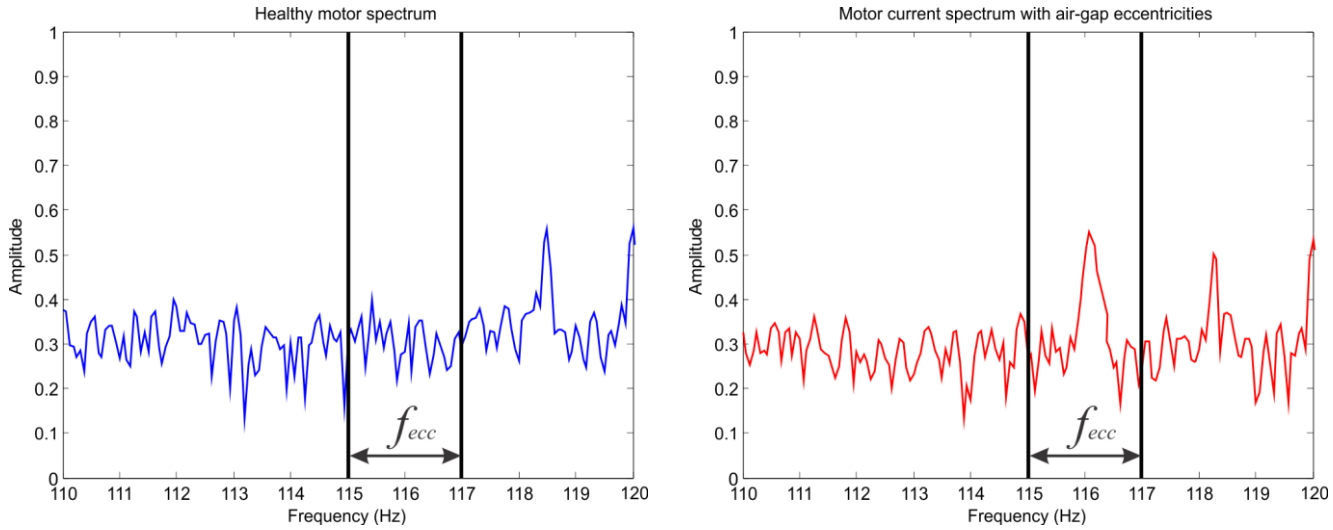

(**a**) (**b**)

Figure 3. Multilayer feed-forward network architecture.

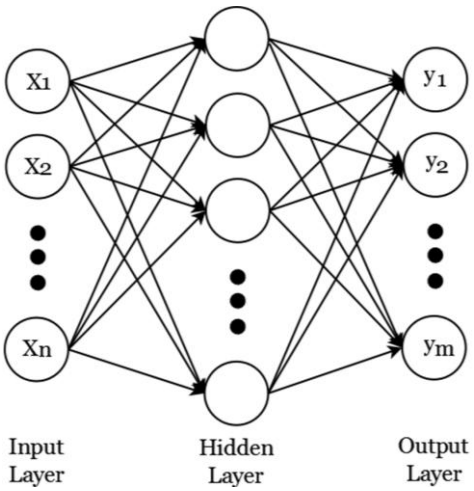

2.3. Variable Speed Drive

In industry the operation of induction motors through variable speed drives (VSDs) is very common, since it allows controlling their rotational speed, extending their useful life, and saving energy [32–35]. There are two different kinds of control in VSDs: Vector control drive and the Scalar control drive. The first one is an excellent driver to handle transients. It also enables fast control of

torque speed. Some disadvantages are the complexity and the high price of the circuit. This control is commonly used in high precision tasks. As for scalar control drives, they are widely used in the industry due to their low-cost, simple design and high immunity to feedback signal errors. That type of control is preferred for simple tasks like those of pumps and fans [47,48]. When the speed varies under vector control drives the frequency content of the monitoring signals are affected by the controller bandwidth. However, it is possible to extract the condition monitoring information from signals derived within the controller [49]. For instance, in [50] rotor failures in induction motors, fed by a vector and scalar control, are diagnosed with three different signals: voltage, current and speed. In scalar control drives the characteristic harmonics of broken rotor bars in current are clearly visible and generate the same speed ripples, contrary to vector control drive where these harmonics are not affected and the speed spectrum is perfect.

3. Methodology

This section shows the proposed methodology for the smart sensor development, the configuration and the block diagram of the FPGA-based smart processor. First, the general structure of the smart sensor is discussed, then the smart processor architecture with the processing stages and finally, the proposed ANN.

3.1. Smart Sensor

The block diagram of Figure 4 shows the proposed smart sensor for fault detection. The system uses a primary sensor (current clamp or Hall-effect sensor) to measure one phase of the stator current in the induction motor connected through a VSD; then, signal conditioning is applied. Subsequently, the conditioned signal is digitalized in the analog-to-digital converter block (ADC). Finally, the digital information is passed through the smart processor that is in charge to assert the motor diagnostic.

Figure 4. Block diagram of the fault detector smart sensor.

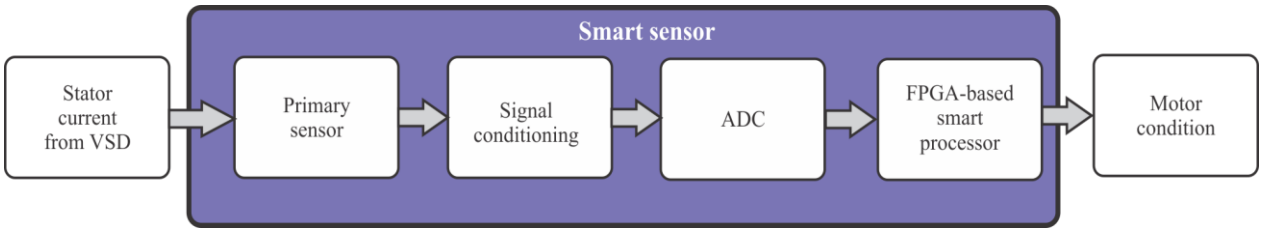

3.1.1. FPGA-Based Smart Processor

The block diagram of the FPGA-based smart processor internal structure to determine the condition of the motor is shown in Figure 5. The outgoing data from the ADC is time windowed with a Hanning window to reduce the leakage in the frequency domain and the frequency operation of the VSD is computed by a frequency estimator. Then, FFT is applied to get the current spectrum. In order to cover motors with different power capabilities and a wide load range the spectrum is normalized according to the magnitude of the fundamental frequency. Afterward, the bands of interest for the different faults are evaluated through the estimation of the RMS value of these selected bands

according to Equations (3) and (4). The selection of the bands of interest is based on intervals between a minimum and maximum slip from 1% to 20% in order to fulfill the NEMA standard of A, B, C and D designs [51]. These slip percentages guarantee a motor load range between 25 to 100%, nevertheless lower values of this range cannot be detected. Finally, the data from each RMS evaluator are inputs of the ANN to deliver the motor condition. Figure 6 shows the smart processing flow up to detect single and multiple-combined faults in induction motors.

Figure 5. Block diagram of the FPGA-based smart processor.

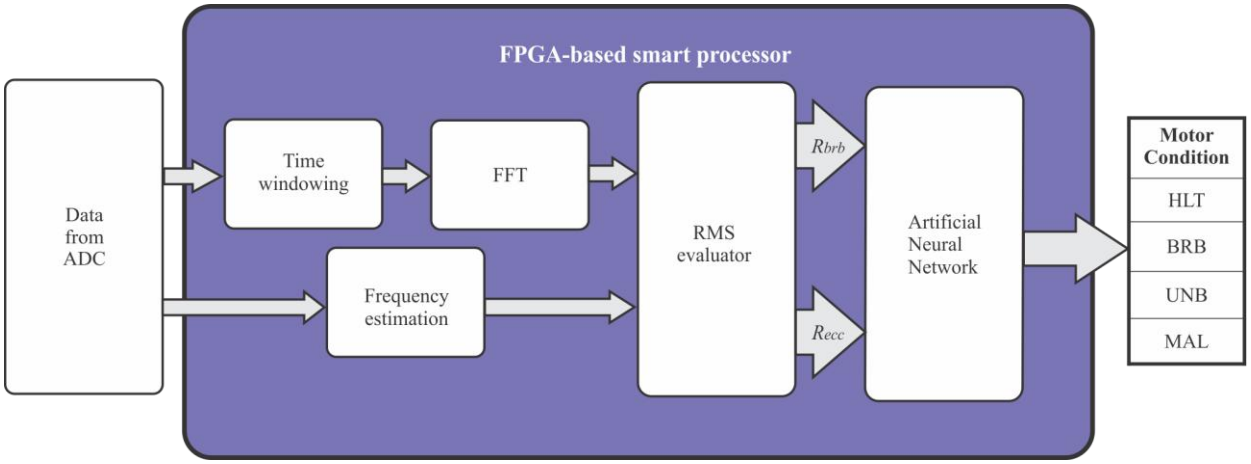

Figure 6. Smart processing flow up.

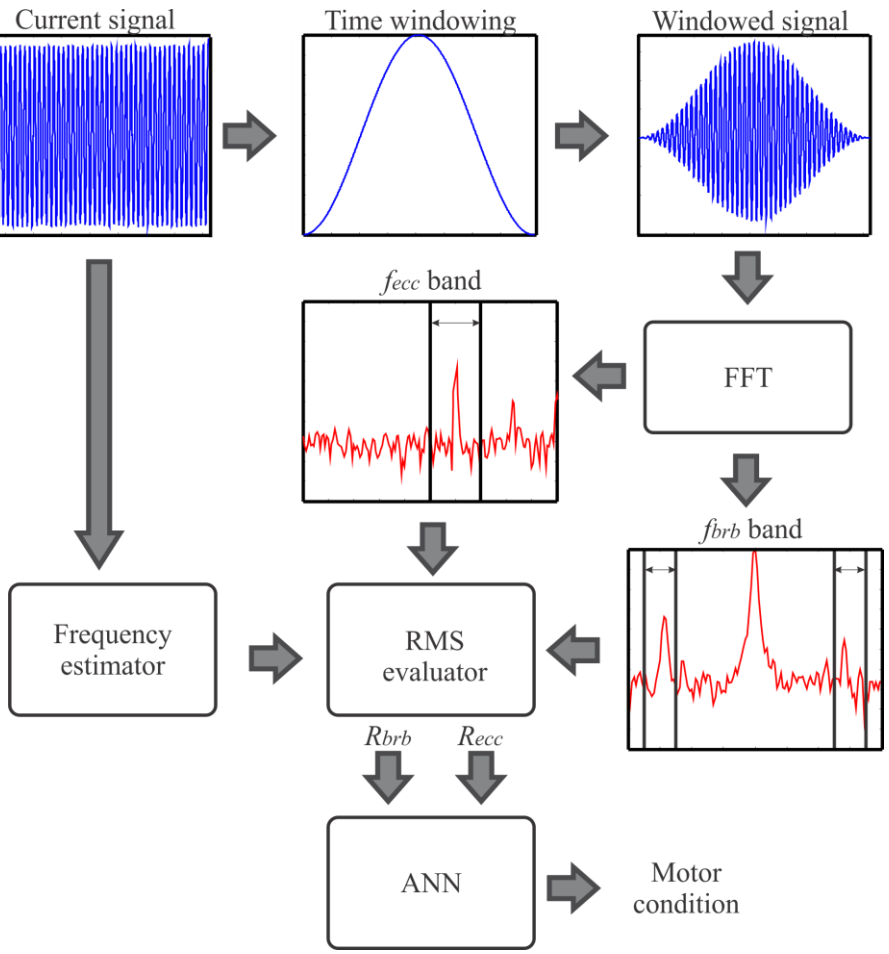

3.2. Proposed ANN

The proposed ANN implements an MFN with two input nodes that receive the RMS value of the left and right sideband components (R_{brb}) and the RMS value of air-gap eccentricities (R_{ecc}) of the stator current from VSD, ten nodes in the hidden layer and four output nodes to detect: healthy motor (HLT), broken rotor bars (BRB), unbalance (UNB), misalignment (MAL) and their combinations. The output nodes correspond to each single fault condition, and if two or more faults are presented at the same time, the corresponding output nodes will be triggered up. Figure 7 shows the proposed ANN.

$$R_{ecc} = \sum_{s=0.01}^{0.20} f\left[1 \pm k\left(\frac{1-s}{p}\right)\right] \tag{5}$$

$$R_{brb} = \sum_{s=0.01}^{0.20} f\left(1 \pm 2ks\right) \tag{6}$$

Figure 7. Proposed ANN.

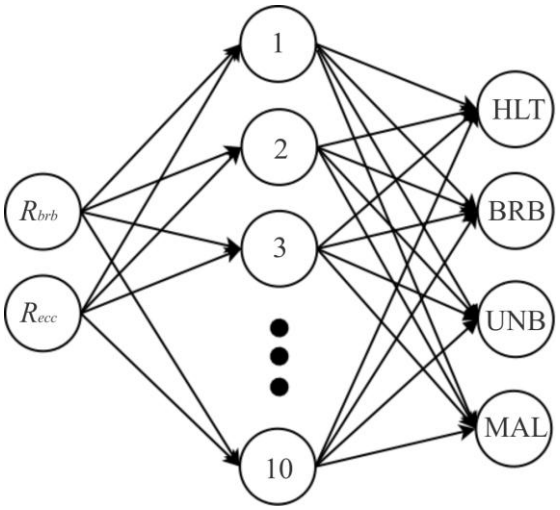

4. Experiments and Results

In this section, the experimental setup and the results are presented for validation the proposed smart sensor. The online fault detection was performed during the steady-state of the induction motor.

4.1. Experimental Setup

The experimental setup consists in using the steady-state current signal provided by a VSD (model WEG CFW08) to the motor under test for detecting the multiple-combined faults and to classify the conditions of the induction motor. The VSD has an operation range from 0 Hz up to 100 Hz using a frequency resolution of 0.01 Hz. Figure 8(a) shows the experiment setup where three different 1-hp three-phase induction motors (model WEG 00136APE48T) are used for testing the performance of the proposed methodology identifying the single and multiple combined fault conditions treated in this work. The tested motors have 2 poles, 28 bars and receive a power supply of 220 V AC. The motor rotational speed is controlled through a VSD at 3 Hz, 30 Hz and 60 Hz. The applied mechanical load is of an ordinary alternator, which represents a quarter (25%) of nominal load for the motor. The current

signal is acquired using a hall-effect sensor model L08P050D15, from Tamura Corporation. A 16-bit 4-channel serial-output sampling analog-to-digital converter ADS8341 from Texas Instrument Incorporated is used in the data acquisition system (DAS). The instrumentation system which was calibrated through the Fluke 435 uses a sampling frequency f_s = 256 Hz obtaining 4,096 samples during 16 seconds of the induction motor steady-state and has a bandwidth of 128 Hz, which covers the VSD operation range. The motor start-up is controlled by a relay in order to automatize the test run. The acquired information is analyzed by the proposed smart sensor that is implemented in a proprietary Spartan 3E XC3S1600 FPGA platform running at 48 MHz that provides the induction motor condition as shown in Figure 8(b). Table 1 summarizes the resource usage of the FPGA.

Figure 8. (**a**) Experiment setup; (**b**) Smart sensor.

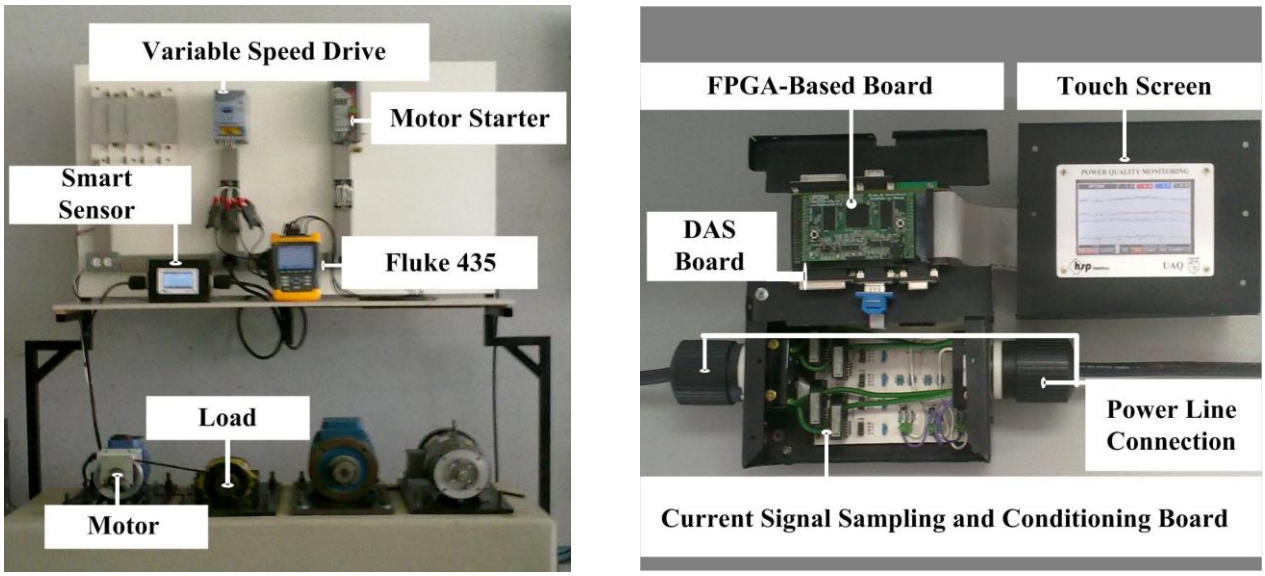

(**a**) (**b**)

Table 1. Resource usage of the FPGA.

Resource utilization	Xilinx Spartan 3E XC3S1600E
Slices	1,757/14,752 (12%)
Flip-flops	638/29,504 (2%)
4-input LUTs	3,270/29,504 (11%)
Maximum operation frequency	53.012 MHz

4.1.1. Single Faults

To produce an artificial broken rotor bar condition it was necessary to drill a 2.0 mm diameter hole in a bar of the rotor without harming the rotor shaft. Figure 9(a) shows the rotor with the broken bar used during the test. The unbalance condition was produced artificially by a bolt in the rotor pulley as shown in Figure 9(b). The misalignment test was carried out by shifting forward the band in the alternator pulley, so that the transverse axes of rotation for the motor and its load were not aligned. Figure 10(a) shows the aligned motor and the Figure 10(b) shows the misaligned motor.

Figure 9. (**a**) Broken rotor bar; (**b**) Unbalance.

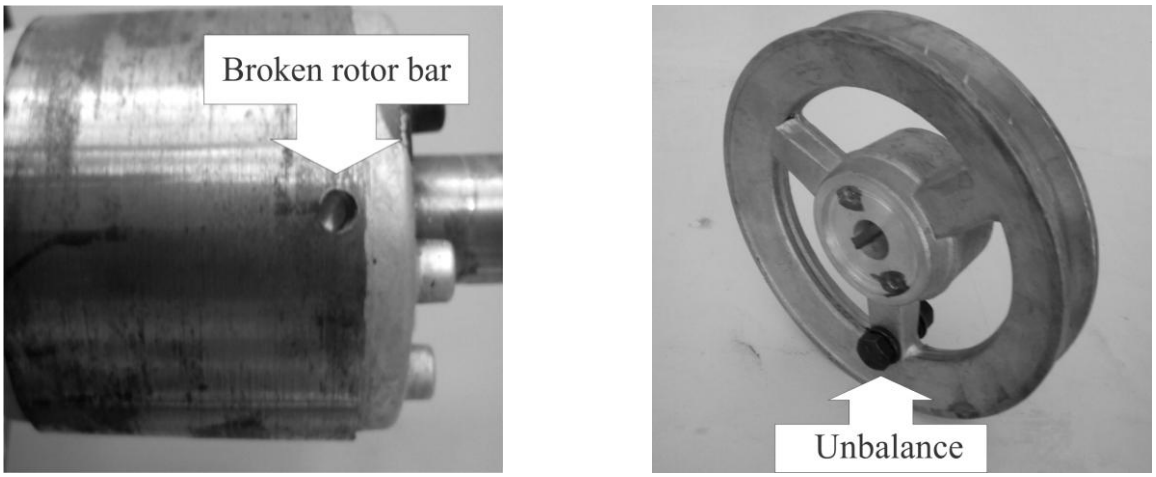

(**a**) (**b**)

Figure 10. (**a**) Motor aligned; (**b**) Motor misaligned.

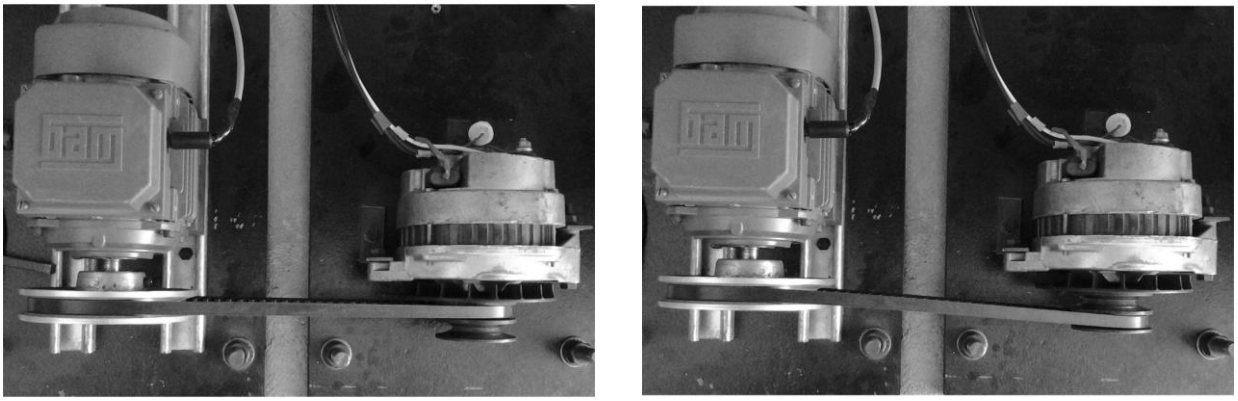

(**a**) (**b**)

4.1.2. Multiple-Combined Faults

The multiple-combined fault conditions were obtained by mixing each single fault with one or two of the remaining faults as shown in Figure 11.

Figure 11. Combination for multiple-combined fault analysis.

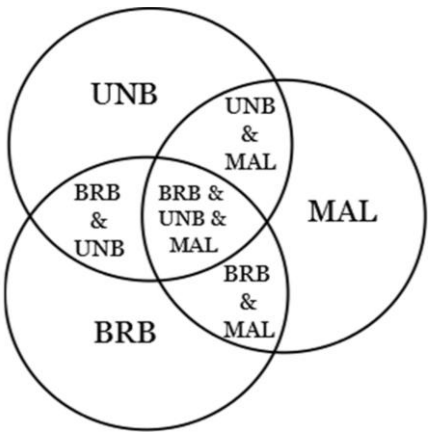

4.1.3. Network Training

The ANN is trained with the back-propagation algorithm to identify single or multiple-combined faults in induction motors. Forty trials are carried out under each motor condition for each study frequency. The training set was obtained with 1,000 random synthetic values for each study frequency within the range $[\mu - \sigma, \mu + \sigma]$, where μ is the mean and σ the standard deviation of the RMS values of spectral components of interest from steady-state of the induction motor on the first five trials. Real values of each fault were used as validation set for the diagnosis. The weights and the biases of each layer in the ANN were obtained offline, using the Matlab neural network toolbox for being implemented on the FPGA for the online diagnosis. The ANN is trained for motors with B NEMA design, since those are used in general applications [51]. The theoretical background shows that the frequency components of the faults do not depend of the power motor capability. Nevertheless, the current magnitude depends of the load and the motor power. So as to minimize those undesired effects that could modify the ANN output the spectrum is normalized before being applied to the ANN. This guarantees the same results in motors with similar characteristics. However, other NEMA designs have different relationship between the fundamental frequency and the fault components because of changes in the current flux density and the stator field [5]. In some of these cases a new training is required for adjusting the calibration of the smart sensor and improving the classification results.

4.2. Fault Identification Results

Table 2 presents the results delivered by the proposed smart sensor during the induction motor condition identification for each frequency studied in order to show the effectiveness of the system. The results include the identification of a healthy condition, a single isolated fault, and the combination of two or three faulty conditions for each study frequency. In order to obtain statistically significant results, 40 tests were performed to acquire the current signals from the induction motor in all treated cases for each study frequency.

Table 2. Effectiveness of the proposed smart sensor on identifying the induction motor condition with one or multiple combined faults.

Induction motor condition	03 Hz Effectiveness (%)	30 Hz Effectiveness (%)	60 Hz Effectiveness (%)
HLT	100	100	80
BRB	80	100	100
UNB	100	100	100
MAL	100	100	100
BRB-UNB	80	100	100
BRB-MAL	90	100	100
UNB-MAL	100	100	100
BRB-UNB-MAL	100	80	90

4.3. Discussion

Three different frequency cases are studied in order to fulfill a range from low to high frequencies: 3 Hz, 30 Hz and 60 Hz. Results of the smart sensor with the motor running at 3 Hz show an

effectiveness of 100% in health motor (HLT), unbalance (UNB), misalignment (MAL), the combination of unbalance and misalignment (UNB-MAL) and the combination of broken bars with unbalance and misalignment (BRB-UNB-MAL); the results for broken rotor bars (BRB), broken rotor bars in combination of unbalance (BRB-UNB) and broken rotor bars combined with misalignment (BRB-MAL) present an effectiveness over 80%. Due to the fact the sideband frequencies at 3 Hz were closer to the fundamental frequency, the conditions with broken bars were more difficult to diagnose. On the other hand, with the motor running at 30 Hz the smart sensor shows an effectiveness of 100% with the exception of BRB-UNB-MAL which presented an 80% effectiveness. Finally, at 60 Hz of the VSD, the smart sensor presents an effectiveness of 100% with the exception of HLT and BRB-UNB-MAL with effectiveness over 80%. A significant characteristic of the proposed smart sensor is the detection of single and multiple-combined faults in VSD-fed induction motors in an automatic way with only a primary sensor, different from the reviewed literature where the results are from single faults or multiple-combined faults interpreted offline by the user from current of the power supply or vibration signals of the induction motor with two or more primary sensors. Table 3 shows the faults detected by the proposed smart sensor (PSS), and the works that fulfill some of the faults detected and their combination. For instance, in [29,30] show online methodologies for the detection of multiple-combined faults of induction motors connected through the power line supply. On the other hand, in [32], reports an offline methodology for the detection of UNB and MAL at different operation frequencies. In a different case, [35] presents a methodology for the detection of different single isolated faults at different operation frequencies over 30 Hz. The PSS offers an online detection of single and multiple-combined faults at different operation frequencies in a wide range from 3 Hz to 60 Hz.

Table 3. Comparison between proposed smart sensor (PSS) and reviewed literature.

Induction motor condition	VSD-fed	Power line supply
BRB	[34], PSS	[7–19,27]
UNB	[32,33,35], PSS	[20]
MAL	[32,35], PSS	[21–23]
BRB-UNB	PSS	[28–31]
BRB-MAL	PSS	[24]
UNB-MAL	PSS	
BRB-UNB-MAL	PSS	

5. Conclusions

This work proposes a new smart sensor for online detection of multiple-combined faults in VSD-fed induction motors using only a Hall-effect current sensor as primary sensor in one-phase of the induction motor, which results in a high portability. The proposed methodology is based on the FFT and an ANN classifier in order to determine the motor condition according to the motor operation frequency controlled by the VSD, the simplicity of this methodology allows analyzing the frequencies of interest excited by the different failures. The FFT spectrum is normalized in order to cover different power motor capabilities and a wide load range. The functionality of the smart sensor was successfully tested in forty tests of each category of the faults and their combinations. Results demonstrate that the

proposed smart sensor is highly efficient in effecting a diagnosis of the induction motor operating over a wide frequency range of the VSD (3, 30 and 60 Hz), different from other works [7–31] that show results from motors fed by the power line supply only or [32–34] that present results from VSD-fed ones, but in a narrow frequency range without combining faults. The obtained results show the versatility of the proposed smart sensor for its use in diverse industrial applications that employ induction motors fed by a VSD. The proposed smart sensor allows the early fault detection benefiting the industry in cost and maintenance time. The proposed smart sensor for online detection of multiple-combined faults in VSD-fed induction motors is based on FPGA technology that provides high computation performance for the proposed methodology, as well as a low-cost, portable and efficient solution. This implementation shows that an FPGA platform is a suitable solution for smart processing units in developing smart sensors.

Acknowledgments

This project was partially supported by CONACyT scholarship (229736), FOFIUAQ-2012, SEP-PIFI (Integral Program of Institutional Support—Universidad de Guanajuato) 2011, and SEP-CONACyT 84723 projects.

References

1. Siyambalapitiya, D.J.; Mclaren, P.G. Reliability improvement and economic benefits of on-line monitoring systems for large induction machines. *IEEE Trans. Ind. Appl.* **1990**, *26*, 1018–1025.
2. Bellini, A.; Filipetti, F.; Tassoni, C.; Capolino, G.A. Advances in diagnostic techniques for induction machines. *IEEE Trans. Ind. Electron.* **2008**, *55*, 4109–4126.
3. Tallam, R.M.; Lee, S.B.; Stone, G.C.; Kliman, G.B.; Yoo, J.; Habetler, T.G.; Harley, R.G. A survey methods for detection of stator related faults in induction machines. *IEEE Trans. Ind. Appl.* **2007**, *43*, 920–933.
4. Nandi, S.; Toliyat, H.A.; Li, X. Condition monitoring and fault diagnosis of electrical motors—A review. *IEEE Trans. Energy Convers.* **2005**, *20*, 719–729.
5. Cusido, J.; Romeral, L.; Ortega, J.A.; Garcia, A.; Riba, J. Signal injection as a fault detection technique. *Sensors* **2011**, *11*, 3356–3380.
6. Rangel-Magdaleno, J.J.; Romero-Troncoso, R.J.; Osornio-Rios, R.A.; Cabal-Yepez, E.; Contreras-Medina, L.M. Novel methodology for online half-broken-bar detection on induction motors. *IEEE Trans. Instrum. Meas.* **2009**, *58*, 1690–1698.
7. Hedayati-Kia, S.; Henao, H.; Mpanda-Mabwe, A.; Capolino, G.A. Wavelet Based Instantaneous Power Analysis for Induction Machine Fault Diagnosis. In *Proceedings of 32nd Annual Conference on IEEE Industrial Electronics (IECON 2006)*, Paris, France, 6–10 November 2006; pp. 1229–1334.
8. Ordaz-Moreno, A.; Romero-Troncoso, R.J.; Vite-Frias, J.A.; Rivera-Gillen, J.R.; Garcia-Perez, A. Automatic online diagnosis algorithm for broken-bar detection on induction motors based on discrete wavelet transform for FPGA implementation. *IEEE Trans. Ind. Electron.* **2008**, *5*, 2193–2202.

9. Ayhan, B.; Chow, M.; Song, M. Multiple discriminant analysis and neural-network-based monolith and partition fault-detection schemes for broken rotor bar in induction motors. *IEEE Trans. Ind. Electron.* **2006**, *53*, 1298–1308.
10. Karami, F.; Poshtan, J.; Poshtan, M. Detection of broken rotor bars in induction motors using nonlinear Kalman filters. *ISA Trans.* **2010**, *49*, 189–195.
11. Jimenez, G.A.; Muñoz, A.O.; Duarte-Mermoud, M.A. Fault detection in induction motors using Hilbert and wavelet transforms. *Electr. Eng.* **2007**, *89*, 205–220.
12. Rabelo-Baccarani, L.M.; Braga-Tavares, J.P.; Rodrigues-Menezes, B.; Matos-Caminhas, W. Sliding mode observer for on-line broken rotor bar detection. *Electr. Pow. Syst. Res.* **2010**, *80*, 1085–1089.
13. Contreras-Medina, L.M.; Romero-Troncoso, R.J.; Cabal-Yepez, E.; Rangel-Magdaleno, J.J.; Millan-Almaraz, J.R. FPGA-based multiple-channel vibration analyzer for industrial applications in induction motor failure detection. *IEEE Trans. Instrum. Meas.* **2010**, *59*, 63–72.
14. Didier, G.; Ternisien, E.; Caspary, O.; Razik, H. A new approach to detect broken rotor bars in induction machines by current spectrum analysis. *Mech. Syst. Signal Process.* **2007**, *21*, 1127–1142.
15. Supangat, R.; Ertugrul, N.; Soong, W.L.; Gray, C.; Hansen, C.; Grieger, J. Detection of broken rotor bars in induction motor using starting-current analysis and effects of loading. *IEEE Proc. Electr. Power Appl.* **2006**, *153*, 848–855.
16. Hedayati-Kia, S.; Henao, H.; Capolino, G.A. Diagnosis of broken-bar fault in induction machines using discrete wavelet transform without slip estimation. *IEEE Trans. Ind. Appl.* **2009**, *45*, 1395–1404.
17. Bellini, A.; Yazidi, A.; Filippetti, F.; Rossi, C.; Capolino, G.A. High frequency resolution techniques for rotor fault detection of induction machines. *IEEE Trans. Ind. Electron.* **2008**, *55*, 4200–4209.
18. Yahia, K.; Cardoso, A.J.M.; Zouzou, S.E.; Gueddidi, S. Broken rotor bars diagnosis in an induction motor fed from a frequency converter: Experimental research. *Int. J. Syst. Assur. Eng. Manag.* **2012**, *3*, 40–46.
19. Kral, C.; Habetler, T.G.; Harley, R.G. Detection of mechanical imbalances of induction machines without spectral analysis of time-domain signals. *IEEE Trans. Ind. Appl.* **2004**, *40*, 1101–1106.
20. Patel, T.H.; Darpe, A.K. Experimental investigations on vibration response of misaligned rotors. *Mech. Syst. Signal Process.* **2009**, *23*, 2236–2252.
21. Salem, S.B.; Bacha, K.; Chaari, A. Support vector machine-based decision for induction motor fault diagnosis using air-gap torque frequency response. *Int. J. Comput. Appl.* **2012**, *38*, doi:10.5120/4686-6812.
22. Patel, T.H.; Darpe, A.K. Vibration response of misaligned rotors. *J. Sound Vib.* **2009**, *325*, 609–628.
23. Benbouzid, M.E.H. A review of induction motors signature analysis as a medium of fault detection. *IEEE Trans. Ind. Electron.* **2000**, *47*, 984–993.
24. Antonino-Daviu, P.; Jover-Rodriguez, M.; Riera-Guasp, M.; Pineda-Sanchez, M. Arkkio, A. Detection of combined faults in induction machines with stator parallel branches through the DWT of startup current. *Mech. Syst. Signal Process.* **2009**, *23*, 2336–2351.

25. Ballal, M.S.; Khan, H.M.; Suryawanshi, R.L.; Sonolikar, R.L. Adaptive neural fuzzy inference system for the detection of inter-turn instulation and bearing wear faults in induction motor. *IEEE Trans. Ind. Eletron.* **2007**, *54*, 250–258.
26. Wang, Y.; He, Z.; Zi, Y. Enhancement of signal denoising and multiple fault signatures detecting in rotating machinery using dual-tree complex wavelet transform. *Mech. Syst. Signal Process.* **2010**, *24*, 119–137.
27. Messaoudi, M.; Sbita, L. Multiple faults diagnosis in induction motor using the MCSA method. *Hyper Sci. Int. J. Signal Image Process.* **2010**, *1*, 190–195.
28. Garcia-Perez, A.; Romero-Troncoso, R.J.; Cabal-Yepez, E.; Osornio-Rios, R.A. The application of high-resolution spectral analysis for identifying multiple combined faults in induction motors. *IEEE Trans. Ind. Electron.* **2011**, *58*, 2002–2010.
29. Romero-Troncoso, R.J.; Saucedo-Gallaga, R.; Cabal-Yepez, E.; Garcia-Perez, A.; Osornio-Rios, R.A.; Alvarez-Salas, R.; Miranda-Vidales, H.; Huber, N. FPGA-based online detection of multiple combined faults in induction motors through information entropy and fuzzy inference. *IEEE Trans. Ind. Electron.* **2011**, *58*, 5263–5270.
30. Cabal-Yepez, E.; Valtierra-Rodriguez, M.; Romero-Troncoso, R.J.; Garcia-Perez, A.; Osornio-Rios, R.A.; Miranda-Vidales, H.; Alvares-Salas, R. FPGA-based entropy neural processor for online detection of multiple combined faults on induction motors. *Mech. Syst. Signal Process.* **2012**, *30*, 123–130.
31. Lebaroud, A.; Clerc, G. Classification of induction machine faults by optimal time-frequency representations. *IEEE Trans. Ind. Electron.* **2008**, *55*, 4290–4298.
32. Obaid, R.R.; Habetler, T.G.; Tallam, R.M. Detecting Load Unbalance and Shaft Misalignment Using Stator Current in Inverter-Driven Induction Motors. In *Proceedings of Electric Machines and Drives Conference (IEMDC 2003)*, Atlanta, GA, USA, 1–4 June 2003; pp. 1454–1458.
33. Blödt, M.; Bonacci, D.; Regnier, J.; Chabert, M.; Faucher, J. On-line monitoring of mechanical faults in variable-speed induction motor drives using the wigner distribution. *IEEE Trans. Ind. Electron.* **2008**, *55*, 522–533.
34. Millan-Almaraz, J.R.; Romero-Troncoso, R.J.; Osornio-Rios, R.A.; Garcia-Perez, A. Wavelet-based methodology for broken bar detection in induction motors with variable-speed drive. *Electr. Power Compon. Syst.* **2011**, *39*, 271–287.
35. Cabal-Yepez, E.; Romero-Troncoso, R.J.; Garcia-Perez, A.; Osornio-Rios, R.A.; Alvarez-Salas, R. Multiple Fault Detection through Information Entropy Analysis in ASD-Fed Induction Motors. In *Proceedings of 8th IEEE International Symposium on Diagnostics for Electrical Machines, Power Electronics & Drives (SDEMPED 2011)*, Bologna, Italy, 5–8 September 2011; pp. 391–396.
36. Rivera, J.; Herrera, G.; Chacon, M.; Acosta, P.; Carrillo, M. Improved progressive polynomial algorithm for self-adjustment and optimal response in intelligent sensors. *Sensors* **2008**, *8*, 7410–7427.
37. Rangel-Magdaleno, J.J.; Romero-Troncoso, R.J.; Osornio-Rios, R.A.; Cabal-Yepez, E. Novel oversampling technique for improving signal-to-quantization noise ratio on accelerometer-based smart jerk sensors in CNC applications. *Sensors* **2009**, *9*, 3767–3789.
38. Granados-Lieberman, D.; Romero-Troncoso, R.J.; Cabal-Yepez, E.; Osornio-Rios, R.A.; Franco-Gasca, L.A. A real-time smart sensor for high-resolution frequency estimation in power systems. *Sensors* **2009**, *9*, 7412–7429.

39. Humin, L.; Weilin, L.; Min, L.; Monti, A.; Ponci, F. Design of smart MVDC power grid protection. *IEEE Trans. Intrum. Meas.* **2011**, *60*, 3035–3046.
40. Rodriguez-Donate, C.; Morales-Velazquez, L.; Osornio-Rios, R.A.; Herrera-Ruiz, G.; Romero-Troncoso, R.J. FPGA-based fused smart-sensor for dynamic and vibration parameter extraction in industrial robot links. *Sensors* **2010**, *10*, 4114–4129.
41. Moreno-Tapia, S.V.; Vera-Salas, L.A.; Osornio-Rios, R.A.; Dominguez-Gonzalez, A.; Stiharu, I.; Romero-Troncoso, R.J. A field programmable gate array-based reconfigurable smart-sensor network for wireless monitoring of new generation computer numerically controlled machines. *Sensors* **2010**, *10*, 7263–7286.
42. Millan-Almaraz, J.R.; Romero-Troncoso, R.J.; Guevara-Gonzalez, R.G.; Contreras-Medina, L.M.; Carrillo-Serrano, R.V.; Osornio-Rios, R.A.; Duarte-Galvan, C.; Rios-Alcaraz, M.A.; Torres-Pacheco, I. FPGA-based fused smart sensor for real-time plant-transpiration dynamic estimation. *Sensors* **2010**, *10*, 8316–8331.
43. Rodriguez-Donate, C.; Osornio-Rios, R.A.; Rivera-Guillen, J.R.; Romero-Troncoso, R.J. Fused smart sensor network for multi-axis forward kinematics estimation in industrial robots. *Sensors* **2011**, *11*, 4335–4357.
44. Depari, A.; Flammini, A.; Marioli, D.; Taroni, A. USB sensor network for industrial applications. *IEEE Trans. Instrum. Meas.* **2008**, *57*, 1344–1349.
45. Son, J.-D.; Niu, G.; Yang, B.-S.; Hwang, D.-H.; Kang, D.-S. Development of smart sensors system for machine fault diagnosis. *Expert Syst. Appl.* **2009**, *9*, 11981–11991.
46. Huang, Y. Advances in artificial neural networks—Methodological development and application. *Algorithms* **2009**, *2*, 973–1007.
47. Holtz, J. Sensorless of induction motor drives. *Proc. IEEE* **2002**, *90*, 1359–1394.
48. *WEG-CFW-08 Frequency Inverter Manual*; WEG Corporation: Jaraguá do Sul, Santa Catarina, Brazil, 2006.
49. Bellini, A.; Filippetti, F.; Franceschini, G.; Tassoni, C. Closed-loop control impact on the diagnosis of induction motors faults. *IEEE Trans. Ind. Appl.* **2000**, *36*, 1318–1329.
50. Menacer, A.; Champenois, G.; Nait-Said, M.S.; Benakcha, A.; Moreau, S.; Hassaine, S. Rotor failures diagnosis of squirrel cage induction motors with different supplying sources. *J. Electr. Eng. Technol.* **2009**, *4*, 219–228.
51. *Motors and Generators*; ANSI/NEMA MG 1-2003 (R2004) Standards Publication; National Electrical Manufacturers Association: Rosslyn, VA, USA, 2011.